Development and characterization of oncolytic adenoviral vectors for the treatment of head and neck cancer

Dissertation submitted to obtain the degree of “Doctor rerum naturalium” (Dr. rer. nat.)
of the faculty of life science at Ulm University

Submitted by

Frederik Wienen

Born in Bad Saulgau

2023

Dean of the faculty of life science at Ulm University:

Prof. Dr. Thorsten Bernhardt

First reviewer:

Prof. Dr. Jan Tuckermann

Second reviewer:

Prof. Dr. Stefan Kochanek

Day doctorate awarded: 21.09.2023

List of publications

Parts of the present study have been previously published in the following publication:

Wienen, F., Nilson, R., Allmendinger, E., Graumann, D., Fiedler, E., Bosse-Doenecke, E., Kochanek, S., and Krutzke, L. (2022). Affilin-based retargeting of adenoviral vectors to the epidermal growth factor receptor. Biomater Adv *144*, 213208. 10.1016/j.bioadv.2022.213208.

Table of contents

1 Abbreviations

°C	Degree Celsius
µm	Micrometer
µM	Micromolar
aa	Amino acid
AAV	Adeno-associated virus
AcOH	Acetic acid
Ad	Adenovirus
ADP	Adenoviral death protein
ALL	Acute lymphoblastic leukemia
ALT	Alanine aminotransferase
Amp	Ampicillin
APS	Ammonium persulfate
AST	Aspartate aminotransferase
BAK	Bcl-2 antagonist/killer protein
BiTE	Bispecific T-cell engager
µBMSC	Bone marrow derived stem cell
bp	Base pair
BSA	Bovine serum albumin
CA	Chloramphenicol
CAF	Cancer associated fibroblast
CAR	Coxsackie- and adenovirus receptor
CAR-T	Chimeric antigen receptor T-cell
CD	Cytosine deaminase
CIP	Calf intestinal phosphatase
cm	Centimeter
CMV	Cytomegalovirus
CPE	Cytopathic effect
CR	Conserved region
CR-1	Complement receptor 1

Abbreviations

CRAd	Conditionally replicating adenoviral vector
Cys	Cysteine
DAPI	4′,6-diamidino-2-phenylindole
DBP	DNA-binding protein
ddH_2O	Double distilled H_2O
DMEM	Dulbecco's modified eagle medium
DMSO	Dimethyl sulfoxide
DNA	Desoxyribonucleic acid
dNTP	Deoxyribonucleotide triphosphate
DPBS	Dulbecco's phosphate buffered saline
dpi	Days post infection
DPP	Dipeptidyl peptidase
DPPIV	Dipeptidyl peptidase 4
dpt	Days post transduction
ds	Double stranded
DSG-2	Desmoglein 2
E.coli	Escherichia coli
EDTA	Ethylenediaminetetraacetic acid
EGF	Epidermal growth factor
eGFP	Enhanced green fluorescence protein
EGFR	Epidermal growth factor receptor
ELISA	Enzyme-linked immunosorbent assay
EMA	European medicines agency
EnAd	Enadenotucirev
EpCAM	Epithelial cell adhesion molecule
ErbB	Erythroblastic leukemia viral oncogene homolog
et al.	Et alii → and others
EtBr	Ethidium bromide
EtOH	Ethanol
E_λ	Extinction at wavelength λ
ε	Extinction coefficient

Abbreviations

FAP	Fibroblast activation protein
FC	Flow cytometry
FCS	Fetal calf serum
FDA	Food and drug administration
FFLuc	Firefly Luciferase
FGF2	Fibroblast growth factor 2
Fig.	Figure
FX	Blood coagulation factor X
g	Gravity
g	Gramm
Gla	Gamma-carboxyglutamic acid
GM-CSF	Granulocyte macrophage-colony stimulating factor
GMP	Good manufacturing practice
h	Hours
H&E	Hematoxylin & Eosin
HAdV	Human adenovirus
HAdV-5	Human adenovirus type 5
HAdV-6	Human adenovirus type 6
HCOH	Formaldehyde
HCRAd-5	Human conditionally replicating adenovirus type 5
hEGF	Human epidermal growth factor
HEPES	4-(2-hydroxyethyl)-1-piperazineethanesulfonic acid
HER	Human epidermal growth factor receptor
hFAP	Human FAP
HNSCC	Head and neck squamous cell carcinoma
HPMA	N-(2-hydroxyprolyl) methacrylamide
hpt	Hours post transduction
HRP	Horse radish peroxidase
HSPG	Heparan sulfate proteoglycans
hTERT	Human telomerase reverse transcriptase
hTfR	Human transferrin receptor

Abbreviations

HV	Helper virus
HVR	Hypervariable region
i.p.	Intraperitoneally
i.t.	Intratumoral
i.v.	Intravenous
IgG	Immunoglobulin G
IgM	Immunoglobulin M
IHC	Immunohistochemistry
IL	Interleukin
ILR2γ	Interleukin 2 receptor gamma chain
ITR	Inverted terminal repeats
IVIS	*In vivo* imaging system
Kana	Kanamycin
kb	Kilo-base
kbp	Kilo-base pair
KC	Kupffer cell
Kd	Dissociation constant
kDa	Kilodalton
KS	Kozak sequence
kV	Kilovolt
l	Liter
LB	Lysogeny broth
LPL	Lipoprotein lipase
LRP	LDL receptor-related protein receptor
M	Molar
mAb	Monoclonal antibody
MEM	Minimum essential medium
MeOH	Methanol
MFI	Mean fluorescence intensity
mg	Milligram
MHC-I	Major histocompatibility complex class I

min	Minutes
ml	Milliliter
MLP	Major late promoter
MLTU	Major late transcription unit
mM	Millimolar
mm	Millimeter
mRNA	Messenger RNA
MSC	Mesenchymal stem cell
n.d.	Not detectable
n.s.	Not statistically significant
NanoLuc	Nano Luciferase
neo	Neomycin
NK	Natural killer (cells)
nm	Nanometer
nM	Nanomolar
NSG	NOD SCID gamma
nt	Nucleotide
Nup214	Nucleoporin 214
o/n	Over night
oAd	Oncolytic adenovirus
oAV	Oncolytic adenoviral vector
OD	Optical density
OD260	Optical density at a wave-length of 260 nm
ori	Origin of replication
OV	Oncolytic virus
PAGE	Polyacrylamide gel electrophoresis
PAMAM	Poly(amidoamine)
Par-4	Prostate apoptosis response-4
PBS	Phosphate buffered saline
PCR	Polymerase chain reaction
PEG	Polyethylene glycol

Abbreviations

PEI	Polyethyleneimine
PFA	Perfluoralkoxy-Polymere
pH	Pondus hydrogenii
pMOI	Particle/physical multiplicity of infection
pRb	Retinoblastoma protein
PSG	Penicillin-Streptomycin-Glutamine
PSMA	Prostate-specific membrane antigen
PSME	PSMA enhancer
pTP	Precursor terminal protein
qPCR	Quantitative real-time PCR
RFU	Response forming unit
RGD motif	Arginine-glycine-aspartic acid motif
RNA	Ribonucleic acid
RPE65	Retinal pigment epithelium-specific 65 kDa protein
rpm	Rounds per minute
RPMI	Roswell Park Memorial Institute
RT	Room temperature
RV	Retrovirus
s.c.	Subcutaneously
SA	Sialic acid
scFv	Single chain variable fragment
SDS	Sodium dodecyl sulfate
sec	Second(s)
SFDA	State and food drug administration
SP	Signal peptide
SPB	Surfactant protein B
Strep	Streptomycin
SV40	Simian virus 40
TAE	Tris-acetate-EDTA
TBE	Tris-borate-EDTA
TBS	Tris-buffered saline

TBS-T	TBS + 0.05% Tween
TCEP	tris(2-carboxyethyl)phosphine
TE	Tris-EDTA
TELT	Tris-EDTA-Lithium-Triton X-100
TEMED	Tetramethyl ethylenediamine
Tet	Tetracycline
TILT	Tumor-infiltrating lymphocyte therapy
TK	Thymidine kinase
TME	Tumor microenvironment
TNF-α	Tumor necrosis factor alpha
TP	Terminal protein
U	Units
V	Volt
V_H	Variable heavy chain
VIT	Vector induced thrombocytopenia
V_L	Variable light chain
VP	Viral particle
VSMC	Vascular smooth muscle cell
WB	Western Blot
WHLW	Ministry of health, labor, and welfare
wt	Wild-type
λ	Lambda → wavelength (nm)
Ψ	Psi → packaging sequence

2 Introduction

2.1 Gene therapy

The field of gene therapy aims to treat or cure diseases by complementing, repairing or reconstituting disordered genes[1] but can be likewise applied as therapeutic approach for anti-cancer therapies[2]. All have in common that they require efficient delivery of the genetic material into the target cell[3,4]. Within 40 years of gene therapy, especially viruses[5] turned out as efficient gene transfer vehicles and up to date various gene therapeutic clinical trials using adenoviruses (Ads), retroviruses (RVs) or adeno-associated viruses (AAVs) as 'gene shuttles' have been employed[6]. Although the field of viral vector-based gene therapy has been subject of several setbacks over the decades[6,7], it has also experienced great progress, leading to successful clinical trials and approval of viral vector-based gene therapeutics[8]. Until 2022, there have been a total of about 3685 gene therapy clinical trials worldwide, from which at least 2179 were based on viral vectors[9]. In 2012 the world's first gene therapeutic drug, Glybera - an AAV for the treatment of lipoprotein lipase (LPL) deficiency, obtained regulatory approval by the European Medicines Agency (EMA)[10,11]. Only few years later, in 2017, a second AAV-based drug, Luxturna, obtained approval by the food and drug administration (FDA) for the treatment of RPE65-linked, inherited retinal dystrophy[12] and in 2019, a third AAV-based drug, Zolgensma, was approved for the treatment of spinal muscular atrophy[13]. Furthermore, also gene therapeutic approaches in the field of oncology experienced success. Chimeric antigen receptor T-cell (CAR-T) therapy, which is based on allogenic or autologous T-cells that have been stably modified *ex vivo* to specifically recognize and eradicate cancerous cells[14], achieved remarkable remission rates of up to 90% in patients suffering from relapsed and refractory acute lymphoblastic leukemia (ALL)[15]. The use of oncolytic viruses (OVs), which infect and eradicate cancer cells due to their cytolytic life-cycle[16] as introduced in more detail in a later section, likewise achieved promising results with several candidates reaching the market. In 2003, Gendicine, a replication-deficient adenovirus encoding for the tumor suppressor p53 was the world's first oncolytic virus that obtained approval for the treatment of head and neck carcinomas in China[17,18]. Only two years later, Oncorine, another adenovirus with selective replication in cancer cells

obtained approval by the Chinese state food and drug administration (SFDA) for the treatment of head and neck squamous cell carcinomas[19]. A further example is Imlygic (T-Vec), a tumor-selective replication-competent oncolytic herpes simplex virus-1 encoding for the granulocyte macrophage-colony stimulating factor (GM-CSF), which achieved approval by the FDA and the EMA in 2015 for the treatment of advanced melanoma[20,21]. Only recently, in 2021, the oncolytic herpes simplex virus-1 (HSV-1) G47Δ showed promising results in clinical studies and thus obtained approval by the Ministry of Health, Labor, and Welfare (WHLW) in Japan for the treatment of glioma[22,23]. Furthermore, there are various ongoing clinical studies investigating different types of oncolytic viruses including adenoviruses, herpes simplex virus, vaccinia virus, reovirus, coxsackie virus or poliovirus, whereof some displaying significant anti-tumor efficacies[24]. Thus, gene therapy represents a promising research field for the treatment of a broad spectrum of various genetic and non-genetic diseases including cancer.

2.2 Oncolytic virotherapy

Oncolytic virotherapy is a growing field of novel anti-cancer therapies[16] and dozens of clinical trials have been conducted up to date[24]. The basic principle of oncolytic virotherapy relies on the self-amplifying characteristic of viruses: initial infection of tumor cells results in virus replication followed by tumor cell lysis and release of viral progeny, which infect neighboring tumor cells[25]. Virus-induced tumor cell lysis additionally stimulates a tumor-directed immune response due to the release of tumor-associated antigens and the induction of inflammatory pathways, which augments the anti-tumor efficacy of OVs[25,26]. OVs are used with the aim to specifically infect and replicate within cancer cells while sparing healthy cells or tissues[16]. Thus, efficient oncolytic virotherapy ideally includes (i) successful delivery of OVs to the tumor site, (ii) tumor cell-specific infection, (iii) tumor-restricted virus replication and (iv) strong induction of a tumor-directed immune activation. To boost the natural characteristics of viruses regarding these requirements, they are often engineered in order to improve their safety and anti-tumor efficacy[27]. Beside virus modifications enabling tumor-specific targeting, cancer cell-restricted virus replication, avoidance of virus particle sequestration and arming of viruses by insertion of therapeutic transgenes into the virus genome are widely used strategies to improve the anti-tumor efficacy of OVs[28].

2.2.1 Adenoviruses in oncolytic virotherapy

Among all OVs investigated, oncolytic adenoviruses (oAds) represent the most frequently used and account for about 40% of clinical trials within the field of oncolytic virotherapy to date[24]. Until now, and as mentioned above, two adenoviral-based OVs, namely Gendicine and Oncorine, achieved approval for the treatment of head and neck cancer in China. Additionally, there are several other oAds enrolled in ongoing clinical trials like ColoAd1, ONCOS-102, DNX-2401 or CG0070[29]. Adenoviruses are genetically stable and integrate into the hosts genome to a negligible extent[30], thus posing minimal risk for insertional mutagenesis. Furthermore, adenoviruses equally infect and replicate within both dividing as well as non-dividing cells, which expands their oncolytic capacity. Additionally, adenoviruses can be produced to high titers and standardized purification protocols allow for final products of high quality.

2.3 Adenoviruses

2.3.1 Classification

Adenoviruses belong to the family of *Adenoviridae* and are subdivided into the five genera *Mastadenoviruses*, *Aviadenoviruses*, *Ichtadenoviruses*, *Siadenoviruses*, and *Atadenoviruses*[31]. First isolated in 1953[32], more than 80 different human adenovirus types have been identified to date[33], which are further grouped in species A-F[34]. Among all adenoviruses identified, human adenovirus type 5 (HAdV-5), which belongs to species C adenoviruses[33,34], is the most investigated and characterized type so far.

2.3.2 Structure

HAdV-5 is a non-enveloped virus with a capsid of ~ 100 nm in diameter, mainly composed out of three structural proteins: fiber, penton base and hexon[35,36]. Hexon is the most abundant surface protein, with a total of 720 hexon monomers assembling into 240 hexon trimers which build up the icosahedral capsid with its 12 vertices[37]. At each of these vertices, five penton base monomers assemble into a pentamer[38]. On top of each pentameric penton base protein, fiber proteins assemble to trimers, which protrude from the viral capsid. The fiber monomer is composed out of a fiber tail, shaft, and a C-terminal globular knob domain[39]. The tail anchors the fiber in the viral capsid and together with the pentameric protein penton base the fiber trimer builds up the viral penton at each vertex of the capsid[40]. Beside their structure-giving properties, fiber, penton base and hexon also exhibit functional tasks. The C-terminal globular knob domain of fiber is essential for the attachment of the HAdV-5 virus particle to its primary receptor coxsackie- and adenovirus receptor (CAR)[41,42]. A so-called “RGD-motif” located within the penton base protein[43] is involved in the host-cell entry due to interaction with cell surface-located $\alpha_v\beta_3$ and $\alpha_v\beta_5$ integrins[44,45]. Solvent exposed regions of the hexon protein comprise three loops, termed L1, L2 and L4[46]. L1 and L2 together feature a total of seven discrete hypervariable regions (HVRs)[47] of which six (HVR1-6) are located within L1 and one (HVR7) within L2. HVRs lack extensive secondary structures and are involved in a variety of different host protein interactions. Distinct amino acid residues located in HVR5 and HVR7 i.e. specifically interact with blood coagulation factor X (FX)[48], which strongly influences the virus tropism *in vivo*[49]. Moreover, hexon significantly accounts to the overall net negative surface charge of the virus particle, which also contributes to the virus tropism[50]. In addition to structural proteins, mature adenoviral particles are further composed of so-called cement (minor) and core proteins. Cement proteins include the viral polypeptides IIIa, VI, VIII, and IX[51], while core proteins include the viral polypeptides IVa2, V, VII, X, the terminal protein (TP) and the adenovirus encoded protease[52]. Cement proteins mainly contribute to capsid stability, intracellular trafficking, and disassembly of the viral capsid at the nucleus[51]. Core proteins are major constituents of the nucleoprotein complex, stabilizing the viral genome and are further involved in genome replication and proteolytic cleavage of protein precursors[52]. A schematic cross-section of an adenovirus particle is illustrated in figure 1.

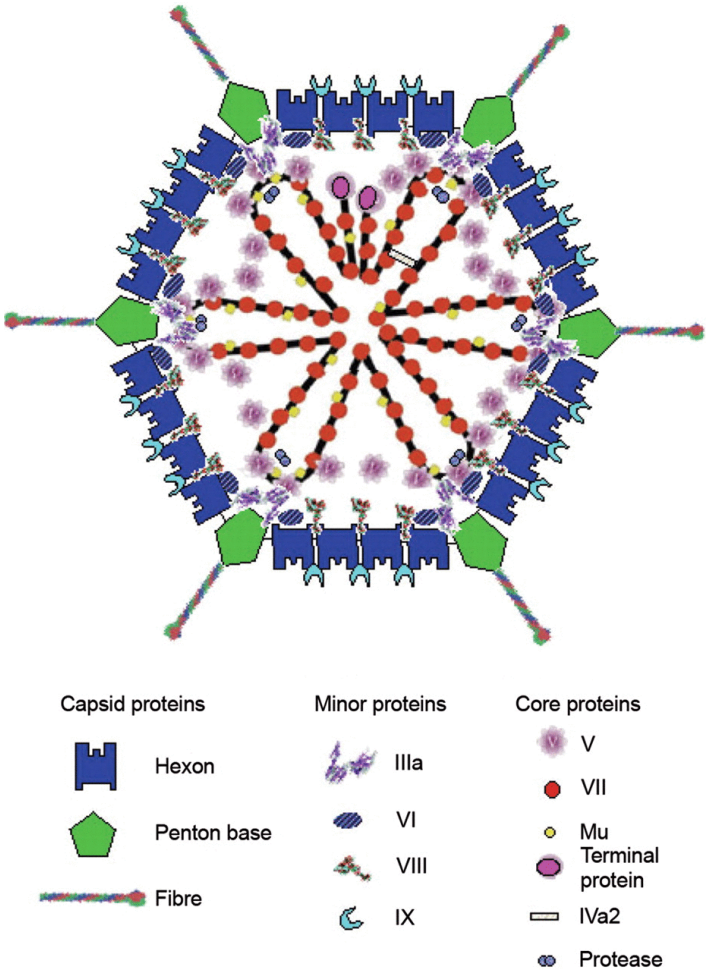

Figure 1: Schematic illustration of an adenovirus capsid cross-section.
Mu = polypeptide X (Russell 2009; Figure 1)

2.3.3 Genome

The HAdV-5 genome is a double-stranded, linear DNA with a size of ~ 36 kbp, first fully sequenced in 1992[53]. The genome is flanked by inverted terminal repeats (ITRs), which form extensive secondary structures[54] and constitute the origin of replication (ori) essential for amplification of the viral genome[55]. At both 5'-ends, the viral terminal protein (TP) is covalently linked to the genome[56], which is involved in DNA replication[57]. At the left site, downstream of the ITR, yet upstream of the coding region *E1A*, the packaging sequence Ψ is localized, which is essential for proper encapsidation of the viral genome into the newly assembled capsid[58–60]. Within the capsid, the genome is tightly packed, facilitated by the viral polypeptides VII, V and Mu (X), which constitute the major components of the nucleoprotein complex[37] and primarily function in DNA condensation[61]. The genome can be subdivided into four early (*E1-E4*) and five late (*L1-L5*) gene regions, termed according to the onset of gene transcription during early and late stages of the viral replication cycle[36]. Early genes mainly fulfill regulatory functions like host cell cycle manipulation and blockage of host cell apoptosis, initiate virus genome replication as well as viral gene transcription, and counteract the host immune defense. Late genes mainly encode for structural proteins involved in capsid assembly and maturation[36]. All viral genes are transcribed by the cellular ribonucleic acid (RNA) polymerase II and extensive alternative splicing results in a multitude of viral transcripts generated during the infection cycle[62]. A schematic illustration of the adenoviral genome is shown in figure 2.

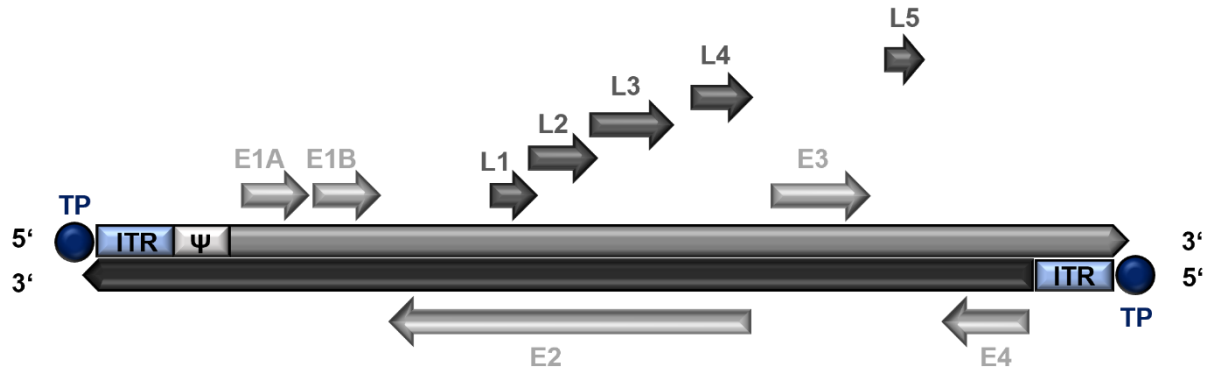

Figure 2: Schematic illustration of the adenoviral genome organization.
ITR: inverted terminal repeat; Ψ: packaging signal; TP: terminal protein; E: early genes; L: late genes.

2.3.4 Replication cycle

2.3.4.1 Cell infection

Human adenoviruses infect a broad range of different cell types, thus cause various diseases in humans ranging from mild infections of the upper respiratory tract to more severe outcomes like pneumonia, pharyngitis, or gastroenteritis[63].

The HAdV-5 replication cycle is initiated by the attachment of the virus particle to the host cell due to a high affinity binding between the fiber knob and its primary receptor CAR[64,65]. Other adenovirus types, however, also use different primary receptors like CD46, Desmoglein-2 or sialic acid[66]. Subsequently, secondary interaction between surface exposed Arg-Gly-Asp (RGD)-motif located within the penton base protein[43] and $\alpha_v\beta_{3/5}$ integrins at the cell surface initiates virus uptake via clathrin-mediated endocytosis, in which several GTPases like dynamin, Rac1, Rab5, Cdc42 and PI3K[67]are involved. During cellular uptake, the fiber is shed from the viral capsid[68] and subsequently the viral capsid becomes progressively disassembled[69]. The viral cysteine protease p23 activates polypeptide VI[70], which by means of an amphipathic helix induces membrane disruption of the early endosome[71–73] and thus mediates release of the virus particle into the cytoplasm. Upon successful escape from the endosome, cellular dynein binds to hexon[74] of the viral capsid and transports the subvirus particle to the nucleus along the microtubular network[74–77], facilitated by polypeptide VI[78]. Arriving at the nucleus, the viral capsid further disassembles and associates with the nuclear pore complex via interactions between hexon and the nucleoporin Nup214[79,80]. Subsequently, the adenoviral genome, together with the core protein VII[81,82], enters the nucleus via a Ran-dependent pathway, involving the CAN/Nup214 nuclear pore complex, histone H1 and the importin Transportin[80,83,84]. A schematic illustration of the adenovirus host cell entry is shown in figure 3.

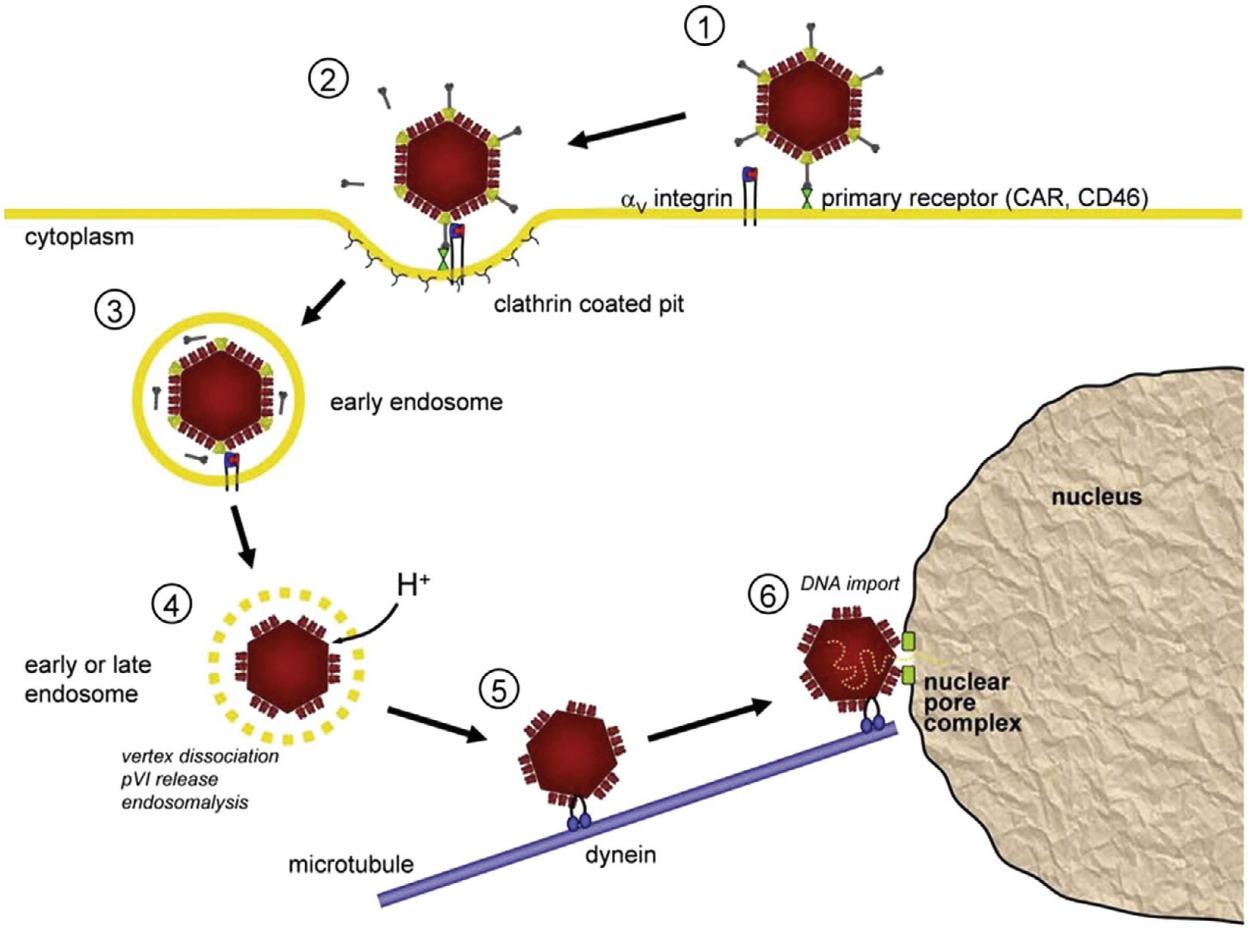

Figure 3: Schematic illustration about the adenovirus host cell entry with subsequent disassembly of the vector capsid in the early endosome, followed by escape of the subvirus particle into the cytosol and transport towards the nucleus along the microtubular network. (Knipe und Howley, Fields virology 2013, Figure 55.12).

2.3.4.2 Early phase

Once the viral genome has been delivered to the nucleus, early viral gene expression is initiated with E1A being the very first gene to be transcribed. Transcription of *E1A* is driven by the constitutively active *E1A* promotor[85], is initiated at ~1 h after host cell infection and is independent from other viral gene products. By alternative splicing of a common precursor mRNA, two *E1A* isoforms, the E1A 12s and 13S proteins with a respective size of 243 amino acids (aa) and 289 aa, are generated. As a major function, E1A proteins induce cell cycle progression into the S-Phase in quiescent cells resting within the G0/G1-Phase[86,87] thus providing favorable conditions for viral replication. Functionally, E1A releases the cellular transcription factor E2F from retinoblastoma protein (pRb), p107

and p130[85,88–91], which enables E2F to induce transcription of S-phase-related gene products. Free E2F also trans-activates the viral *E2* promotor[92] facilitated by the E4-17kDa protein[93], and thus stimulates E2 gene expression[94]. E1A-forced cell cycle entry, however, initiates p53-dependent cellular apoptotic pathways[95,96], which become counteracted by the *E1B* gene products[97]. Like *E1A*, alternative splicing of a common pre-cursor *E1B* mRNA results in the E1B proteins E1B19k and E1B55k[98], both of which prevent cellular apoptosis in a separate mode of action[97]. E1B55k directly binds to and inhibits the function of the tumor suppressor protein p53[97] while E1B19k is a homolog of the cellular anti-apoptotic Bcl-2 protein family[99,100] and mimics the induced myeloid leukemia cell differentiation protein 1[101]. E1B19k complexes with the pro-apoptotic Bcl-2 antagonist/killer (BAK)[101,102] and BAX[103,104] to prevent them to co-oligomerize at the outer mitochondrial membrane[105], which otherwise would result in the release of pro-apoptotic proteins into the cytoplasm[106,107]. Additionally to inducing cell cycle entry, E1A transactivates transcription of all other early genes (*E2-E4*)[85,108,109]. *E2* genes encode for the three viral proteins essential for virus DNA replication including the precursor terminal protein (pTP), the viral DNA-binding protein (DBP) and the adenoviral DNA polymerase[110]. *E3* gene products function within the viral immune evasion, inhibit TNF-α-mediated cellular apoptosis and promote release of viral progeny from the infected host cell[111]. Proteins encoded by *E4* mainly regulate mRNA splicing and thus viral gene expression but also modulate the cell cycle, cell signaling and DNA repair[112].

2.3.4.3 Late phase

After the onset of viral genome replication, late stages of the adenoviral replication cycle are initiated[113], characterized by a manifold upregulation of the viral major late promoter (MLP)[114]. The MLP drives transcription of a ~29 kbp precursor mRNA, the so-called major late transcription unit (MLTU)[115]. All late gene products (*L1-L5*) originate from the MLTU due to extensive alternative splicing. Late genes mainly encode for structural proteins like fiber, penton base and hexon, but also for proteins involved in capsid assembly, proper protein folding and nuclear transport. Assembly and maturation of viral progeny occurs within the nucleus[116]. After assembly, the viral genome becomes packed into the premature capsid[117] and via proteolytic cleavage of core and capsid precursor proteins by

the viral protease, the virion matures into an infectious particle[118]. A sophisticated interplay between various viral proteins[119] as well as accumulation of viral particles and permeabilization of the nuclear membrane, facilitated by the adenoviral death protein (ADP)[120], finally results in host cell lysis and release of viral progeny into the extracellular space. Altogether, the accomplishment of the adenoviral replication cycle requires ~48 h from initial host cell infection[121].

2.4 Adenoviral vectors as gene transfer vehicles

Based on decades of intense scientific research, gene therapy nowadays greatly benefits from adenoviral vectors as gene transfer vehicles in a variety of gene therapeutic attempts[122–124]. Especially the detailed understanding of the adenovirus replication cycle allowed for the generation of highly efficient “gene shuttles” based on replication-deficient HAdV-5 vectors. HAdV-5 vectors transduce their target cell with high efficiency, however, due to deletion of viral genes essential for virus replication, they do not enter a productive replication cycle. Production of such vectors requires cellular systems which trans-complement lacking viral genes essential for vector amplification. Over the years, various vector systems have been developed referred to as 1st, 2nd and 3rd generation vectors, each of which exhibiting specific characteristics required for different gene therapeutic approaches[125].

2.4.1 First generation vectors

Adenoviral vectors of the first generation are characterized by deletion of the *E1* gene region (ΔE1), optionally lacking additionally *E3* (ΔE3). As already described previously, *E1* gene products drive cell cycle progression, initiate transcription of other viral genes, and block cellular apoptosis, thus are essential for virus replication. Deletion of *E1* consequently results in replication-deficient vector particles whose production necessitates *E1* trans-complementing cell systems such as HEK293T[126], N52.E6[127] or PER.C6[128] cells. *E3* gene products mainly counteract cellular immune responses[111,129], are not essential for virus replication *in vitro* and thus do not require any trans-complementation for vector production. The deletion of *E1* and *E3* further allows for the insertion of transgenes up to a size of ~8 kbp. Such 1st generation vectors are often used in basic research for the evaluation of HAdV-5 based gene transfer efficiencies or

investigation of vector tropism and biodistribution by inserting reporter genes such as the (enhanced) green fluorescence protein[130] (eGFP), nano luciferase (NLuc)[131] or firefly luciferase (FFLuc)[132]. Since 1st generation vectors display leaky viral gene expression mediated by cellular factors[133], which renders them highly immunogenic, such vectors are also often used for genetic vaccination[134].

2.4.2 Second generation vectors

Like 1st generation vectors, 2nd generation vectors display deletions of *E1* and optionally *E3*, however, additionally lack (parts of) *E2* and/or *E4*. This reduction of viral genes further reduces their immunogenicity and thus provides prolonged transgene expression levels of 2nd generation vectors[135–138]. Deletion of *E2* and *E4* additionally expands the genomic capacity for the insertion of larger transgenes compared to 1st generation vectors.

2.4.3 Third generation vectors

Adenoviral vectors of the 3rd generation are the most advanced adenoviral vector platform so far and are characterized by the deletion of all viral genes except of the genome-flanking ITRs and the packaging signal Ψ[139,140]. Such vectors provide a high genomic capacity for the insertion of transgenes up to a size of 36 kbp and thus are also referred to as “high-capacity” or “gutless” vectors[140]. However, production of 3rd generation vectors is complex and requires a more sophisticated production system consisting of a helper virus (HV) and an E1-transcomplementing cell line, expressing *cre*-recombinase[141]. The HV, mostly an *E1*-deleted vector, trans-complements for all regulatory and structural viral genes essential for virus replication except of *E1*. The packaging signal located within the HV genome is flanked by *loxP* sites and thus becomes excised by the cellular encoded *cre*-recombinase during vector amplification. Excision of the packaging signal prevents incorporation of HV genomes into newly assembled capsids, while the packaging signal-carrying genome of the 3rd generation vector gets incorporated[141]. Due to steady improvement of this production system, third generation vectors can be produced with minimal HV virus contamination between 0.01-0.02%[142]. Due to lack of viral genes, 3rd generation vectors exhibit substantially low immunogenicity, thus enabling long lasting gene expression and are therefore preferentially used in gene therapeutic approaches requiring long term transgene expression[140].

2.5 Oncolytic adenoviral vectors

Beside their use as classic gene transfer vehicles, adenoviruses are also used in the field of oncolytic virotherapy[143,144]. Different to adenoviral vectors of the 1st, 2nd, and 3rd generation, oncolytic adenoviral vectors (oAVs) retain almost all viral genes and thus remain replication competent. However, they significantly differ from their wild-type counterpart in selectively replicating within cancer cells, but not in healthy cells. Therefore, they are termed 'conditionally replicating' and the respective vectors are referred to as "conditionally replicating adenoviral vectors (CRAds)". There are two major attempts how to turn an adenovirus in a CRAd, which will be introduced in the following section.

2.5.1 Tumor-specific promotors

One strategy to restrict viral replication to cancer cells is the use of tumor-specific promoters to control viral gene expression. One example of such promoters is the human telomerase reverse transcriptase (hTERT) promoter, which is silent in most non-proliferating cells, however, highly active in tumor cells and was used by Kim *et al.* to generate a CRAd with *E1A* expression driven by a modified hTERT promoter (m-hTERT)[145]. A comparable attempt has been conducted by Lee *et al.*, who regulated the adenoviral *E1A* expression by the enhancer element PSME. PSME controls the expression of the prostate-specific membrane antigen (PSMA)[146], which is highly prevalent in prostate cancer[147] and the resulting CRAd replicated selectively in PSMA-positive cells[146]. By using cancer cell type specific promoters, virus replication can be even tighter regulated and restricted to certain cancer types. The surfactant protein B (SPB) promoter i.e. is solely active within adult type II alveolar and bronchial epithelial cells. Doronin *et al.* replaced the adenoviral *E4* promoter by the promoter for SPB and together with some other genetic modification, replication of the resulting CRAd was consequently restricted to lung epithelial cancer cells only[148]. As demonstrated by the given examples, regulation of viral gene expression by tumor specific promotors provides a suitable tool for the generation of CRAds.

2.5.2 Manipulation of adenoviral early genes

Beside regulation of viral gene expression using tumor-specific promoters, cancer cell-selective replication of oAVs can be likewise achieved by genetic modifications of viral genes that manipulate the host cell.

One of such genes is the adenoviral immediate early gene *E1A*. As already described above, *E1A* promotes cell cycle progression into the S-phase and initiates expression of other viral genes essential for virus replication. The E1A protein displays two conserved regions (CR), CR1 and CR2, whereof CR1 directly competes with the transcription factor E2F for the binding to pRb, while CR2 stably complexes with E2F[90]. Due to these interactions, the transcription factor E2F becomes displaced from pRb and set free, resulting in the S-phase entry of the cell. Deletion of a 24 bp stretch in CR1 affecting amino acids 121 to 128 of the E1A polypeptide (E1AΔ24bp) results in a dysfunctional E1A protein unable to bind pRb[149]. Since cancer cells continuously proliferate, often including a dysregulated pRb pathway[150], Fueyo *et al.* rationally designed an E1AΔ24bp mutant adenovirus, which consequently exhibited cancer cell specific replication[151].

Another viral gene that can be mutated to render adenoviruses conditionally replicating is *E1B19k*. In a previous section, it has been introduced that E1B19k counteracts apoptosis by binding to the pro-apoptotic protein BAK. Consequently, adenoviral vectors deleted in *E1B19k* (ΔE1B19k) are unable to block BAK-related apoptotic pathway, which results in apoptosis of the infected cell prior to productive virus replication. As apoptotic pathways are already efficiently suppressed in cancer cells[152], ΔE1B19k vectors can efficiently replicate within such mutated cells yet not in healthy cells. In addition to cancer cell selective replication, E1B19k-deleted CRAds have been shown to exhibit accelerated replication and spread[153–156], indicating that deletion of E1B19k additionally improves their anti-tumor efficacy.

Genetic modifications affecting viral genes involved in the viral immune evasion can be likewise applied to generate CRAds. Here, particularly the E3gp19k protein is of great interest since it retains major histocompatibility complex class I (MHC-I) proteins within the endoplasmic reticulum[157–159]. MHC-I proteins bind and present antigens at the cell surface where they become recognized by cytotoxic T-cells[160]. CRAds harboring a non-functional or even deleted *E3gp19k* gene (ΔE3gp19k) are consequently unable to prevent

MHC-I-mediated presentation of viral antigens, thus rendering the infected cell susceptible to cytotoxic T-cells[161]. Most cancer cells, however, efficiently downregulate MHC-I expression[162], rendering E3gp19k function negligible for virus replication. Thus, E3gp19k-deleted viruses can properly replicate in cancer but not in healthy cells.

2.6 Barriers for oAVs

Oncolytic adenoviral vectors are preferentially administered either locally or systemically via intratumoral (i.t.) or intravenous (i.v.) vector injection. Even though i.t. injection ensures virus delivery to the tumor tissue, the feasibility of this application route greatly depends on the accessibility of the tumor and intratumoral virus spread has been shown to be rather poor[163]. In contrast, i.v. injection facilitates a more even virus distribution throughout the tumor and may also allow to address for potentially emerging metastasis. However, not only but particularly upon i.v. injection, oAVs are subjected to a variety of biological barriers, hampering the delivery of viral particles to the tumor and thus their anti-tumor efficacy. Beside poor tumor transduction efficiencies of oAVs per se, such barriers likewise include both cellular as well as non-cellular off-target interactions, which result in rapid vector particle sequestration and neutralization as schematically represented in figure 4.

2.6.1 Innate and adaptive immune system

HAdV-5-based vectors become rapidly cleared due to various sequestration mechanisms, including innate and adaptive immune responses[164]. While macrophages of the splenic marginal zone[165] have been reported as a source of particle consumption, the majority of vector particles become sequestered by the highly abundant liver residential Kupffer cells (KCs)[50], which account for up to 90% of all macrophages present in the body[166]. Uptake of adenoviral particles by KCs is independent from CAR[167–169] and mainly mediated by scavenger receptor A[170], which recognizes negatively charged molecules[171]. Furthermore, natural antibodies and components of the complement likewise contribute to KC uptake[172] and there is indication that blood coagulation factor IX is also involved[173]. Upon vector phagocytosis, KCs undergo rapid cell death[174], which is amongst others causative for vector-induced toxicity due to the secretion of pro-inflammatory cytokines[175,176]. Additionally to cellular sequestration mechanisms, naturally occurring IgM antibodies and components of the complement bind and opsonize the vector capsid upon entry into the

blood stream[177,178]. Furthermore, the interaction of vector particles with IgMs or Ad specific IgGs in combination with components of the complement mediates binding of particles to erythrocytes via complement receptor 1 (CR-1)[179]. A particularly high seroprevalence against HAdV-5 vectors in the human population[180] represents another major barrier for HAdV-5-based oAVs. HAdV-5-specific IgG antibodies and T-cells, originating from previous HAdV-5 exposure, efficiently recognize and eradicate vector particles[181].

2.6.2 Immune-independent sequestration mechanisms

Beside vector sequestration and neutralization by the innate and adaptive immune system, efficient tumor transduction by HAdV-5 based oAVs is further hampered by off-target cellular interactions.

In addition to the above-mentioned IgM- and complement-mediated particle binding to erythrocytes via CR-1, HAdV-5 likewise binds to human erythrocytes in a CAR-dependent manner[179]. Although erythrocyte binding prolongs the vector blood half-life, cell-bound vector particles become trapped[182], thus unable to transduce their target tissue. However, since only erythrocytes of humans but not those of mice express CAR and CR-1[179], erythrocyte binding is negligible in the murine context.

Another major sink of HAdV-5 is its inherent liver tropism[183]. Those vector particles that evade neutralization and sequestration by KCs, efficiently transduce hepatocytes in a CAR- and integrin-independent manner[167,169,184,185]. Even though a putative heparan sulfate glycosaminoglycan-binding site located within the fiber shaft has been suggested to be at least involved[186,187], blood coagulation factor X (FX) reflects a main mediator of hepatocyte transduction[49,173,188]. Via its N-terminal gamma-carboxyglutamic acid (Gla)-domain, FX binds to HVRs of hexon and bridges vector particles to cell surface-located heparan sulfate proteoglycans (HSPGs)[188,189], leading to hepatocyte transduction[49]. Here, especially N- or O-sulfated HSPGs appear to be substantially involved in the FX-mediated hepatocyte transduction[188]. The pronounced liver tropism of HAdV-5 based vectors is accompanied by severe hepatotoxicity due to tissue damage[190]. As the liver represents the main source for the synthesis of coagulation factors[191], vector-induced hepatocyte death may result in dysregulated coagulation homeostasis[192] as well as inflammatory responses[193], which may contribute to systemic vector toxicity[175,194,195]. To circumvent FX-mediated liver transduction, Alba *et al.* generated an FX binding-ablated HAdV-5

vector, with reduced hepatocyte transduction *in vivo*[48,196]. However, subsequent work by Xu *et al*. identified FX as an efficient shield from natural IgM antibodies[177] and ablation of FX binding results in an augmented IgM-mediated vector neutralization[177]. Thus, even though binding of FX to the viral capsid contributes to vector toxicity and particle sequestration by hepatocyte transduction, it likewise enables evasion from natural IgMs.

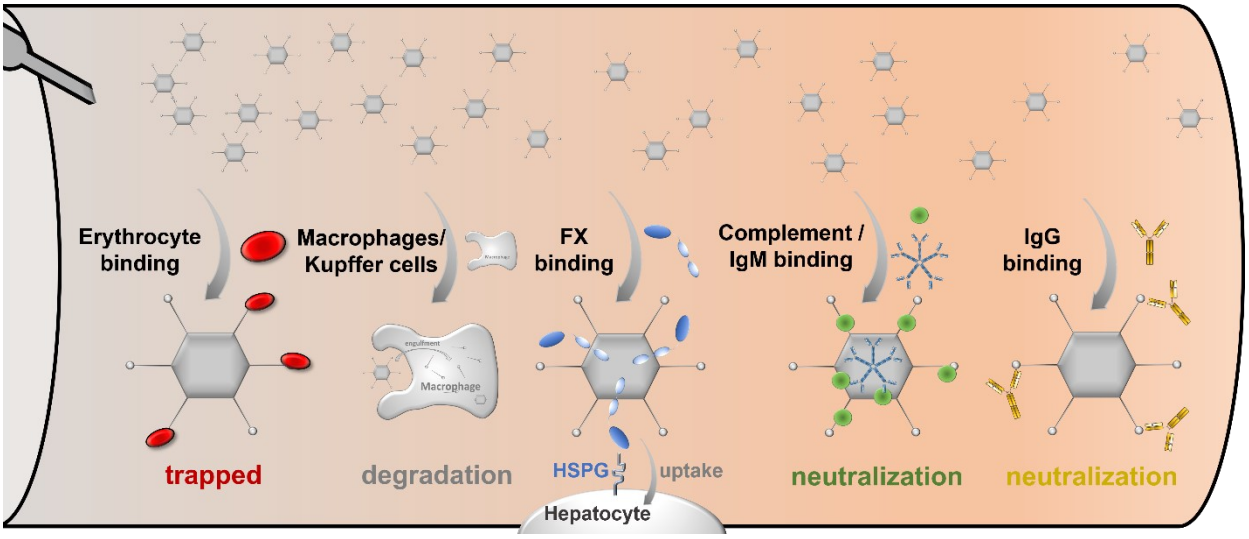

Figure 4: Mechanisms that mediate sequestration and neutralization of HAdV-5-based oAVs.
Binding to erythrocytes traps and renders vector particles non-infectious. Sequestration by macrophages and liver residential Kupffer cells rapidly deprive vector particles from the blood stream. Binding of blood coagulation factor X bridges vector particles towards HSPGs and mediates hepatocyte transduction. In absence of FX-binding, components of the innate immune system including the complement and IgM antibodies bind and neutralize vector particles. Vector-specific IgG antibodies efficiently bind and neutralize vector particles. HSPG: Heparan Sulfate Proteoglycan; IgM: Immunoglobulin M; IgG: Immunoglobulin G.

2.6.3 Inefficient tumor transduction

Vector particles that evaded sequestration are available for tumor transduction. However, efficient tumor tissue infiltration is hampered by various physical barriers[197,198]. A dense tumor stroma surrounding the malignant cell, mainly composed out of non-permissive fibroblasts, tumor vessels, immune cells and extracellular matrix components may generate a physical barrier that limits the anti-tumor efficacy of oncolytic adenoviral vectors[199]. Furthermore, various cancer types show downregulated or even complete

absent expression of the primary adenovirus receptor CAR[200–203], which aggravates successful tumor transduction by HAdV-5-based oAVs. Within solid tumors, lack of lymphatic vessels and hyperpermeability of the tumor vasculature additionally results in interstitial hypertension[204], leading to impaired vessel extravasation of molecules[205] and thus limited tumor infiltration of systemically administered vector particles. Furthermore, intratumoral virus spread has been shown to be severely limited due to tumor stroma components[163].

2.7 Strategies to enhance the therapeutic efficacy of oAVs

To improve the therapeutic efficacy of oncolytic adenoviral vectors, the above-mentioned barriers have to be overcome. To this end, various techniques to circumvent vector sequestration and neutralization but also to improve tumor transduction efficiencies have been applied in order to increase the safety and efficacy of HAdV-5-based oAVs.

2.7.1 Avoiding vector sequestration

One important aspect in the development of oAVs is the improvement of the vector blood half-life after i.v. injection. First, off-target binding of vector particles due to binding to CAR has to be avoided, which can be achieved by a single point mutation affecting the fiber knob domain by which tyrosine at position 477 becomes exchanged for Alanin (Y477A)[206]. Additionally, the profound liver tropism of HAdV-5-based vectors has to be reduced since it reflects the main source of vector particle consumption and the main cause of vector-induced toxicity. This requires both avoiding uptake of particles by KCs and preventing hepatocyte transduction. A simple but efficient strategy to bypass KC uptake is transient KC depletion prior to vector administration[176,207–210], which results in improved vector pharmacokinetics[50,211]. However, KC depletion also augments hepatocyte transduction[208,212], thus increases the risk for liver damage. As already mentioned, KC uptake is mediated by scavenger receptors that recognize negatively charged molecules like HAdV-5 particles. Weaver *et al.* identified HAdV-6, another species C adenovirus[34], to exhibit superior liver transduction efficiencies over HAdV-5, indicating less Kupffer cell uptake and suggested less negatively charged HVRs of HAdV-6 as a reason[213]. Based on these findings, Khare *et al.* generated a HAdV-5/6 chimeric vector by substituting exposed HVR regions of the HAdV-5 capsid by those of HAdV-6. The resulting vector

indeed showed less KC uptake, however, >10 times stronger liver transduction *in vivo*[214]. Since FX represents the main mediator for hepatocyte transduction by HAdV-5-based vectors, Alba *et al.* generated an FX binding-ablated vector by defined capsid mutagenesis[48]. Although the resulting vector exhibited significantly reduced liver transduction after systemic administration[196], subsequent studies identified FX to efficiently shield vector particles from IgM antibodies and the complement[177], rendering FX binding-ablated vectors highly susceptible to neutralization by the innate immune system. Thus, further strategies have been developed to avoid vector neutralization while ablating FX binding to the vector capsid, such as coating of vector particles with immunologically inert polymers. Vector decoration with polyethylene glycol (PEG), N-(2-Hydroxypropyl) methacrylamide (HPMA) or cationic poly(amidoamine) (PAMAM) dendrimers i.e. has been shown to protect vector particles from neutralization[215–217], ablate vector binding to FX and erythrocytes[218], dampen activation of the complement[219,220], reduce vector toxicity[221,222], extend vector plasma circulation[221] and diminish KC uptake[223]. However, such polymer coating is usually realized by either charge- or amine directed attachment of polymers to the vector capsid. As HAdV-5 is highly charged and comprise about 18.000 surface exposed amine groups, such polymer coating results in rather densely packed vector particles, which may negatively interfere with the vector infectivity[215]. To overcome this limitation, Kreppel *et al.* combined both genetic and chemical (geneti-chemical) capsid modification to enable site-specific attachment of protein and non-protein ligands to the vector capsid[224]. They genetically introduced cysteines in solvent-exposed areas of the vector capsid and the thiol groups of these cysteines were used for the covalent coupling of shielding moieties to the vector capsid in a position-specific manner[224–228]. Contrary to the above-mentioned, non-specific polymer coating based on stoichiometric ratios, geneti-chemical capsid modification allows for a more defined shielding density as it is defined by the amount of surface exposed cysteines on the vector capsid. Using this technique, Krutzke *et al.* substituted the shielding capacity of FX by position-specific attachment of PEG moieties to HVR1 of hexon[227]. This HVR1-specific capsid PEGylation prevented binding of FX to the vector capsid, however, likewise protected vector particles from neutralization by murine natural antibodies and the complement and significantly improved vector pharmacokinetics *in vivo*[227].

2.7.2 Improving tumor transduction

Avoiding vector sequestration renders vector particles available for tumor transduction, which is a necessity to harness the full potential of oncolytic virotherapy. Many tumors, however, downregulate or lack sufficient expression of the HAdV-5 primary receptor CAR[200–203] and furthermore, as mentioned before, CAR-binding ablation is mandatory to prevent vector sequestration by human erythrocytes. Thus, different strategies have been developed to address alternative and tumor-specific target receptors. Such vector retargeting can be accomplished by various different strategies[224,229,230], which are schematically illustrated in figure 5.

A first suitable retargeting strategy is (i) the generation of chimeric vectors. Different adenovirus types utilize distinct primary receptors like CD46, desmoglein 2 (DSG-2), CD80, CD86 or sialic acid (SA) for primary host cell attachement[66,231]. Based on this knowledge, various fiber chimeric vectors have been generated by substitution of the HAdV-5 fiber(-knob) by those of other adenovirus types like HAdV-3[232–235], HAdV-7[236], HAdV-11[232,237] or HAdV-35[232,234,237]. Even though this technique is suitable, the tropism of such chimeric vectors remains limited to the repertoire of primary receptors utilized by the respective adenovirus types. Furthermore, most of the adenovirus primary receptors are expressed by a variety of different cell types and thus provide only limited tumor specificity. To circumvent this limitation, (ii) genetic insertion of small peptide sequences into vector capsid proteins has been applied to shift the vector tropism towards novel and more tumor-specific target receptors. Small peptides have been inserted into HVRs of hexon[238], the minor capsid protein IX (IX)[239] or the fiber[240]. Examples for rather unspecific peptide sequences that have been introduced in the viral capsid are the integrin binding RGD-motif[241–244] or poly-lysine motifs[245]. Examples for more target specific peptides that have been successfully introduced to enable vector retargeting towards defined receptors are peptides that bind to the epidermal growth factor receptor (EGFR)[246], HER3/ErbB3- and HER4/ErbB4[247], human transferrin receptor (hTfR)[248] or heparan sulfate containing receptors[245,249]. Although peptide insertion appears promising, it is subjected to restrictions since peptides exceeding a critical size destabilize the vector capsid and thus result in growth-defective vector particles. Furthermore, many tumor-specific targeting ligands do not fold properly upon the incorporation in adenoviral capsid proteins and thus

lose their ability to bind to the respective target receptor[250]. As an alternative, (iii) bispecific adapter molecules provide a suitable tool to alter the adenoviral tropism while maintaining vector capsid integrity[229,251]. Such retargeting molecules consist of two domains by which one of each binds the vector capsid and the other to a tumor-specific target molecule, thus bridging the vector towards alternative target receptors. As a first bispecific adapter molecule, Douglas *et al.* generated in 1996 a conjugate between a neutralizing anti-fiber Fab fragment and folate. This adapter efficiently retargeted adenoviral vectors towards the folate receptor[252]. Since then, a variety of bispecific adapter molecules have been generated to retarget adenoviral vectors towards various targets like the EGFR[253–257], endoglin (CD105)[258], α_v-integrins[259], CD40[260], fibroblast growth factor receptor 2 (FGF2)[261], or epithelial cell adhesion molecule (EpCAM)[262]. Thus, bispecific adapter molecules represent a flexible method for vector retargeting. However, a major disadvantage of this technique is the non-covalent binding of the adapter to the vector capsid, which poses the risk for adapter displacement *in vivo*. Hence, (iv) covalent linkage of targeting ligands to the vector capsid would be beneficial and has been realized using the above-mentioned geneti-chemical capsid modification[224]. By this technique, targeting ligands of the transferrin receptor[224,225], the LDL receptor-related protein receptor (LRP)[226], or the EGFR[228] have been successfully coupled to either hexon[224,225,228], pIX[226] or fiber[228] of the vector capsid. However, there is also evidence that covalent coupling of targeting ligands may interfere with intracellular trafficking pathways and thus impair vector infectivity[226,228].

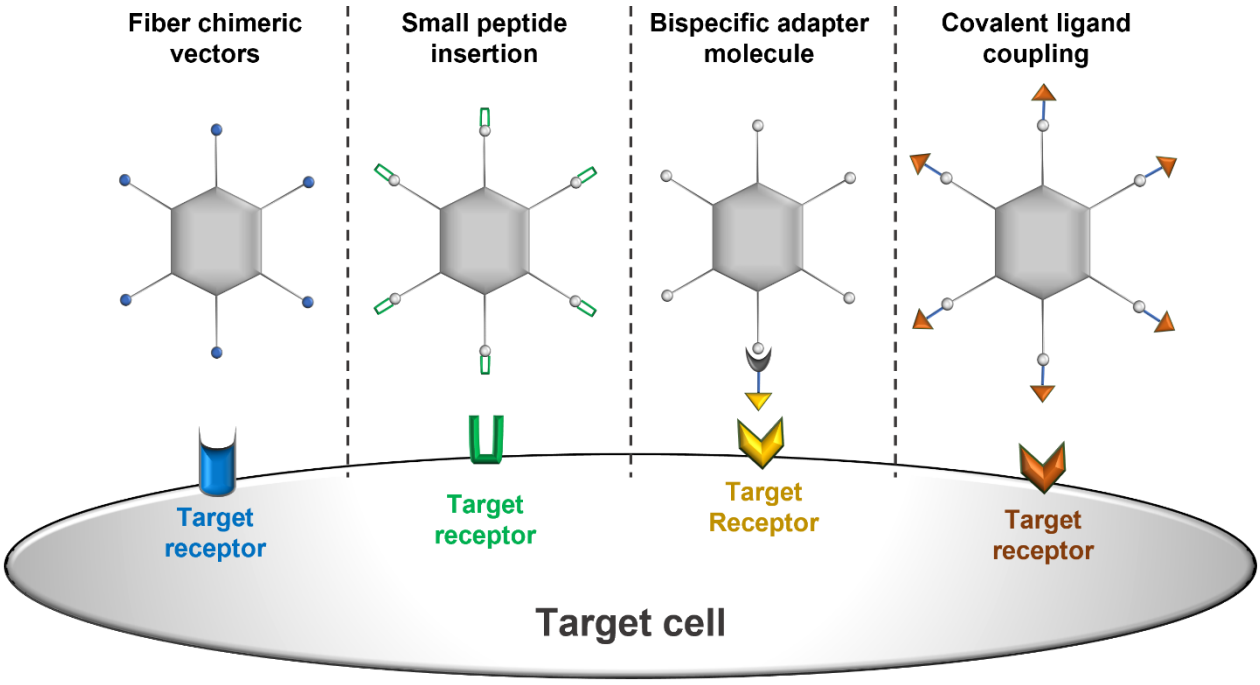

Figure 5: Overview about fiber modification strategies for the retargeting of oAVs.
Left: Chimeric vector with substitution of the fiber-knob from other adenovirus types. Mid left: Genetic insertion of small peptides into the fiber-knob with affinity to the target receptor. Mid right: Bispecific adapter molecule as a bridge between the vector capsid and the target receptor. Right: Covalent ligand coupling by geneti-chemical fiber modification.

2.8 Promising targets for oncolytic virotherapy

There is a manifold of different retargeting strategies and possible-to-address target receptors to improve tumor transduction by oAVs. As the present study focuses on the development of oAVs for the treatment of head and neck squamous cell carcinomas (HNSCC), the epidermal growth factor receptor (EGFR) as well as the fibroblast activation protein (FAP) have been selected as promising targets and will be described in more detail within the following sections.

2.8.1 The epidermal growth factor receptor (EGFR)

Carcinomas of the head and neck arise from malignant transformed epithelial cells of the upper respiratory tract including the oral cavity, pharynx and larynx[263]. Annually, HNSCC accounts for more than 660,000 new cases of cancerous malignancies and 325,000 deaths worldwide, showing steadily increasing incidence[264]. Tobacco consumption[265], alcohol abuse[266] or infection with high risk human papillomavirus (HPV)[267] represent the most relevant risk factors for HNSCC. Once established, HNSCC is an aggressive type of cancer and difficult to treat by conventional treatment strategies such as surgery, chemo- and/or radiotherapy[268]. HNSCC is often accompanied with overexpression of EGFR[269], rendering it an attractive target receptor for HAdV-5-based oncolytic virotherapy. EGFR, also referred to as ErbB-1/Her1, is a transmembrane receptor and belongs to the ErbB receptor family. It consists of a 621 aa extracellular domain, a single 23 aa transmembrane domain and a 542 residue cytoplasmic domain with intrinsic tyrosine kinase activity.[270] Seven binding ligands of EGFR have been identified so far, all of which activate the receptor by binding to its extracellular domain[271]. Upon ligand binding, the EGFR monomer undergoes conformational changes[272] and dimerizes[273–275]. As a consequence, its intracellular tyrosine kinase domains move into spatial proximity[275] and become stimulated, which results in an autophosphorylation of multiple tyrosine residues within the C-terminus of the intracellular EGFR domain[276]. This autophosphorylation initiates intracellular signaling cascades like the RAS-RAF-MEK-ERK MAPK or PI3K-AKT-mTOR pathway, which drive G1/S cell cycle progression and thus cell proliferation[270]. In healthy cells, EGFR activity underlies tight regulation, while cancer cells often display aberrant EGFR activity by either receptor overexpression[277] and/or mutation[278], which consequently results in tumor progression[270] and is tightly linked to poor prognosis[279]. Due to its central role in tumorigenesis and cancer progression, EGFR has become a major target for the development of different anti-cancer therapies[280] such as monoclonal antibodies[281], antibody-drug conjugates[282] or small molecule kinase inhibitors[283]. EGFR-targeted oAVs may provide an efficient treatment strategy for EGFR-positive cancer types like HNSCC.

2.8.2 The fibroblast activation protein (FAP)

Most anti-cancer therapies address the malignant tumor cell. However, solid tumors do not only consist of cancer cells, but also of various other cell types and extracellular matrix components, building up the so-called tumor stroma, which contributes for up to 90% of the total tumor mass[284]. Within the tumor stroma, cancer-associated fibroblasts (CAFs) reflect the most abundant cell type and thus reflect a major cellular constituent of solid tumors[285]. CAFs substantially contribute to tumor progression by secreting growth factors, drive angiogenesis, promote tumor cell invasion and are further linked to drug resistances[285–287]. A prominent characteristic of CAFs is their high expression of the fibroblast activation protein (FAP)[288], which is, with few exceptions[289], almost absent in healthy cells and tissues. FAP is a cell surface located serine protease[290] and belongs to the dipeptidyl peptidase (DPP) family[291]. Structurally, it consist of a large extracellular domain of 734 aa, followed by a single 20 aa transmembrane domain and a short cytoplasmic tail with a size of 6 aa[292]. FAP shares ~50% sequence homology with the ubiquitously expressed dipeptidyl peptidase 4 (DPPIV)[293], another member of the DPP family with which it can form non-covalent heterodimers[294]. However, FAP is proteolytically active only as a glycosylated homodimer[292,295], exhibits collagenolytic activity[290] and is mainly involved within tissue remodeling processes like wound healing or fibrosis[296] but also contributes to embryogenesis[297]. In cancer, FAP is a pro-tumorigenic marker and high FAP expression is associated with poor patient prognosis[296]. Depletion of FAP-expressing CAFs within the tumor stroma thus may have multifaceted benefits for anti-cancer therapies as it could significantly deplete and disrupt the solid tumor, reduce growth factor secretion, inhibit angiogenesis, and may improve the response to other anti-cancer therapies. Thus, due to its specific expression by CAFs, FAP has been suggested as an attractive target for oncolytic virotherapy.

2.9 Aim of the study

Human adenovirus type 5 (HAdV-5)-based oncolytic virotherapy holds promise as efficient anti-cancer therapy. Beside a direct virus-induced cancer cell lysis, the resultant release of tumor-associated antigens stimulates anti-tumor immune responses that additionally support tumor depletion. Systemic vector administration reflects the preferred application route since it allows for improved intratumoral virus distribution and simultaneous addressing of metastases. However, various biological barriers limit efficient tumor cell infection and therewith the anti-tumor efficacy of HAdV-5-based oncolytic vectors. Such barriers include both cellular as well as non-cellular interactions, leading to a dose-limiting vector-induced toxicity and insufficient tumor targeting.

The present study aimed to develop and characterize HAdV-5-based oncolytic vectors that address both improved tumor targeting and reduced toxicity. HAdV-5-based vectors with an epidermal growth factor receptor (EGFR) affinity ligand covalently coupled to either the fiber or hexon protein of the vector capsid were hypothesized to exhibit improved tumor targeting in EGFR-positive tumors and thus will be characterized regarding their oncolytic potential *in vitro* and *in vivo*. With the aim to target cancer-associated fibroblasts (CAFs), which are located in the tumor stroma and thus another promising target for oncolytic virotherapy, a bispecific adapter molecule should be designed that bridges the adenoviral fiber protein to the CAF-specific fibroblast activation protein (FAP) and its re-targeting capacity will be analyzed *in vitro*.

To reduce vector toxicity, a set of conditionally replicating adenoviral vectors (CRAds), carrying different genetic life-cycle modifications suggested to restrict vector replication to tumor cells were to be generated and characterized *in vitro*. Since especially the negative surface charge of HAdV-5 significantly contributes to particle sequestration and vector-induced toxicity, an already existing, surface charge-modified mutant HAdV-5 vector (HexPos3) was hypothesized to exhibit less toxicity and improved tumor targeting and thus planned to become characterized *in vivo* regarding its oncolytic potential. Finally, the most promising vector modifications identified were intended for combination to generate a novel HAdV-5 oncolytic vector with improved anti-tumor efficacy and safety.

3 Materials

3.1 Animals

BALB/c mice were received from Charles River (strain code: 028) and NOD-*scid* *IL2*Rgamma^{null} (NSG) mice (Jackson Laboratory strain #005557) were received from the "Tierforschungszentrum" at Ulm University. While BALB/c mice are immune-competent, NSG mice are severely immune-deficient and thus allow for the engraftment of human tumor xenograft models. The *scid* background eliminates adaptive immunity due to depletion of mature B- and T-cells[298] caused by mutation of the *Prkdc* gene[299,300]. *IL2rg*^{null} comprises a complete null mutation of the *IL2rg* gene, which results in the absence of the interleukin 2 receptor gamma chain (ILR2γ) and thus blocks differentiation of hematopoietic stem cells and natural killer (NK) cells[301]. Mice were kept under ventilated, pathogen-free conditions and were fed with sterilized diet for laboratory rodents. All animal experiments were performed according to the policies and procedures of the institutional guidelines and were approved by the Animal Care Commission of the Government Baden-Württemberg (TVA #1358, #1433).

3.2 Antibiotics

Name	Order Number	Supplier
Ampicillin	K029.1	Roth, Karlsruhe, Germany
Chloramphenicol	A1806	AppliChem, Darmstadt, Germany
Kanamycin	I832.1	Roth, Karlsruhe, Germany
Streptomycin	A1852	AppliChem, Darmstadt, Germany
Tetracycline	A2228	AppliChem, Darmstadt, Germany

3.3 Antibodies

3.3.1 Primary antibodies and Affilin

Name	Order Number	Supplier
mouse α-Fibroblast-Activation-Protein (FC)	BMS 168	ThermoFischer, Rockford, USA
mouse α-human EGF-receptor (FC)	55996	BD Bioscience, Eysins, Switzerland
mouse α-human EGF-receptor (IHC)	MA5–13070	ThermoFischer, Rockford, USA
rat α-mouse CD31 (IHC)	557355	BD Bioscience, Eysins, Switzerland
mouse α-FLAG-M2 (FC, WB, ELISA)	F1804	ThermoFischer, Rockford, USA
Strep-tagged Affilin (α-EGFR)	139819	Navigo Proteins GmbH, Halle, Germany
rabbit α-Strep-Tag	A00626	GenScript, Piscataway Township, New Jersey, United States

3.3.2 Secondary antibodies

Name	Order Number	Supplier
sheep α-mouse-IgG (whole molecule)-FITC	F6257-1ml	ThermoScientific, Rockford, USA
rabbit α-mouse-IgG (whole molecule)-horseradish peroxidase	A9044-2ml	Sigma Aldrich, St. Louis, MO, USA
goat α-rat IgG (H+L) Alexa488	A-11006	Invitrogen, Waltham, Massachusetts, United States

Name	Order Number	Supplier
goat α-mouse-IgG-Alexa594	#A11032	Invitrogen, Waltham, Massachusetts, United States
goat α-rabbit-IgG-Alexa594	#A11037	Invitrogen, Waltham, Massachusetts, United States

3.4 Bacteria

Name	Order Number	Supplier
NEB® 10-beta competent *E.coli*	C3019H	New England BioLabs, Ipswich, MA, USA

3.5 Bacmids

3.5.1 pBeloBacGS66

The HAdV-5 genome was cloned into the pBeloBacGS66 bacmid by *Swa*I digestion[127]. A schematic illustration of the bacmid with the *Swa*I cleavage sites and positions of mutations and transgenes introduced in the present study (see 3.13) is shown in figure 6.

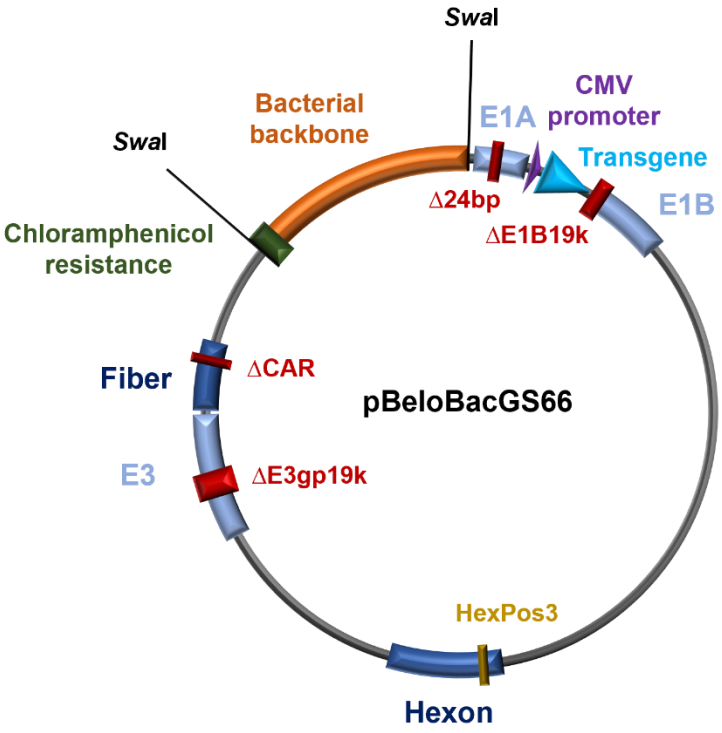

Figure 6: Schematic illustration of the organization of pBeloBacGS66.
Approximate positions of the bacterial backbone harboring the chloramphenicol resistance, *Swa*I restriction sites, the viral genes encoding for E1A, E1B, E3, Hexon and Fiber as well as the CMV promotor and the position of the introduced transgene. Red bars indicate the position of the respective mutations introduced in the present study. The yellow bar represents the position of the HexPos3 mutation.

3.6 Buffers and solutions

Purpose	Name	Composition
Agarose Gel-electrophoresis	DNA loading buffer (10x)	0.25 g Bromphenol blue 12.5 g Glycerol 6 mM EDTA
	TBE-buffer (10x)	225 mM Tris 225 mM Boric Acid 5 mM EDTA
	TAE-buffer (10x)	400 mM Tris 200 mM Acetic Acid 10 mM EDTA
Bacteria cultivation	LB-medium	20 g/l LB dissolved in dH_2O autoclaved
Bacteria lysis	TELT-buffer	50 mM Tris (pH 7.5) 62.5 mM EDTA 2.5 M LiCl 0.4 % Triton X-100
DNA storage	TE-buffer	10 mM Tris 1 mM EDTA pH 8.5
	Tris-Buffer	10 mM Tris pH 8.0
ELISA	Coating-buffer	0.2 M sodium carbonate-bicarbonate, pH 9.6
	Washing-buffer / Sample dilution buffer	DPBS 0.05% Tween20

Purpose	Name	Composition
Flow Cytometry	Flow Cytometry-buffer	DPBS 10 mM EDTA 2% FBS
HAdV-5 vector purification	HEPES-buffer	150 mM / 250 mM NaCl 50 mM HEPES pH 7.4 sterile filtrated (0.2 µm filter)
	CsCl-buffer 1 (1.41 g/ml)	150 mM NaCl 50 mM HEPES 548.5 mg/ml CsCl pH 7.4 sterile filtrated (0.2 µm filter)
	CsCl-buffer 2 (1.27 g/ml)	150 mM NaCl 50 mM HEPES 364.4 mg/ml CsCl pH 7.4 sterile filtrated (0.2 µm filter)
	CsCl-buffer 3 (1.34 g/ml)	150 mM NaCl 50 mM HEPES 454.2 mg/ml CsCl pH 7.4 sterile filtrated (0.2 µm filter)
SDS-PAGE	Cell lysis buffer	1% Triton X-100 in DPBS 1x protease inhibitor
	SDS (10%) solution	100 g SDS dissolved in ddH_2O

Purpose	Name	Composition
SDS-PAGE	8% resolving gel	1 ml 40% Acrylamide/Bisacrylamide (29:1) 1.9 ml 1 M Tris pH 8.8 0.05 ml 10% SDS 0.05 ml 10% APS 0.003 ml TEMED 2.0 ml ddH_2O
	3% stacking gel	0.19 ml 40% Acrylamide/Bisacrylamide (29:1) 0.323 ml 1 M Tris pH 6.8 0.025 ml 10% SDS 0.025 ml 10% APS 0.0025 ml TEMED 1.825 ml ddH_2O
	SDS-loading buffer (10x)	312.5 mM Tris (pH 7.5) 10% SDS 50% Glycerol 1.722 M β-Mercaptoethanol One spoon-tip Bromophenol blue pH 7.0
	Running buffer	25 mM Tris 192 mM Glycine 0.1% SDS
Silver staining	Fixation buffer	50% MeOH 12% AcOH 0.05% HCHO
	Washing buffer	50% EtOH
	Equilibration buffer	0.8 mM $Na_2S_2O_3$

Purpose	Name	Composition
Silver staining	Impregnation buffer	11.78 mM $AgNO_3$ 0.05% HCHO
	Developing buffer	0.57 M Na_2CO_3 0.05% HCOH 15.8 µM $Na_2S_2O_3$
	Stopping buffer	50% MeOH 12% AcOH
Western Blot	Transfer buffer	2 mM Tris 150 mM Glycine 20% MeOH
	TBS-buffer (10x)	500 mM Tris 1.5 M NaCl pH 7.4
	TBS-T	1x TBS-buffer 0.05% Tween20 pH 7.4

3.7 Cell lines

SCC-VII, UM-SCC-11B and UD-SCC-2 cells were kindly provided by Prof. Cornelia Brunner, Clinic for Oto-Rhino-Laryngology, University Medical Center, Ulm

Name	Reference number	Origin
A431 (ATCC)	#CRL-1555	Epidermoid carcinoma, *Homo sapiens*
A549 (ATCC)	#CCL-185	Lung adenocarcinoma, *Homo sapiens*
CAP-T (Cevec)	-	Immortalized amniocytes, *Homo sapiens*
CMT-64 (Sigma)	#10032301	Lung adenocarcinoma, *Mus musculus*
HEK293T (ATCC)	#CRL-1573	Embryonic kidney, *Homo sapiens*
Hepa 1-6 (ATCC)	#CRL-1830	Hepatoma, *Mus musculus*
HSAEpC	C-12642	Human small airway epithelial cells
N52.E6	Ref.:[127]	Immortalized Amniocytes, *Homo sapiens*
UD-SCC-2 (Expasy)	#CVCL_E325	Hypopharyngeal squamous cell carcinoma, *Homo sapiens*
UM-SCC-11B (Expasy)	#CVCL_7716	Laryngeal squamous cell carcinoma, *Homo sapiens*
SCC-VII (Expasy)	#CVCL_V412	Head and neck squamous cell carcinoma ; *Mus musculus*
SK-Mel-28 (ATCC)	#HTB-72	Malignant melanoma, *Homo sapiens*

3.8 Cell culture media and supplements

Reagent	Order number	Supplier
DMEM	41966-029	Gibco, ThermoFisher, Karlsruhe, Germany
FCS	10270-106	Gibco, ThermoFisher, Karlsruhe, Germany
Freestyle™	12338-026	Gibco, ThermoFisher, Karlsruhe, Germany
Growth medium supplement mix	C-39175	PromoCell, Heidelberg, Germany
α-MEM	22561-021	Gibco, ThermoFisher, Karlsruhe, Germany
MEM	31095-029	Gibco, ThermoFisher, Karlsruhe, Germany
DPBS	14190-094	Gibco, ThermoFisher, Karlsruhe, Germany
Penicillin/Streptomycin/ Glutamine (100x)	10378-016	Gibco, ThermoFisher, Karlsruhe, Germany
PEM	12661-013	Gibco, ThermoFisher, Karlsruhe, Germany
RPMI 1640	21875-034	Gibco, ThermoFisher, Karlsruhe, Germany
Small Airway Epithelial Cell Growth Medium	C-21070	PromoCell, Heidelberg, Germany
0.05% Trypsin-EDTA	25300-054	Gibco, ThermoFisher, Karlsruhe, Germany
TrypLE select	12563-011	Gibco, ThermoFisher, Karlsruhe, Germany

3.9 Chemicals and reagents

Name	Order number	Supplier
1 kb DNA ladder	15615-024	Invitrogen, Waltham, Massachusetts, United States
100 bp DNA ladder	15628-050	Invitrogen, Waltham, Massachusetts, United States
1-step ultra TMB-ELISA substrate	34028	ThermoScientific, Rockford, USA
Acetic acid	33209	Sigma-Aldrich, Steinheim, Germany
Acrylamide/Bisacrylamide (29:1)	A515.1	Roth, Karlsruhe, Germany
Albumin Fraction V (BSA)	1844.2	Roth, Karlsruhe, Germany
Ampuwa (ddH_2O)	B230672	Fresenius Kabi, Bad Homburg, Germany
APS	A3678	Sigma-Aldrich, Steinheim, Germany
Argatroban	A0487-5MG	Sigma-Aldrich, Steinheim, Germany
Blocking buffer ELISA	37515	ThermoScientific, Rockford, USA
Bromophenol blue	B-8026	Sigma-Aldrich, Steinheim, Germany
Boric acid	0055	Mallinckrodt Baker B.V., Deventer, Netherlands

Name	Order number	Supplier
Caesium chloride	757306	Roche, Mannheim, Germany
Chloroform	22711.290	VWR Int., Fontenay-sous-Bois, France
CytoFLEX Sheath Fluid	B51503	Beckman Coulter, Brea, California, United States
Dako REAL™ Antibody Diluent	S2022	Dako, Agilent Technologies Inc., Glostrup, Denmark
DMSO	D2650	Sigma-Aldrich, Steinheim, Germany
dATP	N0440S	New England Biolabs, Ipswich, MA, USA
dCTP	N0441S	New England Biolabs, Ipswich, MA, USA
dGTP	N0442S	New England Biolabs, Ipswich, MA, USA
dTTP	N0443S	New England Biolabs, Ipswich, MA, USA
EDTA	A355	AppliChem, Darmstadt, Germany
Eosin G	K31917435	Merck, Darmstadt, Germany
EtOH absolute	51976	Sigma-Aldrich, Steinheim, Germany
Ethidium bromide (EtBr) 0.07%	A2273,0015	AppliChem, Darmstadt, Germany
Fc receptor (human) blocking reagent	120-000-442	Miltenyi Biotec, Bergisch Gladbach, Germany

Name	Order number	Supplier
Fluorescence mounting medium	S3023	Dako Agilent technologies Inc., Glostrup, Denmark
Formaldehyde (37%)	F-8775	Sigmal-Aldrich, Steinheim, Germany
Glycerol	A2926	AppliChem, Darmstadt, Germany
Glycine	A1377	AppliChem, Darmstadt, Germany
Goat serum	X0907	Dako, Agilent technologies Inc., Glostrup, Denmark
Growth factor reduced matrigel	356237	Corning Inc., Corning, NY, USA
HEPES	9105.3	Roth, Karlsruhe, Germany
Hydrochloric acid	UN1789	Merck, Darmstadt, Germany
Isoamyl alcohol	I-9392	Sigma-Aldrich, Steinheim, Germany
Isoflurane	05260-05	Forene, Abbott, Ludwigshafen, Germany
Isopropanol	33539	Sigma-Aldrich, Steinheim, Germany
Kapa SYBR FAST qPCR Master Mix	07-KK4600-05	PEQLAB Biotechnologie, Erlangen, Germany
L-Arabinose	A3256	Sigma-Aldrich, Steinheim, Germany
LB Broth, Lennox	240210	BD, Le Pont de Claix, France

Materials

Name	Order number	Supplier
LB Agar	22700-25	Invitrogen, Karlsruhe, Germany
Lithium chloride	P007.1	Carl Roth, Karlsruhe, Germany
Luminata forte Western HRP-substrate	WBLUF0100	Merck Group, Darmstadt, Karlsruhe
Mayer's Hematoxylin solution	MHS1-100ML	Sigma-Aldrich, Steinheim, Germany
Methanol	33213	Sigma-Aldrich, Steinheim, Germany
Milk powder	T145.2	Roth, Karlsruhe, Germany
o-Phenyldiamine dihydrochloride	P8287-50TAB	Sigma, Steinheim, Germany
Paraformaldehyde	P6148-500G	Sigma-Aldrich, Steinheim, Germany
pEGFP-N1	discontinued	Clontech Laboratories, Saint-Germain-en-Laye, France
PEI MAX	24765-1	Polysciences Inc., Warrington, PA,USA
Phenol	15513-039	Invitrogen, Karlsruhe, Germany
pNL1.1.	N109A	Promega GmbH, Walldorf, Germany
Precision Plus Protein Marker	10022139	Bio-Rad, München, Germany
Protease inhibitor cocktail, cOmplete EDTA-free	118735800001	Roche, Mannheim Germany

Name	Order number	Supplier
ROTI®Block	A151.3	Carl Roth GmbH & Co.Kg, Karlsruhe Germany
SDS	A7249	AppliChem, Darmstadt, Germany
SeaKem® ME Agarose	50010	Lonza, Rockland, ME, USA
Sevofluran Baxter	HDG91175V	Baxter Deutschland GmbH, Unterschleißheim, Germany
Sodium acetate	A1522	AppliChem, Darmstadt, Germany
Sodium bicarbonate	31437	Sigma-Aldrich, Steinheim, Germany
Sodium carbonate	223484	Sigma-Aldrich, Steinheim, Germany
Sodium chloride	31434	Sigma-Aldrich, Steinheim, Germany
Sodium citrate	A2403	AppliChem, Darmstadt, Germany
Sodium hydroxide	A1551	AppliChem, Darmstadt, Germany
Sodium thiosulfate	21,726-3	Sigma-Aldrich, Steinheim, Germany
SuperBlock™ Blocking Buffer in PBS (ELISA)	37518	Thermo Fisher Scientific, Waltham, Massachusetts, United States
β-Mercaptoethanol	M6250	Sigma-Aldrich, Steinheim, Germany
Sucrose	S0389	Sigma-Aldrich, Steinheim, Germany

Materials

Name	Order number	Supplier
Sulfuric acid	258105	Sigma-Aldrich, Steinheim, Germany
TEMED	T9281	Sigma-Aldrich, Steinheim, Germany
Tissue Tek	4583	Sakura, Zoeterwoude, Netherlands
Tris	T1378	Sigma-Aldrich, Steinheim, Germany
Trisodium citrate dihydrate	A2403	AppliChem, Darmstadt, Germany
Tris-phosphate	A6306	AppliChem, Darmstadt, Germany
Triton X-100	A1388	AppliChem, Darmstadt, Germany
Tween 20	9127.1	Roth, Karlsruhe, Germany
VivoGlo™ Luciferin	P1041	Promega, Madison, Wisconsin, United States
Xylol (Isomere)	9713.1	Roth, Karlsruhe, Germany

3.10 Consumables

Name	Order number	Supplier
96-well cell culture dish, flat bottom for qPCR	710880	Biozym, Hess. Oldendorf, Germany
96-well U-bottom plates untreated for flow cytometry	268152	Thermo Fisher Scientific, Waltham, Massachusetts, United States
96-well flat bottom plates NUNC MaxiSorb for ELISA	44-2404	Thermo Fisher Scientific, Waltham, Massachusetts, United States
Amersham™ Protran® Premium 0.45 µm NC	10600003	Sigma Aldrich, Steinheim, Germany
Amicon® Ultra-15 30k	UFC903024	Merck, Darmstadt, Germany
Bepanthen® Augen- und Nasensalbe	PZN: 02182442	Bayer, Leverkusen, Germany
Cell lifter	3008	Costar, Corning, New York, USA
Cell strainer (100 µm)	09012020	Sarstedt, Nümbrecht, Germany
Centrifugation tubes, conical, (200 ml)	376813	Thermo Scientific, Rochester, NY, USA
CytoFLEX Daily QC Fluorospheres	B53230	Beckman Coulter, Fullerton, CA, USA
Electroporation cuvette (25x2 mm gap)	71-2020	EPQLAB Biotechnologies, Erlangen, Germany
Falcon tube (15 ml)	352096	Falcon, Tamaulipas, Mexico
Falcon tube (50 ml)	352070	Falcon, Tamaulipas, Mexico

Name	Order number	Supplier
Filters (0.2 µm)	10462200	GE-Healthcare, Chicago, USA
Glass Pasteur Pipettes	7477 15	Brand, Wertheim, Germany
Hard-Shell 96-Well PCR Plates, low profile, thin wall, skirted, white/clear (qPCR)	HSP9601	Bio-Rad Laboratories, Hercules, California, United States
Hypodermic needle (0.4 x 20 mm) 27G	465 7705	Sterican, BRAUN, Melsungen, Germany
Hypodermic needle (0.9 x 40 mm) 20G	4657519	Sterican, BRAUN, Melsungen, Germany
LucentBlue X-ray film	541090	Biozym, Hess. Oldendorf, Germany
Micro-Fine insulin syringe (0.5 ml)	324876	Backton Dickinson, Franklin Lakes, United States
Microseals	MSB 1001	BIO-RAD Laboratories, Hercules, CA, USA
Nunclon® Δ-coated 96-well cell culture dish, flat bottom	167008	Thermo Fisher Scientific, Waltham, Massachusetts, United States
Nunclon® Δ-coated 24-well cell culture dish, flat bottom	142475	Thermo Fisher Scientific, Waltham, Massachusetts, United States
Nunclon® Δ-coated 6-well cell culture dish, flat bottom	140675	Thermo Fisher Scientific, Waltham, Massachusetts, United States
Nunclon® Δ-coated 6 cm cell culture dish, flat bottom	150288	Thermo Fisher Scientific, Waltham, Massachusetts, United States
Nunclon® Δ-coated 10 cm cell culture dish, flat bottom	150350	Thermo Fisher Scientific, Waltham, Massachusetts, United States
Nunclon® Δ-coated 15 cm cell culture dish, flat bottom	168381	Thermo Fisher Scientific, Waltham, Massachusetts, United States

Name	Order number	Supplier
Omnifix-F® syringe	9161406V	BRAUN, Melsungen, Germany
PCR tubes	230895	NUNC, Langenselbold, Germany
PD-10 column (Seohadex)	17-0851-01	GE Healthcare Amersham, Buckinghamshire, UK
Pipette filter tips [1-10 µl]	022491202	Eppendorf, Hamburg, Germany
Pipette filter tips [20 µl]	70.760.213	Sarstedt, Nümbrecht, Germany
Pipette filter tips [200 µl]	70.760.211	Sarstedt, Nümbrecht, Germany
Pipette filter tips [1000 µl]	70.762.211	Sarstedt, Nümbrecht, Germany
Pipette tips [0.1-20 µl]	073.762	Eppendorf, Hamburg, Germany
Pipette tips [2-200 µl]	073.800	Eppendorf, Hamburg, Germany
Pipette tips [100-1000 µl]	073.843	Eppendorf, Hamburg, Germany
Pipettes (stripettes) [5 ml]	4487	Costar, Corning, NY, USA
Pipettes (stripettes) [10 ml]	4488	Costar, Corning, NY, USA
Pipettes (stripettes) [25 ml]	4489	Costar, Corning, NY, USA
Pipettes (stripettes) [50 ml]	4490	Costar, Corning, NY, USA

Name	Order number	Supplier
Safe-lock tubes [1.5 ml]	0030 123.328	Eppendorf, Hamburg, Germany
Safe-lock tubes [2 ml]	00030 123.344	Eppendorf, Hamburg, Germany
Scalpel	BA220	Braun, Tuttlingen, Germany
Sentina® Ambidextrous NP Latex	141 392	Lohmann & Rauscher GmbH&Co KG, Neuwied, Germany
SHIELDskin™, orange nitrile 260	67 6233	SHIELDScientific, Bennekom, Netherlands
SHIELDskin™, eco nitrile PF 250	625123	SHIELDScientific, Bennekom, Netherlands
Superfrost™ Plus glas sildes	J1800AMNZ	Thermo Fisher Scientific, Waltham, Massachusetts, United States
SuperSignal™ West Pico PLUS Chemiluminescent Substrate	34578	Thermo Fisher Scientific, Waltham, Massachusetts, United States
Syringe [2 ml]	4646027V	Braun, Tuttlingen, Germany
Syringe [1 ml]	300013	Luer Lok, BD Plastipak, Heidelberg, Germany
Syringe [50 ml]	300865	Luer Lok, BD Plastipak, Heidelberg, Germany
Wheaton® Tissue Grinder	358103	Wheaton, Millville, NJ
Ultraclear centrifuge tubes	344059	Beckman Coulter, GmbH, Krefeld, Germany
Uncoated 15 cm cell culture dish	83.3903	Sarstedt, Nümbrecht, Germany

3.11 Devices

Name	Supplier
Agarose gel documentation	Gel Jet imager, Intras, Göttingen, Germany
Agfa CP1000	X-ray film developing device, AGFA, Mortsel, Belgien
Hoefer™ HE33 Agarose gel running chambers	Thermo Fisher Scientific, Waltham, Massachusetts, United States
Autoclave	Varioklav Steam Sterilizer, Thermo Fisher Scientific, Rockford, IL, USA
Bacteria incubator	Heraeus B15, Thermo Fisher Scientific, Rockford, IL, USA
Bacteria incubator	Edmund Bühler Labortechnik TH15, KS-15
Biophotometer	Eppendorf, Hamburg, Germany
Block heater	HBT-21-32, HLC Haep Labor Consult, Bovenden, Germany
Cell culture incubator	Heraeus BBD 6220, Thermo Fisher Scientific, Rockford, IL, USA
CytoFLEX Flow Cytometer	Beckman Coulter GmbH, Krefeld, Germany

Name	Supplier
Centrifuges	Heraeus Multifuge 3s-r, Thermo Fisher Scientific, Rockford, IL, USA
	Microliter centrifuge 5424R, Eppendorf, Hamburg, Germany
	Sorvall RC6 Plus with F21 or F10S rotor, Thermo Fisher Scientific, Rockford, IL, USA
	Optima XE-90 Ultracentrifuge with SW 41 Rotor, Beckman Coulter, Brea, California, United States
	Heraeus Biofuge fresco, Thermo Fisher Scientific, Rockford, IL, USA
	Specttrafuge Mini Centrifuge C1301, Labnet International, Woodbrigde, NY, USA
Electroporator	Micropulser, Bio-Rad, München, Germany
Fluorescence microscope	Zeiss Axio Scope 2 plus with Axia-Cam MRm camera; Carl Zeiss, Göttingen, Germany
Fridge	Hera Freeze -80°C, Thermo Fisher Scientific, Rockford, IL, USA
Desiccator 467-2120	Kartell, Noviglio, Italy
Hotplate stirrer	Heidolph MR 3001K, Heidolph, Schwabach, Germany
Leica cm 3050 s Cryostat	Leica, Wetzlar, Germany

Materials

Name	Supplier
Microscope	Leica DM IL, Leica, Wetzlar, Germany
Multiscan Ex 96-well plate reader	Thermo Fisher Scientific, Rockford, IL, USA
NanoDrop 3300	Thermo Fisher Scientific, Rockford, IL, USA
Neubauer cell-counting chamber	BLAUBRAND®-Zählkammers, Wertheim, Germany
Binocular	Nikon SMZ-2B, Nikon, Minato, Präfektur Tokio, Japan
Power supply (SDS-PAGE and Western Blot)	PowerPac HC, Bio-Rad, München, Germany
GloMax® luminometer	Promega, Madison, Wisconsin, United States
Mini Protean 3 Cell	Bio-Rad Laboratories, Hercules, California, United States
pH meter	MP225, Mettler, Toledo, Scherzenbach, Switzerland
PCR thermocycler	TECHNE Thermocycler FT GENE 5D Techgene, LabTech int., Buckhardtsdorf, Germany
Phosphoscreen cassette	Storage, molecular dynamics, Amersham, Nümbrecht germany
Shaker MHR20/23	HLC Haep Labor Consult, Bovenden, Germany
Tube rotator	Snijders Scientific, Tilburg, Holland
Waterbath SUB-14	Grant, Cambridge, UK

Name	Supplier
qPCR cycler	Tratagene Mx 3005P, Aglient Technologies, La Jolla, CA, USA
IVIS 200 in vivo Imaging System	Caliper Life Science, Waltham, Massachusetts, United States
Dark Reader Transilluminator	Clare Chemical Research, Dolores, Colorado, United States

3.12 Enzymes

Name	Order Number	Supplier
*Afl*II restriction enzyme	R0520	New England Biolabs, Ipswich, MA, USA
*Afl*III restriciton enzmye	R0541	New England Biolabs, Ipswich, MA, USA
Alkaline phosphatase, Calf Intenstinal (CIP)	M0290L	New England Biolabs, Ipswich, MA, USA
*Ase*I restriction enzyme	R0526	New England Biolabs, Ipswich, MA, USA
Benzonase	E1014	Merck Millipore, Burlington, MA, USA
*Dra*I restriction Enzyme	R0129	New England Biolabs, Ipswich, MA, USA
*EcoR*V restriction enzyme	R0195	New England Biolabs, Ipswich, MA, USA
*Hind*III restriction enzyme	R0104	New England Biolabs, Ipswich, MA, USA

Name	Order Number	Supplier
*Kpn*I restriction Enzyme	R3142	New England Biolabs, Ipswich, MA, USA
*Not*I restriction enzyme	R0189	New England Biolabs, Ipswich, MA, USA
*Pvu*I restriction Enzyme	R3150	New England Biolabs, Ipswich, MA, USA
Q5® High-Fidelity DNA Polymerase	M0491S	New England Biolabs, Ipswich, MA, USA
*Swa*I restriction enzyme	R0604	New England Biolabs, Ipswich, MA, USA
T4 DNA ligase	M0203L	New England Biolabs, Ipswich, MA, USA
*Xho*I restriction enzyme	R0146	New England Biolabs, Ipswich, MA, USA

3.13 HAdV-5 vectors

All HAdV-5 vectors used were based on the GenBank ID: AY339865.1.

3.13.1 Modifications of the vector life cycle

3.13.1.1 Replication-deficient first-generation vectors

All first generation HAdV-5 vectors carried a complete deletion of the *E1* gene region (GenBank ID: AY339865.1, nucleotide (nt) sequence from nt 1 to 440 and from nt 3,523 to 35,935), rendering them replication deficient and were generated preceding to the present study by the Department of Gene Therapy at Ulm University.

3.13.1.2 (Conditionally) replication-competent vectors

Wild-type HAdV-5wt

HAdV-5wt carried the full-length HAdV-5 genome (GenBank ID: AY339865.1).

E1AΔ24bp mutation

HAdV-5 vectors carry the E1AΔ24bp mutation, referring to a 24 bp deletion within the *E1A* gene region[151] (GenBank ID: AY339865.1 nt 919 to 943), which encodes for the E1A 12S protein. Due to this mutation, binding of E1A 12S to the retinoblastoma protein (pRb) is prevented and hinders E1A-mediated cell cycle progression into the S-Phase, thus restricts virus replication to proliferating cells[151].

ΔE1B19k mutation

HAdV-5 vectors carry the E1B19k mutation, referring to a 147 bp deletion within the *E1B19k* gene region[302] (GenBank ID: AY339865.1 nt 1770 to 1916), which results in a non-functional E1B19k protein. Healthy cells with functional apoptotic pathways, thus are assumed to undergo rapid apoptosis upon infection with an E1B19k mutant, while virus replication remains feasible in malignant cells.

ΔE3gp19k

HAdV-5 vectors carry the E3gp19k mutation, referring to a 712 bp deletion within the *E3* gene region (GenBank ID: AY339865.1 nt 28738 to 29450), which deletes the *E3gp19k* gene. The E3gp19k protein binds to MHC class I (MHC-I) proteins and prevents antigen presentation at the host cell surface. Thus, cells infected with an E3gp19k mutant should become rapidly recognized and eradicated by the host immune system. To maintain the stop codon of the upstream located *E3-6.7k*, the start codon of *E3gp19k* was additionally mutated (…**ATG**A… to …**ATA**A…).

3.13.2 Modifications of the vector capsid

HexPos3

HAdV-5 vectors carry the HexPos3 capsid mutation harbored a 13 aa deletion of mainly negatively charged aa within HVR1 of hexon, which were replaced by four consecutive positively charged lysine residues (EEEDDDNEDEVDE → KKKK; GenBank ID: AY339865.1 nt 19280-19318).

ΔCAR

HAdV-5 vectors carry the ΔCAR mutation harbored a single aa substitution within the fiber knob domain from tyrosine to alanine at aa position 477 (Y477A), which has been shown to significantly reduce binding of HAdV-5 particles to their primary attachment receptor CAR[303].

3.13.3 Geneti-chemical modification of the vector capsid

FiberAffilin

A solvent exposed cysteine, flanked by flexible glycine-rich linkers was genetically introduced into the HI-loop of the fiber knob (Protein ID: AAQ19310.1, position: downstream of G543, LIGGG-C-GGGID). Attachment of Affilin was achieved by covalent cysteine linkage between the surface exposed cysteine of the vector capsid and a C-terminal cysteine of Affilin, using a bismalemidohexane linker preceding to the present study by the Department of Gene Therapy at Ulm University[228].

HexonAffilin

A solvent exposed cysteine was genetically introduced into HVR1 of hexon (Protein ID: AAQ19298, D151C). Attachment of Affilin was achieved by covalent linkage between the surface exposed cysteine of the vector capsid and a C-terminal cysteine of Affilin, using a bismalemidohexane linker preceding to the present study by the Department of Gene Therapy at Ulm University[228].

3.13.4 Genetic introduction of reporter genes

Enhanced green fluorescence protein (eGFP)

Instead of *E1*, all replication deficient vectors harbored the enhanced green fluorescence protein (eGFP) reporter cassette under regulation of the human cytomegalovirus (CMV) promotor with a C-terminal simian virus 40 poly(A) (SV40 poly(A)) signal sequence (subcloned from pEGFP-N1 (Clontech Laboratories, Saint-Germain-en-Laye, France).

eGFP-NanoLuciferase

Most (conditionally) replicating HAdV-5 vectors were equipped with the eGFP-NanoLuciferase reporter cassette (subcloned from pNL1.1. plasmid, N109A, Promega) inserted between E1A/E1B open reading frames (GenBank ID: AY339865.1 nt 1648/1649) and driven by the human CMV promotor. eGFP and NanoLuciferase were genetically fused by a 15 aa linker (GWWWFWWWWFWWWWF) and C-terminally flanked by the SV40 poly(A) signal sequence.

FireflyLuciferase

The conditionally replicating vectors HCRAd-5_ΔCAR and HCRAd-5-HexPos3_ΔCAR were equipped with the Firefly Luciferase reporter cassette (firefly luciferase GeneBank ID: MK484107.1, nt 283 to 1932), inserted between E1A/E1B open reading frames (GenBank ID: AY339865.1 nt 1648/1649), driven by the human CMV promotor and C-terminally flanked by the SV40 poly(A) signal sequence.

3.13.5 List of viruses and vectors used in the present study

Name	Life cycle modification	Transgene	Inserted mutations
HAdV-5wt	Replication competent	eGFP + NanoLuciferase	-
HAdV-5	Replication deficient	eGFP	ΔE1
HAdV-5_ΔCAR	Replication deficient	eGFP	ΔE1 ΔCAR
HAdV-5_ΔCAR FiberAffilin	Replication deficient	eGFP	ΔE1 ΔCAR Affilin covalently coupled to the fiber knob
HAdV-5_ΔCAR HexonAffilin	Replication deficient	eGFP	ΔE1 ΔCAR Affilin covalently coupled to hexon

Name	Life cycle modification	Transgene	Inserted mutations
HAdV-5_ΔCAR HexPos3	Replication deficient	eGFP	ΔE1 ΔCAR HexPos3
HAdV-5 E1AΔ24bp	Conditionally replicating	eGFP + NanoLuciferase	E1AΔ24bp
HAdV-5 E1AΔ24bp ΔE1B19k	Conditionally replicating	eGFP + NanoLuciferase	E1AΔ24bp ΔE1B19k
HAdV-5 E1AΔ24bp ΔE1B19k ΔE3gp19k	Conditionally replicating	eGFP + NanoLuciferase	E1AΔ24bp ΔE1B19k ΔE3gp19k
HCRAd-5 ΔCAR	Conditionally replicating	FireFly Luciferase	E1AΔ24bp ΔE1B19k ΔE3gp19k ΔCAR
HCRAd-5 HexPos3 ΔCAR	Conditionally replicating	FireFly Luciferase	E1AΔ24bp ΔE1B19k ΔE3gp19k HexPos3 ΔCAR

3.14 Kits

Name	Order Number	Supplier
Counter-Selection BAC Modification Kit Red/ET Recombination	K002 *(discontinued)*	GeneBridges, Heidelberg, Germany
GenElute Mammalian Genomic DNA Miniprep Kit	G1N350	Sigma-Aldrich, Steinheim, Germany
PCR purification Kit (250)	28106	QIagen, Hilden, Germany
Qiagen Large Construction Kit (10)	12462	Qiagen, Hilden, Germany
Qiagen Plasmid Midi Kit (100)	12145	Qiagen, Hilden, Germany
QIAmp DNA Mini Kit	51306	Qiagen, Hilden, Germany
QIAquick Gel Extraction Kit	28704	Qiagen, Hilden, Germany

3.15 PCR primers

3.15.1 Primers for homologous recombination

All primers used were commercially purchased synthetic oligos. Bold nucleotides are complementary to the respective PCR template. Underlined nucleotides are complementary to the target bacmid.

3.15.1.1 Primers for the insertion of NanoLuciferase between E1A/E1B

rpsL-neo NanoLuciferase oligos (template provided by the Kit)	
Forward primer	**5'**-AGTTCGTGACCGCCGCCGGGATCACTCTCGGCATGGACGAGCTGTACAAGG**GCCTGGTGATGATGGCGGGATCG-3'**
Reverse primer	**5'**-AACCTCTACAAATGTGGTATGGCTGATTATGATCTAGAGTCGCGGCCGCTT**CAGAAGAACTCGTCAAGAAGGCG-3'**
NanoLuciferase insertion oligos (template: pNL1.1 (Promega))	
Forward primer	**5'**-AGTTCGTGACCGCCGCCGGGATCACTCTCGGCATGGACGAGCTGTACAAGGGTGGTGGTGGTTCTGGTGGTGGTGGTTCTGGTGGTGGTGGTTCT**GTCTTCACACTCGAAGATTTCGTTG-3'**
Reverse primer	**5'**-AACCTCTACAAATGTGGTATGGCTGATTATGATCTAGAGTCGCGGCCGCTT**TACGCCAGAATGCGTTCGCACAG-3'**

3.15.1.2 Primers to generate E1AΔ24bp-carrying vectors

rpsL-neo E1AΔ24bp oligos (template provided by the Kit)	
Forward primer	**5'**-AGCAGCCGGAGCAGAGAGCCTTGGGTCCGGTTTCTATGCCAAACCTTGTAG**GCCTGGTGATGATGGCGGGATCG-3'**
Reverse primer	**5'**-CAAGACCTGCAACCGTGCCCGGGGTGCTCCACATAATCTAACACAAACTC**TCAGAAGAACTCGTCAAGAAGGCG-3'**
E1AΔ24bp oligos (template: commercially purchased synthetic oligo)	
Forward primer	**5'-CCGGTTTCTATGCCAAACCTTGTA-3'**
Reverse primer	**5'-CGTATTCCTCCGGTGATAATGACA-3'**

3.15.1.3 Primers to generate E1BΔ19k-carrying vectors

rpsL-neo E1BΔ19k oligos (template provided by the Kit)	
Forward primer	**5'**-CGCCGTGGGCTAATCTTGGTTACATCTGACCTCATGGAGGCTTGGGAGTG**GGCCTGGTGATGATGGCGGGATCG-3'**
Reverse primer	**5'**-CCAGAAAATCCAGCAGGTACCCCCCGCTCAGATGGGTTTCTTCGCTCCAT**TCAGAAGAACTCGTCAAGAAGGCG-3'**
E1BΔ19k oligos (template: commercially purchased synthetic oligo)	
Forward primer	**5'-TTACATCTGACCTCATGGAGGCTT-3'**
Reverse primer	**5'-TCAGATGGGTTTCTTCGCTCCATT-3'**

3.15.1.4 Primers to generate ΔE3gp19k-carrying vectors

rpsL-neo ΔE3gp19k oligos (template provided by the Kit)	
Forward primer	**5'**-ATTTATTGTCAGCTTTTTAAACGCTGGGGTCGCCACCCAAGATGATTAGG**GGCCTGGTGATGATGGCGGGATCG-3'**
Reverse primer	**5'**-GGTTGTGTTGGTCATCTCTGTTAGGGTGGGTCGCTGTAGTTGGACTGGAA**TCAGAAGAACTCGTCAAGAAGGCG-3'**
ΔE3gp19k oligos (template: commercially purchased synthetic oligo)	
Forward primer	**5'-TTCTCTGCCTAAGGCTCGCCGCCT-3'**
Reverse primer	**5'-TAGCGGCGGCCGCGTTGGTTGTGT-3'**

3.15.1.5 Primers to generate Firefly luciferase-carrying vectors

rpsL-neo Firefly Luciferase oligos (template provided by the Kit)	
Forward primer	**5'**-TGCAGTCGACGGTACCGCGGGCCCGGGATCCACCGGTCGCCAC CATG**GGCCTGGTGATGATGGCGGGATCG-3'**
Reverse primer	**5'**-GTGATGCTATTGCTTTATTTGTAACCATTATAAGCTGCAATAAACAA GTT**TCAGAAGAACTCGTCAAGAAGGCG-3'**
Firefly Luciferase oligos (template: in the lab available bacmid)	
Forward primer	**5'-TGCAGTCGACGGTACCGCGGGCCCGGGATCCACCGGTCGCCAC CATGGAAGACGCCAAAAACATAAAGAAAGG-3'**
Reverse primer	**5'-GTGATGCTATTGCTTTATTTGTAACCATTATAAGCTGCAATAAAC AAGTT-3'**

3.15.1.6 Primers to generate ∆CAR-carrying vectors

rpsL-neo ∆CAR oligos (template provided by the Kit)	
Forward primer	**5'**-GATTTGACGAAAATGGAGTGCTACTAAACAATTCCTTCCTGGACCCAGAA **GGCCTGGTGATGATGGCGGGATCG-3'**
Reverse primer	**5'**-GCGTTTGTATAGGCTGTGCCTTCAGTAAGATCTCCATTTCTAAAGTTCCA **TCAGAAGAACTCGTCAAGAAGGCG-3'**
∆CAR oligos (template: in the lab available bacmid)	
Forward primer	**5'-AACTTTGTGGACCACACCAGC-3'**
Reverse primer	**5'-TGCACTTGGAGTTGTGTCTCC-3'**

3.15.1.7 Primers to generate HexPos3-carrying vectors

rpsL-neo HexPos3 oligos (template provided by the Kit)	
Forward primer	**5'**-CAAATCCTTGCGAATGGGATGAAGCTGCTACTGCTCTTGAAATAAACCTA**GGCCTGGTGATGATGGCGGGATCG**-**3'**
Reverse primer	**5'**-CCAGAATAAGGCGCCTGCCCAAATACGTGAGTTTTTTGCTGCTCAGCTTG**TCAGAAGAACTCGTCAAGAAGGCG**-**3'**
HexPos3 oligos (template: in the lab available bacmid)	
Forward primer	**5'**-**TTTTAAGCCCTACTCTGGCACTGC**-**3'**
Reverse primer	**5'**-**CCTTCGACACCTATTTGAATACCC**-**3'**

3.15.2 qPCR primers

Primer for amplification of the HAdV-5 *E4* gene region	
Forward primer	**5'**-TAGACGATCCCTACTGTACG-**3'**
Reverse primer	**5'**-GGAAATATGACTACGTCCGG-**3'**
Primer for amplification of human *β-actin*	
Forward primer	**5'**-GCTCCTCCTGAGCGCAAG-**3'**
Reverse primer	**5'**-CATCTGCTGGAAGGTGGACA-**3'**
Primer for amplification of murine *β-actin*	
Forward primer	**5'**-CAAGGAGTGCAAGAACACAG-**3'**
Reverse primer	**5'**-GCCTTGGAGTGTGTATTGAG-**3'**

3.16 Plasmids

3.16.1 pBSK-CMV

The pBSK-CMV expression plasmid was used for cloning of pBSK-CMV_H1-FAP5(V_H-V_L)-S11(V_H-V_L)-FLAG and pBSK-CMV_hFAP by *Not*I digestion. A schematic illustration is shown in figure 7.

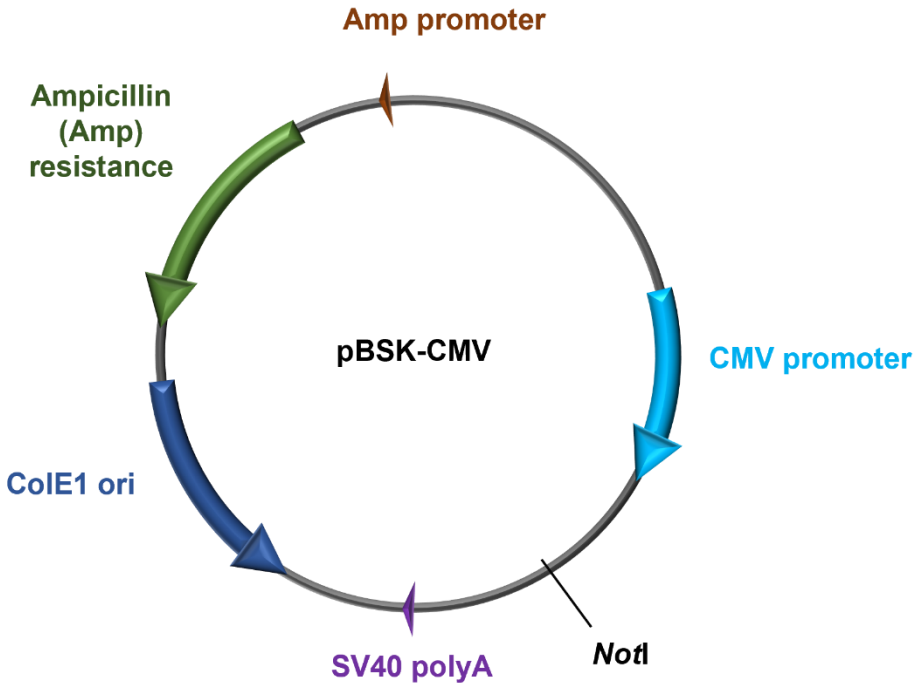

Figure 7: Schematic illustration of the organization of pBSK-CMV
Shown are the approximate positions of the Ampicillin resistance gene, the Ampicillin promoter, CMV promoter, the origin of replication (ColE1 ori) and the position of the *Not*I restriction site used for cloning. Amp: Ampicillin, ColE1 ori: origin of replication.

3.17 Software

Name	Purpose
ChemCapture	Software for Gel Jet imager
CytExpert	Software for Beckman Coulter CytoFlex
GLOMAX	Software for Promega GloMax Luminometer
Leica Application Suite	Imaging Program for fluorescence microscope
Living Image®	Imaging program for IVIS 200 *in vivo* Imaging System
Microsoft Office 365	Data analysis, word processing
RStudio software (version 4.1.2)	Statistical analysis
Serial Cloner (version 2.6.1)	*In silico* cloning, sequence analysis

4 Methods

4.1 Nucleic acid methods

4.1.1 Determination of DNA concentrations by optical density measurement

DNA samples were diluted 1:100 in ddH_2O and extinction was measured at a wavelength of 260 nm. Based on the path length of the cuvette (1 cm) and a given extinction coefficient of 0.02 $\frac{\mu l}{ng * cm}$, DNA concentrations were calculated based on the Lambert-Beer's law according to the following formula:

$$c = \frac{E_\lambda}{\varepsilon_\lambda * d}$$

λ = wavelength [nm]

E_λ: extinction at a wavelength of 260 nm

d = path length of the cuvette

c = DNA concentration [ng/µl]

ε_λ = extinction coefficient at wavelength λ $\left[\frac{\mu l}{ng * cm}\right]$

4.1.2 DNA precipitation

The sample volume was determined and 10% of sodium acetate (3 M, pH 5.2) were added. The sample was mixed with 2.5-fold the sample volume of 100% EtOH, carefully inverted and centrifuged at 20,817 x *g* for 15 min. The supernatant was removed and the obtained pellet was overlayed with 250 µl 70% EtOH. Again, the sample was centrifuged as described, and the obtained pellet was air-dried. Depending on the intended use, precipitated DNA was finally dissolved in an appropriated amount of either ddH_2O, Tris- or TE-buffer and stored at 4 °C.

4.1.3 Enzymatic DNA digestion

4.1.3.1 Qualitative restriction analysis

For qualitative restriction analysis, 200 ng DNA were digested at the temperature optimum of the respective restriction enzyme for 2 h. The composition of a single reaction mix is listed in table 1.

Table 1: Reaction mix for qualitative restriction analysis

Component	Volume
DNA sample (200 ng/µl)	1 µl
Reaction buffer (10x)	2 µl
Restriction enzyme	1 µl
ddH_20	16 µl
Total volume	**20 µl**

4.1.3.2 Preparative DNA digestion

For preparative DNA digestion, 15 µg of DNA were digested at the temperature optimum of the respective restriction enzyme, o/n. The composition of a single reaction mix is listed in table 2.

Table 2: Reaction mix for preparative restriction analysis

Component	Volume
DNA sample (1 µg/µl)	15 µl
Reaction buffer (10x)	10 µl
Restriction enzyme	5 µl
ddH_20	70 µl
Total volume	**100 µl**

4.1.3.3 Linearization of HAdV-5 genomes from bacmid DNA

For linearization of HAdV-5 genome-containing bacmid pBeloBacGS66 (see 3.5.1), 10 µg of bacmid DNA were digested with *Swa*I in a total volume of 100 µl at 25 °C, o/n. The composition of a single reaction mix is listed in table 3.

Table 3: Reaction mix for linearization of HAdV-5 genome containing bacmid pBeloBacGS66

Component	Volume
DNA sample (1 µg/µl)	10 µl
Reaction buffer (10x)	10 µl
*Swa*I	5 µl
ddH_20	75 µl
Total volume	**100 µl**

4.1.4 Qualitative agarose gel electrophoresis

Qualitative agarose gel electrophoresis was performed using 1% agarose gels dissolved in TBE-buffer containing EtBr (1 drop per 50 ml gel). Enzymatically digested DNA (see 4.1.3.1) was mixed with 2.2 µl DNA loading buffer (10x), loaded onto the gel and separated at 120 V for 1-4 h. To determine fragment sizes, 7 µl of 1 kb DNA ladder were additionally loaded onto the gel and DNA was visualized by UV-exposure using the Gel Jet imager device.

4.1.5 Purification of DNA fragments with a length > 7 kbp

DNA fragments larger than 7 kbp and *Swa*I digested Bacmid DNA (see 4.1.3.3) were separated using 1% agarose gels dissolved in TAE-buffer containing EtBr (1 drop per 50 ml gel) at 120 V for 2-4 h. The DNA fragment of the expected size was cut out from the gel, sliced into pieces, and transferred into a 2 ml reaction tube. The gel weight was determined, mixed with an equal amount of phenol (v/w) and snap-frozen in liquid nitrogen. Subsequently, the sample was slowly thawed at RT and centrifuged at 20,817 x *g* for 15 min. The obtained upper phase was transferred into a new 2 ml reaction tube and the sample volume was determined. An equal amount of chloroform-isoamyl

alcohol (24:1) was added to the sample, thoroughly mixed for ~ 1 min, and centrifuged at 20,817 x *g* for 15 min. Again, the upper phase was transferred into a new 1.5 ml reaction tube and the sample volume was determined. Subsequently, the sample was mixed with ice-cold isopropanol according to 0.7-fold the sample volume and incubated at -20 °C for 30 min. The sample was centrifuged at 20,817 x *g* for 30 min, the supernatant removed and the obtained pellet was resuspended in 150 µl TE-buffer. Finally, the DNA was precipitated as described in 4.1.2, dissolved in an appropriate amount of TE-buffer and stored at 4 °C.

4.1.6 Polymerase chain reaction (PCR) for homologous recombination

DNA fragments used for homologous recombination (see 4.4.6) were generated by PCR. The used primers and templates are listed in the Materials section (see 3.15.1).

4.1.6.1 Amplification of rpsL-neo cassette containing fragments

DNA fragments carrying the rpsL-neo cassette were amplified using primers harboring a 24 bp sequence complementary to the rpsL-neo template (GeneBridges) with additional 50 bp 5'-overhangs complementary to the target HAdV-5 bacmid sequence (see 3.15.1). PCR reactions were prepared and performed as listed in table 4 and table 5.

Table 4: Sample preparation for amplification of a rpsL-neo containing DNA fragment.

Component	Volume	Final concentration
Q5 reaction buffer (5x)	80 µl	1x
Q5 enhancer (5x)	80 µl	1x
dNTPs (10 mM)	8 µl	200 µM
Foreward primer (10 µM)	20 µl	0.5 µM
Reverse primer (10 µM)	20 µl	0.5 µM
DNA template (rpsL-neo cassette)	4 µl	0.5 ng/µl
Q5 High-Fidelity Polymerase (1 U/µl)	4 µl	0.01 U/µl
ddH2O	**Ad. 400 µl**	**-**

Table 5: Thermocycle protocol for the generation of rpsL-neo containing DNA fragments.

Step	Temperature	Time	Cycles
Initial heat	98 °C	30 sec	1
Denaturation	98 °C	10 sec	25
Annealing	60 °C	30 sec	
Elongation	72 °C	1.5 min	
Final elongation	72 °C	2 min	1
Storage	4 °C	∞	-

4.1.6.2 Amplification of insertion oligos

Insertion oligos, harboring the mutated sequence of interest flanked by sequences homologous to the target HAdV-5 bacmid were amplified from commercially acquired template oligos or DNA constructs available in the laboratory. The used primers are listed in the Materials section (see 3.15.1). PCR reactions were prepared and performed as listed in table 6 and table 7, respectively.

Table 6: Sample preparation for the amplification of an insertion oligo.

Component	Volume	Final concentration
Q5 reaction buffer (5x)	80 µl	1x
Q5 enhancer (5x)	80 µl	1x
dNTPs (10 mM)	8 µl	200 µM
Foreward primer (10 µM)	20 µl	0.5 µM
Reverse primer (10 µM)	20 µl	0.5 µM
DNA template	4 µl	0.5 ng/µl
Q5 High-Fidelity Polymerase (1 U/µl)	4 µl	0.01 U/µl
ddH2O	**Ad. 400 µl**	**-**

Table 7: Thermocycle protocol for the generation of an insertion oligo.

Step	Temperature	Time	Cycles
Initial heat	98 °C	30 sec	1
Denaturation	98 °C	10 sec	25
Annealing	58-63 °C	30 sec	
Elongation	72 °C	30 sec/kb	
Final elongation	72 °C	2 min	1
Storage	4 °C	∞	-

4.1.7 Purification of DNA fragments with a length < 7kbp

DNA fragments smaller than 7 kbp were purified using the QIAquick® Gel Extraction Kit (250) (Qiagen). First, DNA fragments were separated by agarose gel electrophoresis using an 1% agarose gel dissolved in TAE buffer containing EtBr (1 drop per 50 ml gel) at 120 V for 2-4 h. PCR fragments were cut out from the gel, transferred into a 2 ml reaction tube and the sample weight was determined. Three volumes the gel weight of buffer QG (Qiagen) were added and incubated at 50 °C. Once the gel was completely dissolved, the sample was loaded onto a QIAquick spin column (Qiagen), centrifuged at 20,817 x *g* for 1 min and the flow through was discarded. To remove any remaining gel from the column, 500 µl of buffer QG were added, centrifuged at 20,817 x *g* for 1 min and the flow through again was discarded. For washing, 750 µl of buffer PE (Qiagen) were added to the column, centrifuged as described and the flow through was discarded. Washing was repeated once, followed by an additional centrifugation step at 20,817 x *g* to remove any remaining washing buffer from the column. To elute bound DNA, the column was placed onto a new 1.5 ml reaction tube, 50 µl of ddH_2O were added, incubated at RT for 10 min and centrifuged at 20,817 x *g* for 1 min. DNA concentrations were determined as described in 4.1.1 and samples were stored at 4 °C until further use.

4.1.8 Quantitative real time polymerase chain reaction (qPCR)

qPCR was used to quantify the amount of adenoviral genome copy numbers within DNA samples by detection of the adenoviral *E4* gene region. DNA concentrations of samples were determined as described in 4.1.1 and diluted in ddH_2O to a final concentration of 10 ng/µl. Samples were normalized to the β-actin copy numbers in the respective sample. Isolated and purified HAdV-5 genome DNA with defined genome copy numbers/µl was used as a reference. The used primers to amplify *E4* and *β-actin* are listed in the Material section 3.15.2. The composition of a single qPCR reaction mix and the used thermocycle protocol are listed in table 8 and table 9, respectively.

Table 8: Composition of a single qPCR reaction mix.

Component	Volume	Final concentration
KAPA SYBR FAST qPCR Master Mix (2x)	10 µl	1x
Forward primer [10 µM]	0.4 µl	200 nM
Reverse primer [10 µM]	0.4 µl	200 nM
Template [10 ng/µl]	2 µl	1 ng/µl
ddH2O	**Ad. 20 µl**	**-**

Table 9: Thermocycle protocol for qPCR analysis.

Step	Temperature	Time	Cycles
Initial heat	95 °C	10 min	1
Denaturation	95 °C	30 sec	40
Annealing&Elongation	60 °C	20 sec	
Melting curve	50-95 °C	15 sec / 1 °C increment	1
Storage	4 °C	∞	1

4.1.9 Cloning of pBSK-CMV_H1-FAP5(V_H-V_L)-S11(V_H-V_L)-FLAG

4.1.9.1 Design of the FAP5-S11-FLAG bispecific adapter molecule

The FAP5-S11-FLAG bispecific adapter molecule was designed by genetic fusion of the two single chain variable fragments (scFv) scFvFAP5 and scFvS11, binding the fibroblast activation protein and adenovirus fiber knob, respectively. To this end, the two subdomains of the respective scFv, consisting out of the variable heavy (V_H) and variable light (V_L) chain derived from either the FAP binding antibody mAb FAP5[304] or the HAdV-5 fiber knob binding scFvS11[253] were genetically fused via flexible glycine-serine linkers ($(G_4S)_3$) and the resultant scFvFAP5 and scFvS11 were fused to each other by a short glycine-serine linker (G_4S). An N-terminal signal peptide (H1)[305] as well as a C-terminal FLAG-Tag were added for protein secretion and detection, respectively. Upstream of the start codon, a Kozak-sequence was introduced and *Not*I restriction sites were added at both the 5'- and 3'-ends for subsequent cloning. The corresponding DNA sequence was codon optimized for *homo sapiens* expression and synthesized by GeneArts. A schematic illustration of the design of the H1-FAP5(V_H-V_L)-S11(V_H-V_L)-FLAG expression cassette is shown in figure 8.

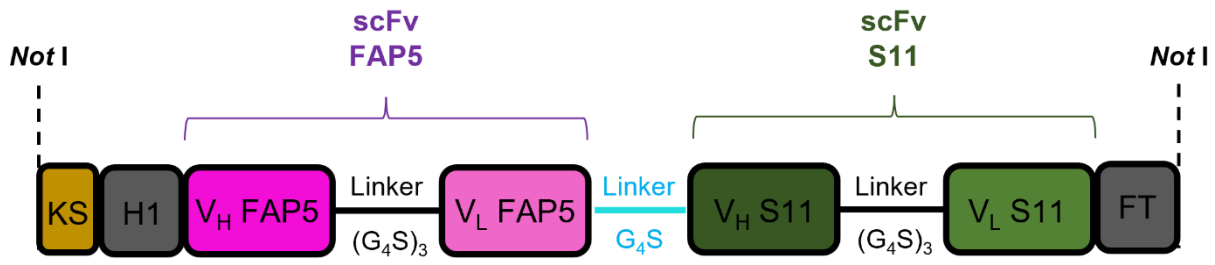

Figure 8: Genetic design of the H1-FAP5(V_H-V_L)-S11(V_H-V_L)-FLAG expression cassette.
KS: Kozak sequence; H1: signal peptide; V_H: variable heavy chain, V_L: variable light chain; scFv: single chain variable fragment, FT: FLAG-Tag.

4.1.9.2 Generation and purification of the H1-FAP5(V_H-V_L)-S11(V_H-V_L)-FLAG insert

The H1-FAP5-S11-FLAG plasmid (GeneArts) was digested with *Not*I as described in 4.1.3.2. The digested DNA was separated by agarose gel electrophoresis and prepared as described in 4.1.7. The purified insert was eluted in 20 µl ddH_2O, DNA concentration was determined as described in 4.1.1 and the sample was short-term stored at 4 °C.

4.1.9.3 Linearization, dephosphorylation and purification of pBSK-CMV

The pBSK-CMV plasmid (see 3.16.1) was digested with *Not*I as described in 4.1.3.2. The next day, 0.5 µl calf intestinal (alkaline) phosphatase (CIP) was added to the reaction mix and incubated at 45 °C for 45 min to remove 5'-phosphate groups from the free DNA ends. Subsequently, the linearized and dephosphorylated DNA was purified by phenol extraction. To this end, the reaction mix was adjusted to 100 µl with TE-buffer, an equal volume of phenol was added and sample thoroughly mixed for ~1 min. The sample was centrifuged at 20,817 x *g* for 5 min and the upper phase was transferred into a new 1.5 ml reaction tube. The sample volume was determined, an equal amount of chloroform-isoamyl alcohol (24:1) was added and thoroughly mixed for ~ 1 min. After centrifugation at 20,817 x *g* for 5 min, the upper phase was transferred into a new 1.5 ml reaction tube and the sample volume was determined. The sample was mixed with 0.7-fold the sample volume of ice-cold isopropanol, gently inverted, and incubated at -20 °C for 1 h, followed by centrifugation at 20,817 x *g* for 15 min. The obtained DNA was resuspended in TE-buffer, precipitated as described in 4.1.2, dissolved in an appropriate amount of TE-buffer and stored at 4 °C.

4.1.9.4 Ligation of the H1-FAP5(V_H-V_L)-S11(V_H-V_L)-FLAG insert and linearized pBSK-CMV

The *Not*I-digested and purified H1-FAP5(V_H-V_L)-S11(V_H-V_L)-FLAG insert described in 4.1.9.2 was ligated with the *Not*I-digested and dephosphorylated linear pBSK-CMV vector DNA described in 4.1.9.3. For ligation, insert and vector DNA were mixed to a molecular ratio of 5:1 (insert:vector) in 8 µl ddH_2O and 1 µl of T4 ligase buffer (10x) as well as 1 µl T4 ligase were added and incubated at RT for 30 min. Subsequently, 1 µl of the ligation mix was transformed in *E.coli* DH10β as described in 4.4.1 and bacteria were plated onto

LB-agar plates supplemented with 100 µg/ml Ampicillin and incubated at 37 °C o/n. The next day, single clones were picked and inoculated for small-scale plasmid preparation as described in 4.4.2. One clone carrying the correct pBSK-CMV_H1-FAP5(V_H-V_L)-S11(V_H-V_L)-FLAG plasmid was finally used for large-scale plasmid preparation as described in 4.4.3.

4.1.10 Cloning of pBSK-CMV_hFAP

The full-length amino acid sequence of human fibroblast activation protein (hFAP) was obtained from the UniProt data base (UniProt ID: Q12884). Upstream of the start codon, a Kozak sequence was added and *Not*I restriction sites were introduced at the 5'- and 3'-ends. The corresponding DNA sequence was codon optimized for *homo sapiens* expression and synthesized by GeneArts. Subsequent cloning of pBSK-CMV_hFAP was analogously performed as described for pBSK-CMV_H1-FAP5(V_H-V_L)-S11(V_H-V_L)-FLAG in section 4.1.9.

4.1.11 Isolation of viral DNA

Viral DNA was isolated from 200 µl viral stock solution (see 4.6.1.3) using the QIAmp DNA Mini Kit (250) (Qiagen) according to the manufacturers protocol. Eluted DNA was precipitated as described in 4.1.2 and finally resuspended in 20 µl TE-buffer at 4 °C o/n. The next day, the DNA concentration was determined as described in 4.1.1 and genome integrity was validated by enzymatic restriction analysis (see 4.1.3.1) and agarose gel electrophoresis (see 4.1.4). The obtained band patterns were compared to theoretical restriction patterns.

4.1.12 DNA extraction from tissue samples

DNA extractions from organs and tumors were performed using the GenElute Mammalian Genomic DNA Miniprep Kit (SigmaAldrich). A small piece of tissue (~ 10 mg) was incubated in 180 µl lysis buffer T (Kit) supplemented with 20 µl Proteinase K (Kit) at 56 °C, o/n. The next day, 20 µl RNAse were added, briefly vortexed and incubated at RT for 2 min. As a next step, 200 µl of Lysis buffer C (Kit) were added, thoroughly vortexed (10-15 sec) and incubated at 70 °C for 10 min. Meanwhile, a nucleic acid binding column was equilibrated by adding 500 µl column preparation solution (Kit), followed by

centrifugation at 20,817 x *g* for 1 min. The flow through was discarded, 200 µl 100% EtOH were added to the sample and thoroughly vortexed. The sample was loaded onto the equilibrated nucleic acid binding column and centrifuged at 20,817 x *g* for 10 min. The column was washed twice by adding 500 µl wash buffer (Kit), followed by centrifugation at 20,817 x *g* for 1 min. To elute bound DNA, 200 µl Tris-buffer were added, incubated at RT for 10 min and subsequently centrifuged at 20,817 x *g* for 1 min. Samples were either stored short-term at 4 °C or frozen at -20 °C for long term storage.

4.2 Protein based methods

4.2.1 SDS-PAGE

Either 100 µg total protein (CAP-T cell lysates) or 27µl of 18x concentrated CAP-T cell culture supernatant (see 4.5.6) was mixed with 10x SDS-loading buffer and heated at 96 °C for 5 min. Denatured samples were loaded on a 8% resolving gel with a 5% stacking gel and separated at 100 V for 2-4 h in SDS-running buffer. To determine protein sizes, 7 µl of Precision Plus Protein marker were loaded.

4.2.2 Silver staining

Silver staining was used to validate vector stock purity after vector purification (see 4.6.1). To this end, $1x10^{10}$ VPs were separated by SDS-PAGE (see 4.2.1) and protein bands were subsequently visualized by silver staining: First, protein gels were fixed in fixation buffer for 30 min and subsequently washed in 50% EtOH for 15 min. Proteins were equilibrated in equilibration buffer for 1 min, followed by three consecutive washing steps in ddH_2O for ~ 20 sec each. Next, proteins were impregnated in impregnation buffer for 20 min and again washed three times as described. Proteins were finally visualized by incubation in developing solution for 1-10 min. Finally, staining was stopped first by washing the gel in ddH_2O and subsequent transfer into stop solution for 5 min.

4.3 Biochemical methods

4.3.1 Western Blot analysis for detection of FAP5-S11-FLAG

Samples from SDS-PAGE (4.2.1) were transferred to a nitrocellulose membrane using wet-blot blotting technique at 100 V for 45 min in transfer buffer. The membrane was blocked in blocking buffer (TBS-T-buffer containing 5% skim milk powder) at RT for 1 h and subsequently incubated with primary antibody mouse α-FLAG-M2 (diluted 1:250 in TBS-T) at 4 °C, o/n, rotating. The membrane was washed three times in TBS-T for 15 min each and incubated with secondary antibody rabbit α-mouse-IgG (whole molecule)-HRP (diluted 1:20,000 in blocking buffer) at RT for 1 h. The membrane was washed as described and incubated in Super Signal West Pico solution for ~ 1 min. Signals were detected using an X-ray film (Amersham HyperfilmTM ECL) that was exposed to the membrane for ~3-5 min and developed using the Agfa CP 100 developing device.

4.3.2 ELISA to detect binding of FAP5-S11-FLAG to the HAdV-5 capsid

96-well flat bottom Maxi sorb ELISA plates were coated with $1x10^9$ vector particles per well, dissolved in 100 µl ELISA coating buffer at 4 °C, o/n. The next day, plates were washed three times with 200 µl/well washing buffer and blocked with 150 µl/well SuperBlock™ at RT for 1 h. Plates were washed five times as described and 150 µl/well of 18x concentrated CAP-T cell culture supernatant (see 4.5.6) at the indicated dilution were added. Plates were incubated at RT for 1 h and subsequently washed five times as described. Subsequently, 150 µl/well of primary antibody mouse α-FLAG-M2 (1:2000 in DPBS) were added and incubated at RT for 1 h. Again, plates were washed five times as described and incubated with 150 µl/well of secondary antibody rabbit α-mouse-IgG (whole molecule)-HRP antibody (1:10,000 in DPBS) at RT for 1 h. Plates were washed as described and 100 µl/well of 1-step ultra TMB-ELISA substrate were added and incubated at RT for 5-30 min. Substrate turnover was stopped by adding 100 µl of 2 M H_2SO_4 and quantified by optical density measurement at 450 nm using the Multiscan EX ELISA-Reader.

4.3.3 Detection of cell surface receptor expression and FAP5-S11-FLAG binding to hFAP by flow cytometric analysis

Indicated cells were washed with DPBS and detached using TrypLE select. Fully detached cells were resuspended in DPBS containing 10% FBS and subsequently centrifuged at 180 x *g* for 10 min. Cells were washed twice with DPBS, resuspended in an appropriate volume of DPBS containing 0.5% FCS (PBS/FCS) and counted as described in 4.5.3. As a next step, cells were diluted to a final concentration of $1x10^6$ cells/ml in PBS/FCS and incubated with 5 µl/ml human Fc receptor (human) blocking reagent at 4 °C for 30 min, rotating. Subsequently, cells were washed twice with 200 µl PBS/FCS and $2x10^5$ cells were incubated with indicated primary antibodies at 4 °C for 1 h. Cells were washed three times as described and incubated with indicated secondary antibodies at 4 °C for 1 h in the dark. After incubation with antibodies, cells were again washed as described, resuspended in an appropriate volume of PBS/FCS and analyzed by flow cytometric analysis using the CytoFLEX flow cytometer.

4.3.3.1 Detection of EGFR

A549, UD-SCC-2, UM-SCC-11B and SK-Mel-28 cells were incubated with primary mouse α-human EGF receptor antibody (diluted 1:100 in PBS/FCS) and secondary sheep α-mouse IgG-FITC antibody (diluted 1:50 in PBS/FCS).

4.3.3.2 Detection of the human fibroblast activation protein (hFAP)

HEK293T, HeLa, HEK293ThFAP, and HeLahFAP (both established by transient transfection (see 4.5.4) with pBSK-CMV_hFAP (see 4.1.10)) cells were incubated with primary mouse α-fibroblast activation protein antibody (diluted 1:200 in PBS/FCS) and secondary sheep α-mouse IgG-FITC antibody (diluted 1:50 in PBS/FCS).

4.3.3.3 Binding of FAP5-S11-FLAG to hFAP

HEK293T, HeLa, HEK293ThFAP and HeLahFAP (both established by transient transfection (see 4.5.4) with pBSK-CMV_hFAP (see 4.1.10)) were incubated with 18x concentrated cell culture supernatants of pBSK-CMV_H1-FAP5(V_H-V_L)-S11(V_H-V_L)-FLAG transfected CAP-T cells (see 4.5.6) at 4 °C for 1 h. As a negative control, 18x concentrated cell culture supernatants of untransfected CAP-T cells were used. Cells were washed three times with 200 µl PBS/FCS and incubated with primary mouse α-FLAG-M2 antibody (diluted 1:200 in PBS/FCS) and secondary sheep α-mouse IgG-FITC antibody (diluted 1:50 in PBS/FCS).

4.3.4 Immunohistochemical staining of cell lines

SK-Mel-28 or UD-SCC-2 cells were seeded on glass slides within 24-plates as described in 4.5.3 and cultivated under standard conditions, o/n. The next day, cells were washed with 500 µl DPBS and fixed in 4% PFA at RT for 15 min. Cells were washed twice with DPBS and blocked with blocking buffer (5% BSA, 10% FCS, dissolved in DPBS) at RT for 1 h. Subsequently, cells were incubated with 250 µl of the indicated antibodies. All antibodies and Affilin were diluted in REAL™ antibody diluent and cell nuclei were stained with 4′,6-diamidino-2-phenylindole (DAPI) at RT for 1 min. After staining, cells were covered with fluorescence mounting medium for fluorescence microscopic evaluation.

4.3.4.1 Detection of EGFR

Cells were incubated with primary antibody mouse α-EGFR (diluted 1:100) at 4 °C, o/n. The next day, cells were washed three times with DPBS and incubated with secondary antibody goat α-mouse IgG-Alexa488 (diluted 1:500) at RT for 3 h.

4.3.4.2 Binding of Affilin to EGFR

Cells were incubated with Strep-tagged Affilin (250 nM) at 4 °C, o/n. The next day, cells were washed three times with DPBS and incubated with rabbit α-Strep Tag antibody (diluted 1:500) at RT for 1 h. Cells again were washed three times with DPBS and incubated with secondary antibody goat α-rabbit-IgG-Alexa594 (diluted 1:500) at RT for 3 h.

4.3.5 Immunohistochemical staining of snap-frozen tumor sections

Cryo-sections of snap-frozen and TissueTek embedded tissue samples with a thickness of 6 µm were prepared using the Leica cryostat and air-dried at RT, o/n. The next day, tissue sections were fixed twice in ice-cold acetone for 15 min and blocked with blocking buffer (5% BSA and 10% goat serum dissolved in DPBS) at RT for 1 h. To analyze for tissue vascularization, sections were incubated with primary antibody rat α-mouse CD31 (diluted 1:200) and secondary antibody goat α-rat IgG Alexa488 (diluted 1:500). For detection of EGFR, sections were incubated with primary antibody mouse α-EGFR (diluted 1:100) and secondary antibody goat α-mouse-IgG Alexa594 (diluted 1:500). Binding of Affilin was analyzed using Strep-tagged Affilin (250 nM) followed by incubation with rabbit α-Strep-Tag antibody (diluted 1:500) at RT for 1 h and secondary antibody goat α-rabbit-IgG Alexa594 (diluted 1:500). All antibodies and Affilin were diluted in REAL™ Antibody diluent. Incubation with primary antibodies and Affilin was performed at 4 °C o/n and after three consecutive washing steps by incubation in DPBS for 5 min each, tissue sections were incubated with secondary antibodies at RT for 3 h. After three additional washing steps, cell nuclei were stained with DAPI at RT for ~ 1 min, washed again three times and covered with fluorescence mounting medium for fluorescence microscopic evaluation.

4.4 Bacteria based methods

4.4.1 Transformation of *Escherichia coli* (*E.coli*) DH10β

E.coli DH10β were thawed on ice and diluted 1:10 in ddH_2O in a final volume of 20 µl. As a next step, 100 ng of either plasmid or bacmid DNA, dissolved in 1 µl ddH_2O were added, gently mixed, and incubated on ice for ~1 min. Cells were transferred into a precooled electroporation cuvette and electroporated (electric field strength of E = 12.5 kV/cm). Subsequently, cells were swiftly transferred to 500 µl LB medium and incubated at 37 °C and 800 rpm for 30 min, if not stated otherwise. Cells were plated onto LB-agar dishes containing the respective selection antibiotic(s) and incubated at 37 °C for 12-16 h, if not stated otherwise.

4.4.2 Small scale plasmid preparation

A single colony of *E.coli* DH10β transformed with either pBSK-CMV_H1-FAP5(V_H-V_L)-S11(V_H-V_L)-FLAG (see 4.1.9) or pBSK-CMV_hFAP (see 4.1.10) was inoculated into 1.8 ml LB-medium containing 100 µg/ml ampicillin and incubated at 37 °C at 800 rpm, o/n. The next day, 10 µl of the o/n culture was used to inoculate 1.8 ml of fresh LB-medium containing 100 µg/ml ampicillin followed by cultivation at 37 °C at 800 rpm over the day. The remaining o/n culture was centrifuged at 20,817 x *g* and supernatant was aspirated. The obtained pellet was resuspended in 200 µl TELT-buffer and incubated at 96 °C for 3 min, followed by incubation on ice for additional 5 min. Subsequently, the lysate was centrifuged at 20,817 x *g* for 10 min to precipitate cell debris and the cleared supernatant was transferred into a new 1.5 ml reaction tube. The sample was mixed with 100 µl of ice-cold isopropanol, gently inverted several times and again centrifuged at 20,817 x *g* for 10 min. Supernatant was aspirated and precipitated DNA was overlayed with 100 µl of 70% EtOH. After centrifugation at 20,817 x *g* for 10 min, the supernatant was removed, the obtained DNA pellet was air-dried several minutes and dissolved in 20 µl TE-buffer. To verify for the correct plasmid sequence of pBSK-CMV_H1-FAP5(V_H-V_L)-S11(V_H-V_L)-FLAG and pBSK-CMV_hFAP, 5 µl of purified plasmid DNA were used for enzymatic DNA digestion (see 4.1.3.1) and subsequent agarose gel electrophoresis (see 4.1.4). One clone showing the correct band pattern was chosen to inoculate large scale plasmid preparation. To this end, 200 ml of LB-medium containing 100 µg/ml Ampicillin were inoculated with 50 µl of the over day culture of the respective clone and cultivated at 37 °C and 300 rpm, o/n.

4.4.3 Large scale plasmid preparation

Large scale plasmid preparations were performed using the Qiagen Plasmid Midi Kit according to the manufactures protocol. Inoculated o/n culture (see 4.4.2) was centrifuged at 4,400 x *g* for 20 min, the supernatant was discarded and the obtained bacteria pellet resuspended in 10 ml buffer P1 (resuspension buffer). Subsequently, 10 ml buffer P2 (lysis buffer) were added, gently inverted, and incubated at RT for 5 min. Cell lysis was stopped by addition of 10 ml buffer P3 (neutralization buffer), gentle mixing and incubation on ice for 15 min, followed by centrifugation at 26,640 x *g* for 30 min. A genomic-tip 500G

DNA purification column (Qiagen) was equilibrated with 10 ml buffer QBT (equilibration buffer) and the cleared cell lysate was loaded onto the column. The column was washed twice with 30 ml buffer QC (wash buffer) and bound plasmid DNA was eluted by adding 15 ml buffer QF (elution buffer). Subsequently, 10.5 ml of ice-cold isopropanol were added to the eluate, gently inverted, and incubated at -20 °C for at least 1 h. Afterwards, the solution was centrifuged at 2,241 x *g* for 30 min and the supernatant was discarded. The obtained DNA pellet was resuspended in 300 µl TE-buffer and precipitated as described in 4.1.2. The obtained DNA pellet was air dried, resuspended in an appropriate volume of TE-buffer and stored at 4 °C until further use.

4.4.4 Small scale bacmid preparation

Small scale bacmid preparation was performed using buffers of the Qiagen Plasmid Maxi Kit. A single colony of transformed *E.coli* DH10β (see 4.4.1) was inoculated into 1.8 ml of LB-medium containing the respective antibiotic(s) and incubated at 37 °C and 800 rpm, o/n if not stated otherwise. The next day, and in case of a planned large-scale bacmid preparation, 5 ml of fresh LB-medium containing the respective antibiotic(s) was inoculated with 50 µl of the o/n culture and incubated at 37 °C and 800 rpm over the day. The remaining o/n culture was centrifuged at 20,817 x *g* for 1 min, the supernatant was aspirated and the obtained pellet resuspended in 200 µl buffer P1 (resuspension buffer). As a next step, 200 µl buffer P2 (lysis buffer) were added, gently mixed, and incubated at RT for 5 min. Subsequently, 200 µl buffer P3 (neutralization buffer) were added, mixed, and incubated on ice for 15 min. Cell debris was separated by centrifugation at 20,817 x *g* for 15 min and the cleared supernatant was transferred into a new 1.5 ml reaction tube. The cleared cell lysate was mixed with 500 µl ice-cold isopropanol, gently inverted several times, incubated at -20 °C for at least 1 h and subsequently centrifuged at 20,817 x *g* for 15 min. The supernatant was gently removed and precipitated DNA was overlaid with 70% EtOH, followed by centrifugation at 20,817 x *g* for 15 min. Again, the supernatant was removed and the obtained DNA pellet was air dried and dissolved in 25 µl deionized water for 1 h at 37 °C. For enzymatic digestion analysis (see 4.1.3.1), 20 µl of the obtained DNA sample was used and analyzed by agarose gel electrophoresis (see 4.1.4). One clone showing the correct band pattern was chosen to inoculate large scale bacmid preparation.

To this end, 1 l of LB-medium, containing the respective antibiotic(s) was inoculated with the over day culture of the respective clone and incubated at 37 °C and 300 rpm, o/n.

4.4.5 Large scale bacmid preparation

Large scale bacmid purification was performed using the Qiagen large construction Kit. A single colony of bacmid-transformed *E.coli* DH10β (see 4.4.1) was inoculated into 5 ml LB-medium containing the respective antibiotic(s) and cultivated at 37 °C and 300 rpm over day. The obtained bacteria culture was used to inoculate 1 l of LB-medium containing the respective antibiotic(s) following cultivation at 37 °C at 300 rpm, o/n. The next day, bacteria were harvested by centrifugation of the o/n culture at 4,400 x *g* for 20 min. The supernatant was discarded and the obtained pellet was resuspended in 40 ml buffer P1 (resuspension buffer). As a next step, 40 ml buffer P2 (lysis buffer) were added, inverted several times, and incubated at RT for 5 min. To stop cell lysis, 40 ml of buffer P3 (neutralization buffer) were added to the lysate, inverted several times, and incubated on ice for 15 min. Cell debris was separated by centrifugation at 26,640 x *g* for 30 min and the cleared cell lysate was transferred into a new 50 ml falcon through a cell strainer to remove any remaining cell debris. Cleared cell lysate was mixed with ice-cold isopropanol according to 0.7-fold the volume of the lysate, gently inverted several times, and incubated at -20 °C for at least 1 h. The sample was centrifuged at 26,640 x *g* for 30 min and supernatant was discarded. The obtained DNA pellet was gently overlaid with 70% EtOH and again centrifuged at 26,640 x *g* for 30 min. Again, the supernatant was discarded and the obtained DNA pellet was air-dried several minutes. Subsequently, 10 ml of buffer P1, P2 and P3 each were mixed, centrifuged at 2,241 x *g* for 10 min and the obtained clear phase was transferred into a new 50 ml falcon. A genomic-tip 500G DNA purification column was equilibrated with 10 ml of equilibration buffer QBT (Qiagen). The air-dried DNA was resuspended in a total volume of 20 ml buffer P1/P2/P3 and added to the equilibrated genomic-tip 500G DNA purification column. After the sample has passed through, the column was washed twice with 30 ml buffer QC (wash buffer) and DNA was subsequently eluted into a new 50 ml falcon tube by adding 15 ml of pre-warmed (65 °C) buffer QF (elution buffer) to the column. The obtained eluate was overlayed with 10.5 ml ice-cold isopropanol, gently inverted several times, incubated at -20 °C for at least 1 h and subsequently centrifuged at 2,241 x *g* for 20 min. Supernatants were discarded and the

obtained DNA pellet was air-dried for several minutes. After resuspending the DNA in 300 µl TE-buffer, it was precipitated as described in 4.1.2, dissolved in 25-50 µl TE-buffer and stored at 4 °C.

4.4.6 Homologous recombination

To generate HAdV-5 mutants, site-directed mutagenesis was performed using the Red/ET Counter-Selection BAC Modification Kit by Gene Bridges.

4.4.6.1 Basic principle of homologous recombination in bacteria

Homologous recombination provides the possibility to perform site-directed mutagenesis at any region within bacmid DNA in bacteria. It relies on the *E.coli* DH10β strain, which inherently harbors resistance against streptomycin (Strep) due to a single point mutation within the *rpsL* gene. In a first step, *E.coli* DH10β become co-transformed with bacmid DNA encoding the HAdV-5 genome and the Red/ET plasmid encoding the lambda phage proteins redα (a 5'->3´ exonuclease) and redβ (DNA annealing protein) under regulation of an L-Arabinose-inducible promotor. As a second step, a functional rpsL-neo cassette becomes inserted into the region of interest within the target bacmid DNA via homologous recombination, mediated by the redα and redβ proteins. Insertion of the rpsL-neo cassette re-sensitizes *E.coli* DH10ß for streptomycin, however, confers resistance against kanamycin. Thus, bacteria harboring a bacmid with the inserted rpsL-neo cassette can be efficiently selected using kanamycin. In a third step, the rpsL-neo cassette becomes substituted by a sequence of interest, likewise mediated by the redα and redβ proteins. Consequently, bacteria become kanamycin sensitive, however, streptomycin resistant again, which allows for final counter-selection of bacteria harboring the desired mutated bacmid DNA. The required DNA fragments, either encoding the rpsL-neo cassette or the sequence of interest are generated by PCR and carry flanking sequences that are homologous to the region of interest within the target bacmid. The primers and templates used to generate these fragments are listed in section 3.15.1. A schematic illustration about the basic principle of homologous recombination is shown in figure 9.

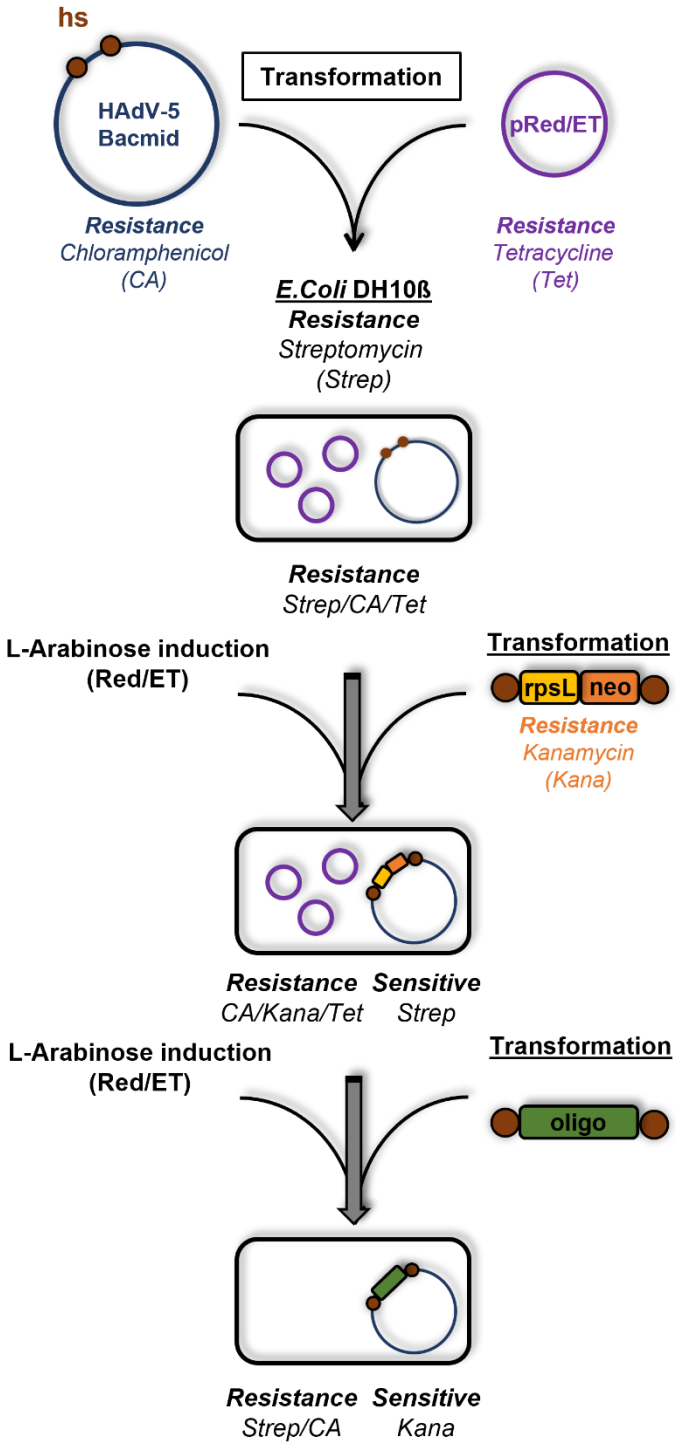

Figure 9: Schematic workflow of homologous recombination in *E.coli* DH10ß using the Red/ET counter selection BAC modification Kit.
hs=homologous sequences; Strep=Streptomycin; CA=Chloramphenicol; Kana=Kanamycin; Tet=Tetracycline

4.4.6.2 Protocol of homologous recombination

Streptomycin (Strep)-resistant *E.coli* DH10β were transformed as described in 4.4.1 with 10 ng Red/ET plasmid (encoding tetracycline (Tet) resistance) and 100 ng bacmid DNA (see 3.5.1) carrying the respective HAdV-5 genome (encoding chloramphenicol (CA) resistance), plated onto LB-agar plates supplemented with 20 µg/ml CA, 20 µg/ml Strep and 3 µg/ml light-sensitive Tet and cultivated at 30 °C in the dark, o/n.

After 24 h, about 10 single colonies were pooled into 1.8 ml LB(CA/Strep/Tet)-medium and cultivated at 30 °C and 800 rpm in the dark, o/n. The next day, 1.4 ml of fresh LB(CA/Strep/Tet)-medium was inoculated with 10 µl of the o/n culture and incubated at 30 °C and 800 rpm in the dark for exactly 2 h. As a next step, 50 µl of freshly prepared L-Arabinose solution (100 mg/ml dissolved in LB-medium) were added to the culture and incubated at 35 °C and 800 rpm for 1 h to induce expression of the redα and redβ proteins. To re-establish electro-competence, bacteria were centrifuged at 16,356 x *g* at 4 °C, washed twice with 1 ml of ice-cold ddH_2O and resuspended in 20 µl ice-cold ddH_2O. Bacteria were transformed with 200 ng of PCR-amplified rpsL-neo fragment (see 4.4.1) and regenerated in 500 µl LB-medium at 30 °C and 800 rpm for 1 h. After regeneration, bacteria were plated onto LB-agar plates supplemented with 20 µg/ml CA, 3 µg/ml Kanamycin (Kana) and 3 µg/ml Tet and cultivated at 30 °C in the dark for 24 h.

The next day, single colonies were picked and resuspended in 50 µl LB-medium. Half of the volume was used to inoculate 1.8 ml of either LB(CA/Kana/Tet)- or LB(CA/Strep/Tet)-medium, respectively following cultivation at 30 °C and 800 rpm in the dark, o/n. LB(CA/Strep/Tet) cultures were used as a negative selection for successful insertion of the rpsL-neo cassette, as bacteria harboring a functional rpsl-neo cassette become Strep-sensitive. The next day, o/n cultures were evaluated for bacteria growth and only colonies grown in LB(CA/Kana/Tet)-medium but not in LB(CA/Strep/Tet)-medium were further used. Subsequently, 1.4 ml fresh LB(CA/Kana/Tet)-medium was inoculated with 10 µl of o/n cultures and put on ice until needed (see below). The remaining o/n cultures were used for small scale bacmid preparation as described in 4.4.4 and purified bacmid DNA was analyzed by enzymatic restriction analysis (see 4.1.3.1) for correct insertion of the rpsL-neo cassette. The previously inoculated 1.4 ml culture of one positive

clone was incubated at 30 °C and 800 rpm in the dark for exactly 2 h, followed by induction of redα and redβ expression by addition of L-Arabinose as described above. Electro-competence was re-established as described and bacteria were transformed with 200 ng of PCR fragment, encoding the mutated sequence of interest. After regeneration in 500 µl LB-medium at 37 °C for 1 h, bacteria were plated onto LB(CA/Strep)-agar plates and incubated at 37 °C, o/n. The next day, single colonies were picked and resuspended in 50 µl LB-medium, from which half of the volume was used to inoculate either 1.8 ml LB(CA/Strep)- or LB(CA/Kana)-medium, respectively followed by cultivation at 37 °C at 800 rpm, o/n. This time, LB(CA/Kana) cultures were used as a negative selection as those bacteria with successful insertion of the mutation-carrying DNA fragment become Kana-sensitive due to substitution of the rpsL-neo cassette. Consequently, only single clones growing in LB(CA/Strep)-, however, not LB(CA/Kana)-medium were used for further analysis.

The next day, 5 ml of fresh LB(CA/Strep)-medium was inoculated with 50 µl of o/n culture and cultivated at 37 °C and 300 rpm over the day. The remaining o/n cultures were used to perform small scale bacmid preparation as described in 4.4.4 and purified bacmid DNA was analyzed for correct insertion of the mutated DNA sequence by enzymatic restriction analysis (see 4.1.3.1). The over day culture of one clone showing the expected band pattern was used to inoculate large scale bacmid preparation as described in 4.4.5.

4.5 Cell culture methods

4.5.1 Cultivation of adherent cell lines and primary cells

Adherent cell lines and primary cells were cultured on 15 cm dishes at 37 °C, 5% CO_2 and 90% relative humidity, further referred to as standard conditions. Cells were incubated in the respective cell culture media listed in table 10. Dulbecco's Modified Eagle Medium (DMEM), Minimum Essential Medium (MEM) and α-MEM were supplemented with 10% fetal bovine serum (FCS) and 1x Penicillin-Streptomycin-Glutamine (PSG). Small Airway Epithelial Cell Growth Medium was supplemented with growth medium supplement mix. For maintenance, cells were passaged twice a week. To this end, cells were washed with 10 ml Dulbecco's Phosphate Buffered Saline (DPBS) once and incubated with 3 ml 0.05% trypsin-EDTA solution under standard conditions. Fully detached cells were resuspended

in fresh cell culture medium and seeded onto new 15 cm dishes, according to the split ratios of the respective cell line listed in table 10.

Table 10: Cell culture media and split ratios for the respective cell lines and primary cells

Adherent cell culture

Cell line	Medium	Split ratio
A431	DMEM	1:10
A549	MEM	1:8
CMT-64	DMEM	1:8
N52.E6	MEM	1:3
HEK293T	DMEM	1:12
Hepa 1-6	α-MEM	1:5
SCC-VII	RPMI	1:7
SK-Mel-28	DMEM	1:3
UD-SCC-2	DMEM	1:6
UM-SCC-11B	DMEM	1:10
HSAEpC (primary cells)	Small Airway Epithelial Cell Growth Medium	1:2

4.5.2 Cultivation of CAP-T suspension cells

CAP-T cells were cultured in protein expression medium (PEM) in 125 ml shaking flasks at 175 rpm under standard conditions. For maintenance, cell densities were adjusted twice a week. To this end, cells were counted as described in 4.5.3 and diluted to a final density of $5x10^5$ cell/ml within a total volume of 30 ml.

4.5.3 Cell counting and cell seeding

10 µl of cell suspension was transferred into a Neubauer counting chamber. Cell numbers within four big squares, according to a volume of 0.1 µl were counted and the average cell count was calculated. Cell concentrations were calculated according to the given formula:

$$\mathrm{c\ (cells/ml)} = \mathrm{\emptyset\ cell\ count} * 10^4 * \mathrm{dilution\ factor}$$

For seeding, cells were diluted to the desired concentration in a volume according to the respective seeding format. Cell numbers and volumes used for respective plate formats are listed in table 11.

Table 11: Cell amounts and volumes used for cell seeding according to the respective format

Format	Cells/well	Volume/well
96-well plate	2×10^4	200 µl
24-well plate	1×10^5	1 ml
6-well plate	5×10^5	3 ml
6 cm dish	1×10^6	5 ml

4.5.4 Transfection of adherent cell lines

Cells were seeded as described in 4.5.3 and cultivated under standard conditions, o/n. The next day, cells were washed once with DPBS and fresh cell culture medium was added. DNA transfection was performed using the PEI MAX transfection reagent. PEI MAX and DNA in a quantitative ratio of 3:1 were separately diluted in equal volumes of serum free cell culture medium according to the respective transfection format listed in

table 12. Subsequently, the PEI MAX solution was added to the DNA, vortexed for ~5 sec, incubated at RT for 10 min and added to the cells.

Table 12: Amounts of DNA and PEI MAX used for transfection of adherent cells at the respective format

Format	DNA	PEI MAX
24-well plate	500 ng in 25 µl	1.5 µg in 25 µl
	750 ng in 25 µl	2.25 µg in 25 µl
	1 µg in 25 µl	3 µg in 25 µl
6-well plate	2 µg in 150 µl	6 µg in 150 µl
6 cm dish	5 µg in 500 µl	15 µg in 500 µl

4.5.5 Transfection of CAP-T suspension cells

CAP-T cells were counted as described in 4.5.3 and $4.5x10^7$ cells were transferred into a 15 ml falcon tube and centrifuged at 180 x *g* for 10 min. Supernatants were aspirated and cells were resuspended in 10 ml fresh Freestyle medium, followed by centrifugation at 180 x *g* for 10 min. The supernatant again was aspirated and cells were resuspended in 3 ml Freestyle medium. As a next step, 45 µg of DNA and 135 µg of PEI MAX were separately diluted in 1.5 ml of Freestyle medium each. The PEI MAX solution was added to the DNA, vortexed for ~ 5 sec, incubated for 10 min at RT and added to the prepared cell suspension. Cells were cultivated under the described conditions (see 4.5.2) for 5 hours before 9 ml PEM were added to the cells, followed by further incubation at 175 rpm under standard conditions.

4.5.6 Production of the FAP5-S11-FLAG bispecific adapter molecule

The FAP5-S11-FLAG bispecific adapter molecule was produced in CAP-T suspension cells. To this end, cells were transfected with the pBSK-CMV_H1-FAP5(V_H-V_L)-S11(V_H-V_L)-FLAG expression plasmid as described in 4.5.5. Five days after transfection, cells and cell culture supernatants were harvested by centrifugation at 180 x *g* for 10 min. Depending on the intended use, supernatants were either sterile filtrated through a 0.45 µm filter or loaded onto a 30 kDa cut off Amicon and centrifuged at 4500 x *g* until 18x concentrated.

4.6 HAdV-5 vector methods

4.6.1 Production of HAdV-5 vectors

E1-deleted HAdV-5 vectors were amplified and produced in *E1*-transcomplementing N52.E6 cells. Replication competent and conditionally replicating HAdV-5 vectors were amplified and produced in A549 cells.

4.6.1.1 Transfection of cells with linearized HAdV-5 genome

A549 and N52.E6 cells were seeded onto 24-well plates as described in 4.5.3. The next day, cells were transfected with linearized (see 4.1.3.3) and purified (see 4.1.5) bacmid DNA carrying the HAdV-5 genome as described in 4.5.4.

4.6.1.2 Vector amplification

Transfected A549 or N52.E6 cells from 4.6.1.1 were cultivated for 5-10 days under standard conditions until a cytopathic effect was observed. If cells tend to overgrow, they were expanded to 6 cm dishes. As soon as a cytopathic effect became visible, cells were harvested by scraping and lysed by three consecutive freeze-thaw cycles by snap-freezing them in liquid nitrogen and thawing at 37 °C. The obtained cell lysates were used for re-infection of new cells in a 10 cm dish format. Two days after re-infection, cells were harvested and again subjected to freeze-thaw lysis as described. The obtained cell lysates were used to re-infect two 15 cm dishes and infected cells again were harvested and lysed 48 h after re-infection. Volumes ranging between 2 µl and 100 µl of the obtained cell lysates were finally utilized to infect 6 cm dishes for titration experiments in order to

determine the optimal volume of lysate for re-infection of 15 cm dishes. Finally, twenty 15 cm dishes were infected with the optimal amount of cell lysate.

4.6.1.3 Vector purification by CsCl-gradient ultracentrifugation

Infected cells from 4.6.1.2 (20x15 cm dishes) were harvested by scraping 48 h post infection, centrifuged at 300 x *g* for 10 min and the obtained cell pellet was resuspended in 3 ml HEPES-buffer. Cells, infected with HAdV-5-HexPos3 vectors were resuspended in HEPES-buffer containing 250 mM NaCl to avoid charge-mediated binding of vector particles to cell debris. HAdV-5 vectors were purified by two consecutive CsCl-gradients for the removal of cell culture related impurities and incomplete vector particles. Subsequently, a size exclusion chromatography was performed to desalt the vector-containing sample.

Vector-infected and harvested cells were lysed by three consecutive freeze-thaw cycles, centrifuged at 1942 x *g* for 10 min and the obtained supernatant was used for vector purification (vector sample). In case of HexPos3 capsid-mutated vectors, vector samples were incubated with five units benzonase at 37 °C for 30 min to digest cellular nucleic acids. As a next step, a discontinuous CsCl-gradient was prepared. To this end, 3 ml of CsCl-buffer 1 (ϱ=1.41 g/ml) were gently overlayed with 5 ml of CsCl-buffer 2 (ϱ=1.27 g/ml) within an Ultraclear centrifugation tube. On top of the gradient, the vector sample was loaded and centrifuged at 176,000 x *g* at 4 °C for 2 h using the Optima XE-90 Ultracentrifuge. The obtained vector band was aspirated by punctuation of the tube using a syringe with Sterican® 0.9 x 40 mm 20G canula and was collected in new Ultraclear centrifugation tube. As a second purification step, a continuous CsCl-gradient was performed. To this end, the sample was mixed with CsCl-buffer 3 (ϱ1.34 g/ml) and centrifugated at 176,000 x *g* at 4 °C for 20 h. The formed vector band again was aspirated as described, in which care was taken to not exceed a total sample volume of 2.5 ml. A PD-10 column was equilibrated with 5 x 5 ml HEPES buffer. Subsequently, the vector sample with a total volume of 2.5 ml was added to the column and the flow through was discarded. For elution, 5 ml of HEPES buffer were added and five fractions of 1 ml each were collected. Fractions two and three, containing the purified and desalted vector

particles, were pooled and the total volume was determined. The sample was supplemented with 10% glycerol, aliquoted and stored at -80 °C.

4.6.1.4 Determination of vector particle titers

Vector particle titers of purified vectors (see 4.6.1.3) were determined by optical density measurement. To this end, 40 µl of purified virus stock solution (see 4.6.1.3) were mixed with 2 µl of 10% SDS and 158 µl of HEPES buffer and heated to 56 °C for 10 min. For blank measurement, the virus stock solution was replaced by 36 µl HEPES-buffer and 4 µl glycerol. Subsequently, the optical density of the sample was measured at a wavelength of 260 nm (OD_{260}) and titers were calculated, utilizing the empirically determined equation that 1.1 x 10^9 viral particles per µl equals one OD_{260} unit. Due to sample dilution of 1:5, the titer was calculated by the following formula:

$$c\left(\frac{\text{Viral particles}}{\mu l}\right) = OD_{260} * (1.1 * 10^9) * 5$$

4.6.2 HAdV-5 cell transduction and infection

Cells were seeded onto nunclon® Δ-coated, flat bottom 96-Well plates as described in 4.5.3 and cultivated under standard conditions, o/n. The next day, cells were washed once with 100 µl DPBS and 100 µl of serum free cell culture medium was added per well. For transduction assays, HAdV-5 vectors were dissolved in 100 µl serum free cell culture medium to the indicated particle multiplicity of infection (pMOI) and added to the cells. For transduction assays in murine plasma, vector particles/well dissolved in a total volume of 2 µl were mixed with 10 µl NOD SCID gamma (NSG) plasma and incubated at 37 °C for 10 min. Pre-incubated vector particles were diluted in serum free cell culture medium to a final volume of 100 µl and added to the cells. Three hours post transduction (hpt), the vector-containing medium was removed, cells were washed once with 200 µl DPBS and 200 µl fresh cell culture medium ware added per well. Transduction efficiencies were evaluated 24 hpt using flow cytometric analysis as described in 4.6.5.

4.6.3 Crystal violet staining for cytotoxicity assay

Cells were seeded onto nunclon® Δ-coated, flat bottom 96-Well plates as described in 4.5.3 and cultivated under standard conditions, o/n. The next day, 100 µl of cell culture medium were removed from each well and substituted with 100 µl of fresh cull culture medium containing either HAdV-5wt or the respective conditionally replicating vector at the indicated pMOI. Depending on the cell line, infected cells were cultivated under standard conditions for 7-14 days to allow for virus replication and spread. After the indicated period, cells were stained using crystal violet: First, the vector-containing medium was removed and cells were washed twice with 200 µl DPBS. Cells were fixed in 100 µl 4% PFA at RT for 15 min, followed by washing once with DPBS. Fixed cells were stained by adding 50 µl of 0.1% crystal violet solution dissolved in ddH_2O per well for ~2 min. After removal of the crystal violet solution, cells were washed three times with DPBS and were subsequently air dried for several minutes before pictures were taken.

4.6.4 Retargeting of HAdV-5 vectors to the fibroblast activation protein

Retargeting of eGFP-encoding HAdV-5-based vectors to the human fibroblast activation protein (hFAP) was evaluated in HEK293T cells transiently expressing hFAP (HEK293ThFAP). To this end, HEK293T cells were seeded onto 6-Well plates as described in 4.5.3 and transfected with pBSK-CMV_hFAP as described in 4.5.4. As a negative control, HEK293T cells were transfected with an empty plasmid pBSK-CMV (see 3.16.1), which has been generated previously to the present study by the Department of Gene Therapy at University Ulm. Twenty-four hours post transfection, 1 x 10^9 VPs of HAdV-5_ΔCAR (referring to a pMOI of 1000) were mixed with 3 ml sterile filtrated cell culture supernatant of pBSK-CMV_H1-FAP5(V_H-V_L)-S11(V_H-V_L)-FLAG-transfected CAP-T cells (see 4.5.6) and incubated at RT for 30 min, rotating. As a control, HAdV-5_ΔCAR vectors were analogously incubated in either cell culture supernatant of untransfected CAP-T cells or fresh PEM medium. HEK293T and HEK293ThFAP cells were washed once with DPBS and pre-incubated HAdV-5_ΔCAR particles were added to the cells. Three hours post transduction, the vector-containing supernatants were aspirated, cells were washed twice with DPBS and 3 ml of fresh cell culture medium were

added per well. Transduction efficiencies were evaluated 24 hpt by fluorescence microscopy.

4.6.5 Evaluation of transduction efficiencies by flow cytometry

Cells, transduced with eGFP-encoding HAdV-5 vectors were washed with DPBS once and detached with TrypLE select (96-well plate: 50 µl; 24-well plate: 100 µl; 6-well plate: 250 µl). Once cells were detached, equal volumes of Flow Cytometry-buffer were added, cells rinsed, and 100-200 µl of cell suspension were transferred into U-bottom 96-Well plates. Transduction efficiencies were evaluated using the CytoFLEX flow cytometer. Viable cell populations were gated according to their forward and sideward scattered characteristics and single cells were gated according to the forward scatter height and width of the viable cell population. Transduction efficiencies were evaluated by quantification of eGFP-positive cells or the mean fluorescence intensity (MFI) within a total of 8000 cells according to the single cell population.

4.7 *In vivo* experiments

4.7.1 Murine plasma

Murine blood was anticoagulated with 1 µg/µl Argatroban dissolved in DPBS. To remove blood cells, samples were centrifuged at 800 x *g* for 10 min, the cleared plasma was transferred into a new 1.5 ml reaction tube and stored at -20 °C.

4.7.2 Establishment of xenograft models

Two days before subcutaneous tumor cell injection, A431, UM-SCC-11B, and SK-Mel-28 cells were split onto 15 cm dishes according to their split ratios (see 4.5.1) and cultivated under standard conditions to sub-confluency. At the day of tumor cell injection, cells were detached with TrypLE select and resuspended in cell culture medium (see 4.5.1). Cells were centrifuged at 180 x *g* for 10 min and supernatants were discarded. Cells were washed twice with 10 ml DPBS and centrifuged as described. Washed cells were resuspended in 1 ml DPBS and counted as described in 4.5.3 using three independent 1:100 dilutions of the cell suspension. Subsequently, cells were diluted to the required concentration. For a single injection, A431 (cell numbers injected: $5x10^5$, $1x10^6$, $5x10^6$),

UM-SCC-11B (cell numbers injected: $5x10^5$, $1x10^6$, $3.3x10^6$) and SK-Mel-28 (cell numbers injected: $5x10^5$, $1x10^6$, $5x10^6$) were diluted in 50 µl aliquots and thoroughly mixed with 50 µl growth factor reduced Matrigel. Subsequently, cells were subcutaneously injected into previously razored left flanks of NSG mice using Omnifix-F® 1 ml syringes with Sterican® Ø20 0.40 x 20 mm 27G cannulas. For tumor growth kinetic studies, 8-10 weeks old NSG mice were used. Upon tumor cell injection, mice were daily monitored regarding their body weight and tumor growth. Tumor lengths and widths were measured using an electronic caliper. The corresponding tumor volumes were calculated using the following formula.

$$\text{Tumor volume} = 0.5 \times \text{length} \times \text{width}^2$$

When tumors reached a maximum size of 15 mm in diameter, mice were euthanized by means of deep sevoflurane narcotization and subsequent bleeding. Tumors were excised and snap-frozen in liquid nitrogen.

4.7.3 *In vivo* vector biodistribution and tumor transduction studies

UD-SCC-2 and SK-Mel-28 xenografts were established in 8-10 weeks old female NSG mice as described in 4.7.2. For vector biodistribution and tumor transduction studies, *E1*-deleted and eGFP-expressing vectors were used. For biodistribution studies, $2x10^{10}$ vector particles, dissolved in 100 µl DPBS were administered via tail vein injection after 14 days of tumor growth using Omnifix-F® 1 ml syringes with Sterican® Ø20 0.40 x 20 mm 27G cannulas. For tumor transduction studies, $1x10^{10}$ vector particles dissolved in 50 µl DPBS were intratumorally injected after 28 days of tumor growth via three radial dispersed injection channels using Omnifix-F® insulin syringes. Three days after vector injection, mice were euthanized as described, organs and tumors were harvested and snap-frozen in liquid nitrogen. Additionally, tissue samples of tumors and livers were fixed in 2% PFA (dissolved in DPBS) at 4 °C for 24 h and subsequently dehydrated in 20% sucrose (dissolved in ddH_2O) at 4 °C for additional 24 h. PFA-fixed and dehydrated tissue samples were embedded into TissueTek and frozen at -80 °C for subsequent preparation of tissue sections.

4.7.4 Liver uptake early after vector injection

To investigate liver uptake of vector particles early after vector injection, 8-10 weeks old BALB/c mice were intravenously injected via the tail vein with $2x10^{10}$ vector particles dissolved in 100 µl DPBS using Omnifix-F® 1 ml syringes with Sterican® Ø20 0.40 x 20 mm 27G cannulas. Twenty minutes after vector injection, mice were euthanized as described, livers were harvested and snap-frozen in liquid nitrogen.

4.7.5 Survival studies

UD-SCC-2 xenografts were established in 6-8 months old male and female NSG mice as described in 4.7.2. For survival studies, the Firefly Luciferase-expressing conditionally replicating vectors HCRAd-5_ΔCAR and HCRAd-5-HexPos3_ΔCAR were used. After 21 days of tumor growth, mice were intravenously injected via the tail vein with either 100 µl DPBS or $2x10^{10}$ vector particles dissolved in 100 µl DPBS. Upon vector injection, tumor growth was monitored by daily measurement of tumor volumes (see 4.7.2). Additionally, IVIS measurements for *in vivo* detection of Firefly Luciferase activity were performed 2, 3, 7, 14, 21, 28, 35, 43, 49, and 56 days after vector injection (see 4.7.6). Mice were sacrificed when tumors reached a size of 15 mm in diameter or when animals showed significant signs of toxicity.

4.7.6 *In vivo* bioluminescence imaging

In vivo bioluminescence imaging was performed using the IVIS 200 imaging system. Mice, i.v. injected with Firefly Luciferase-expressing vectors were intraperitoneally (i.p) injected with 300 µl VivoGlo® luciferin (10 mg/ml dissolved in DPBS) and subsequently narcotized by mild isoflurane anesthetization while eyes were protected with eye ointment. Following substrate injection and anesthetization, mice were placed into the IVIS 200 imaging system chamber and pictures were taken at different exposure times (30 sec – 5 min) using the following settings: Binning 4; F/Stop 4; Field of view 4; subject height 1.5 cm.

4.7.7 Fluorometric analysis of liver homogenates

A small piece of snap-frozen and thawed liver tissue (see 4.7.3) was transferred into 200 µl TBS-buffer containing 1x protease inhibitor and homogenized using a bullet blender. Subsequently, the homogenate was cleared by two consecutive centrifugation steps at 20,817 x *g* for 5 min, while after each centrifugation the cleared supernatant was transferred into a new 1.5 ml reaction tube. Cleared samples were diluted 1:10 in Tris-buffer and protein concentrations were determined by optical density measurement at a wavelength of 280 nm. The fluorescence intensity of 2 µl sample was measured using the NanoDrop 3300 device at an excitation and emission wavelength of 488 and 512 nm, respectively. Results were finally calculated as the relative fluorescence unit (RFU) per µg protein.

4.7.8 Fluorescence microscopic evaluation of PFA-fixed liver sections

Cryo-sections of PFA-fixed and TissueTek embedded frozen liver samples with a thickness of 6 µm were prepared using the Leica cryostat. For the analysis of vector-induced eGFP expression, sections were directly covered with fluorescence mounting medium (Dako) and evaluated by fluorescence microscopy.

4.7.9 H&E staining of tissue sections

Cryo-sections of PFA-fixed and TissueTek embedded frozen tumor and liver samples with a thickness of 6 µm were prepared using the Leica cryostat. For H&E staining, sections were fixed in ice-cold acetone twice and subsequently air-dried. As a next step, sections were incubated in Mayer's Hematoxylin solution for 3 min followed by steady washing in tap water for 10 min. Subsequently, sections were incubated with Eosin solution (0.5% in ddH_2O) for 1 min, followed by short washing in ddH_2O for ~5-10 sec. For dehydration, sections were subjected to an ascending alcohol series by consecutive incubation in 70%, 96% and 100% EtOH for 30 sec, 1 min and 4 min, respectively. As a last step, sections were incubated in Xylol for 4 min twice and covered with Eukitt® prior to microscopic evaluation.

4.8 Statistical analysis

If not stated otherwise, all experiments were repeated at least three times. Statistical analyses were performed by either unpaired two-sample (Welch's) student's T-test or Wilcox test utilizing RStudio software (version 4.1.2). *p*-values ≤0.05 were considered statistically significant and results are given as mean ± standard deviation.

5 Results

5.1 Retargeting of adenoviral vectors towards the epidermal growth factor receptor (EGFR)

The epidermal growth factor receptor (EGFR) is overexpressed in many types of HNSCC and was thus expected as an attractive target receptor for oncolytic adenoviral vectors. The Affilin molecule is an ubiquitin-based, 10 kDa high affinity ligand of EGFR[306] and capsid modification of HAdV-5-based vectors with Affilin was hypothesized to enable efficient vector retargeting towards EGFR. Prior to the present study, two Affilin capsid-modified vectors, based on an eGFP-encoding, *E1*-deleted and CAR binding-ablated parental vector (HAdV-5_ΔCAR) were generated by the Department of Gene Therapy at University Ulm. Affilin has been coupled to the vector capsid by a covalent thioetherlinkage between a C-terminal cysteine of Affilin and genetically introduced and surface-exposed cysteines within either the fiber (HAdV-5_ΔCAR_FiberAffilin) or hexon (HAdV-5_ΔCAR_HexonAffilin) protein, using a bismalemidohexane linker[228] (schematically shown in figure 10). First *in vitro* experiments preceding to the present study already revealed beneficial *in vitro* characteristics for the Affilin-decorated vectors, including (i) significantly enhanced transduction efficiencies in EGFR-expressing cancer cells (ii) less binding to blood coagulation factor X (FX) (iii) absent neutralization by the complement- and natural IgM antibodies and (iv) less uptake by murine macrophages.[228] Based on these promising data, the Affilin-decorated vectors were further investigated regarding their oncolytic potential both *in vitro* and *in vivo*.

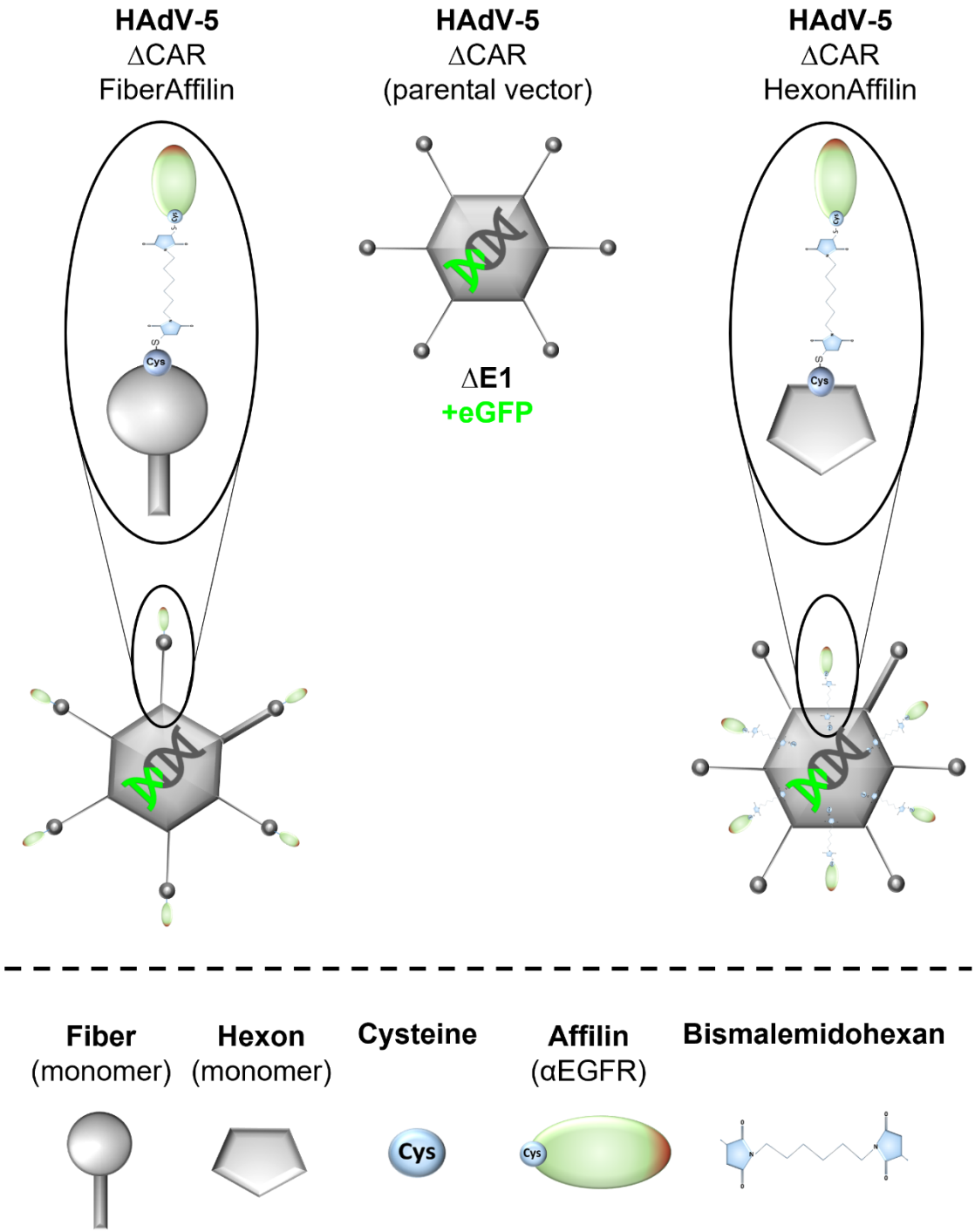

Figure 10: Generation of Affilin-decorated vectors
The Affilin-decorated vectors HAdV-5_ΔCAR_FiberAffilin and HAdV-5_ΔCAR_HexonAffilin were generated by covalent cysteine linkage of the EGFR affinity ligand Affilin to either the fiber or hexon capsid protein of the eGFP-encoding, *E1*-deleted and CAR binding-ablated vector HAdV-5_ΔCAR, using a bismalemidohexan linker.

5.1.1 EGFR-mediated cell transduction of Affilin-decorated vector particles *in vitro*

To reconfirm the already observed enhanced transduction efficiencies of the Affilin-decorated vectors in an EGFR-dependent manner, transduction assays were performed in a set of cancer cell lines *in vitro*. A549, UM-SCC-11B, UD-SCC-2 and SK-Mel-28 cells were characterized regarding their EGFR expression levels by immunostaining and subsequent flow cytometric analysis (Figure 11A). Among these cell lines, UD-SCC-2 cells showed highest EGFR expression levels followed by UM-SCC-11B and A549 cells. SK-Mel-28 cells showed almost absent EGFR expression and thus were chosen as an EGFR-negative control. As a next step, transduction efficiencies of the Affilin-decorated vectors were investigated. Compared to the vector control HAdV-5_ΔCAR, both Affilin-decorated vectors showed significantly improved transduction efficiencies in all cell lines tested (Figure 11B). Regarding EGFR-positive cells, HAdV-5_ΔCAR_FiberAffilin showed consistently higher transduction efficiencies than HAdV-5_ΔCAR_HexonAffilin. In contrast, transduction efficiencies of both vectors in EGFR-negative SK-Mel-28 cells were at comparable levels. Importantly, transduction efficiencies of the Affilin-decorated vectors increased in correlation to EGFR expression levels of the respective cell lines, indicating that transduction was EGFR-dependent. To prove that the Affilin-decorated vectors transduce the cell via EGFR, a competition assay was performed (Figure 11C). Preincubation of UM-SCC-11B cells with human epidermal growth factor (hEGF), the natural ligand of EGFR, significantly inhibited cell transduction by HAdV-5_ΔCAR_FiberAffilin, proving that capsid modification with Affilin mediated an EGFR-specific host cell transduction.

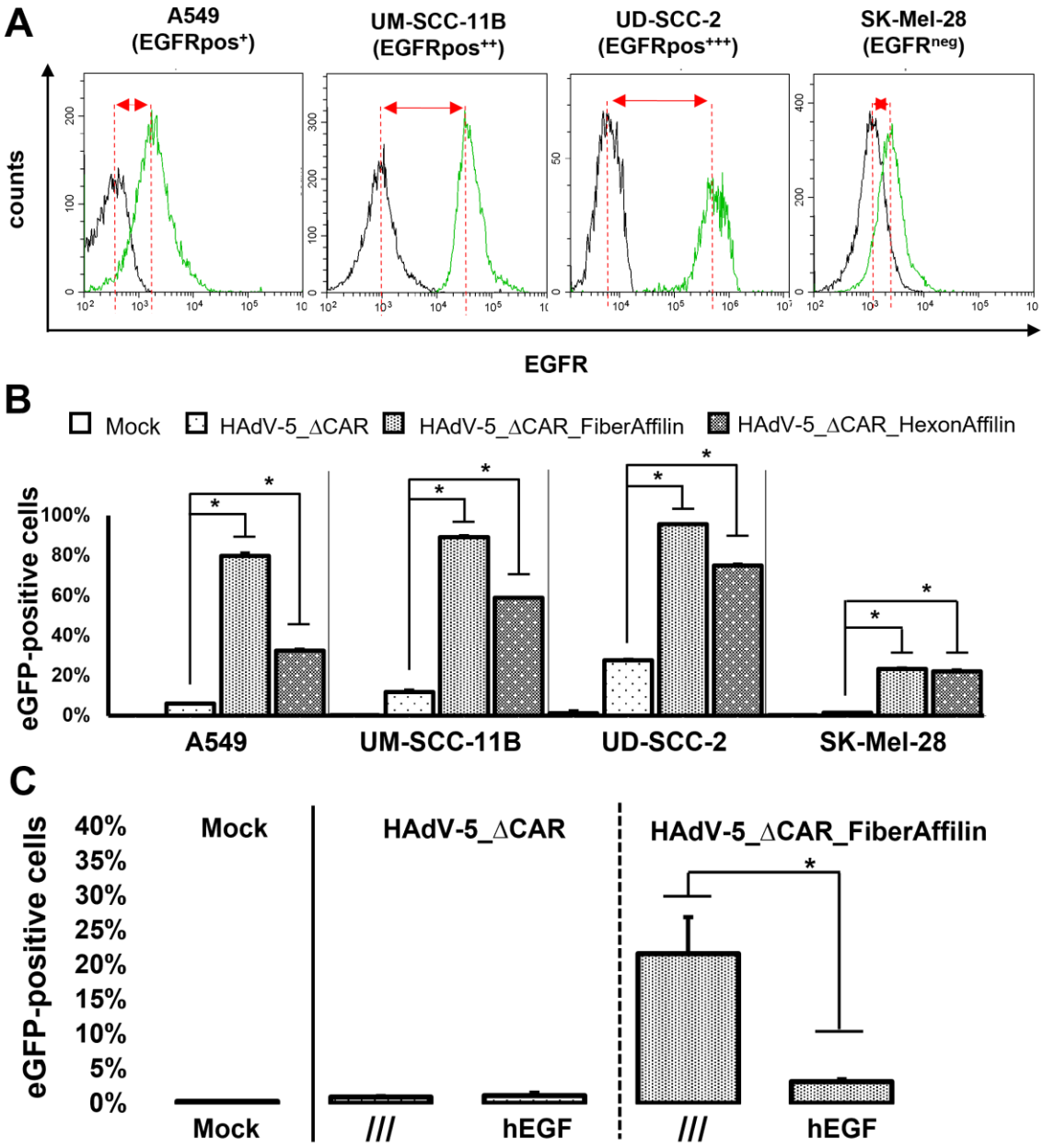

Figure 11: Affilin-decorated vectors transduce cells in an EGFR-specific manner
(A) EGFR expression by A549, UM-SCC-11B, UD-SCC-2 and SK-Mel-28 cells was detected by immunostaining and subsequent flow cytometry. EGFR was detected using mouse α-EGFR primary antibody and FTIC-labeled α-mouse-IgG secondary antibody. Black lines indicate mock treated cells. Green lines indicate cells treated with α-EGFR antibody. Shift between cell populations (red arrows) indicates the extent of EGFR expression. **(B)** A549, UM-SCC-11B, UD-SCC-2 and SK-Mel-28 cells were transduced with HAdV-5_ΔCAR, HAdV-5_ΔCAR_FiberAffilin or HAdV-5_ΔCAR_HexonAffilin with pMOI 1000 and eGFP-positive cells were quantified 24 hpt by flow cytometry. n=3; *=p<0.05. **(C)** UM-SCC-11B cells were preincubated with either PBS (///) or human epidermal growth factor (hEGF) prior to transduction with HAdV-5_ΔCAR or HAdV-5_ΔCAR_FiberAffilin at pMOI 1000 and eGFP-positive cells were quantified by flow cytometry 24 hpt. n=3; *=p<0.05. (Wienen *et al.* 2022, Figure 1b, d and e; CC BY-NC-ND 4.0, https://creativecommons.org/licenses/by-nc-nd/4.0/)

5.1.2 NOD/SCID Gamma mouse plasma enhances transduction efficiencies of Affilin-decorated vectors

The Affilin-decorated vectors showed significantly enhanced transduction efficiencies in EGFR-positive cancer cells. To investigate potential effects of NOD SCID Gamma (NSG) mouse plasma components, which might negatively affect transduction efficiencies of the Affilin-decorated vectors in later *in vivo* studies, transduction of A549, UM-SCC-11B, UD-SCC-2 and SK-Mel-28 cells by HAdV-5_ΔCAR, HAdV-5_ΔCAR_FiberAffilin and HAdV-5_ΔCAR_HexonAffilin was analyzed in either presence or absence of NSG mouse plasma (Figure 12). Interestingly, presence of NSG mouse plasma further increased the already enhanced transduction efficiencies of both Affilin-decorated vectors in all cell lines tested, while transduction efficiencies of the parental vector HAdV-5_ΔCAR remained almost unaffected. Here the transduction-enhancing effect of murine plasma was even more pronounced for HAdV-5_ΔCAR_HexonAffilin than for HAdV-5_ΔCAR_FiberAffilin. Thus, NSG mouse plasma does not negatively affect but even enhances transduction efficiencies of the Affilin-decorated vectors *in vitro*, which could be beneficial regarding their tumor transduction efficiencies *in vivo*.

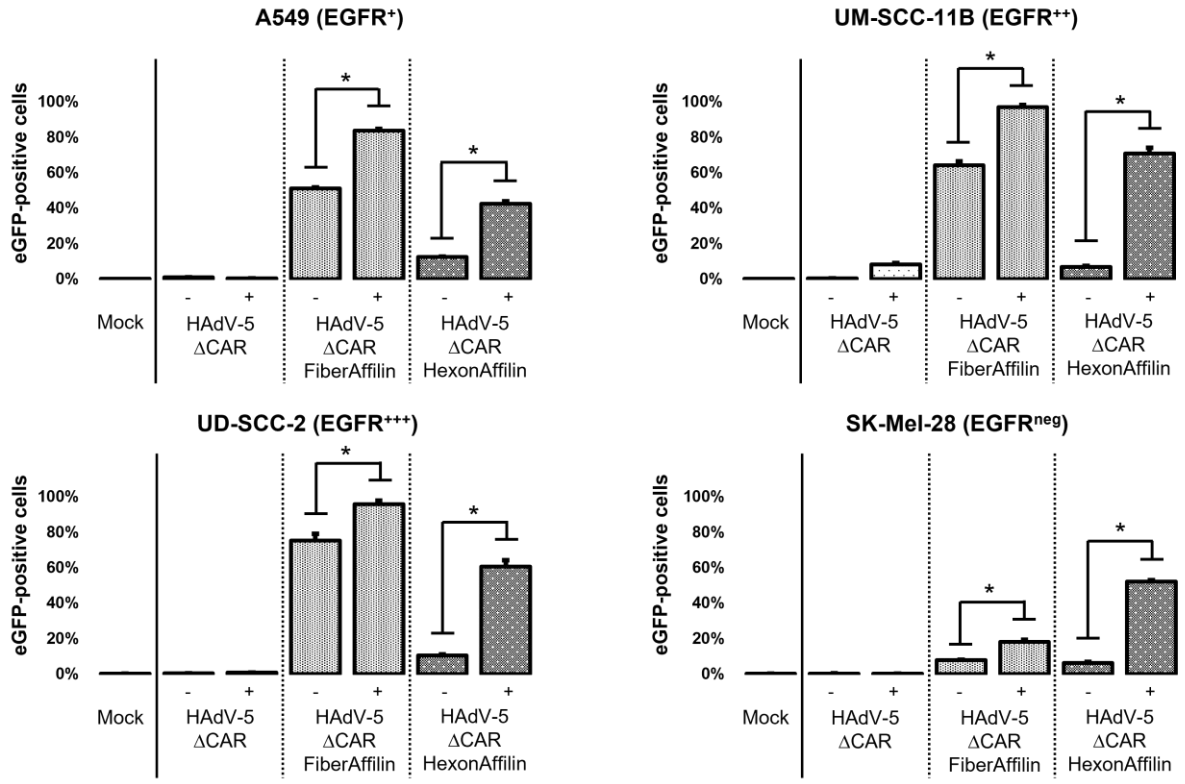

Figure 12: NSG mouse plasma improves transduction efficiencies of Affilin-decorated vectors *in vitro*

A549, UM-SCC-11B, UD-SCC-2 and SK-Mel-28 cells were transduced with either HAdV-5_ΔCAR, HAdV-5_ΔCAR_FiberAffilin or HAdV-5_ΔCAR_HexonAffilin with pMOI 1000 in either absence (-) or presence (+) of NSG mouse plasma. Transduction efficiencies were evaluated 24 hpt by flow cytometric analysis. n=3; *=p<0.05. (Wienen *et al.* 2022, Figure 3; CC BY-NC-ND 4.0, https://creativecommons.org/licenses/by-nc-nd/4.0/)

5.1.3 Establishment of subcutaneous xenograft tumor mouse models

To further investigate the oncolytic potential of the Affilin-decorated vectors *in vivo*, human xenograft tumor mouse models based on EGFR-positive and EGFR-negative cancer cell lines were established with special focus on two characteristics that are moderate tumor growth and good vascularization. To this end, different cell numbers of the EGFR-positive cell lines A431 (cell numbers injected: $5x10^5$, $1x10^6$, $5x10^6$), UD-SCC-2 (cell numbers injected: $2x10^6$, $6x10^6$), UM-SCC-11B (cell numbers injected: $5x10^5$, $1x10^6$, $3.3x10^6$) as well as the EGFR-negative cell line SK-Mel-28 (cell numbers injected: $5x10^5$, $1x10^6$, $5x10^6$) were subcutaneously injected into left flanks of NSG mice. The take rate for all xenografts was 100% and tumor growth was assessed by daily measurement of the tumor length and width with subsequent calculation of the tumor volume. Best tumor growth of A431, UM-SCC-11B, UD-SCC-2 and SK-Mel-28 tumors were observed after subcutaneous injection of $5x10^5$, $5x10^5$, $2x10^6$ and $5x10^6$ tumor cells, respectively (Figure 13). A431 tumors showed aggressive and inhomogeneous growth with a maximum of 22 days until tumors reached the termination criteria. Thus, the A431 xenograft model was excluded for further *in vivo* studies and was not further characterized in this study. UM-SCC-11B and SK-Mel-28 xenografts, however, showed moderate and uniform tumor growth, fitting the intended growth characteristics. UD-SCC-2 xenografts showed slow tumor growth at the beginning, which turned into an almost exponential growth phase at around 30 days after tumor cell injection.

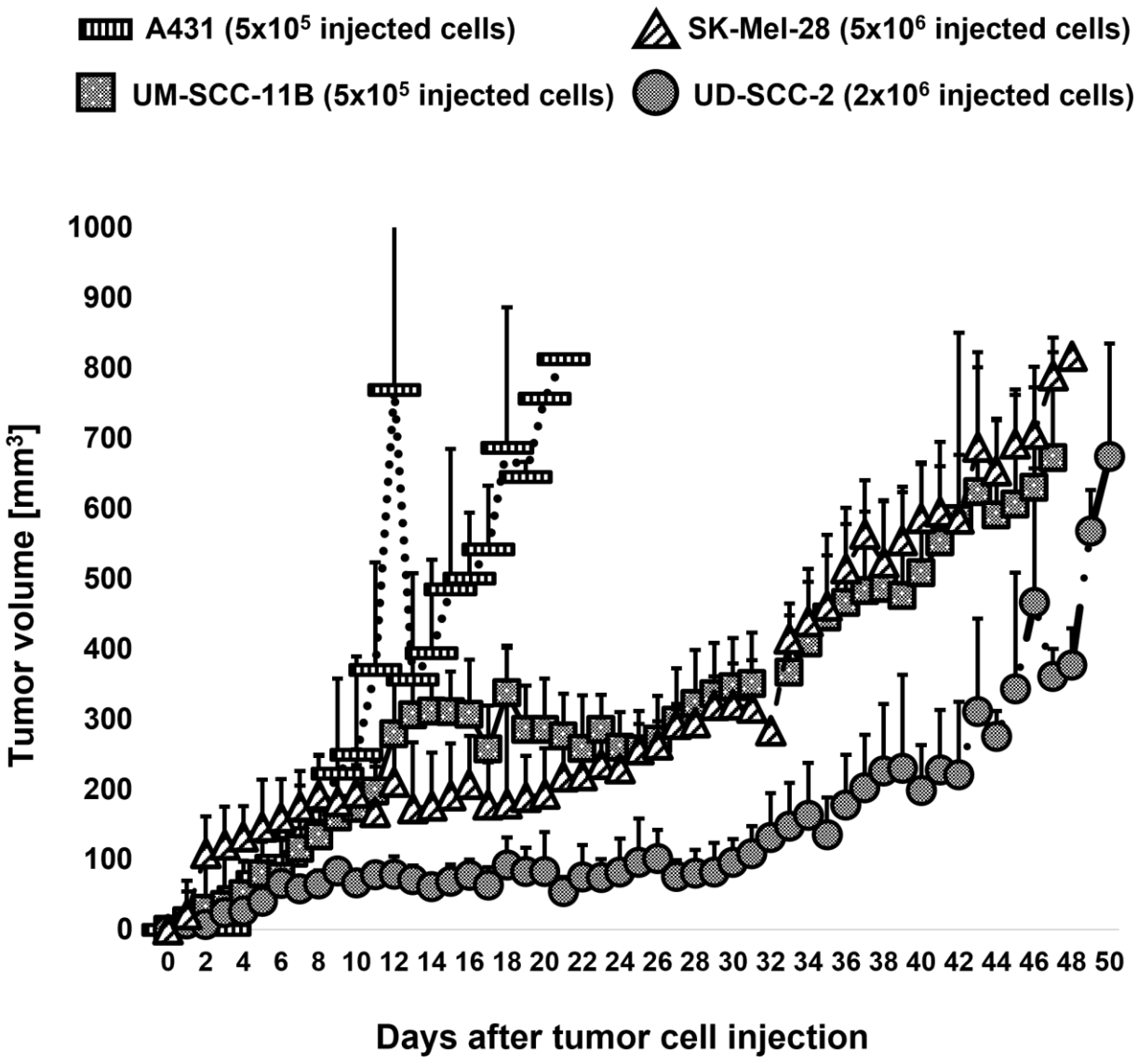

Figure 13: Growth kinetics of A431, UM-SCC-11B, UD-SCC-2 and SK-Mel-28 subcutaneous xenograft models

NSG mice were subcutaneously injected with the indicated cell numbers of A431, UM-SCC-11B, UD-SCC-2 and SK-Mel-28 cells. After tumor cell injection, tumor growth was daily monitored by measurement of tumor length and width using an electronic caliper and tumor volumes were calculated. Results are shown as mean tumor sizes ± standard deviation. A431, UM-SCC-11B, SK-Mel-28: n=8 ; UD-SCC-2: n=6 .The UD-SCC-2 xenograft model was established and characterized by Robin Nilson, Department of Gene Therapy, University Ulm (Adapted from Nilson *et al*. 2023, Figure 1S; CC BY-NC-ND 4.0, https://creativecommons.org/licenses/by/4.0/)

Since proper tumor vascularization is mandatory for efficient vector delivery to the tumor after intravenous vector injection, as a next step, vascularization of UM-SCC-11B, UD-SCC-2 and SK-Mel-28 tumors was analyzed by immunohistochemical staining of tumor sections for the endothelial marker CD31 (Figure 14).

Tumor sections of UM-SCC-11B xenografts showed abundant CD31 staining at the tumor periphery but almost no CD31-positive cells were detected in the tumor interior, indicating insufficient vascularization in inner areas of the tumor. These findings were in line with observations that UM-SCC-11B tumors appeared slightly necrotic after excision (data not shown), which was also indicated by less DAPI staining within inner areas of the tumor sections. Thus, despite favorable tumor growth, UM-SCC-11B xenografts were excluded for further *in vivo* studies due to insufficient tumor vascularization and emerging tumor necrosis. However, UD-SCC-2 and SK-Mel-28 xenografts showed abundant CD31 staining at both, the tumor periphery, and the tumor interior. In addition, no tumor necrosis was noted in neither tumor model after tumor excision, further confirmed by uniform DAPI staining throughout the tumor sections. Thus, due to moderate tumor growth and uniform tumor vascularization, UD-SCC-2 and SK-Mel-28 xenografts were chosen as respectively EGFR-positive and EGFR-negative human tumor xenograft models for further *in vivo* studies.

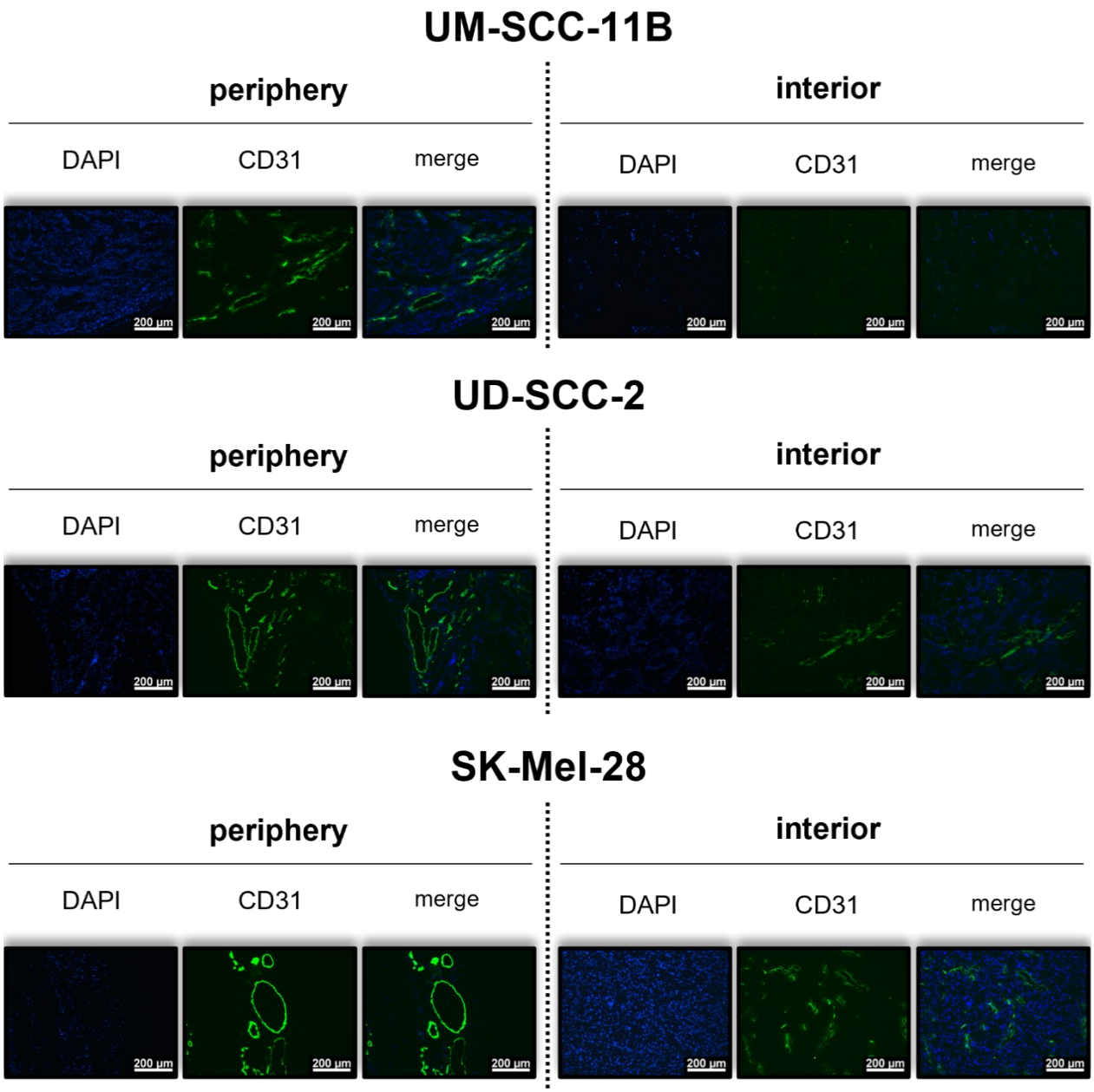

Figure 14: Vascularization of subcutaneous UM-SCC-11B, UD-SCC-2 and SK-Mel-28 xenograft models

After excision of subcutaneously grown UM-SCC-11B, UD-SCC-2 and SK-Mel-28 tumors, samples were snap-frozen, embedded into Tissue Tek and tumor vascularization was analyzed in tumor sections by immunohistochemical staining for CD31. CD31 was detected using rat-α-mouseCD31 primary antibody and Alexa488-labeled α-rat-IgG secondary antibody. Cell nuclei were stained with DAPI. Shown are pictures from UM-SCC-11B, UD-SCC-2 and SK-Mel-28 tumors excised after 48, 39 and 49 days of tumor growth, respectively. Immunohistochemical staining of UD-SCC-2 tumor sections was performed by Robin Nilson, Department of Gene Therapy, University Ulm.

5.1.4 Intravenous injection of Affilin-decorated vectors does not lead to improved tumor targeting in EGFR-positive tumors *in vivo*

After establishment of suitable EGFR-positive and EGFR-negative tumor xenograft models, tumor targeting of the Affilin-decorated vectors was investigated *in vivo*. UD-SCC-2 and SK-Mel-28 tumor xenografts were established in NSG mice as described and after 14 days of tumor growth, $2x10^{10}$ vector particles of either HAdV-5_ΔCAR, HAdV-5_ΔCAR_FiberAffilin or HAdV-5_ΔCAR_HexonAffilin were intravenously injected. Three days after vector administration, mice were euthanized, organs and tumors were harvested and tumor targeting was analyzed by quantification of intratumoral vector genome copy loads using qPCR analysis (Figure 15).

Vector genomes of HAdV-5_ΔCAR were detected in both xenograft models, with genome copy numbers being higher in SK-Mel-28 tumors than in UD-SCC-2 tumors. In line with absent EGFR expression by SK-Mel-28 cells *in vitro*, most intratumoral vector genome copy numbers were below the detection limit for HAdV-5_ΔCAR_FiberAffilin and HAdV-5_ΔCAR_HexonAffilin in SK-Mel-28 tumors (Figure 15B). However, compared to HAdV-5_ΔCAR, neither HAdV-5_ΔCAR_FiberAffilin nor HAdV-5_ΔCAR_HexonAffilin showed improved tumor targeting in EGFR-positive UD-SCC-2 tumors (Figure 15A) and tumor uptake of HAdV-5_ΔCAR_HexonAffilin was even less compared to HAdV-5_ΔCAR_FiberAffilin. Thus, despite significantly enhanced EGFR-specific transduction efficiencies *in vitro*, intravenous injection of HAdV-5_ΔCAR_FiberAffilin and HAdV-5_ΔCAR_HexonAffilin did not lead to enhanced tumor transduction in EGFR-positive UD-SCC-2 tumor xenografts.

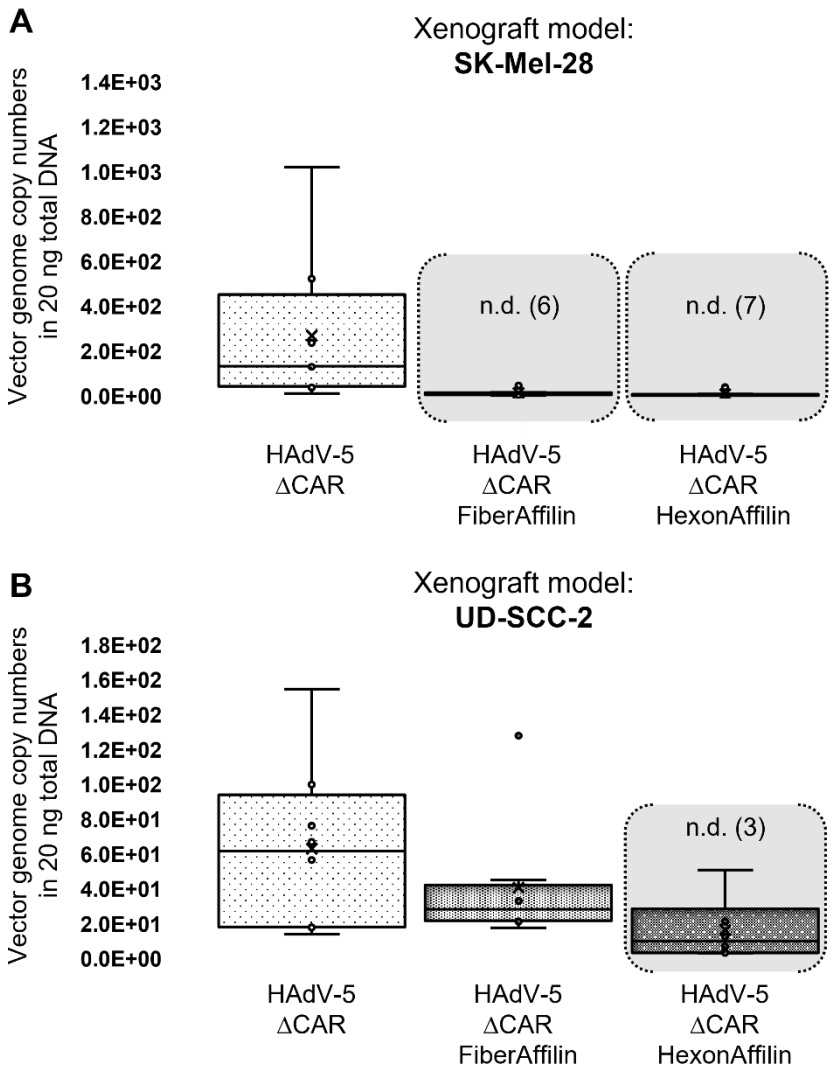

Figure 15: Affilin-decorated vectors do not exhibit improved tumor transduction after intravenous injection

NSG mice bearing subcutaneous SK-Mel-28 (A) or UD-SCC-2 (B) tumors were intravenously injected with $2x10^{10}$ vector particles of either HAdV-5_ΔCAR, HAdV-5_ΔCAR_FiberAffilin or HAdV-5_ΔCAR_HexonAffilin after 14 days of tumor growth. Three days after vector injection, tumors were harvested and intratumoral vector genome copy numbers were quantified by qPCR analysis. n=8. Greyish backgrounds highlight data sets with values below the detection range with n.d. (x) indicating the number of values below the detection range. n.d. = not detectable. (As author adapted from Wienen *et al.* 2022, Figure 5; CC BY-NC-ND 4.0, https://creativecommons.org/licenses/by-nc-nd/4.0/)

5.1.5 Affilin-decorated vectors exhibit less liver uptake upon *i.v.* injection

Neither HAdV-5_ΔCAR_FiberAffilin nor HAdV-5_ΔCAR_HexonAffilin showed elevated tumor targeting in UD-SCC-2 tumor-bearing NSG mice after intravenous vector injection. Since HAdV-5-based vectors are known to have a pronounced liver tropism after systemic administration[49], particle consumption by the liver was hypothesized as the cause for absent tumor transduction. Thus, liver tropism of the Affilin-decorated vectors was analyzed by assessment of fluorescence intensities and quantification of vector genome copy numbers within livers of vector injected mice using fluorometric analysis and qPCR analysis, respectively (Figure 16A, B).

Independent of the respective xenograft, both methods revealed a significantly reduced liver tropism of the Affilin-decorated vectors compared to HAdV-5_ΔCAR. Interestingly, liver uptake of HAdV-5_ΔCAR_HexonAffilin was even more diminished compared to HAdV-5_ΔCAR_FiberAffilin, as indicated by a further reduction of vector genome copy numbers detected by qPCR analysis (Figure 16B). These observations were further confirmed by fluorescence microscopy of corresponding liver sections derived from UD-SCC-2 xenograft-bearing mice (Figure 16C). High amounts of eGFP-positive cells were observed in liver sections of mice treated with HAdV-5_ΔCAR, indicating pronounced hepatocyte transduction. In contrast, substantially lower amounts of eGFP-positive cells were observed in liver sections of mice injected with HAdV-5_ΔCAR_FiberAffilin and HAdV-5_ΔCAR_HexonAffilin. In line with qPCR analysis, liver sections of mice treated with HAdV-5_ΔCAR_HexonAffilin showed the lowest number eGFP-positive cells.

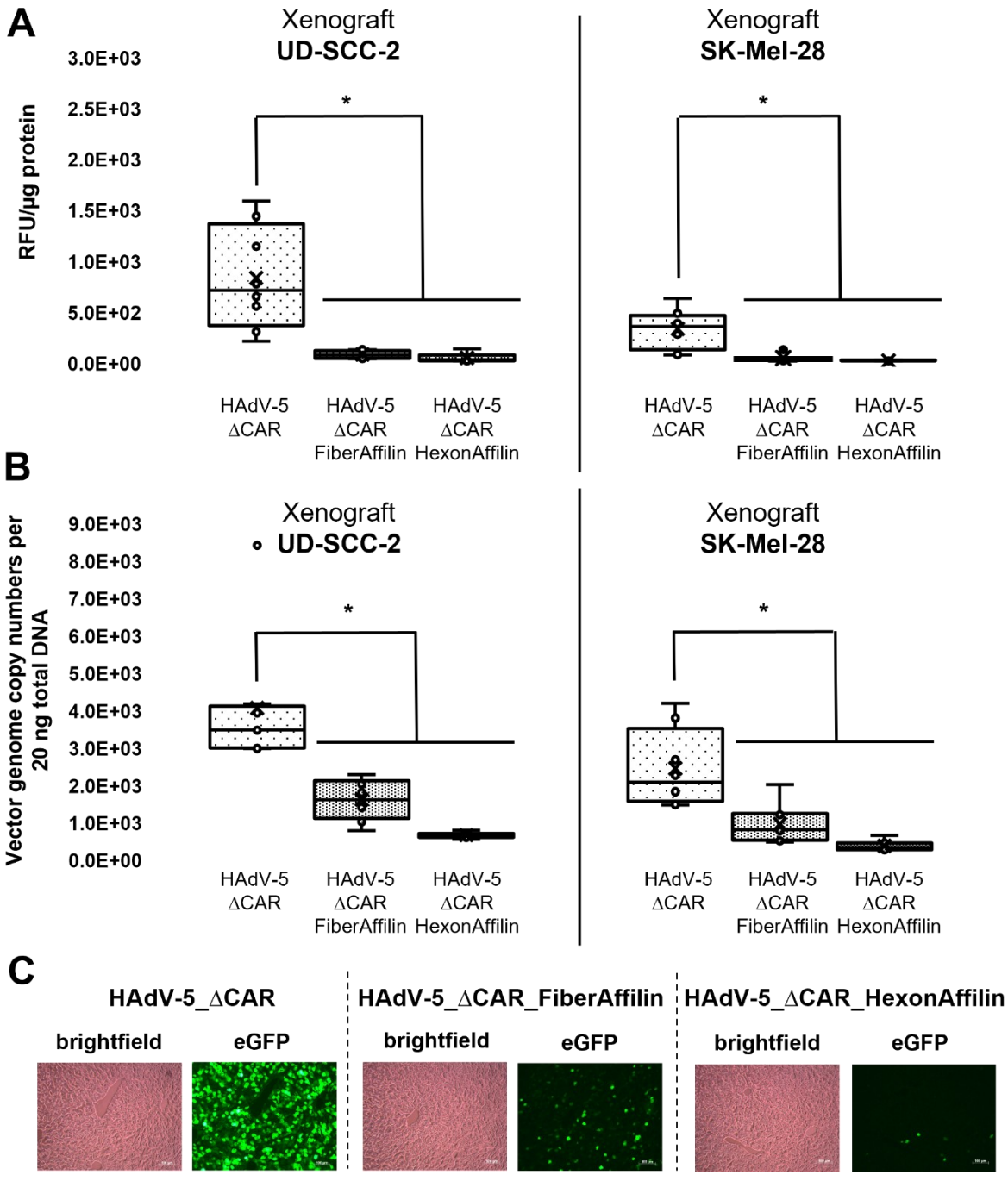

Figure 16: Affilin-decorated vectors exhibit significantly reduced liver tropism after intravenous injection into tumor-bearing NSG mice.

NSG mice bearing subcutaneous UD-SCC-2 or SK-Mel-28 xenografts were intravenously injected with $2x10^{10}$ vector particles of HAdV-5_ΔCAR, HAdV-5_ΔCAR_FiberAffilin or HAdV-5_ΔCAR_HexonAffilin after 14 days of tumor growth. Three days after vector injection, livers were harvested and eGFP expression levels as well as vector genome copy numbers were quantified by **(A)** fluorometric analysis and **(B)** qPCR analysis, respectively. Hepatocyte transduction was further confirmed by **(C)** fluorescence microscopy for eGFP-positive cells in corresponding liver sections of mice bearing UD-SCC-2 xenografts. n = 8; * = $p<0.05$. RFU: response forming unit. (*Wienen et al.* 2022, Figure 4a, b, c; CC BY-NC-ND 4.0, https://creativecommons.org/licenses/by-nc-nd/4.0/)

Beside hepatocyte transduction, particle consumption by liver residential Kupffer cells additionally may lead to a rapid blood clearance of HAdV-5-based vectors within minutes after systemic administration[50]. To exclude an extensive uptake of the Affilin-decorated vectors by Kupffer cells, BALB/c mice were intravenously injected with either PBS, or $2x10^{10}$ vector particles of HAdV-5_ΔCAR, HAdV-5_ΔCAR_FiberAffilin or HAdV-5_ΔCAR_HexonAffilin and vector genome copy numbers within livers were analyzed 20 minutes after vector administration. Compared to HAdV-5_ΔCAR, both Affilin-decorated vectors showed significantly diminished vector loads in livers early after injection (Figure 17). As seen with samples harvested from tumor-bearing NSG mice after 72 h (Figure 16), HAdV-5_ΔCAR_HexonAffilin again showed the lowest vector genome copy numbers of all vectors injected, followed by HAdV-5_ΔCAR_FiberAffilin and HAdV-5_ΔCAR.

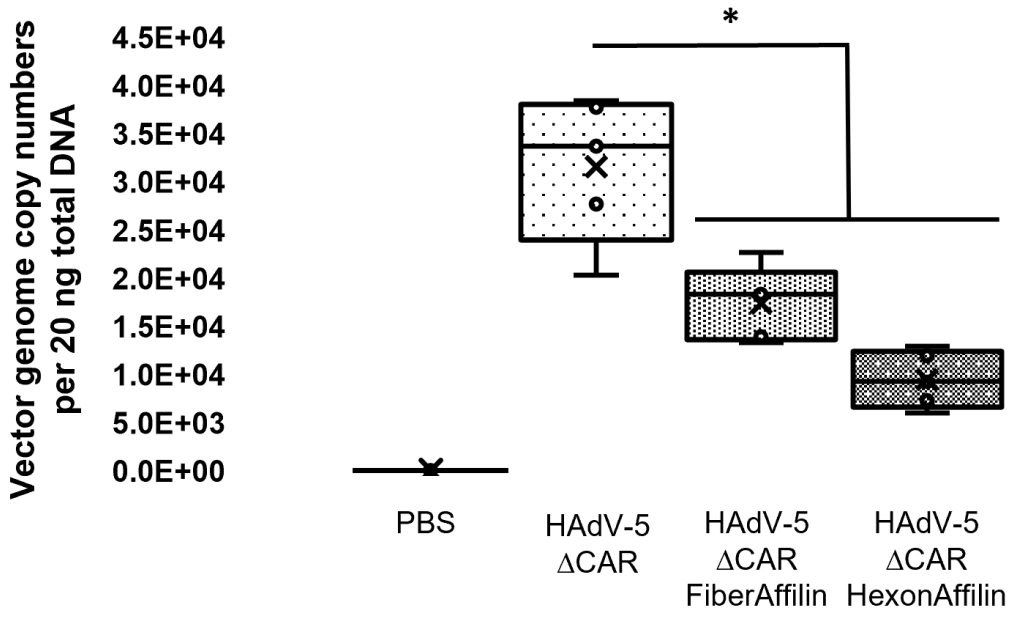

Figure 17: Significantly reduced liver uptake of Affilin-decorated vectors in BALB/c mice early after intravenous vector injection

BALB/c mice were intravenously injected with either PBS or $2x10^{10}$ vector particles of HAdV-5_ΔCAR, HAdV-5_ΔCAR_FiberAffilin or HAdV-5_ΔCAR_HexonAffilin. Twenty minutes after vector injection, livers were harvested and analyzed for vector genome copy numbers by qPCR analysis. n = 5; * = $p<0.05$. (Wienen *et al.* 2022, Figure 4d, CC BY-NC-ND 4.0, https://creativecommons.org/licenses/by-nc-nd/4.0/)

5.1.6 UD-SCC-2 xenografts exhibit abundant EGFR expression but poor tumor vascularization after 14 days of tumor growth

To analyze whether poor tumor targeting by the i.v. injected Affilin-decorated vectors was caused by either an insufficient tumor vascularization or absent EGFR expression in the tumor at the day of vector injection, immunohistochemical staining for both the endothelial marker CD31 and EGFR was performed in tumor sections of UD-SCC-2 and SK-Mel-28 xenografts after 14 days of tumor growth. Tumor sections of SK-Mel-28 xenografts were used as a negative control for the EGFR staining method and *in vitro* cultivated UD-SCC-2 and SK-Mel-28 cells were stained analogously. Confirming previous flow cytometric analysis (Figure 11A), UD-SCC-2 cells showed distinct EGFR staining *in vitro* while SK-Mel-28 cells appeared almost EGFR negative (Figure 18A). Tumor sections of UD-SCC-2 xenografts also showed abundant EGFR staining while almost no EGFR was detected in tumor sections of SK-Mel-28 xenografts (Figure 18B). However, compared to SK-Mel-28 xenografts, only minor CD31 expression was detected in tumor sections of UD-SCC-2 xenografts, indicating weak tumor vascularization of the latter at the day of vector injection (Figure 18B). In addition, vascularization within UD-SCC-2 tumors appeared exclusively within areas of absent EGFR expression (Figure 18B; merge), most probably stromal tissue of murine origin (Figure 18B; red arrows).

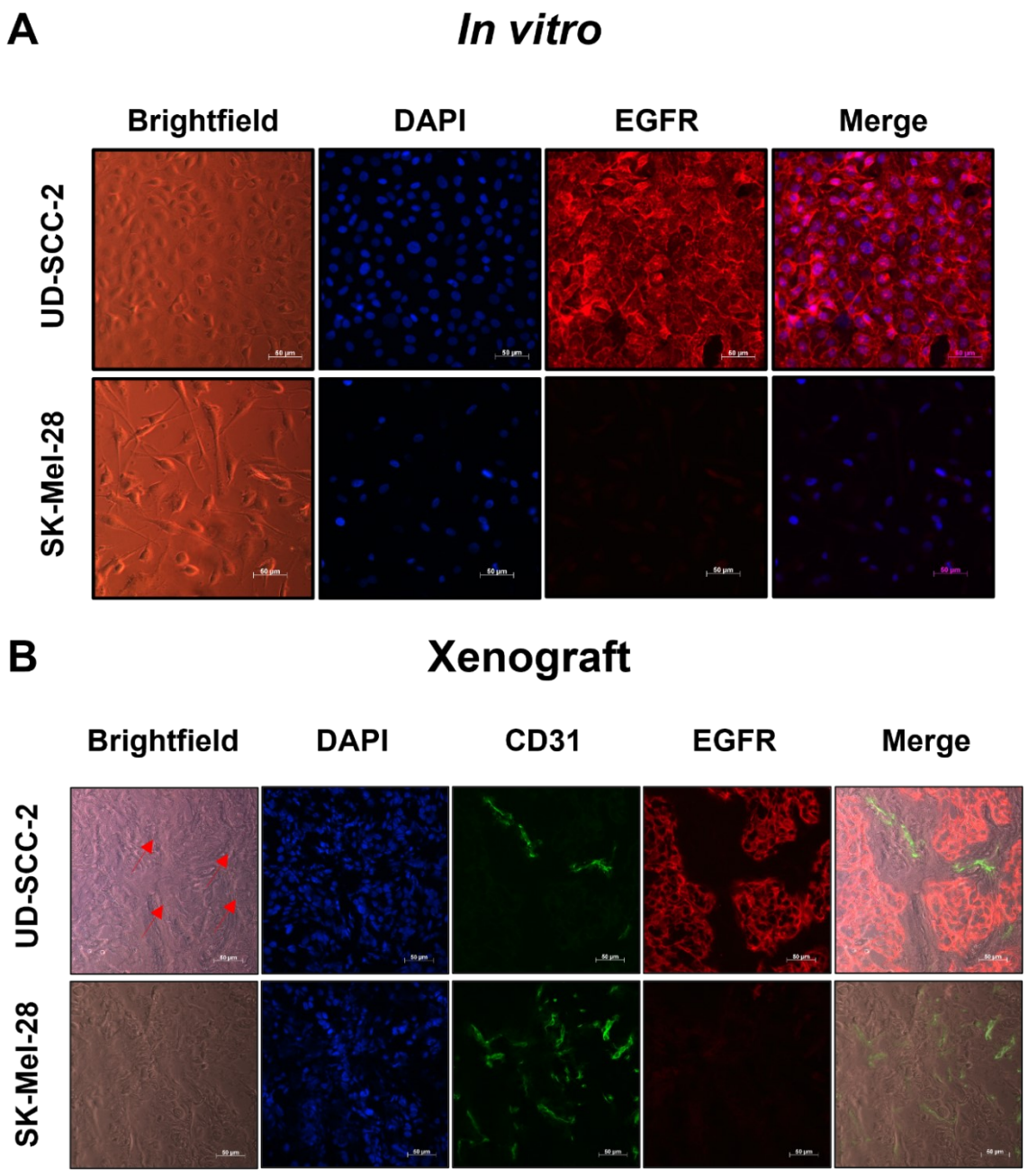

Figure 18: UD-SCC-2 xenografts show abundant EGFR expression but weak vascularization after 14 days of tumor growth

Immunochemical staining was performed of **(A)** *in vitro* cultivated UD-SCC-2 and SK-Mel-28 cells and **(B)** UD-SCC-2 and SK-Mel-28 xenografts established in NSG mice after 14 days of tumor growth. EGFR was detected using mouse-α-EGFR primary antibody and Alexa594-labeled α-mouse-IgG secondary antibody. CD31 was detected using rat-α-CD31 primary antibody and Alexa488-labeled α-rat-IgG secondary antibody. Cell nuclei were stained with DAPI. Red arrows indicate areas of absent EGFR expression. (Wienen *et al.* 2022, Figure 6; CC BY-NC-ND 4.0, https://creativecommons.org/licenses/by-nc-nd/4.0/)

5.1.7 Affilin-decorated vectors exhibit altered organ tropism *in vivo*

Tumor transduction by intravenously injected Affilin-decorated vectors was suggested to be in part hampered by an insufficient tumor vascularization at the day of vector injection. Furthermore, HAdV-5_ΔCAR_FiberAffilin and HAdV-5_ΔCAR_HexonAffilin were also shown to exhibit a significantly reduced liver tropism after intravenous injection (Figure 16, Figure 17). Thus, an altered organ tropism as a possible cause of particle consumption was suggested. To this end, vector genome copy numbers within lungs, spleens, kidneys and hearts of vector-injected, tumor-bearing NSG mice harvested three days after vector injection, were quantified by qPCR analysis (Figure 19).

Independent of the respective xenograft used, both Affilin-decorated vectors showed significantly reduced vector loads within the spleen, lung, and kidney. Here, HAdV-5_ΔCAR_HexonAffilin again showed the lowest vector genome copy number of all vectors injected, followed by HAdV-5_ΔCAR_FiberAffilin and HAdV-5_ΔCAR, as likewise observed in previous qPCR analyses of the liver (Figure 16). However and interestingly, this relative vector distribution pattern was reversed in the heart, in which HAdV-5_ΔCAR_HexonAffilin showed the highest genome vector copy numbers followed by HAdV-5_ΔCAR_FiberAffilin and HAdV-5_ΔCAR in descending order.

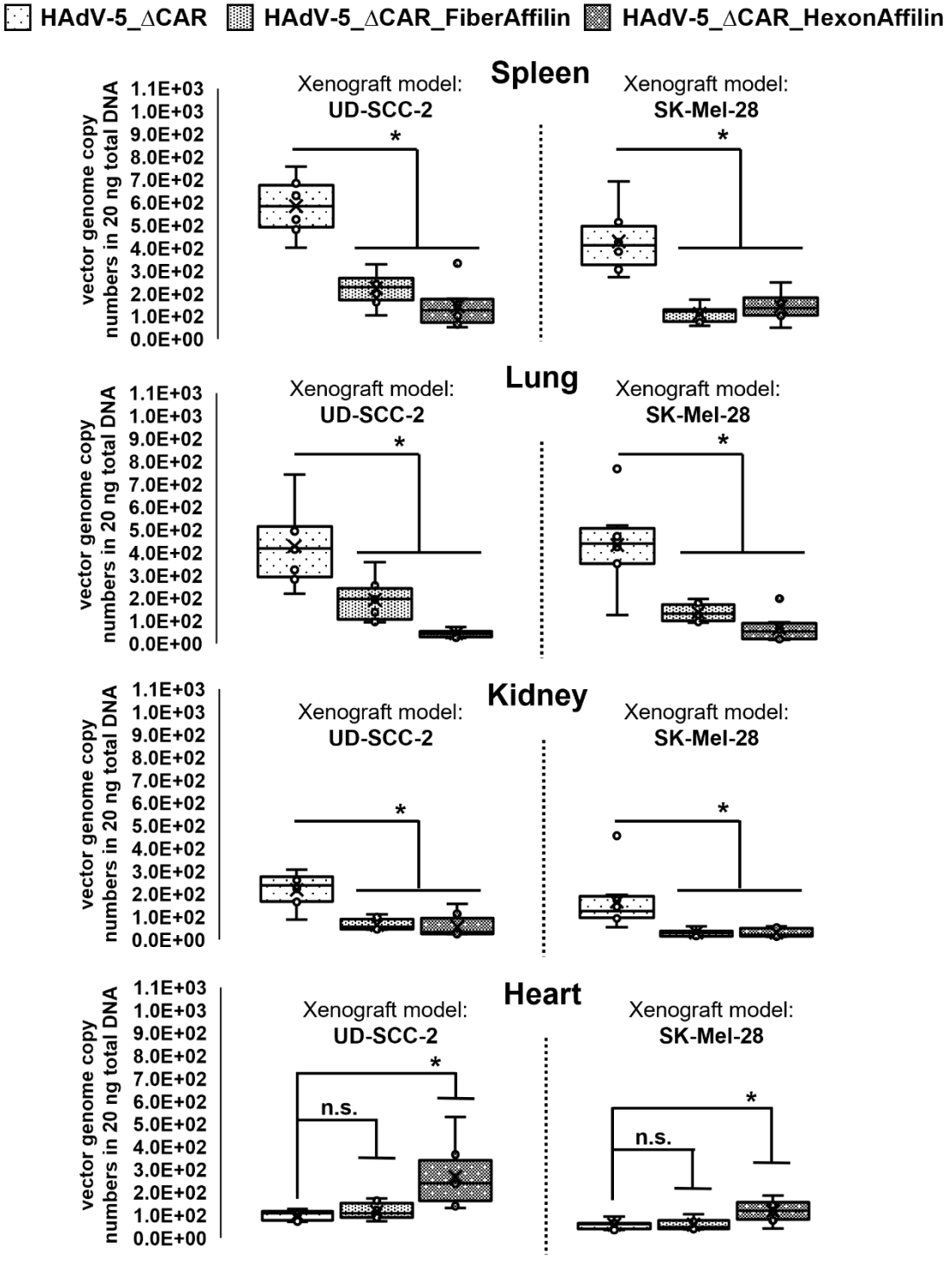

Figure 19: Affilin-decorated vectors exhibit elevated heart tropism after intravenous injection

NSG mice bearing UD-SCC-2 or SK-Mel-28 xenografts were intravenously injected with $2x10^{10}$ vector particles of HAdV-5_ΔCAR, HAdV-5_ΔCAR_FiberAffilin or HAdV-5_ΔCAR_HexonAffilin after 14 days of tumor growth. Three days after vector injection, mice were euthanized and vector genome copy numbers in spleens, lungs, kidneys, and hearts were quantified by qPCR analysis. n =8; * = $p<0.05$; n.s. = not significant. (As author adapted from Wienen *et al.* 2022, Figure 7b; CC BY-NC-ND 4.0, https://creativecommons.org/licenses/by-nc-nd/4.0/)

5.1.8 Affilin-decorated vectors exhibit enhanced transduction efficiencies in murine cells *in vitro*

The heart reflects the first organ to be reached by intravenously injected vectors. As EGFR is expressed in the cardiac tissue[307–310] and human and murine EGFR share ~95% sequence homology, it was hypothesized that Affilin-decorated vector particles may also show an EGFR-dependent increased transduction of murine cells. To address this question, *in vitro* transduction assays using the murine cell lines SCC-VII, Hepa 1-6 and CMT-64 were performed (Figure 20). Interestingly, transduction efficiencies of HAdV-5_ΔCAR_FiberAffilin and HAdV-5_ΔCAR_HexonAffilin were significantly increased compared to HAdV-5_ΔCAR in all murine cell lines tested. HAdV-5_ΔCAR_HexonAffilin showed the highest transduction efficiencies, consistent with results obtained from murine heart samples in biodistribution analysis (Figure 19).

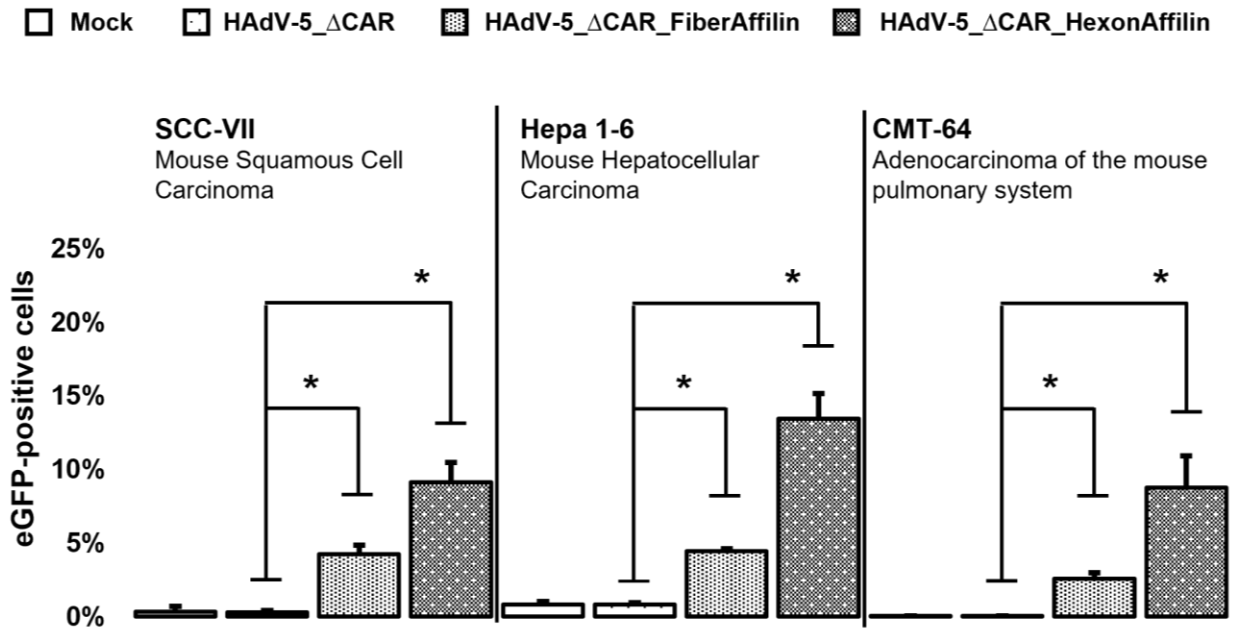

Figure 20: Affilin-decorated vectors exhibit improved transduction efficiencies in murine cell lines

The murine cell lines SCC-VII, Hepa 1-6 and CMT-64 were transduced with either HAdV-5_ΔCAR, HAdV-5_ΔCAR_FiberAffilin or HAdV-5_ΔCAR_HexonAffilin with pMOI 1000 and eGFP-positive cells were quantified 24 hpt by flow cytometry. n=3, * = $p<0.05$. (As author adapted from Wienen *et al.* 2022, Figure 7c; CC BY-NC-ND 4.0, https://creativecommons.org/licenses/by-nc-nd/4.0/)

5.1.9 Inaccessibility of EGFR in *in vivo* xenograft tumors

Insufficient tumor vascularization and off-target transduction of murine cells were suggested as possible reasons for an insufficient tumor transduction by Affilin-decorated vector particles after intravenous injection. To circumvent these limitations and to investigate whether capsid modification with Affilin improves tumor transduction in EGFR-positive tumors *per se*, an intratumoral vector injection was performed. Therefore, $1x10^{10}$ vector particles of HAdV-5_ΔCAR or HAdV-5_ΔCAR_FiberAffilin were intratumorally injected into EGFR-positive UD-SCC-2 tumor-bearing NSG mice after 28 days of tumor growth. Three days after vector injection, tumors were harvested and transduction efficiencies were analyzed by fluorometric measurement and qPCR analysis (Figure 21A). Intratumoral injection of HAdV-5_ΔCAR_FiberAffilin did not lead to enhanced but even diminished transduction of EGFR-positive UD-SCC-2 tumors compared to HAdV-5_ΔCAR. To investigate the accessibility of EGFR for binding of Affilin in the tumor *in vivo*, immunohistochemical staining in UD-SCC-2 xenografts with Strep-tagged Affilin molecules was performed (Figure 21B). Tumor sections of SK-Mel-28 xenografts were used as negative control and *in vitro* cultured UD-SCC-2 and SK-Mel-28 cells were stained analogously to verify the EGFR specificity of Affilin. As expected, distinct binding of Affilin to UD-SCC-2 but not to SK-Mel-28 cells was detected *in vitro*, indicating EGFR specificity. However, neither in tumor sections of SK-Mel-28 nor UD-SCC-2 xenografts, binding of Affilin was detected, which may indicate absent or even significantly diminished binding of Affilin to EGFR in UD-SCC-2 tumors and thus may explain absent tumor transduction by Affilin-decorated vector particles *in vivo*.

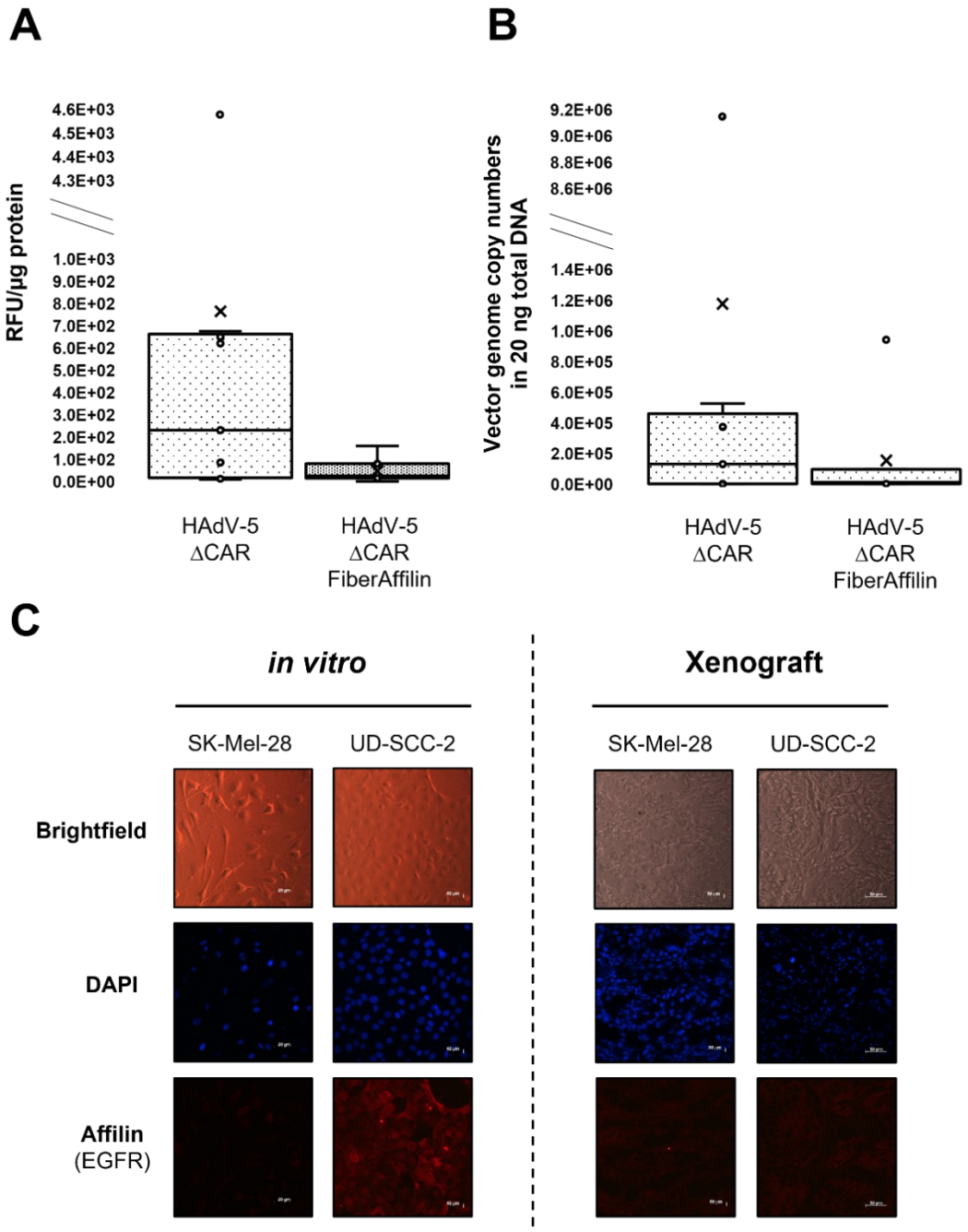

Figure 21: Reduced tumor transduction by Affilin-decorated vectors upon i.t. administration *in vivo* and absent binding of Affilin in EGFR-positive xenografts.
NSG mice bearing UD-SCC-2 xenografts were intratumorally injected with $1x10^{10}$ vector particles of either HAdV-5_ΔCAR_FiberAffilin or HAdV-5_ΔCAR after 28 days of tumor growth and transduction efficiencies were evaluated three days after vector injection by **(A)** fluorometric measurement of intratumoral eGFP expression and **(B)** qPCR analysis of intratumoral vector genome copy numbers (n=8). **(C)** Immunohistochemical staining of *in vitro* cultured SK-Mel-28 and UD-SCC-2 cells (left panel) and sections of respective *in vivo* xenograft tumors grown for 21 days in NSG mice (right panel), using Strep-tagged Affilin. Strep-tagged Affilin was detected using mouse-α-Strep primary antibody and Alexa594-labeled α-mouse-IgG secondary antibody. Cell nuclei were stained with DAPI. (Wienen *et al.* 2022, Figure 8; CC BY-NC-ND 4.0, https://creativecommons.org/licenses/by-nc-nd/4.0/)

5.2 Retargeting of adenoviral vectors towards the fibroblast activation protein (FAP)

The EGFR was shown to be a difficult to address receptor for tumor-targeting by oncolytic adenoviral vectors. Additionally, the tumor stroma was suggested to contribute to an insufficient vector delivery to the tumor cell after intravenous vector injection. As a rational, a direct targeting of the tumor stroma was aimed to overcome these limitations and to improve tumor transduction by oncolytic adenoviral vectors. Cancer associated fibroblasts (CAF) are the most abundant cell type within the tumor stroma of solid tumors[285] and thus represent an attractive target cell type for oncolytic virotherapy. CAFs express the fibroblast activation protein (FAP) to high levels[288] whereas FAP expression in healthy cells and tissues is almost completely absent[289], rendering it a highly specific tumor marker. Thus, FAP represents a promising target for efficient tumor-targeting by oncolytic adenoviral vectors.

To retarget HAdV-5-based vectors towards FAP, a bispecific adapter molecule was designed by genetic fusion of two single chain variable fragments (scFv) binding to the HAdV-5 fiber knob (scFvS11) and FAP (scFvFAP5). scFvS11 was previously described by the working group of Watkins *et al*.[253], is well characterized, and was already used in various retargeting approaches[253,254,258]. The scFvFAP5 was generated by genetic fusion of the variable heavy (V_H) and variable light (V_L) domain of the monoclonal antibody (mAb) FAP5[304] via a flexible glycine-serine $(G_4S)_3$ linker. The same linker was used to fuse the V_H and the V_L of scFvS11. Both scFv were genetically fused to each other via a short G_4S linker. Additionally, an N-terminal signal peptide (H1) and a C-terminal FLAG-Tag were attached for protein secretion and detection, respectively. A schematic representation of the genetic arrangement of the FAP5-S11-FLAG bispecific adapter molecule and the suggested retargeting strategy is shown in figure 22.

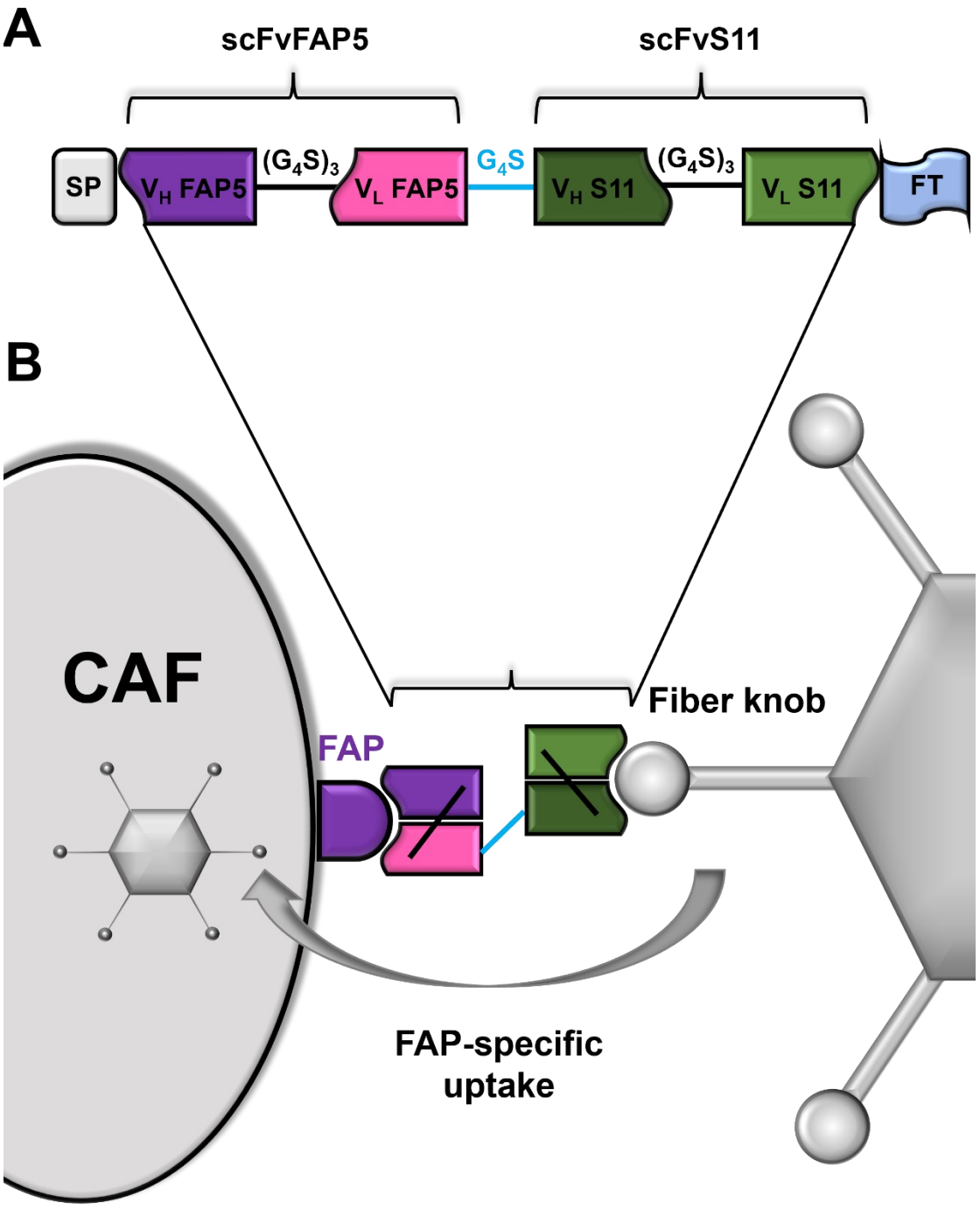

Figure 22: Schematic representation of the FAP5-S11-FLAG bispecific adapter molecule
The FAP5-S11-FLAG bispecific adapter molecule was generated by genetic fusion of scFvFAP5 and scFvS11 binding the fibroblast activation protein (FAP) and HAdV-5 fiber knob, respectively **(A)**. An N-terminal signal peptide (H1) and a C-terminal FLAG-Tag (FT) were attached for protein secretion and detection, respectively. Transduction of cancer associated fibroblasts (CAFs) by HAdV-5-based vectors using the FAP5-S11-FLAG is suggested to be mediated by bridging the adenoviral fiber knob to FAP located at the cell surface **(B)**. V_H: variable heavy chain; V_L: variably light chain, scFv: single chain variable fragment.

5.2.1 Production of FAP5-S11-FLAG bispecific adapter molecule

For production of the FAP5-S11-FLAG bispecific adapter molecule, CAP-T cells were transfected with an expression plasmid, encoding the CMV promoter-driven H1-FAP5-S11-FLAG gene. Five days post transfection, cells and cell culture supernatants were harvested and analyzed by Western Blot analysis for protein expression and secretion (Figure 23). FAP5-S11-FLAG was detected in both CAP-T cell lysates and supernatants at the expected size of ~52 kDa, confirming successful protein expression and secretion. Cell culture supernatants were 18x concentrated in order to increase the FAP5-S11-FLAG concentration.

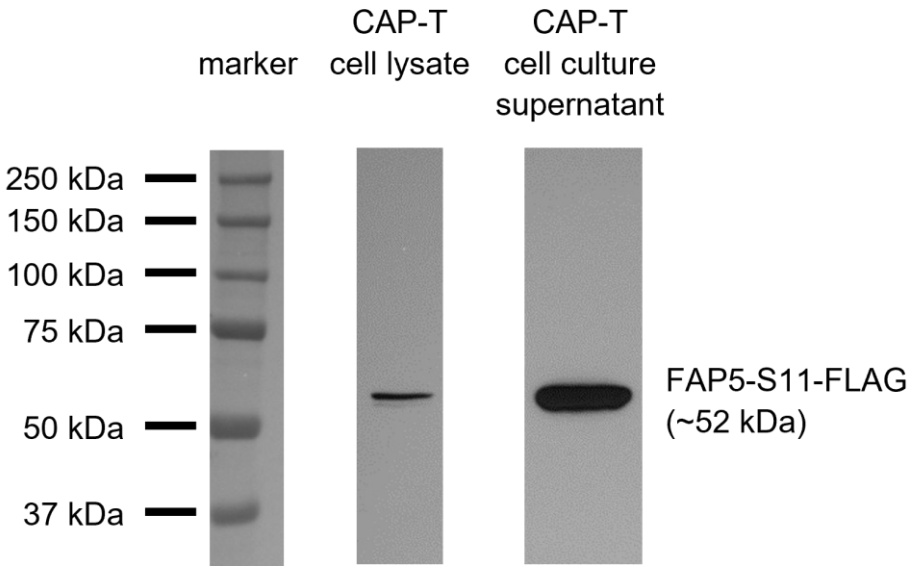

Figure 23: Successful expression and secretion of FAP5-S11-FLAG bispecific adapter molecule by CAP-T cells
CAP-T cells were transfected with pBSK-CMV_H1-FAP5-S11-FLAG and expression and secretion of FAP5-S11-FLAG was analyzed by Western Blot five days post transfection. Either 100 µg total protein of cell lysate or 27 µl of 18-fold concentrated cell culture supernatant were loaded and FAP5-S11-FLAG was detected using mouse-α-FLAG-M2 primary antibody and HRP-labeled α-mouse-IgG secondary antibody.

5.2.2 Plasmid transfection induces transient expression of the human fibroblast activation protein (hFAP) in HEK293T and HeLa cells

To evaluate an FAP5-S11-FLAG-mediated FAP-dependent cell transduction by retargeted adenoviral vectors, FAP was transiently expressed in two different cell lines. HEK293T and HeLa cells were transfected with the pBSK-CMV_hFAP expression plasmid, encoding a CMV promoter-controlled human FAP (hFAP) (further referred to as HEK293ThFAP and HeLahFAP, respectively) and hFAP expression was analyzed by flow cytometry 24 hours post transfection (Figure 24). Preliminary data showed that endogenous hFAP expression was neither detected in HEK293T nor HeLa cells. In contrast, HEK293ThFAP and HeLahFAP showed distinct hFAP expression with ~41% and ~56% of hFAP-positive cells, respectively.

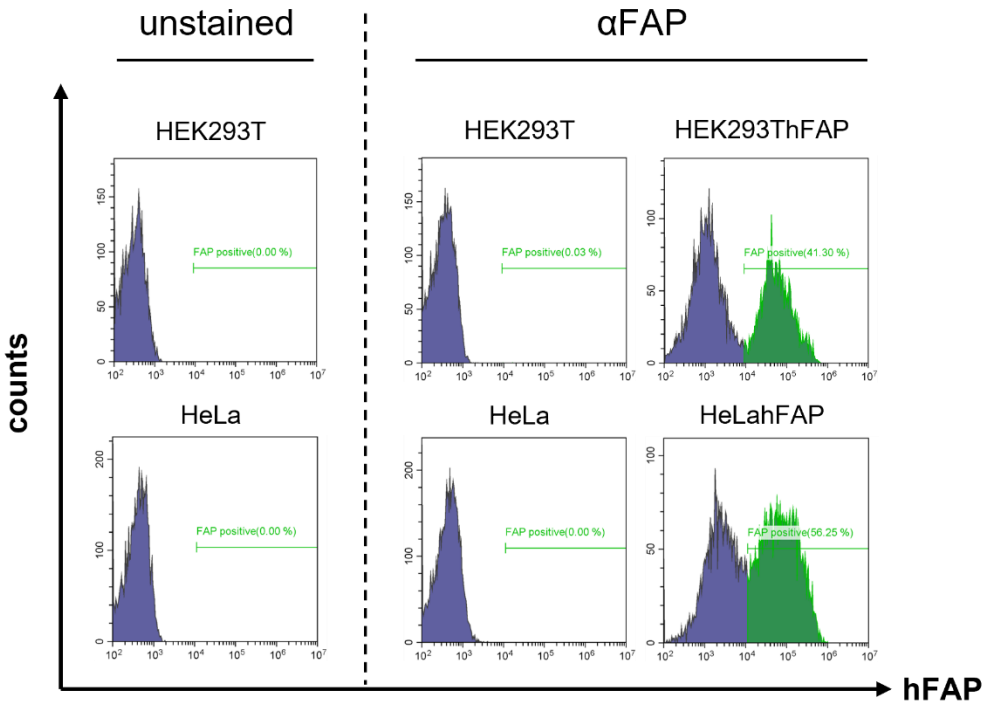

Figure 24: Transfection of HeLa and HEK293T cells with pBSK-CMV_hFAP induces hFAP expression
HEK293T and HeLa cells were transfected with pBSK-CMV_hFAP and hFAP expression was detected using mouse-α-FAP primary antibody and FITC-labeled α-mouse-IgG secondary antibody 24 hpt. Blue cell populations represent hFAP-negative cells, green cell populations indicate hFAP-positive cells. n=2

5.2.3 FAP5-S11-FLAG exhibits bispecific binding to hFAP and HAdV-5

Binding of FAP5-S11-FLAG to both hFAP and the adenovirus capsid is mandatory for an efficient retargeting of adenoviral vectors towards hFAP. Thus, the bispecific binding capacity of FAP5-S11-FLAG was investigated.

First, binding to hFAP was analyzed by flow cytometric analysis in HEK293ThFAP and HeLahFAP cells, at which HEK293T and HeLa cells were used as a negative control. Cells were incubated with supernatants of untransfected or pBSK-CMV_H1-FAP5(V_H-V_L)-S11(V_H-V_L)-FLAG-transfected CAP-T cells. Cell surface binding of the adapter molecule was detected using an α-FLAG antibody and hFAP expression was detected using an α-hFAP antibody (Figure 25).

Preliminary data confirmed distinct hFAP expression in HEK293ThFAP and HeLahFAP cells, while HEK293T and HeLa cells were hFAP negative. In line with hFAP expression, FAP5-S11-FLAG showed distinct binding to HEK293ThFAP and HeLahFAP, however, not to HEK293T or HeLa cells. In addition, in none of the samples background signals were detected for CAP-T cell culture supernatants lacking the FAP-S11-FLAG (ctrl). Thus, the FAP5-S11-FLAG bispecific adapter molecule within CAP-T cell culture supernatants was shown to specifically bind to membrane-associated hFAP in both HEK293ThFAP and HeLahFAP cells.

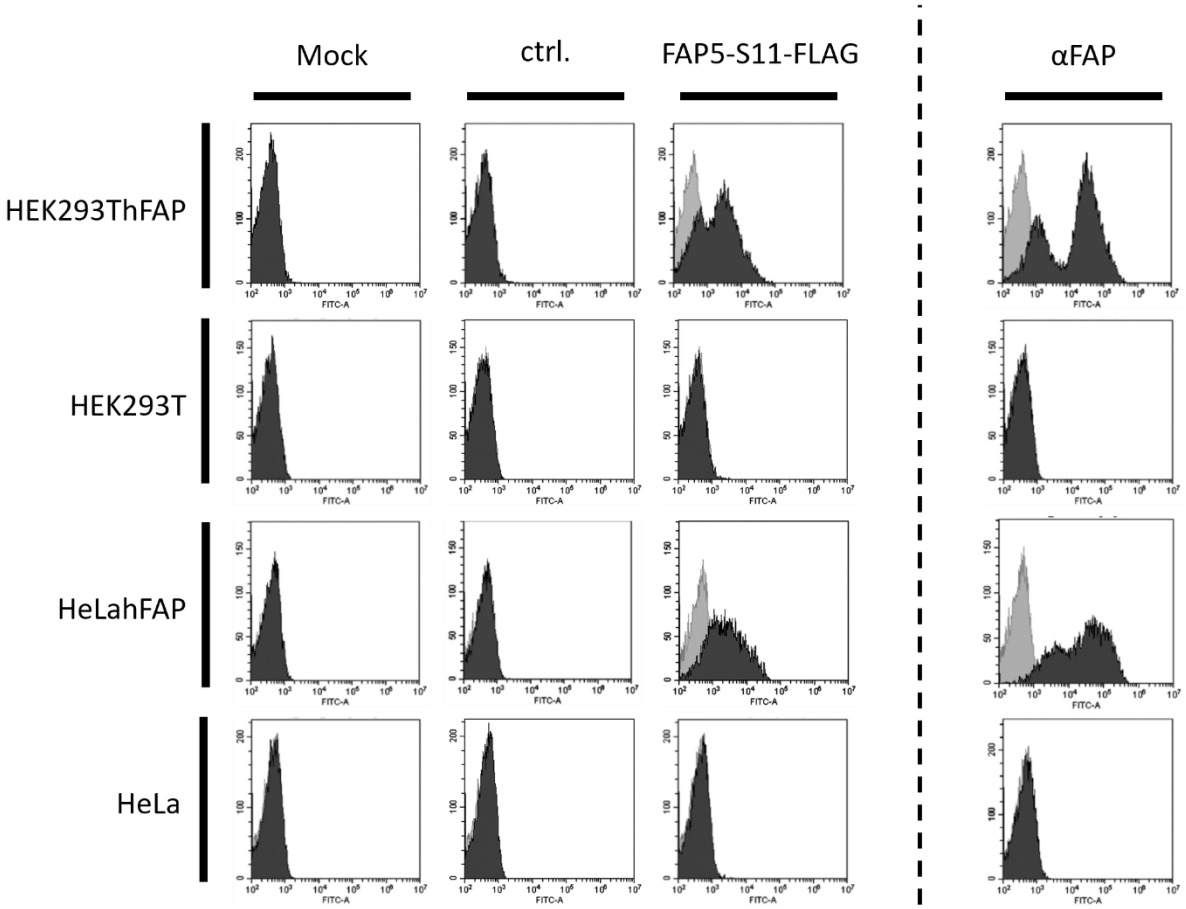

Figure 25: FAP5-S11-FLAG specifically binds to membrane-associated hFAP
hFAP expression was analyzed in HEK293T, HEK293ThFAP, HeLa, and HeLahFAP cells using mouse α-FAP primary antibody and FITC-labeled α-mouse-IgG secondary antibody (αFAP). Binding of FAP5-S11-FLAG to hFAP was analyzed by incubation of cells with 18x concentrated FAP5-S11-FLAG-containing CAP-T cell culture supernatants (FAP5-S11-FLAG). Cell surface binding of FAP5-S11-FLAG was detected using mouse α-FLAGM2 primary antibody and FITC-labeled α-mouse-IgG secondary antibody. CAP-T cell culture supernatants lacking the FAP5-S11-FLAG bispecific adapter molecule (ctrl) were used as a negative control. Bright grey cell populations indicate untreated cells. Dark grey cell populations indicate cells treated with the indicated regimen. n=1

Having confirmed that FAP5-S11-FLAG binds to membrane-associated hFAP, its binding to the adenovirus capsid was analyzed by ELISA. HAdV-5- and HAdV-5_ΔCAR-coated ELISA plates were incubated with CAP-T cell culture supernatants containing FAP5-S11-FLAG or supernatants of untransfected CAP-T cells (ctrl) in different dilutions and vector-bound FAP5-S11-FLAG was detected using α-FLAG antibody (Figure 26). Preliminary data confirmed FAP5-S11-FLAG bound similarly to both HAdV-5 and HAdV-5_ΔCAR particles in a dilution dependent manner. Thus, the ΔCAR mutation was shown not to interfere with binding of FAP5-S11-FLAG to the vector capsid.

Taken together, this data indicated that the FAP5-S11-FLAG bispecific adapter molecule bound to both cell surface-expressed hFAP and the adenoviral capsid.

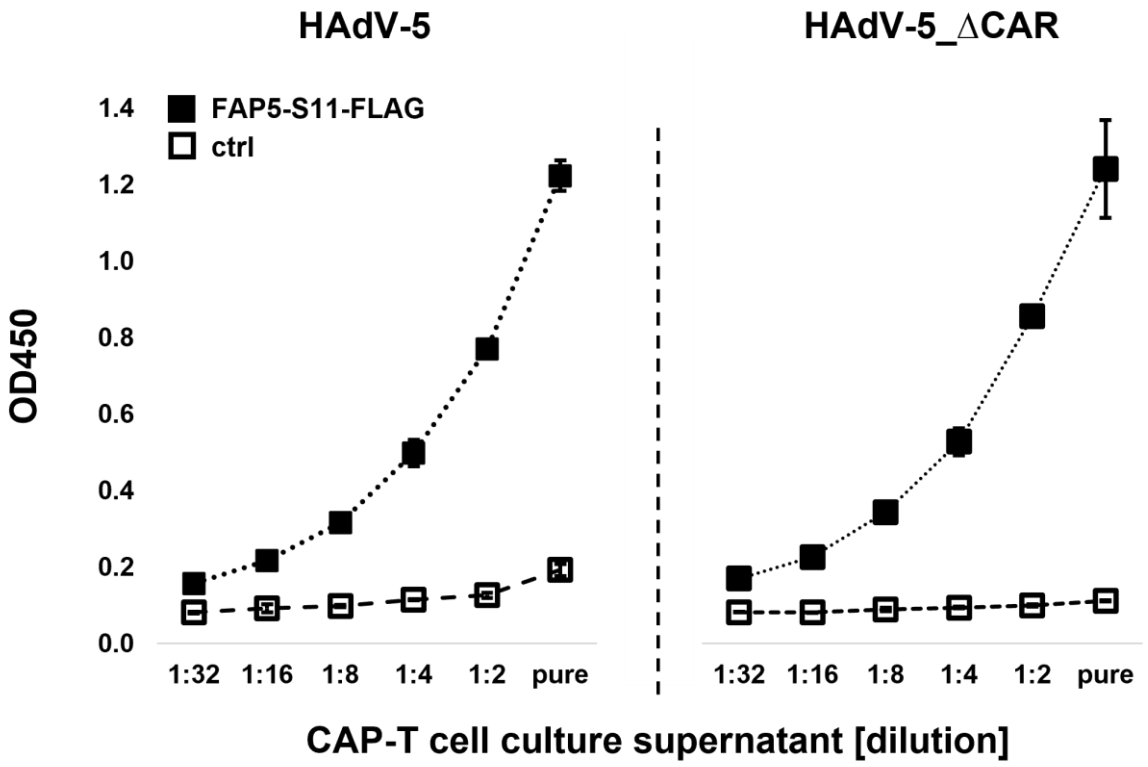

Figure 26: FAP5-S11-FLAG binds to HAdV-5 and HAdV-5_ΔCAR vector particles
ELISA plates coated with $1x10^{10}$ vector particles per well of either HAdV-5 and HAdV-5_ΔCAR were incubated with CAP-T cell culture supernatants either containing FAP5-S11-FLAG or not (ctrl). FAP5-S11-FLAG was detected using mouse-α-FLAGM2 primary antibody and HRP-labeled α-mouse-IgG secondary antibody. Optical densities were measured at a wavelength of 450 nm (OD450). n=1

5.2.4 FAP5-S11-FLAG retargets HAdV-5_ΔCAR vectors towards hFAP

The FAP5-S11-FLAG bispecific adapter molecule was shown to exhibit bispecific binding capacity to hFAP and the adenovirus capsid. To investigate whether HAdV-5-based vectors can be retargeted towards hFAP-expressing cells by the FAP5-S11-FLAG bispecific adapter molecule, a retargeting assay was performed. To avoid CAR-mediated cell transduction, the HAdV-5_ΔCAR vector was used. Vector particles were pre-incubated with either CAP-T cell culture supernatants containing the

FAP5-S11-FLAG, CAP-T cell culture supernatants lacking the FAP5-S11-FLAG (ctrl) or fresh cell culture medium (PEM). Subsequently, samples were used for transduction of HEK293T or HEK293ThFAP cells and transduction efficiencies were evaluated after 24 hours by fluorescence microscopic evaluation for eGFP-positive cells (Figure 27).

Preliminary results revealed almost no transduction of HEK293T and HEK293ThFAP cells by HAdV-5_ΔCAR pre-incubated in CAP-T cell culture supernatants lacking the FAP5-S11-FLAG or PEM. Pre-incubation of HAdV-5_ΔCAR particles in CAP-T cell culture supernatants containing the FAP5-S11-FLAG in turn resulted in a substantial transduction of HEK293ThFAP cells, however, not HEK293T cells. Thus, this preliminary data indicated that the bispecific adapter molecule FAP5-S11-FLAG mediates retargeting of HAdV-5-based vectors towards hFAP-expressing cells.

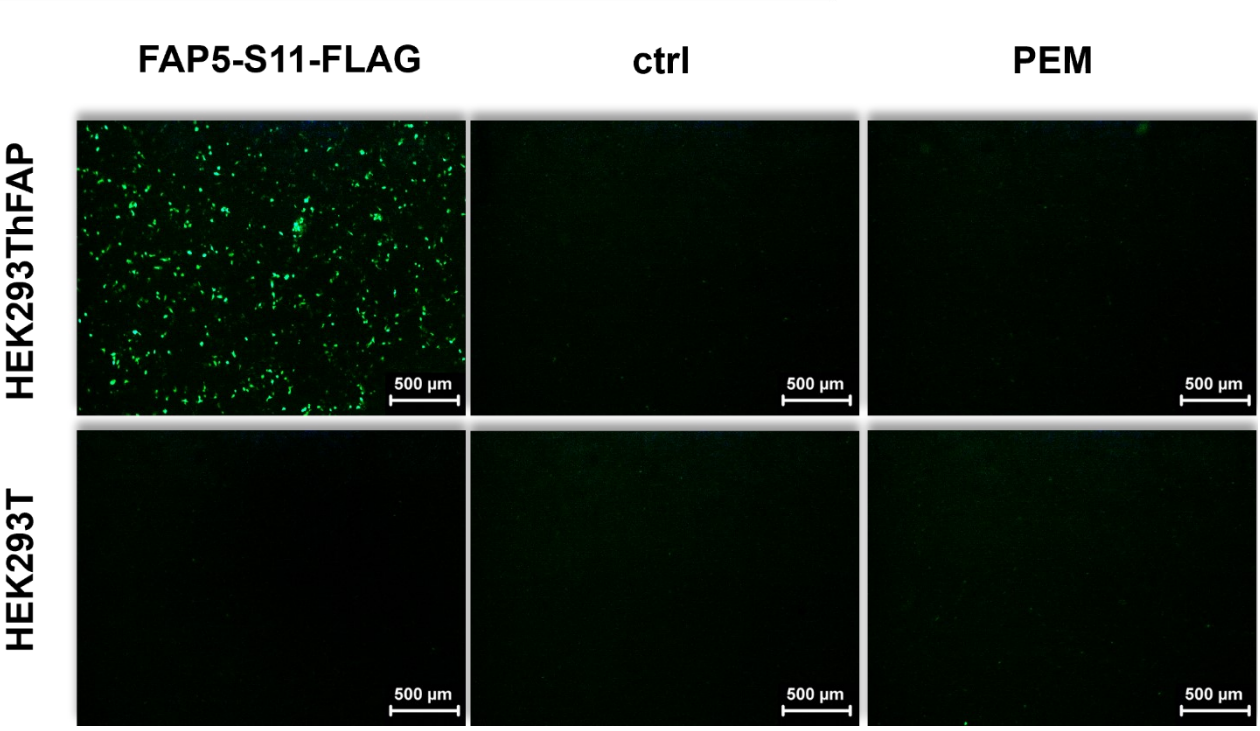

Figure 27: Successful retargeting of HAdV-5-based vectors to hFAP-expressing cells by bispecific FAP5-S11-FLAG adapter molecule

HEK293ThFAP and HEK293T cells were transduced with pMOI 1000 of HAdV-5_ΔCAR pre-incubated in either CAP-T cell culture supernatants containing FAP5-S11-FLAG, CAP-T cell culture supernatants lacking FAP5-S11-FLAG (ctrl) or fresh CAP-T cell culture medium (PEM). Transduction efficiencies were evaluated 24 hpt by fluorescence microscopy for eGFP-positive cells. n=1

5.3 Tumor targeting by a surface-charge modified HAdV-5 hexon mutant oncolytic vector

Hexon is the most abundant structural capsid protein of HAdV-5 particles and negatively charged amino acids within the HVR1 region of hexon mainly contribute to the overall negative surface charge of HAdV-5 virions. By previous work in the Department of Gene Therapy at University Ulm, a HAdV-5 mutant vector was generated in which a stretch of 13 predominately negatively charged amino acids within the HVR1 region of the hexon protein were deleted and substituted by four consecutive positively charged lysine residues (Figure 28). The obtained mutant vector HAdV-5-HexPos3 exhibited a significantly reduced overall negative surface charge and showed remarkably increased transduction efficiencies in human cancer cell lines in a CAR-independent manner as shown by a CAR binding-ablated HAdV-5-HexPos3_ΔCAR vector.[311] Due to these advantageous characteristics, the HAdV-5-HexPos3_ΔCAR vector was further characterized regarding its potential as an oncolytic virus *in vitro* and *in vivo*.

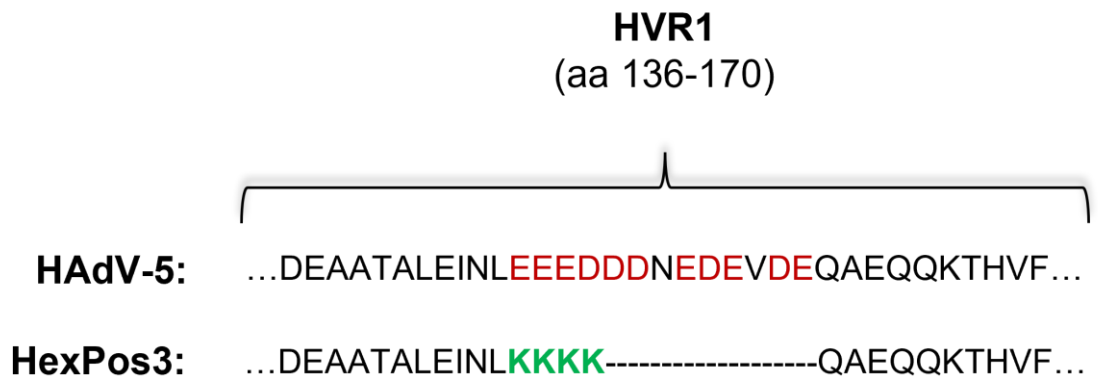

Figure 28: Partial HVR1 amino acid sequence of wild-type HAdV-5 and HAdV-5-HexPos3.
To generate the HAdV-5-HexPos3 vector, a 13 aa spanning stretch of mainly negatively charged amino acids (red letters) within the HVR1 region of hexon were deleted and partially replaced by four consecutive positively charged lysins (green letters). HVR1: hyper variable region 1.

5.3.1 NSG mouse plasma significantly enhances transduction of HAdV-5-HexPos3_ΔCAR in human cancer cell lines

HAdV-5-HexPos3_ΔCAR was previously shown to exhibit significantly enhanced transduction efficiencies in human cancer cell lines in a CAR-independent manner *in vitro*[311]. With the aim to assess potential effects of murine blood plasma components to the HAdV-5-HexPos3_ΔCAR infectivity prior to *in vivo* experiments, transduction assays in presence of NSG mouse plasma were performed. HAdV-5-HexPos3_ΔCAR and a control vector lacking the HexPos3 capsid modification (HAdV-5_ΔCAR) were used to transduce SK-Mel-28, A549, UD-SCC-2 and UM-SCC-11B cancer cells in either presence or absence of murine NSG plasma (Figure 29).

As already reported for A549 and UM-SCC-11B cells[311], HAdV-5-HexPos3_ΔCAR exhibited significantly enhanced transduction efficiencies in all cancer cell lines tested in the absence of murine plasma, including UD-SCC-2 and SK-Mel-28 (Figure 29A). Compared to HAdV-5_ΔCAR, transduction efficiencies of HAdV-5-HexPos3_ΔCAR in SK-Mel-28, A459, UD-SCC-2 and UM-SCC-11B cells were increased ~4.5-, ~11-, ~14-, and ~40-fold, respectively. Interestingly, NSG mouse plasma further improved transduction efficiencies of HAdV-5-HexPos3_ΔCAR in SK-Mel-28, A549 and UD-SCC-2 cells ~51-, ~12.8-, and ~9.8-fold, respectively while transduction efficiencies in UM-SCC-11B cells remained almost unaffected. In contrast, transduction efficiencies of HAdV-5_ΔCAR in presence of NSG mouse plasma remained unaffected in UD-SCC-2, SK-Mel-28 and A549 cells, while a ~7-fold increase was observed in UM-SCC-11B cells (Figure 29B). Taken together, HAdV-5-HexPos3_ΔCAR was shown to exhibit significantly enhanced, CAR-independent transduction efficiency in various different human cancer cell lines, which is further enhanced by NSG mouse plasma. This suggested HAdV-5-HexPos3_ΔCAR as a promising oncolytic virus candidate that needs to be further investigated *in vivo*.

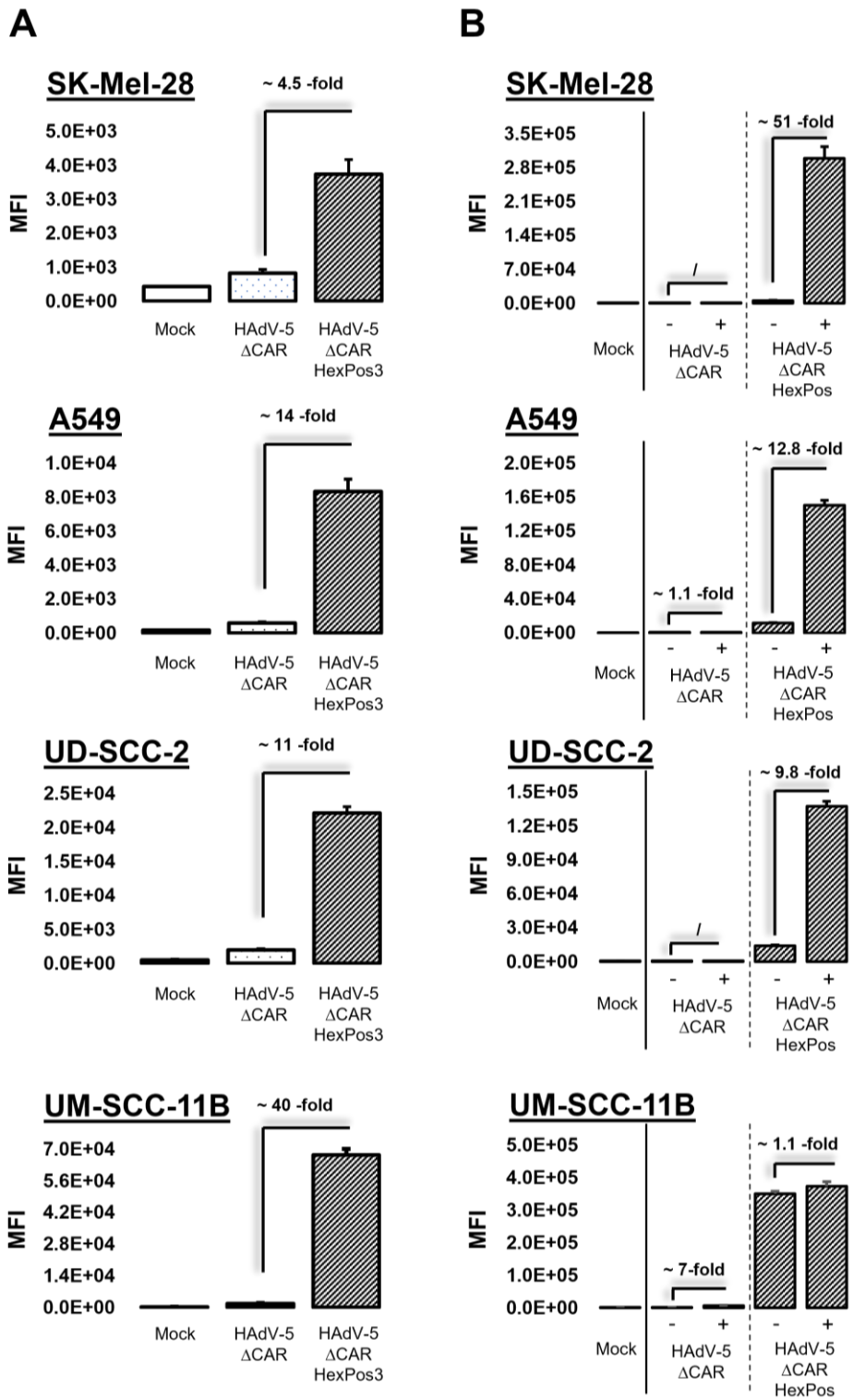

Figure 29: NSG mouse plasma improves transduction of human cancer cell lines by HAdV-5-HexPos3_ΔCAR *in vitro*

SK-Mel-28, A549, UD-SCC-2 and UM-SCC-11B cells were transduced with pMOI 1000 of either HAdV-5_ΔCAR or HAdV-5-HexPos3_ΔCAR **(A)** alone or **(B)** in either absence (-) or presence (+) of murine NSG mouse plasma. Transduction efficiencies were evaluated by quantification of mean fluorescence intensities (MFI) 24 hpt using flow cytometry. Results are given as mean ± standard deviation (n=3).

5.3.2 HAdV-5-HexPos3_ΔCAR exhibits significantly reduced off-target tissue tropism and improved tumor targeting after intravenous injection

HAdV-5-HexPos3_ΔCAR showed significantly improved transduction efficiencies in human cancer cell lines *in vitro* that was further improved in presence of NSG mouse plasma. To investigate tumor targeting and biodistribution of HAdV-5-HexPos3_ΔCAR *in vivo*, subcutaneous UD-SCC-2 xenograft-bearing NSG mice were intravenously injected with either HAdV-5-HexPos3_ΔCAR or HAdV-5_ΔCAR after 14 days of tumor growth. Three days after vector injection, mice were euthanized, organs and tumors were harvested and vector genome copy numbers within lungs, spleens, kidneys, hearts, livers, and tumors were analyzed by qPCR analysis (Figure 30A).

Except for the heart, HAdV-5-HexPos3_ΔCAR showed significantly reduced vector loads in all organs analyzed, including the liver, the main off-target organ of HAdV-5-based vectors. The reduced liver uptake of HAdV-5-HexPos3_ΔCAR was further confirmed by fluorescence microscopic evaluation of liver sections, in which almost no eGFP-positive cells were observed (Figure 30B). In contrast, abundant eGFP-positive cells were observed in liver sections of mice injected with HAdV-5_ΔCAR confirming the pronounced liver tropism of unmodified HAdV-5-based vectors. However and interestingly, significantly increased intratumoral vector loads were detected for HAdV-5-HexPos3_ΔCAR leading to a ~29-fold increased tumor/liver ratio compared to HAdV-5_ΔCAR (Figure 30A). Thus, due to its reduced off-target organ uptake and significantly increased tumor uptake, these data indicated an improved tumor targeting and potentially reduced vector toxicity of HAdV-5-HexPos3_ΔCAR *in vivo* after i.v. injection.

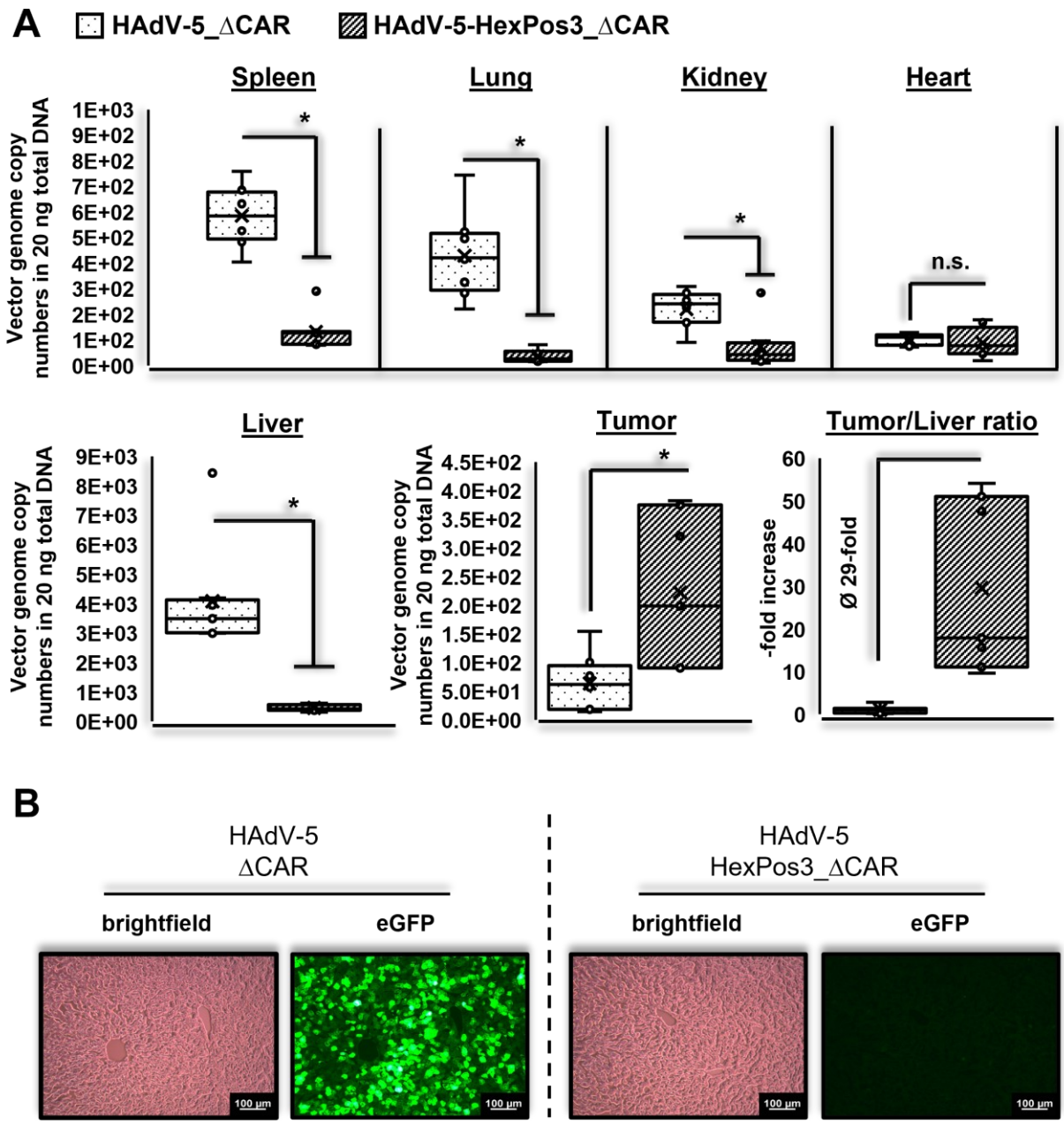

Figure 30: HAdV-5-HexPos3_ΔCAR exhibits improved tumor targeting and less off-target organ tropism after intravenous injection

Subcutaneous UD-SCC-2 tumor-bearing NSG mice were intravenously injected with $2x10^{10}$ vector particles of either HAdV-5_ΔCAR or HAdV-5-HexPos3_ΔCAR after 14 days of tumor growth. Three days after vector injection, organs and tumors were harvested and **(A)** vector genome copy numbers within spleens, lungs, kidneys, livers, and tumors were quantified by qPCR analysis and tumor/liver ratios were calculated. n=7-8; * = $p<0.05$; n.s. = not significant. Hepatocyte transduction by HAdV-5_ΔCAR and HAdV-5-HexPos3_ΔCAR was additionally evaluated by **(B)** fluorescence microscopic evaluation of liver sections. Shown are representative pictures from mice i.v. injected with either HAdV-5_ΔCAR or HAdV-5-HexPos3_ΔCAR. Data set for HAdV-5_ΔCAR shown in (A) has been published in Wienen *et al.* 2022, Figure 4b; Figure 5a; Figure 7b;

To exclude that the diminished liver transduction by HAdV-5-HexPos3_ΔCAR was not caused by a rapid vector clearance due to an elevated particle uptake by Kupffer cells, BALB/c mice were intravenously injected with either PBS, or $2x10^{10}$ vector particles of either HAdV-5_ΔCAR or HAdV-5-HexPos3_ΔCAR and vector genome copy numbers within livers were analyzed by qPCR analysis 20 minutes after vector injection (Figure 31). Compared to HAdV-5_ΔCAR, HAdV-5-HexPos3_ΔCAR showed slightly, however, not statistically significant elevated genome copy numbers in the liver 20 minutes after vector injection, indicating that HAdV-5-HexPos3_ΔCAR was not excessively taken up by liver residential Kupffer cells.

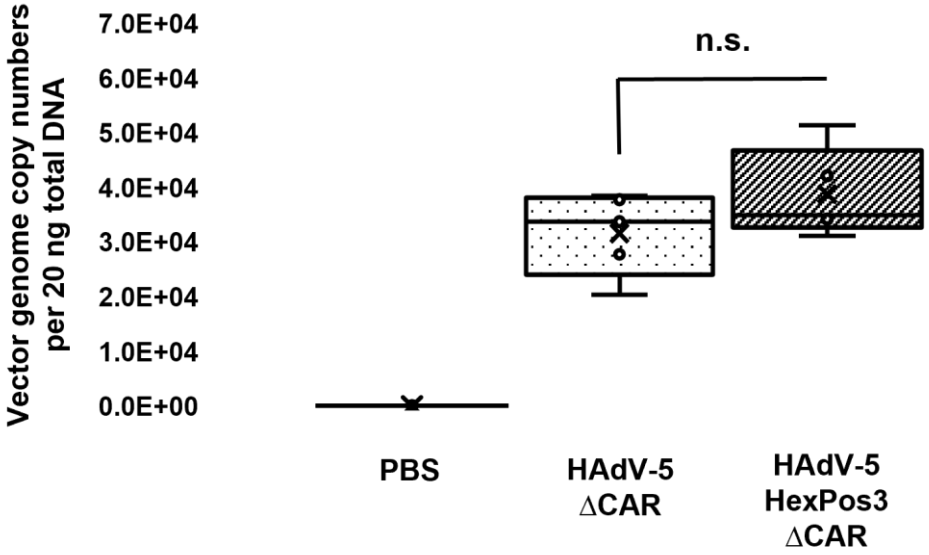

Figure 31: HAdV-5-HexPos3_ΔCAR does not exhibit elevated uptake into the liver early after intravenous vector injection
BALB/c mice were intravenously injected with either PBS or $2x10^{10}$ particles of either HAdV-5_ΔCAR or HAdV-5-HexPos3_ΔCAR. Twenty minutes after vector injection, livers were harvested and vector genome copy numbers were analyzed by qPCR analysis. n=5; n.s. = not significant. Data for PBS and HAdV-5_ΔCAR published in Wienen *et al.* 2022, Figure 4d; CC BY-NC-ND 4.0, https://creativecommons.org/licenses/by-nc-nd/4.0/

5.3.3 Generation of conditionally replicating adenoviral vectors

HAdV-5-HexPos3_ΔCAR showed significantly improved tumor targeting and reduced off-target organ tropism compared to the unmodified control vector HAdV-5 _ΔCAR after intravenous injection, indicating an improved oncolytic potential and reduced vector toxicity *in vivo*. However, tumor lysis requires virus replication, which necessarily increases the risk of vector-induced side-effects due to virus replication in healthy cells and tissues. To overcome this limitation and to improve the safety of oncolytic adenoviral vectors, conditionally replicating adenoviral vectors (CRAds) were designed, which should predominately replicate in cancer cells with aberrant cell cycle control. Based on the HAdV-5 wild-type virus (HAdV-5wt), three CRAds were generated by successive genetic mutations within cell cycle modulatory viral genes that are essential for virus replication in healthy cells, however, negligible in cancer cells. A first CRAd was generated by deletion of a 24 bp stretch within the CR1 region of *E1A* (HAdV-5_E1AΔ24bp). This mutation was previously shown to ablate binding of E1A to the retinoblastoma protein, which prevents E1A-mediated S-phase induction in quiescent healthy cells[312]. A second CRAd was generated by partial deletion of the *E1B19k* gene (HAdV-5_E1AΔ24bp_ΔE1B19k). During virus replication, E1B19k blocks apoptosis due to binding to the pro-apoptotic proteins BAK[101,102] and BAX[103,104]. Healthy cells infected by a ΔE1B19k vector thus should rapidly undergo apoptosis before onset of productive virus replication. Furthermore, E1B19k is suggested to interact with the adenoviral death protein (ADP)[313], which is involved in host cell lysis at late stages of viral replication[120] and deletion of E1B19k was shown to accelerate viral progeny release[153–156]. A third CRAd additionally harbored a partial deletion of the *E3gp19k* gene (HAdV-5_E1AΔ24bp_ΔE1B19k_ΔE3gp19k) without affecting other *E3*-encoded genes. E3gp19k inhibits MHC class I (MHC-I)-mediated viral antigen presentation by the infected cell during virus replication[157–159]. Healthy cells infected by a ΔE3gp19k vector thus should be rapidly recognized and eradicated by the host immune system. All CRAds were equipped with a CMV promoter-driven eGFP-NanoLuciferase fusion reporter cassette inserted in a non-coding region between *E1A* and *E1B*. A schematic representation of the genomic arrangement is illustrated in figure 32.

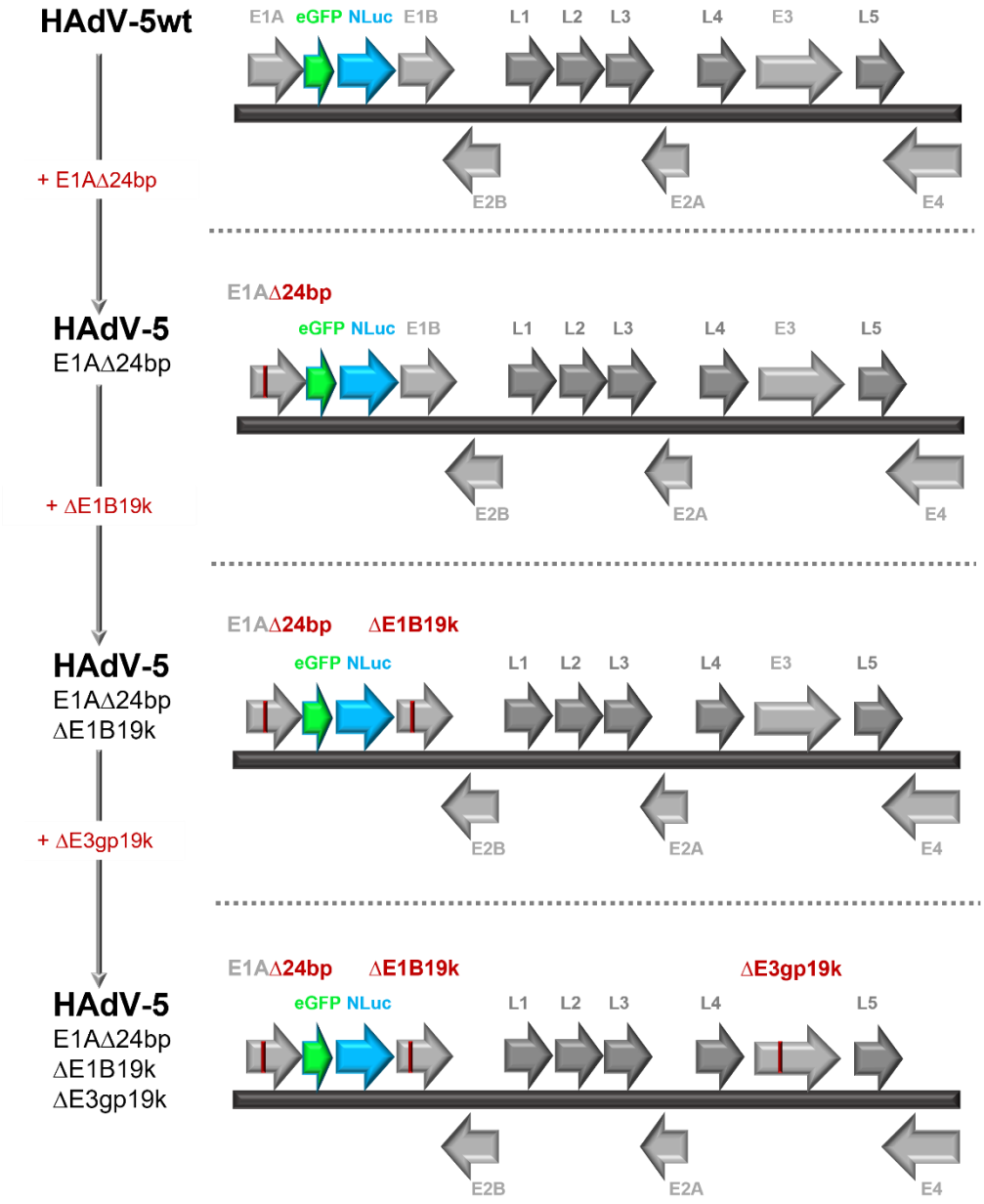

Figure 32: Genomic arrangement of the generated CRAds
Based on the HAdV-5 wild-type virus (HAdV-5wt), HAdV-5_E1AΔ24bp was generated by a defined 24 bp deletion within the CR1 region of *E1A*. Further partial deletions of *E1B19k* and *E3gp19k* sequences resulted in HAdV-5_E1AΔ24bp_ΔE1B19k and HAdV-5_E1AΔ24bp_ΔE1B19k_ΔE3gp19k, respectively. HAdV-5wt and all CRAds were equipped with a CMV promoter-driven eGFP-NanoLuciferase (eGFP-NLuc) reporter cassette inserted between *E1A* and *E1B*. The illustrations shown schematically represent the double stranded (ds) DNA genome of HAdV-5wt and the respective CRAds. E = early gene regions; L = late gene regions

All CRAds were produced to normal titers and vector integrities at the genomic and physical levels were verified by enzymatic restriction analysis and genome sequencing, respectively (data not shown). Purity of the respective vector preparations were additionally verified by silver staining (data not shown). Infectivity of the generated CRAds was verified by transduction assays using A549 and UD-SCC-2 cells (Figure 33). All CRAds showed transduction efficiencies comparable to HAdV-5wt in both cell lines analyzed, indicating comparable infectious titers.

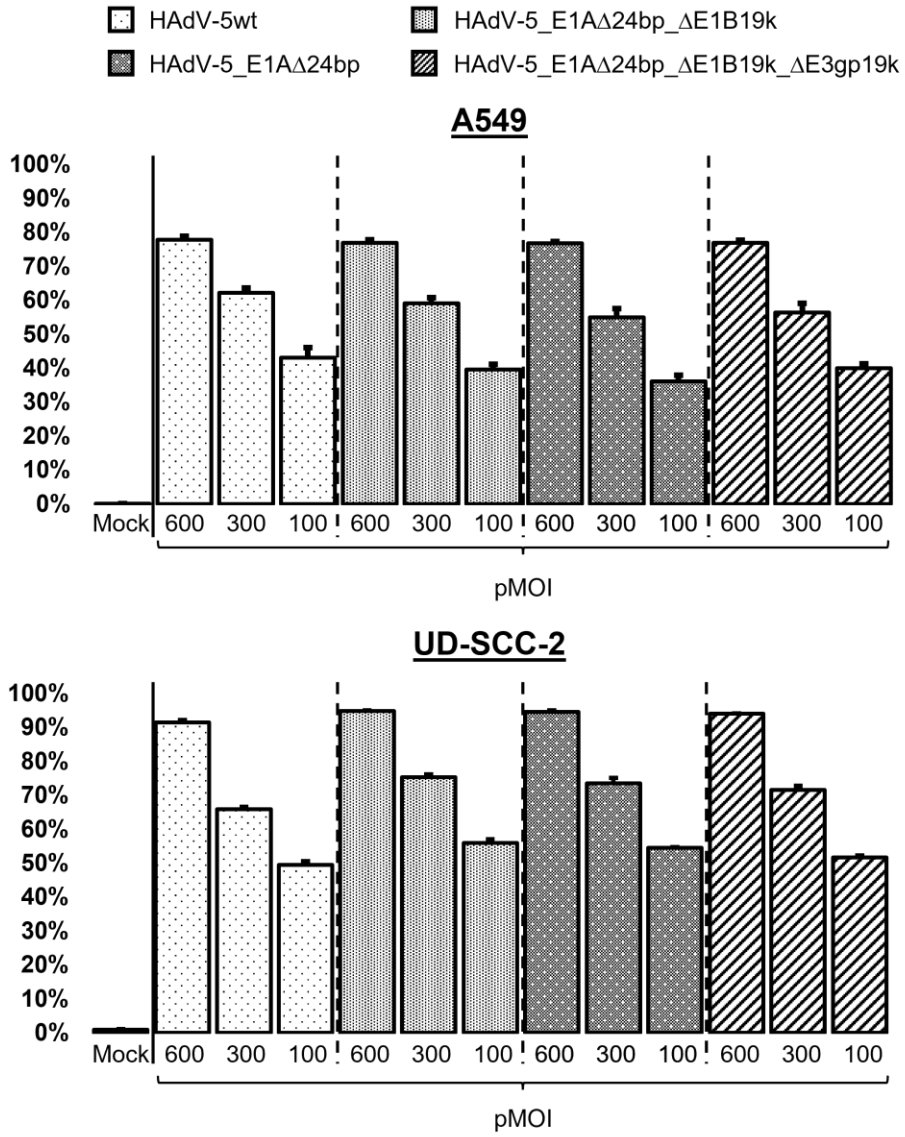

Figure 33: Comparable infectivity of HAdV-5wt and CRAds
A549 and UD-SCC-2 cells were infected with HAdV-5wt, HAdV-5_E1AΔ24bp, HAdV-5_E1AΔ24bp_ΔE1B19k and HAdV-5_E1AΔ24bp_ΔE1B19k_ΔE3gp19k with the indicated pMOI and eGFP-positive cells were evaluated 24 hpi by flow cytometry. n=3

5.3.4 E1B19k-deleted adenoviral vectors showed improved oncolytic potential and selective replication in cancer cells *in vitro*

CRAds are designed to preferentially replicate in and lyse cancer cells while not harming healthy cells or tissues. To investigate the oncolytic potential of the generated CRAds *in vitro*, a cytotoxicity assay was performed in SK-Mel-28, UD-SCC-2 and A549 human cancer cell lines. To further investigate whether replication of the generated CRAds was restricted to cancer cells, an analogous assay was performed in human primary, non-cancerous HSAEpC cells. Cells were infected with low pMOI ranging from 1 to 0.031 in serial 1:2 dilutions and virus replication-induced cytotoxicity was evaluated after indicated incubation times by crystal violet staining of remaining cells (Figure 34).

Compared to HAdV-5wt, both E1B19k-deleted CRAds, HAdV-5_E1AΔ24bp_ΔE1B19k and HAdV-5_E1AΔ24bp_ΔE1B19k_ΔE3gp19k, showed significantly improved cell lysis in all cancer cell lines tested while in contrast cell lysis by HAdV-5_E1AΔ24bp appeared to be impaired compared to HAdV-5wt. This effect was most pronounced in UD-SCC-2 cells in which almost no cell lysis by HAdV-5wt and HAdV-5_E1AΔ24bp was observed, while in contrast HAdV-5_E1AΔ24bp_ΔE1B19k and HAdV-5_E1AΔ24bp_ΔE1B19k_ΔE3gp19k lysed almost all cells at all pMOIs tested. Importantly, primary HSApC cells were not lysed by HAdV-5_E1AΔ24bp_ΔE1B19k and HAdV-5_E1AΔ24bp_ΔE1B19k_ΔE3gp19k infection, indicating strictly restricted replication of these CRAds to cancer cells. In contrast, HAdV-5wt and HAdV-5_E1AΔ24bp showed almost complete cell lysis in primary HSApC cells at all pMOIs tested, indicating for insufficient cancer cell restricted replication. Since HAdV-5_E1AΔ24bp_ΔE1B19k_ΔE3gp19k showed the most efficient cancer cell lysis but absent replication in primary cells, it was considered the most promising CRAd for further *in vivo* studies and will be further referred to as HCRAd-5 in all following experiments.

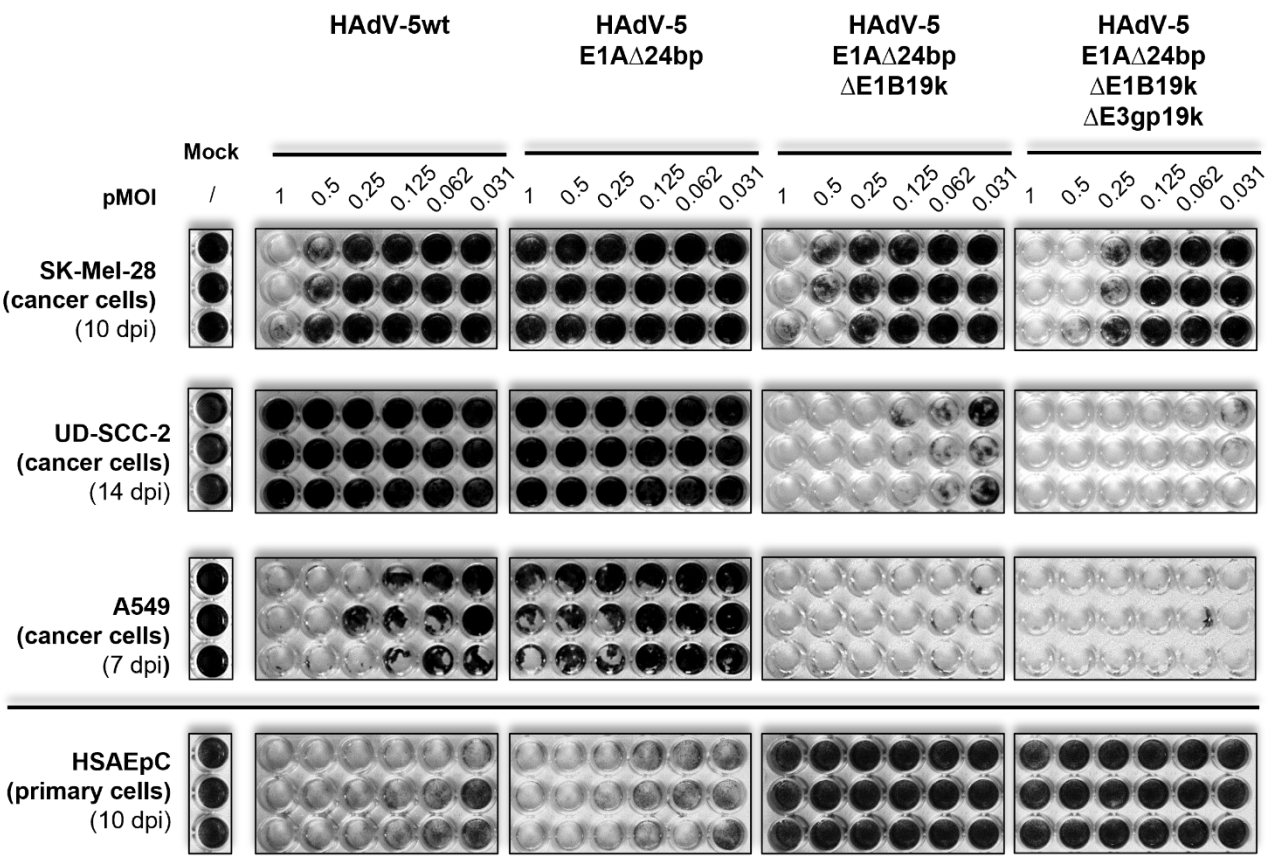

Figure 34: *E1B19k* deletion improves the oncolytic potential of HAdV-5-based CRAds and restricts virus replication to cancer cells *in vitro*.
SK-Mel-28, UD-SCC-2, A549 and non-cancerous primary HSAEpC cells were infected with HAdV-5wt, HAdV-5_E1AΔ24bp, HAdV-5_E1AΔ24bp_ΔE1B19k and HAdV-5_E1AΔ24bp_ΔE1B19k_ΔE3gp19k with the indicated pMOI. After the indicated time periods, remaining cells were washed with PBS, fixed in 4% PFA and stained by crystal violet. n=3-4. dpi = days post infection.

To visualize the spread of HAdV-5wt and CRAds, UD-SCC-2 cells were infected with low pMOI and additionally evaluated for eGFP-positive cells by fluorescence microscopy at six days post infection (Figure 35). Only few eGFP-positive cells were observed in wells infected with HAdV-5wt and HAdV-5_E1AΔ24bp, indicating limited viral spread. Distinct spread, however, was observed for both of the E1B19k-deleted CRAds, as indicated by comet-like shaped eGFP-positive cell clusters. Fitting to the results obtained by crystal violet staining, additional deletion of E3gp19k resulted in even enhanced spread compared to solely deletion of E1B19k.

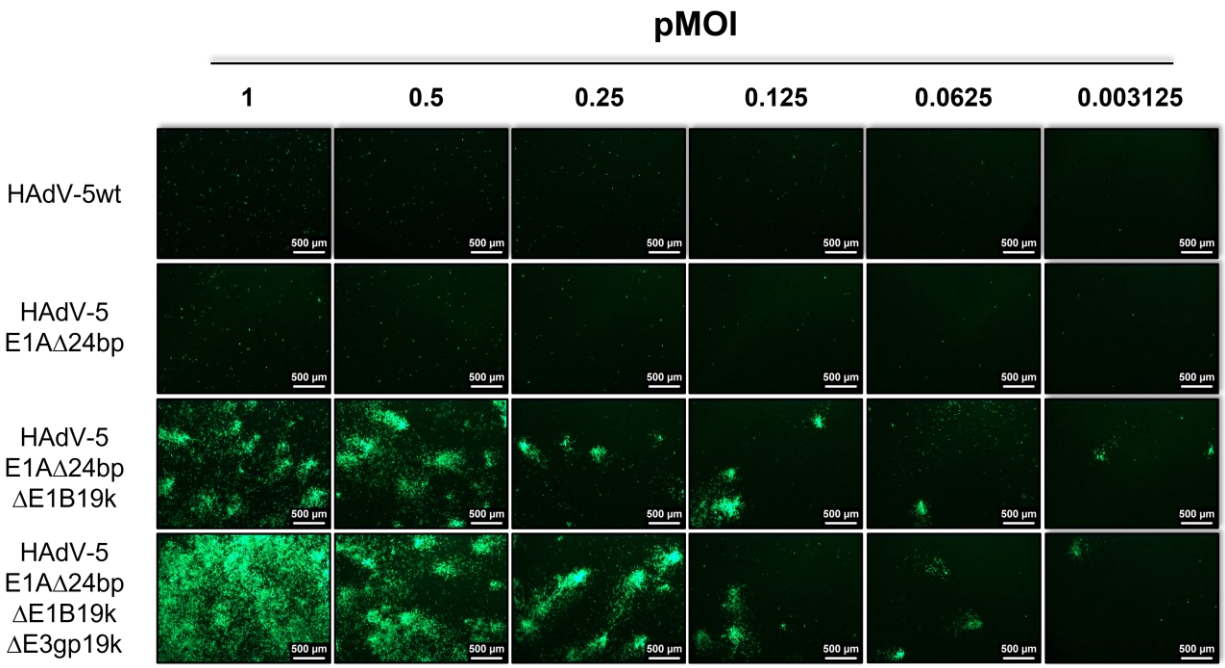

Figure 35: Deletion of E1B19k significantly enhances spread of CRAds in UD-SCC-2 cells
UD-SCC-2 cells were infected with either HAdV-5wt, HAdV-5_E1AΔ24bp, HAdV-5_E1AΔ24bp_ΔE1B19k or HAdV-5_E1AΔ24bp_ ΔE1B19k_ΔE3gp19k with the indicated pMOI. Six days post infection, cells were evaluated for viral spread by fluorescence microscopic evaluation of eGFP-positive cells. Shown are representative pictures of n=3.

5.3.5 HexPos3 capsid mutation significantly reduces virus toxicity after i.v. injection

HCRAd-5 (HAdV-5_E1AΔ24bp_ ΔE1B19k_ΔE3gp19k) showed efficient cancer cell lysis and absent replication in primary cells *in vitro*, indicating improved oncolytic potential and vector safety. To further improve tumor targeting and to reduce off-target organ tropism *in vivo* after i.v. vector injection, the previously described HexPos3 and ΔCAR capsid mutations were genetically introduced into HCRAd-5, generating the HCRAd-5-HexPos3_ΔCAR vector and its respective control counterpart HCRAd-5_ΔCAR. Both vectors were equipped with a CMV promoter-driven firefly luciferase reporter gene inserted between *E1A* and *E1B* and their oncolytic potential was investigated *in vivo*. To this end, subcutaneous UD-SCC-2 tumor-bearing NSG mice were intravenously injected with either PBS or $2x10^{10}$ vector particles of HCRAd-5-HexPos3_ΔCAR or HCRAd-5_ΔCAR. Different from previous *in vivo* experiments, vector injection was performed after 21 days of tumor growth in order to allow for better tumor vascularization. Anti-tumor efficacies and tumor targeting were respectively evaluated by daily measurements of tumor sizes and *in vivo* detection of vector-derived luciferase expression, the latter being analyzed by IVIS measurement at 2, 3, 7, 14, 21, 28, 35, 43, 46, and 56 days after vector injection.

Already 48 h after vector injection, HCRAd-5_ΔCAR-injected mice showed treatment related adverse side-effects including a rapid drop of their body weight, impaired activity and agility, diminished skin turgor and reduced tactile stimulation, altogether indicating severe toxicity. In contrast, mice treated with HCRAd-5-HexPos3_ΔCAR behaved like PBS-injected mice and showed no signs of toxicity throughout the entire observation period. Fitting to previous biodistribution analysis, IVIS measurement revealed strong luciferase expression in the liver of HCRAd-5_ΔCAR-injected mice at 48 h post vector administration, while hepatic luciferase expression was weak or absent in HCRAd-5-HexPos3_ΔCAR- or PBS-injected mice, respectively (Figure 36). A rapid deterioration in the general health condition of HCRAd-5_ΔCAR-injected mice necessitated to sacrifice respective mice.

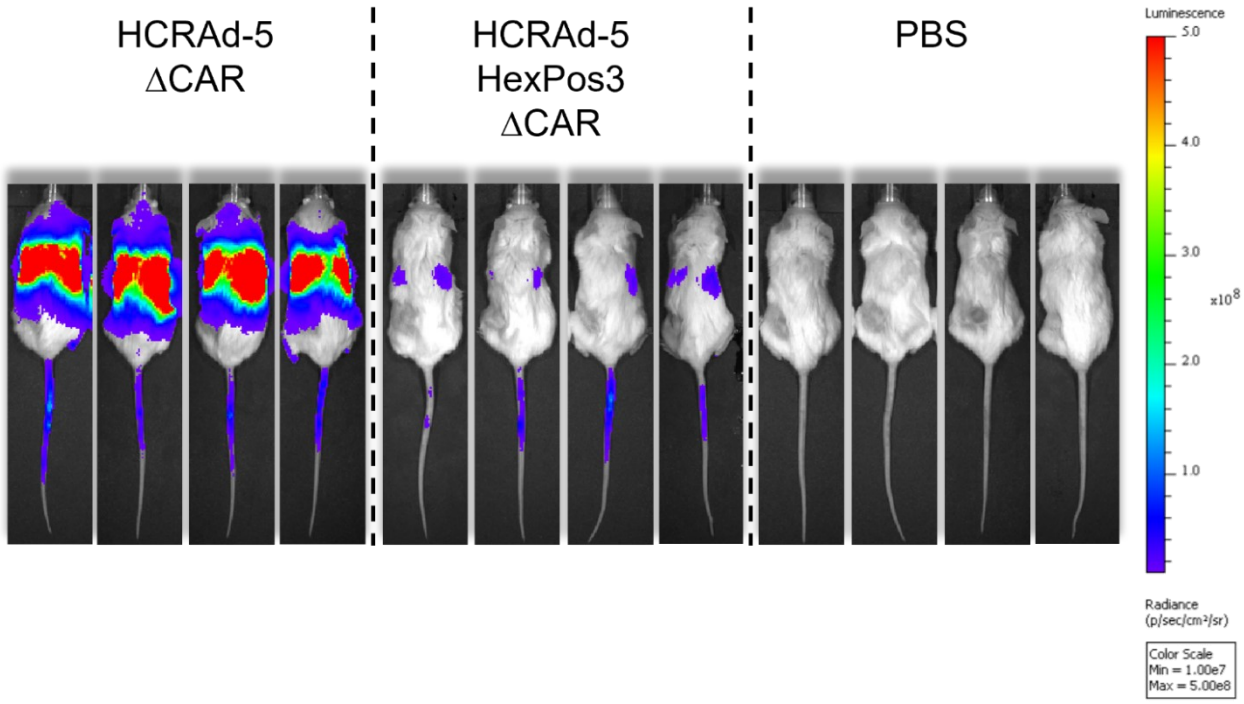

Figure 36: HCRAd-5-HexPos3_ΔCAR exhibits reduced liver tropism and significantly reduced vector toxicity after i.v. injection

Subcutaneous UD-SCC-2 tumor-bearing NSG mice were intravenously injected with either PBS or $2x10^{10}$ vector particles of HCRAd-5_ΔCAR or HCRAD-5-HexPos3_ΔCAR after 21 days of tumor growth. Forty-eight hours after vector injection, mice were narcotized, intraperitoneally injected with 200 µl firefly luciferase substrate and luciferase activities were analyzed by the IVIS 200 *in vivo* imaging system. Shown are representative images of four mice from each group (n=12).

5.3.6 Intravenous injection of HCRAd-5_ΔCAR causes severe hepatic damage in NSG mice

Intravenous injection of HCRAd-5_ΔCAR resulted in severe vector-induced toxicity necessitating the sacrifice of respective mice 48 hours post vector administration. Interestingly, blood samples of all HCRAd-5_ΔCAR-injected mice were observed to exhibit severely impaired coagulation (data not shown). Given that and due to the abundant luciferase expression within livers of HCRAd-5_CAR-injected mice, hepatic damage was hypothesized to be a possible reason for the observed toxic side-effects. Thus, aspartate aminotransferase (AST) and alanine aminotransferase (ALT) concentrations were analyzed in serum samples of HCRAd-5_ΔCAR- and PBS-injected mice (Figure 37A). AST and ALT serum concentrations of PBS-injected mice were 73.87 ± 14.50 U/l and 31.73 ± 3.96 U/l, respectively and were set as baseline levels. In contrast, AST and ALT serum concentrations of HCRAd-5_ΔCAR-injected mice were 17148.33 ± 6825.04 U/l and 7888.33 ± 2780.49 U/l, respectively and accordingly elevated 232- and 249-fold. Additionally, hematoxylin-eosin (H&E) staining was performed in liver sections of mice injected with HCRAd-5_ΔCAR or PBS. While no pathologic alterations were observed in liver sections of PBS-injected mice, liver sections of HCRAd-5_ΔCAR injected mice revealed a massive plan lobular tissue damage indicated by swollen and apoptotic appearing hepatocytes (Figure 37B), most probably due to pronounced hepatocyte transduction by HCRAd-5_ΔCAR. Thus, massively elevated AST and ALT serum concentrations and an altered tissue architecture in liver sections of HCRAd-5_ΔCAR-injected mice indicated for a severe vector-induced hepatic damage caused by intravenously injected HCRAd-5_ΔCAR.

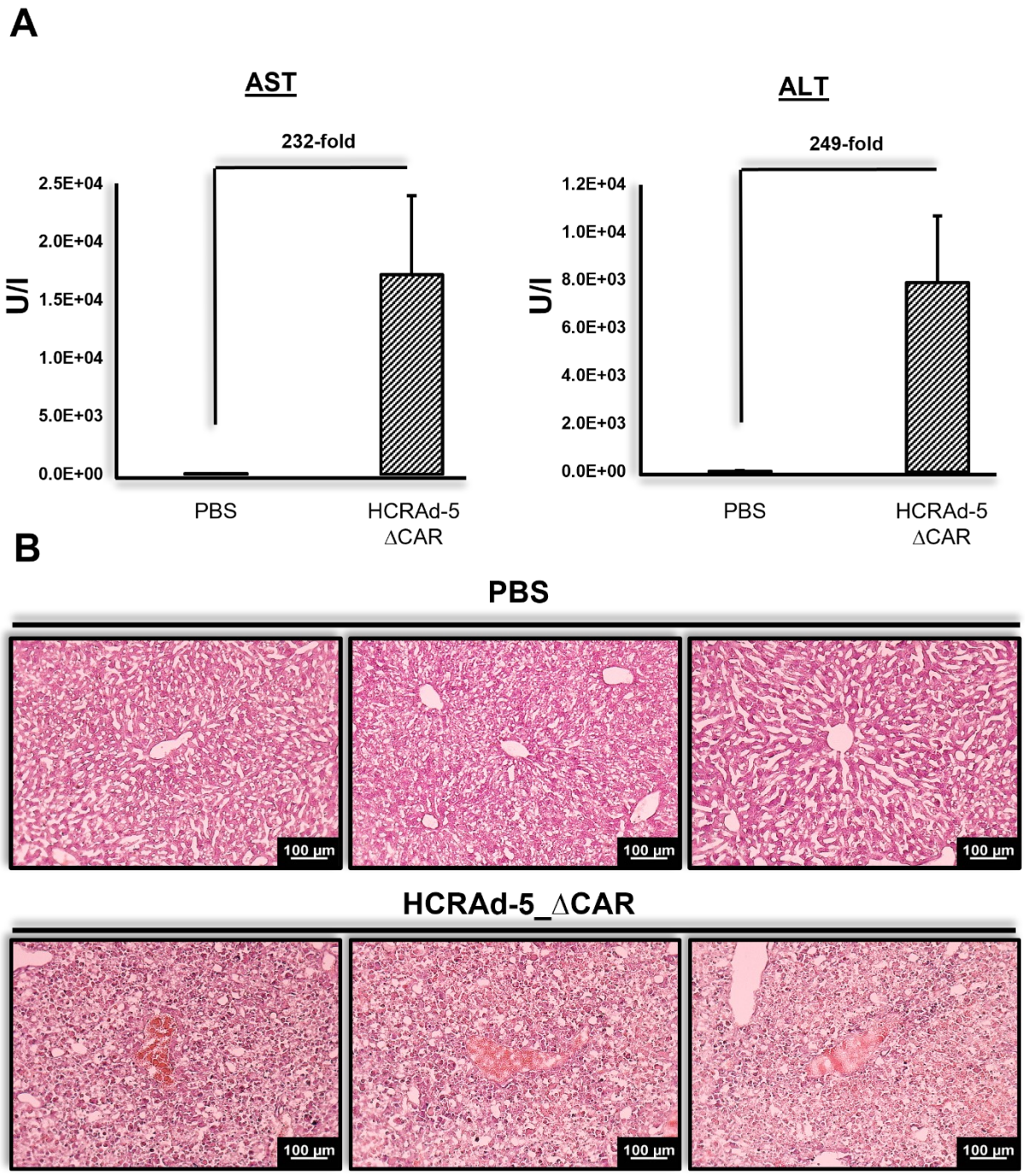

Figure 37: HCRAd-5_ΔCAR induces severe hepatic damage in NSG mice after intravenous injection

Subcutaneous UD-SCC-2 tumor-bearing NSG mice were intravenously injected with either PBS or $2x10^{10}$ vector particles of HCRAd-5_ΔCAR after 21 days of tumor growth. Due to severe vector-induced toxicity, HCRAd-5_ΔCAR-injected mice were euthanized 48 h after vector injection (n=12). To investigate potential liver damages caused by HCRAd-5_ΔCAR, **(A)** AST and ALT serum concentrations of PBS- and HCRAd-5_ΔCAR-injected mice were analyzed (n=10-12) and **(B)** H&E staining of liver sections of mice injected with PBS or HCRAd-5_ΔCAR was performed. Shown are representative pictures of three mice from each group. AST: Aspartate aminotransferase, ALT: Alanine aminotransferase

5.3.7 Successful tumor transduction by HCRAd-5-HexPos3_ΔCAR after single intravenous injection

HCRAd-5-HexPos3_ΔCAR showed significantly reduced vector toxicity after intravenous injection in UD-SCC-2 tumor-bearing NSG mice compared to HCRAd-5_ΔCAR. To further analyze biodistribution and tumor transduction of HCRAd-5-HexPos3_ΔCAR after intravenous injection, *in vivo* luciferase expression was analyzed by IVIS measurements at 3, 7, 14, 21, 28, 35, 43, 49, and 56 days after virus injection (Figure 38). Since PBS-injected mice did not exhibit any luciferase expression (Figure 36), IVIS measurements were only conducted with HCRAd-5-HexPos3_ΔCAR vector-injected mice.

Three days after vector injection, all mice injected with HCRAd-5-HexPos3_ΔCAR showed luciferase activity in the liver (Figure 38), however, significantly lower compared to those detected in HCRAd-5_ΔCAR-injected mice 48 h after vector injection (Figure 36). In addition, and fitting to previous biodistribution analysis (Figure 30), luciferase activities at varying intensities were also detected at tumor sites, indicating successful tumor transduction by HCRAd-5-HexPos3_ΔCAR after intravenous injection (Figure 38, red arrows). While luciferase expression in the liver continuously decreased over time, luciferase expression at tumor sites first increased up to day 7 before it also started to decrease. However, one tumor showed continuous luciferase activity up to day 56 after vector injection, suggesting intratumoral vector replication (Figure 38, subgroup “high”). Thus, beside a significantly reduced toxicity, HCRAd-5-HexPos3_ΔCAR additionally showed improved and partially persisting tumor transduction, likely leading to intratumoral virus replication after a single intravenous injection in some of the animals.

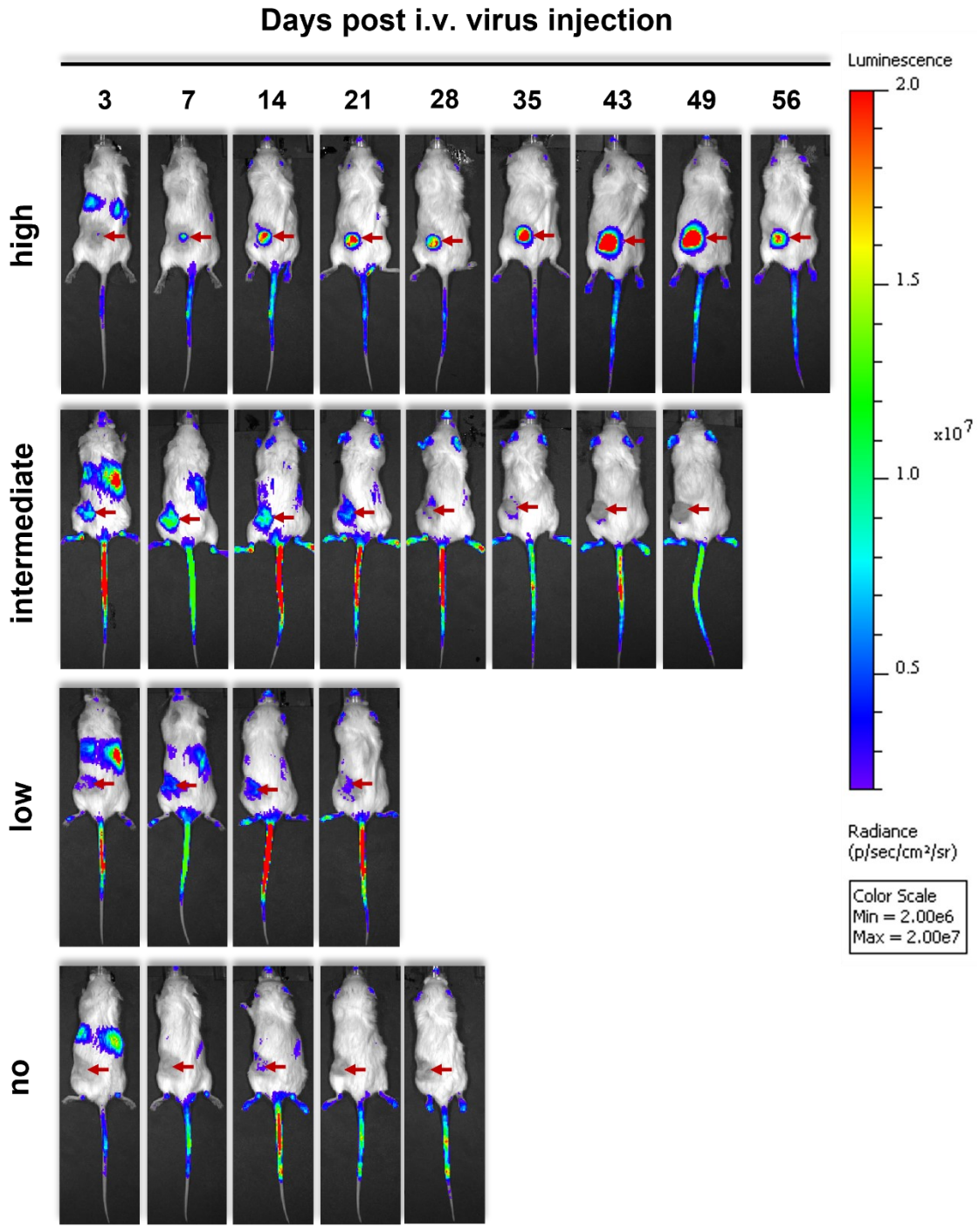

Figure 38: Substantial and persisting tumor infection by HCRAd-5-HexPos3_ΔCAR *in vivo*
Subcutaneous UD-SCC-2 tumor-bearing NSG mice were intravenously injected with $2x10^{10}$ vector particles of HCRAd-5-HexPos-3_ΔCAR after 21 days of tumor growth. After 3, 7, 14, 21, 28, 35, 43, 49, and 56 days of vector injection, mice were narcotized, intraperitoneally injected with 200 µl luciferase substrate and luciferase activity was analyzed by IVIS 200 *in vivo* imaging system. Mice were subgrouped in 'high', 'intermediate', 'low', and 'no' according to their luciferase expression levels at tumor sites. Shown are representative pictures of one mouse per subgroup over time. Tumor sites are indicated by red arrows. n=12

To analyze a potential anti-tumor effect of HCRAd-5-HexPos3_ΔCAR, Kaplan-Meier survival analysis was performed with mice being sacrificed when tumors reached a maximum size of 15 mm in diameter (Figure 39A). Due to the severe vector-induced toxicity of HCRAd-5_ΔCAR, a direct comparison between HCRAd-5_ΔCAR and HCRAd-5-HexPos3_ΔCAR regarding their anti-tumor efficacy was not possible in this experiment, since all mice injected with HCRAd-5_ΔCAR had to be euthanized already 48 h after vector injection.

Compared to the PBS group, HCRAd-5-HexPos3_ΔCAR-injected mice showed slightly prolonged survival rates in the Kaplan-Meier survival analysis (Figure 39A), leading to an increased mean survival of 9 days (Figure 39B). However, it is noteworthy, that among the HCRAd-5-HexPos3_ΔCAR-injected mice no direct correlation of luciferase activities at tumor sites detected by the IVIS measurement and prolonged survival of the respective mice was observed. An inhomogeneous tumor growth in all mice, which significantly influenced the time span until tumor size-based discontinuation criteria were reached, further complicated the interpretation of the obtained results. To investigate a potential tumor disruption by HCRAd-5-HexPos3_ΔCAR due to intratumoral virus replication, H&E staining of tumor sections from tumors excised at the end point of HCRAd-5-HexPos3_ΔCAR- and PBS-injected mice was performed (Figure 39C). Here, tumors of both, PBS- as well as HCRAd-5-HexPos3_ΔCAR-injected mice showed partially disrupted tumor textures, most probably due to emerging tumor necrosis at late stages of tumor growth. Taken together, HAdV-5-HexPos3_ΔCAR was shown to exhibit significantly diminished vector toxicity, reduced off-target organ tropism and improved tumor targeting with partially long-lasting intratumoral virus replication, which may cause prolonged survival of UD-SCC-2 tumor-bearing NSG mice after a single intravenous injection.

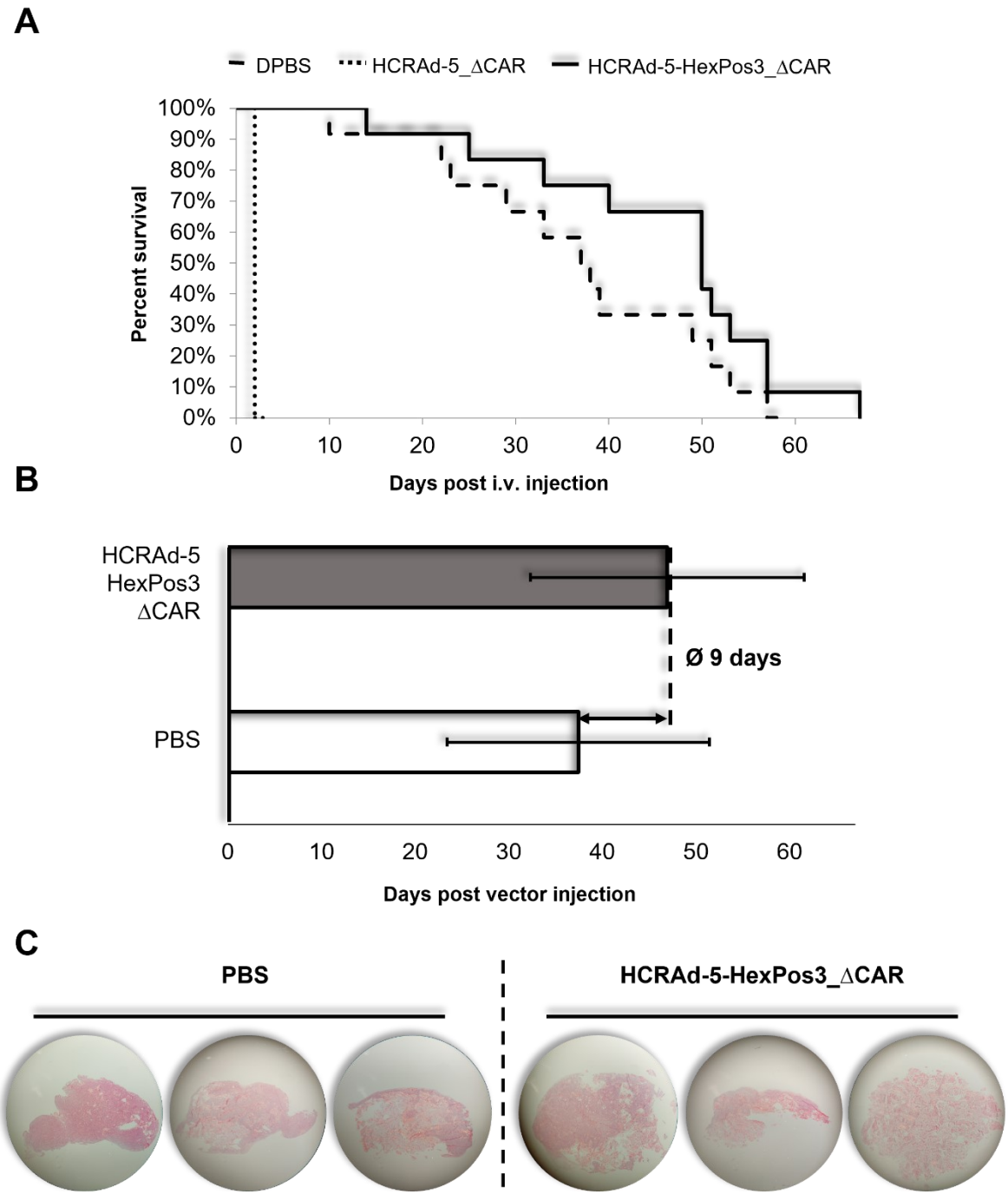

Figure 39: Intravenous injection of HCRAd-5-HexPos3_ΔCAR leads to prolonged survival of UD-SCC-2 tumor-bearing NSG mice

Subcutaneous UD-SCC-2 tumor-bearing NSG mice were intravenously injected with either PBS or $2x10^{10}$ vector particles of HCRAd-5_ΔCAR and HCRAd-5-HexPos3_ΔCAR (n=12). Mice were sacrificed upon severe signs of toxicity or when tumors reached a maximum size of 15 mm in diameter. Anti-tumor effects were analyzed by **(A)** Kaplan-Meier survival analysis and **(B)** calculation of mean survival rates. **(C)** After tumor excision at the end point, H&E staining of tumor sections was performed to evaluate tumor tissue textures. Shown are representative pictures of three mice either injected with PBS or HCRAd-5-HexPos3_ΔCAR.

6 Discussion

6.1 Strengths and weaknesses of oncolytic virotherapy

Oncolytic virotherapy is at the forefront as novel anti-cancer therapy. Compared to conventional treatment regimens like surgery or radiotherapy, it provides a rather mild intervention, causing significantly less patient burden. Different to other, more invasive anti-cancer therapies like chemotherapy or monoclonal antibodies (mAb), oncolytic viruses greatly benefit from their self-amplifying characteristics as they autonomously replicate upon initial tumor cell infection[314] and thus may require only a single administration. Virus-induced tumor cell lysis further may stimulate anti-tumor immune responses due to the release of cancer cell specific antigens[315], additionally augmenting anti-tumor efficacies. Today, most oncolytic viruses developed are based on human adenovirus type 5 (HAdV-5), which can be attributed to its well understood biology, good safety profile, genetic stability, ease in genetic manipulation and beneficial manufacturing properties[316]. However, HAdV-5-based oncolytic virotherapy is still confronted with several biological barriers, limiting its anti-tumor efficacy[317,318]. Tumor cells often lack expression of the HAdV-5 primary receptor CAR[200–203], which hampers efficient tumor transduction by HAdV-5-based oncolytic vectors. A heterogenous tumor constitution including a dense tumor stroma and extracellular matrix components additionally aggravates efficient tumor infiltration by vector particles and limits intratumoral virus spread[163]. Poor tumor transduction efficiencies may result in extensive off-target organ transduction, having vector-induced toxicities as a consequence. Especially the strong liver tropism of HAdV-5 pose risks for severe hepatotoxicity[183]. Rapid vector sequestration from the bloodstream due to cellular and non-cellular off-target interactions additionally limits an efficient delivery of vector particles to the tumor upon systemic administration[50,318]. An improved and specific tumor targeting, while avoiding common vector sequestration mechanisms and toxicities, thus reflects a decisive requirement for efficient anti-cancer virotherapy by HAdV-5 based oncolytic vectors.

To address the issue of poor tumor transduction efficiencies by HAdV-5-based oncolytic vectors, the present study focused on the development and characterization of HAdV-5-based oncolytic vectors with improved tumor transduction efficiencies and less

vector toxicity, particularly dedicated to the treatment of head and neck squamous cell carcinoma (HNSCC). Retargeting strategies based on geneti-chemical capsid modification[224], bispecific adapter molecules and genetic capsid mutation were applied. In a first attempt, HAdV-5 based vectors retargeted towards the epidermal growth factor receptor (EGFR) were characterized regarding their tumor transduction efficiencies and biodistribution profiles *in vitro* and *in vivo*. By means of a bispecific adapter molecule, it was further investigated whether the fibroblast activation protein (FAP) may provide a suitable tumor stroma-target for HAdV-5-based oncolytic virotherapy. Furthermore, a charge-modified HAdV-5 capsid mutant[311] was thoroughly characterized regarding its biodistribution properties, tumor transduction efficiencies, toxicity and therapeutic efficacy both *in vitro* and *in vivo*. The data gathered in the present study highlight still existing barriers for HAdV-5-based oncolytic virotherapy, however, likewise provide insights into how to potentially overcome these limitations and develop HAdV-5-based oncolytic vectors with improved anti-tumor efficacies.

6.2 Capsid modification with Affilin efficiently retargets adenoviral vectors towards EGFR *in vitro* but does not improve tumor transduction *in vivo*

Head and neck squamous cell carcinomas (HNSCC) reflect an aggressive type of cancer with high recurrence[319], necessitating effective treatment strategies. As the EGFR is frequently overexpressed in most types of HNSCC[269], in the present study HAdV-5-based vectors retargeted against the EGFR were investigated regarding their oncolytic potential *in vitro* and *in vivo*. Prior to the present study, these vectors have been generated by means of geneti-chemical capsid modification[224]: The EGFR affinity ligand Affilin has been covalently coupled to either the fiber (HAdV-5_ΔCAR_FiberAffilin) or hexon (HAdV-5_ΔCAR_HexonAffilin) protein of the vector capsid in a position-specific manner[228] using genetically introduced surface-exposed cysteines. Experiments preceding to the present study already revealed promising *in vitro* characteristics for these Affilin-decorated vectors, including less susceptibility to known vector sequestration mechanisms such as less macrophage uptake, reduced binding to blood coagulation factor X (FX) and absent neutralization by the complement or innate immune system[228]. Based on these

encouraging data, further experiments were performed in the present study to assess the oncolytic potential of the Affilin-decorated vectors *in vitro* and *in vivo*.

First *in vitro* experiments confirmed enhanced transduction efficiencies of HAdV-5_ΔCAR_FiberAffilin and HAdV-5_ΔCAR_HexonAffilin in an EGFR-dependent manner, indicating that capsid modification with Affilin enables an efficient vector targeting towards EGFR. The fiber-Affilin modification resulted in consistently higher transduction efficiencies than the hexon-Affilin modification. This may be caused by a hampered intracellular trafficking of HAdV-5_ΔCAR_HexonAffilin upon vector endocytosis. After endocytosis, HAdV-5 particles have to escape from the early endosome to become transported towards the nucleus to deliver their genome. Affilin binds to EGFR with high affinity (Kd = 10.9 nM)[306] and endosome acidification upon initial vector endocytosis may only insufficiently resolve the high affinity interaction between Affilin and EGFR, thus trapping HAdV-5_ΔCAR_HexonAffilin particles within the early endosome. Such vector particles that successfully escaped into the cytoplasm may be further hampered in their cytoplasmic trafficking. HAdV-5 particles become transported towards the nucleus along the microtubular network, mediated by cellular dynein[74]. As dynein binds to HVR1[320], which likewise reflects the coupling site of Affilin in case of HAdV-5_ΔCAR_HexonAffilin[228], Affilin may interfere with dynein binding and thus hampers particle transport to the nucleus. As a result, HAdV-5_ΔCAR_HexonAffilin particles deliver their genome less efficiently and thus become less infectious. In case of HAdV-5_ΔCAR_FiberAffilin, the interaction between Affilin and EGFR may be of low impact, as the fiber becomes shed from the capsid during vector uptake[68].

Presence of murine plasma, however, enhanced the transduction efficiencies of both Affilin-decorated vectors significantly *in vitro* suggesting favorable tumor transduction efficiencies *in vivo*. However and unexpectedly, upon i.v. injection neither HAdV-5_ΔCAR_FiberAffilin nor HAdV-5_ΔCAR_HexonAffilin showed improved but even diminished uptake into both EGFR-positive and EGFR-negative tumors. Initial suggestions about a strong liver tropism of particles as the cause for absent tumor transduction, however, were not confirmed, as both vectors showed significantly diminished hepatocyte transduction compared to the unmodified vector control HAdV-5_ΔCAR. Additionally, both Affilin-decorated vectors showed less liver uptake early after i.v. injection, indicating less sequestration by liver residential Kupffer cells, which

would have been another possible source for particle consumption[50]. Nonetheless, both Affilin-decorated vectors were previously reported to exhibit an accelerated blood clearance[228], which indicated another source of particle consumption. Strikingly, HAdV-5_ΔCAR_HexonAffilin showed even less liver uptake and hepatocyte transduction than HAdV-5_ΔCAR_FiberAffilin, even though it was reported to be faster cleared from the bloodstream[228].

6.3 An unfavorable tumor constitution and on-target/off-tumor binding prevents efficient tumor transduction by i.v. injected Affilin-decorated vectors

To further unravel the cause for the absent tumor transduction by Affilin-decorated vectors in EGFR-positive tumors, the constitution of the UD-SCC-2 xenografts was investigated in more detail. Efficient tumor transduction by i.v. injected vector particles requires sufficient target receptor expression in the tumor[321] and proper tumor vascularization for successful particle delivery via the cardiovascular system. Both requirements were investigated for the UD-SCC-2 tumor xenografts at the day of vector injection using immunohistochemical staining for EGFR and CD31. Fitting to strong EGFR expression levels in UD-SCC-2 cells *in vitro*, abundant EGFR expression was likewise verified within the UD-SCC-2 xenografts. Lack of target receptor expression as the cause for absent tumor transduction by the Affilin-decorated vectors thus was excluded. However, although UD-SCC-2 xenografts displayed distinct intratumoral vessels when stained after 39 days of tumor growth, vascularization was significantly less developed after 14 of tumor growth, when vectors were injected. Such poor tumor vascularization may hampered efficient delivery of vector particles to the tumor via the bloodstream. Furthermore, neoplastic vessels were embedded into a dense tumor stroma, most likely of murine origin and distal from the EGFR-expressing target cell. Thus, additionally to an improper tumor vascularization, spatial inaccessibility of the EGFR-expressing tumor cell may be another possible explanation for the insufficient tumor transduction by the Affilin-decorated vectors in EGFR-positive UD-SCC-2 tumors after i.v. vector injection.

HAdV-5_ΔCAR_FiberAffilin and HAdV-5_ΔCAR_HexonAffilin were previously reported to exhibit an accelerated blood clearance[228], indicating rapid particle sequestration after i.v.

injection. Since the liver as a source of particle consumption was already excluded, an altered organ tropism was hypothesized, so biodistribution analysis were performed to analyze vector uptake into the lung, spleen, kidney and heart of vector-injected mice. Here, elevated vector loads within the cardiac tissue were observed for both HAdV-5_ΔCAR_FiberAffilin and HAdV-5_ΔCAR_HexonAffilin, indicating enhanced transduction efficiencies in murine cardiac cells. In line with this hypothesis, both vectors showed significantly enhanced transduction efficiencies in murine cell lines *in vitro*. Since host cell transduction by the Affilin-decorated vectors was shown to be EGFR-specific, the elevated transduction efficiencies in murine cells suggest vector uptake via the murine EGFR. Human EGFR shares 94.8% sequence homology with its murine counterpart as it can be identified by standard protein sequence alignment (UniProtID: Q01279 vs. P00533). Such similarity offers great potential for cross-reactivities by EGFR-binding ligands between human and murine EGFR as it has been already observed for murine EGF, which likewise binds to human EGFR, though with lower affinity[322]. EGFR-targeting drugs like small molecule tyrosine kinase inhibitors i.e. are also pharmacologically active in mice[308], thus cross-reactivity for Affilin between human and murine EGFR can be considered possible. Hence, elevated particle uptake in the heart thus may be a result of vector binding to EGFR expressed within the cardiac tissue, which would be in line with reports about EGFR to be essential for proper heart development and function[307–310]. EGFR mutant mice were reported to develop enlarged semilunar valves[307,310], hyperplasic left ventricles and suffered from heart failures leading to premature death[307], indicating the presence and necessity of EGFR in the heart.

However, even though uptake levels of the Affilin-decorated vectors into the cardiac tissue were elevated, the total number of detected vector genomes was still low, thus unlikely to be the sole origin of particle consumption. As binding of Affilin to murine EGFR can be considered and EGFR reflects a ubiquitously expressed receptor, a broadly distributed on-target/off-tumor binding of the Affilin-decorated vectors can be assumed. Proper function of the vasculature i.e. depends on EGFR expression by vascular smooth muscle cells (VSMCs)[323,324]. VSMCs surround the vascular lumen, build up most of the blood vessel wall and help to regulate blood pressure by vasoconstriction and vasodilatation[325]. EGFR is involved in basal VSMC homeostasis[323] and loss of EGFR in VSMCs causes arterial hypotension[324]. Their abundancy within the cardiovascular system and their

localization directly adjacent to the endothelial monolayer of the blood vessel thus renders VSMCs an easy-to-access cell type for i.v. injected vectors. Binding to EGFR expressed by VSMCs thus reflects a likely source for particle consumption, which may explain the accelerated blood clearance of the Affilin-decorated vectors[228].

Strikingly, HAdV-5_ΔCAR_HexonAffilin seemed to be substantially more affected by such on-target/off-tumor sequestration mechanisms as evident by its even elevated uptake levels into the cardiac tissue. Here, the total number of Affilin molecules coupled to the vector capsid may be causative. Hexon reflects the most abundant capsid protein of an adenoviral particle with 720 hexon monomers assembling into 240 trimers. Fiber in turn contributes to the adenoviral capsid with only 36 monomers assembling into 12 trimers. Each of these monomeric fiber or hexon proteins have been genetically equipped with a single surface-exposed cysteine to enable the site-directed covalent attachment of a terminal cysteine-bearing Affilin molecule. The coupling efficiencies have been reported to be 60% and 10% to fiber and hexon, respectively[228]. Stoichiometrically, this results in a total amount of ~21 Affilin molecules coupled to HAdV-5_ΔCAR_FiberAffilin and ~72 Affilin molecules coupled to HAdV-5_ΔCAR_HexonAffilin. Thus, HAdV-5_ΔCAR_HexonAffilin vectors are covered with ~3.4-times more Affilin molecules than HAdV-5_ΔCAR_FiberAffilin vectors, enabling for more receptor binding possibilities and thus may explain the even elevated uptake levels of HAdV-5_ΔCAR_HexonAffilin into the cardiac tissue. Strikingly, HAdV-5_ΔCAR_HexonAffilin likewise exhibited superior transduction efficiencies in murine cell lines *in vitro*, which contradicted results previously obtained in human cell lines. As mentioned in a previous section, the diminished transduction efficiency of HAdV-5_ΔCAR_HexonAffilin in human cell lines was hypothesized to originate from the high-affinity binding between Affilin and EGFR, which may trap the vector particle within the early endosome. Based on the suggestion that Affilin binds to murine EGFR with lower affinity, acidification of the early endosome upon vector endocytosis may be sufficient to resolve the low affinity bond between Affilin and murine EGFR, resulting in higher transduction efficiencies of HAdV-5_ΔCAR_HexonAffilin in murine cells compared to human cells.

6.4 Inaccessibility of EGFR in *in vivo* xenografts hampers tumor transduction by Affilin-decorated vectors

HNSCC often affects areas of the upper respiratory tract, thus being accessible for local vector administration. To circumvent vector sequestration after i.v. injection and to investigate whether capsid modification with Affilin might enhances tumor transduction in EGFR-positive tumors *per se*, an intratumoral vector injection of HAdV-5_ΔCAR and HAdV-5_ΔCAR_FiberAffilin was performed in UD-SCC-2 xenografts. Surprisingly, i.t. injection did not result in improved but even diminished tumor transduction efficiencies by HAdV-5_ΔCAR_FiberAffilin. As HAdV-5_ΔCAR_FiberAffilin showed remarkable transduction efficiencies in UD-SCC-2 cells *in vitro* and EGFR was proven to be abundantly expressed in UD-SCC-2 xenografts, an impaired accessibility of EGFR for the Affilin ligand *in vivo* was suggested. Using immunohistochemical staining, binding of Affilin to EGFR-positive UD-SCC-2 cells *in vitro* was confirmed, however, no binding was observed for UD-SCC-2 tumor sections. As epidermal growth factor (EGF) efficiently inhibited transduction of UD-SCC-2 cells by HAdV-5_ΔCAR_FiberAffilin *in vitro*, absent binding of Affilin to EGFR *in vivo* might be a result of EGFR occupation within the tumor by one of its natural ligands[271]. Upon ligand binding, EGFR undergoes conformational changes and dimerizes[273], which may contribute to an inaccessibility of the Affilin epitope. Stroma-derived fibroblasts are known to secrete various growth factors[285] including EGFR binding ligands such as transforming growth factor-α (TGF-α)[326,327]. As a dense tumor stroma was observed in UD-SCC-2 tumors, growth factors, probably originating from stroma-derived fibroblasts, might bind and occupy EGFR *in vivo*. These findings let suggest that the tumor stroma not only represents a physical barrier for the Affilin-decorated vectors after i.v. injection, but also contributes to an inaccessibility of EGFR due to secretion of EGFR-binding ligands. The even diminished transduction efficiencies of HAdV-5_ΔCAR_FiberAffilin compared to HAdV-5_ΔCAR upon i.t. injection might be further explained by the reduced binding of FX to HAdV-5_ΔCAR_FiberAffilin[228], as FX is known to be a potent enhancer of adenoviral transduction[328].

6.5 The fibroblast activation protein as a suitable target for oncolytic adenoviral vectors

Stromal tissue of solid tumors can account for most of the total tumor mass and cancer associated fibroblasts (CAFs) comprise the most abundant cellular constituent of the tumor stroma[285]. Several aspects suggest CAFs as an attractive target cell type to increase the therapeutic efficacy of oncolytic adenoviruses. CAFs promote tumor angiogenesis[329], modulate the extracellular matrix[330], suppress immune responses and secrete growth factors driving tumor progression[331]. Targeting and destroying CAFs by oncolytic adenoviral vectors thus may not only help to disrupt the tumor but may also break-down the tumor growth-promoting microenvironment. However, fibroblasts are hardly transduced by HAdV-5-based vectors due to insufficient expression of the primary adenovirus receptor CAR[332]. To achieve efficient transduction of CAFs by HAdV-5-based vectors, the fibroblast activation protein (FAP), a cell surface located serine protease[290], was suggested a suitable target antigen as it represents a highly specific tumor marker, almost exclusively expressed by CAFs within the tumor stroma[333]. As a retargeting strategy, the bispecific adapter molecule FAP5-S11-FLAG was generated, being a genetic fusion between two single chain variable fragments, binding FAP[304] and the adenovirus fiber knob[253].

FAP5-S11-FLAG was shown to bind both cell surface-located human FAP (hFAP) and the adenoviral capsid. The ΔCAR mutation of applied HAdV-5_ΔCAR vectors did not affect FAP5-S11-FLAG binding to the capsid. An *in vitro* retargeting assay using HEK293T cells transiently expressing hFAP (HEK293ThFAP) confirmed that HAdV-5_ΔCAR was successfully retargeted towards hFAP by means of FAP5-S11-FLAG. This finding suggested hFAP as a promising tumor stroma target for HAdV-5-based oncolytic vectors. However, one limitation of the here reported data is that experiments were performed in cells of epithelial origin with artificial and only transient hFAP expression, which does not perfectly match the mesenchymal origin of CAFs in the tumor stroma. FAP is a serine protease[290] that is catalytically active only as a glycosylated homodimer (FAP/FAP)[292,295], however, also forming heterodimers with CD26/Dipeptidyl-peptidase-4 (DPP4)[294] (FAP/DPP4). Even though the dimerization status of hFAP within the HEK293ThFAP cells used in the present study was not investigated, it can be assumed that overexpression of

hFAP predominantly results in the formation of FAP/FAP homodimers. There is indication that heterodimerization may influences binding of some FAP antibodies[334], consequently FAP/DPP4 heterodimerization may likewise result in an impeded binding of FAP5-S11-FLAG to hFAP. Thus, if transduction of primary CAFs by adenoviral vectors is feasible remains to be investigated. However, it has been revealed that stromal fibroblasts of epithelial cancers solely express FAP, while only barely DPP4[293], suggesting that predominantly FAP/FAP homodimers rather than FAP/DPP4 heterodimers may be present in CAFs. The FAP5 parental antibody mAb FAP5[304] was shown to bind FAP in pancreatic, lung and colon carcinoma xenograft models[304], indicating that FAP5-S11-FLAG most likely binds to FAP expressed by CAFs as well. Thus, successful retargeting of HAdV-5-based vectors towards CAFs by means of FAP5-S11-FLAG seems promising and would be in line with previous reports about FAP-targeted HAdV-5-based vectors. Pang *et al.* generated FAP-targeted adenoviral vectors by genetic insertion of small FAP-binding peptides into the fiber of the adenoviral capsid and showed increased transduction efficiencies in primary gastric CAFs by these vectors *in vitro*[335]. Continuing *in vivo* studies further revealed significantly inhibited tumor growth in gastric cancer xenografts after repeated i.v. injection of these FAP-targeted vectors[335]. Even though this is, to the best of our knowledge, the only report about oncolytic adenoviral vectors directly targeted towards FAP, there have been several other attempts to indirectly target CAFs by means of oncolytic adenoviruses. De Sostoa *et al.* generated the oncolytic adenovirus ICO15K-FBiTE, which encoded an FAP-directed bispecific T-cell engager (BiTE)[336]. BiTEs are a type of bispecific adapter molecule, binding to a specific cell surface antigen and the CD3 receptor on T-cells, thus bridging cytotoxic T-cells to the bound target cell[337]. ICO15K-FBiTE enabled BiTE-induced T-cell-mediated cytotoxicity in FAP^+ cells *in vitro* and subsequent *in vivo* studies showed increased intratumoral T-cell accumulation, depletion of stromal tissue and significantly delayed tumor growth in A549 and HPAC xenografts upon i.t. injection of ICO15K-FBiTE[336]. A comparable study was performed by Freedman *et al.*, who armed another oncolytic adenovirus, Enadenotucirev (EnAd) with a FAP-targeted BiTE[338]. The BiTE-expressing EnAd induced T-cell-mediated cell death of CAFs *in vitro* and *ex vivo* infection of solid prostate cancer biopsies led to activation and infiltration of $PD1^+$ cells[338]. However, despite such encouraging results obtained by FAP-targeted oncolytic virotherapy, possible side-effects need to be considered as well. Bone

marrow-derived stem cells (BMSCs) for example endogenously express FAP[339] and thus represent a potential off-target cell type for FAP-targeted anti-tumor therapies. Indeed, FAP-targeted chimeric antigen receptor-T (CAR-T) cells have been reported to have limited anti-tumor efficacy but induced severe bone marrow toxicity in preclinical *in vivo* studies[340]. However, contrary data were generated by Kakarla *et al.*, who reported anti-tumor efficacies of FAP-targeted CAR-T cells in pre-clinical studies with absence of any severe adverse events[341].

Taken together, the data obtained in the present study indicate that FAP might be a promising target for HAdV-5 based oncolytic virotherapy. Data from several other studies support this suggestion and provide encouraging results that FAP-directed anti-cancer therapies can be highly effective. However, the efficacy and safety of oncolytic adenoviral vectors targeted against FAP should be thoroughly evaluated. Thus, continuing experiments, both *in vitro* and *in vivo*, are needed to obtain further insights into the antitumor efficacy and safety of FAP-targeted HAdV-5-based oncolytic vectors.

6.6 HexPos3 capsid mutation improves biodistribution properties and tumor uptake of i.v. injected HAdV-5 vectors *in vivo*

Efficient tumor transduction and low vector toxicity is essential for the therapeutic success of oncolytic virotherapy. Previously, the HAdV-5-HexPos3_ΔCAR vector was generated, exhibiting a reduced overall net negative surface charge[311] due to partial replacement of 13 mainly negatively charged amino acids within HVR1 of hexon by four positively charged lysine residues. HAdV-5-HexPos3_ΔCAR was shown before to exhibit significantly improved and CAR-independent transduction efficiency in human cancer cell lines[311] and thus was considered a promising candidate for oncolytic virotherapy. Hence, in the present study, its oncolytic potential was thoroughly investigated *in vitro* and *in vivo*. First *in vitro* transduction assays confirmed the remarkably enhanced transduction efficiency of HAdV-5-HexPos3_ΔCAR in human cancer cell lines and murine plasma had even enhancing effects on the transduction efficiency. *In vivo*, HAdV-5-HexPos3_ΔCAR showed a favorable biodistribution profile after i.v. injection into UD-SCC-2 tumor-bearing NSG mice with either equal or reduced off-target uptake in lung, spleen, kidney, and heart, however, elevated tumor uptake compared to the control vector HAdV-5_ΔCAR.

Furthermore, HAdV-5-HexPos3_ΔCAR showed no elevated liver uptake compared to HAdV-5_ΔCAR early after i.v. injection into BALB/c mice, indicating that HAdV-5-HexPos3_ΔCAR was likely not affected by excessive sequestration via liver residential Kupffer cells. Most interestingly, HAdV-5-HexPos3_ΔCAR further showed almost absent hepatocyte transduction despite verified and substantial binding of biologically functional FX[311], a main mediator of hepatocyte transduction by HAdV-5-based vectors *in vivo*[49]. Thus, this data may indicate for another, yet still unknown mechanism of hepatocyte transduction by HAdV-5-based vectors *in vivo*, potentially involving HVR1 of hexon. Based on the significantly reduced hepatocyte transduction and elevated tumor uptake, HAdV-5-HexPos3_ΔCAR further exhibited an about 29-fold improved tumor to liver ratio compared to the unmodified control vector HAdV-5_ΔCAR, which pointed to an improved oncolytic potential and significantly reduced vector toxicity of HAdV-5-HexPos3_ΔCAR after i.v. injection in NSG mice.

6.7 Absence of E1B19k protein improves the oncolytic potential of adenoviral vectors and restricts replication to cancer cells

Replication deficient HAdV-5-HexPos3_ΔCAR showed favorable biodistribution properties and significantly increased tumor uptake after i.v. injection, rendering it a promising candidate for efficient HAdV-5-based oncolytic virotherapy. Tumor lysis, however, requires virus replication, which, considering vector safety, should be tightly restricted to cancer cells to avoid damage of healthy cells and tissues. With the aim to generate a conditionally replicating HAdV-5-HexPos3_ΔCAR oncolytic vector, three conditionally replicating adenoviral vectors (CRAds), based on the HAdV-5 wild-type virus (HAdV-5wt) were generated by successive mutations within the viral early gene regions *E1A* (E1AΔ24bp), *E1B19k* (ΔE1B19k) and *E3gp19k* (ΔE3gp19k). The resultant CRAd's HAdV-5_E1AΔ24bp, HAdV-5_E1AΔ24bp_ΔE1B19k and HAdV-5_E1AΔ24bp_ΔE1B19k_ΔE3gp19k were characterized regarding their oncolytic potential and cancer cell specific replication *in vitro* using both cancer and primary cells.
Contrary to previous reports[151], in the present study the E1AΔ24bp mutation did not restrict virus replication to cancer cells, since primary cells were efficiently lysed upon infection by HAdV-5_E1AΔ24bp. Moreover, HAdV-5_E1AΔ24bp showed less efficient

spread in cancer cells compared to HAdV-5wt, indicating that the E1AΔ24bp mutation lowers the oncolytic potential of HAdV-5-based oncolytic vectors. In contrast, HAdV-5_E1AΔ24bp_ΔE1B19k showed distinctly improved cancer cell lysis and accelerated spread compared to HAdV-5wt in all cancer cell lines tested, and almost absent replication in primary cells. Even though the underlying mechanism is not completely understood so far, previously it has been shown that absence of the E1B19k protein results in an expedited viral release from the infected host cell and thus to more efficient viral spread[153–156]. Further, the E1B19k interferes with the adenovirus death protein (ADP), thus absent E1B19k protein may enhance host cell lysis and contribute to an early release of viral progeny from the infected cell[120,313]. ADP, which is expressed at low levels during early phases of the adenoviral infection cycle becomes highly amplified during late stages[342] and is required for efficient cell lysis and release of viral progeny[343]. An adenoviral vector overexpressing ADP showed improved spread in cancer cells[344] while ADP-deleted vectors spread less efficiently and show a small plaque forming phenotype[343]. Interestingly, the small plaque forming phenotype of an ADP-deleted vector could be readily compensated by abrogation of the E1B19k function[345] and localization of both ADP[346] and E1B19k[347] at the nuclear membrane during viral infection may be indicative for an interaction between both proteins to regulate viral release.

Further, E1B19k binds to the pro-apoptotic protein Bax and thereby prevents virus-induced host cell apoptosis[103]. This is a possible explanation for the tightly restricted replication of E1B19k-deleted vectors to cancer cells with aberrant apoptotic pathways, while absence of E1B19k during vector replication in primary cells probably results in rapid apoptosis of the infected cell, which would prevent productive vector replication and spread. Strikingly, absence of E3gp19k protein further improved cancer cell-specific replication efficiency of HAdV-5-based oncolytic vectors as shown by the even enhanced spread of HAdV-5_E1AΔ24bp_ΔE1B19k_ΔE3gp19k in cancer cells. This observation was unexpected, since E3gp19k is known to be involved in the adenoviral immune evasion due to prevention of MHC I-mediated antigen presentation by the infected cell[157–159] and thus has no known host cell cycle modulatory function *in vitro*. The underlying mechanism for the improved spread of HAdV-5_E1AΔ24bp_ΔE1B19k_ΔE3gp19k in cancer cells thus remains unsolved for the time being and requires further investigation. However, one possible explanation might be the shortened genome of

HAdV-5_E1AΔ24bp_ΔE1B19k_ΔE3gp19k due to deletion of *E3gp19k* (712 bp). HAdV-5wt and all *in vitro* characterized CRAds generated in the present study harbored the genetically introduced eGFP-NanoLuciferase reporter gene, which expands the vector genome by ~3.7% (1355 bp) its original size and potentially interferes with efficient packaging of the vector genome into newly assembled capsids[348]. Deletion of *E3gp19k* may compensated for this limitation, resulting in a larger subset of infectious viral progeny and thus may explain the even enhanced spread of HAdV-5_E1AΔ24bp_ΔE1B19k_ΔE3gp19k compared to HAdV-5_E1AΔ24bp_ΔE1B19k in cancer cells.

6.8 HexPos3 capsid mutation significantly reduces hepatotoxicity of conditionally replicating HAdV-5 vectors

To investigate the anti-tumor efficacy of an HexPos3 capsid mutated vector *in vivo*, the HexPos3 and ΔCAR capsid mutations were genetically introduced into the previously characterized CRAd HAdV-5_E1AΔ24bp_ΔE1B19k_ΔE3gp19k, generating the HCRAd5-HexPos3_ΔCAR vector and a respective counterpart control vector, lacking the HexPos3 capsid-mutation, HCRAd-5_ΔCAR. Anti-tumor efficacies of both vectors were investigated in UD-SCC-2 tumor-bearing NSG mice after i.v. vector injection.

HCRAd-5-HexPos3_ΔCAR was well tolerated, as all HCRAd-5-HexPos3_ΔCAR-injected mice behaved like the PBS-injected group throughout the whole observation period of the experiment without any physical anomalities regarding their general health condition. In sharp contrast, HCRAd-5_ΔCAR-injected mice showed distinct signs of vector-induced toxicity already 48 hours after vector injection, indicated by a rapid drop in body weight, reduced tactile stimulation, diminished skin turgor and reduced activity. Subsequent IVIS measurement displayed pronounced luciferase activities at sites of the liver in all HCRAd-5_ΔCAR injected mice, indicating strong liver transduction. At the same time, HCRAd5-HexPos3_ΔCAR-injected mice showed only minor luciferase activities in the liver, confirming data from previous biodistribution analysis that showed almost absent hepatocyte transduction by the replication deficient HAdV-5-HexPos3_ΔCAR vector.

Vector-induced toxicities of HCRAd-5_ΔCAR necessitated a premature euthanasia of all HCRAd-5_ΔCAR–injected mice 48 hours after vector injection. Strikingly, blood samples

collected from HCRAd-5_ΔCAR-injected mice showed impaired coagulation and mice partially displayed internal bleedings. Serum analysis revealed drastically elevated aspartate aminotransferase (AST) and alanine aminotransferase (ALT) levels, indicating severe hepatic injury[349]. Subsequent H&E staining of liver sections confirmed this assumption as a massive disruption of the liver architecture with abundant hepatocyte death was histologically identified.

Hepatotoxicity is a known complication upon i.v. injection of HAdV-5-based vectors, partially having fatal outcome[183]. Various factors have been identified to contribute to this effect including the injected vector dose, viral gene expression[194,195], KC uptake[175] or vector interactions with blood factors[173]. In the present study, vector-induced toxicities were solely observed in HCRAd-5_ΔCAR-injected mice, however, not in mice injected with its replication deficient counterpart HAdV-5_ΔCAR. These findings strongly indicated that neither the injected vector dose nor hepatocyte transduction *per se* were causative for the HCRAd-5_ΔCAR-induced toxicity, but solely the conditionally replicating phenotype of HCRAd-5_ΔCAR. The major paradox, however, is that murine hepatocytes should not support productive HCRAd-5_ΔCAR replication. First, hepatocytes are quiescent cells[350] thus replication of conditionally replicating HCRAd-5_ΔCAR vector particles should be efficiently prevented. Furthermore, murine cells are generally not permissive for growth of human adenoviruses and do not support late stages of the HAdV-5 replication cycle, due to various biological barriers[351,352]. Liver damage due to hepatocyte lysis induced by a completed viral life cycle thus can be rather excluded. However, onset of early HAdV-5 gene expression has been reported to partially occur also in murine cells[351] and may have already toxic effects to the affected hepatocyte. In line with this hypothesis, Engler *et al.* reported about hepatotoxicity in immunodeficient beige/scid mice upon i.v. injection of a conditionally replicating HAdV-5 vector, which correlated with viral E1A expression and induced tumor necrosis factor-α (TNF-α) release in the liver[195]. TNF-α in turn is a pleiotropic cytokine, highly involved within liver homeostasis and likewise induces hepatocyte proliferation as a response to liver injury as a unique feature of the liver[353,354]. TNF-α release as a result of viral E1A expression thus may engage liver regenerative processes[355], initiating hepatocyte proliferation. Proliferating hepatocytes in turn may support the onset of early stages of HCRAd-5_ΔCAR replication, including vector genome amplification[351]. Intranuclear accumulation of vector

genomes mimics DNA double strand breaks, which senses the cellular DNA repair machinery[356] to induce cell-cycle arrest and apoptosis[357,358], which could not be counteracted by HCRAd-5_ΔCAR due to lack of the E1B19k protein. Hepatocyte apoptosis may promote further release of TNF-α in the liver, enforcing hepatocyte proliferation and thus creating a self-amplifying feedback-loop that progressively drives viral gene expression and genome amplification, leading to apoptosis of further hepatocytes. The abundant hepatocyte transduction in combination with onset of hepatocyte proliferation potentially supporting early stages of vector replication thus may explain the pathogenesis of the HCRAd-5_ΔCAR-induced hepatotoxicity.

Liver damage is further correlated with abnormalities in blood coagulation[192]. As hepatocytes are the main source for *de novo* synthesis of coagulation factors[191], most of which having a blood plasma half-life of a few days[359], the abundant hepatocyte death caused by HCRAd-5_ΔCAR may likewise explain the impaired blood coagulation and internal bleedings observed in HCRAd-5_ΔCAR-injected mice. I.v. injection of adenoviral vectors additionally poses risk to induce so-called "vector-induced thrombocytopenia (VIT)"[360–363], which occurs within hours after vector injection[361]. Depending on severity, thrombocytopenia may also result in impaired blood coagulation and bleedings[364], such as observed in HCRAd-5_ΔCAR-injected mice. However, VIT is dose-dependent[362] and platelet counts usually recover within days after vector injection[360,362]. Based on the data gathered in the present study showing that i.v. injection of replication deficient HAdV-5_ΔCAR at the same dose than HCRAd-5_ΔCAR did not result in any vector-induced toxicities, VIT seems rather unlikely causative for the impaired blood coagulation and bleedings observed in HCRAd-5_ΔCAR-injected mice.

6.9 Insufficient intratumoral spread limits the anti-tumor efficacy of HAdV-5-HexPos3_ΔCAR

HCRAd-5-HexPos3_ΔCAR showed absent toxicity and successful tumor transduction after i.v. injection in UD-SCC-2 tumor-bearing NSG mice. However, luciferase activities at sites of the tumor peaked at seven days after vector injection and then continuously declined over time. Even though HCRAd-5-HexPos3_ΔCAR-injected mice showed slightly prolonged overall survival rates compared to the PBS-injected group, a direct correlation

between intratumoral luciferase expression levels and prolonged survival of the respective mice was not verifiable, indicating insufficient intratumoral vector replication and spread. As a first possible explanation, tumor necrosis at late stages of tumor growth as observed in H&E staining of tumor sections was suggested to generate a virucidal environment limiting efficient vector replication and spread. However, impaired intratumoral spread of wild-type HAdV-5 has been already reported before and was hypothesized to be primarily caused by *"tumor-supporting structures"* of murine origin abundantly present within human xenografts established in immune-deficient mice[163]. The microscopic appearance of the UD-SCC-2 xenografts used in the present study likewise showed clustered tumor cells tightly embedded into a dense stromal tissue, most likely of murine origin as well. As human adenoviruses cannot productively replicate within murine cells[351,352], such abundant stromal tissue most probably represents a major barrier that prevents proper intratumoral vector replication and spread. Moreover, and as already introduced in more detail in a previous section, the major cellular constituent of the tumor stroma are fibroblasts, which by themselves are only hardly transduced by HAdV-5 based vectors due to lack of CAR expression[332]. However, in that point of view, HexPos3 capsid mutated oncolytic vectors might have an advantage over their unmodified counterpart in a clinical setting. Nilson *et al.* reported that HexPos3 capsid mutated HAdV-5 vectors efficiently transduce human mesenchymal stem cells (MSCs)[311] in a CAR-independent manner and a conditionally replicating HexPos3 capsid-mutated CRAd was shown to lyse MSCs with high efficacy[365]. As MSCs share various characteristics with fibroblasts[366], the data provided by Nilson *et al.* let suggest that HCRAd-5-HexPos3_ΔCAR in an entirely human context might exhibits enhanced oncolytic potential over unmodified HAdV-5-based oncolytic vectors as it may transduces and lyses tumor stroma residential fibroblasts more efficiently.

6.10 Critical view on retargeting strategies for the improvement of tumor transduction efficiencies of HAdV-5-based oncolytic vectors

Efficient tumor transduction is a prerequisite for successful oncolytic virotherapy and represents a major obstacle for systemic HAdV-5-based anti-cancer therapy. One aspect that prevents efficient tumor transduction by HAdV-5-based vectors is inaccessibility,

downregulation, or even absent expression of the HAdV-5 primary receptor CAR in solid tumors. To address this issue, HAdV-5-based vectors have been retargeted towards various different cell surface proteins overexpressed by tumor cells. Respective targeting ligands have been applied either genetically, chemically or geneti-chemically[367–371], all of which having their advantages and disadvantages, which will be considered in this section.

Genetic capsid modifications such as capsid-chimeric vectors or incorporation of small peptide ligands into the capsid particularly have the advantage to be inherited to viral progeny, supporting efficient re-infection of neighboring cancer cells and vector spread through the tumor tissue. Moreover, vector production and purification can be easily scaled up and adapted to GMP-compliant guidelines[372,373], providing the possibility for industrial manufacturing. However, especially the insertion of larger peptides into the vector capsid poses the risk to negatively interfere with the vector stability[374] potentially ending up in unfeasible vector rescue[375] or low yield vector production. Furthermore, the inserted peptide must properly fold within the reducing environment of the cytoplasm to be biologically active and in order to recover viable and genetically retargeted vectors[250]. Thus, the choice of suitable retargeting peptides, not interfering with vector stability is limited.

In contrast, capsid modification on a chemical basis does not affect vector capsid integrity as the retargeting moiety becomes attached to the matured particle. Furthermore, it is ensured that the retargeting ligand is properly folded and thus biologically active. However, chemical attachment of retargeting moieties is often charge-mediated or amine-directed, which may result in densely coated and non-infectious vector particles[215]. A more site-specific attachment can be realized using bispecific adapter molecules, which bind to defined regions of the capsid[229,251]. However, even though this technique prevents a too dense particle coating, the adapter can become displaced from the capsid as it is merely non-covalently attached. This is particularly important during *in vivo* and clinical application since vector particles interact with several blood components[318], which may compete with the adapter for respective capsid binding sites. Here, coupling of the retargeting ligand by geneti-chemical capsid modification[369] provides a suitable method to avoid displacement of the position-specifically attached retargeting ligand. Genetically introduced surface-exposed cysteine residues are used to attach maleimide-bearing

linkers or maleimide-bearing molecules to the vector capsid in a site-specific manner. The resultant covalent thioether bond provides a robust, non-displaceable linkage of the ligand to the vector capsid. However, the scalability of chemical and geneti-chemical capsid modifications remains challenging and requires sophisticated production protocols to meet GMP demands. Furthermore, both modification strategies are not passed on to progeny and thus solely allow for the initial vector targeting.

Independent of the respective retargeting method, tumor targeting ligands always harbor the risk for potential off-target interactions as observed in the present study with the EGFR-targeted Affilin-decorated vectors. Most target receptors, though overexpressed in cancer cells, are likewise often present in healthy cells and tissues, which may result in off-target transduction and adverse events. Thus, biodistribution profiles must be thoroughly investigated to assess the safety of retargeted adenoviral vectors. Moreover, retargeting of HAdV-5-based oncolytic vectors towards alternative target receptors alone may not be sufficient but requires simultaneous avoidance of vector particle sequestration by the several biological barriers as discussed in more detail before.

6.11 Vector detargeting as a more efficient retargeting strategy

With the intention to improve tumor transduction efficiencies of HAdV-5-based vectors, a large number of different vectors retargeted towards alternative target receptors overexpressed by cancer cells have been developed. However, even though *in vitro* experiments often show promising results, biological barriers *in vivo* often limit efficient tumor transduction by HAdV-5-based oncolytic vectors. Especially i.v. injection of retargeted vector particles frequently results in abundant off-target organ transduction and/or rapid particle sequestration accompanied by adverse side effects. In particular, the pronounced liver tropism of HAdV-5-based vectors may result in severe hepatic damage[183]. Avoiding such off-target interactions may significantly improve the safety and therapeutic efficacy of HAdV-5-based anti-cancer virotherapy. This suggestion is supported by the data gathered in the present study, showing that HCRAd-5-HexPos3_ΔCAR, which exhibited a significantly diminished liver tropism and absent toxicity, showed slightly improved therapeutic efficacy. Reduced vector toxicities may allow for the administration of higher and/or repeated vector doses, increasing the probability for a greater subset of vector particles to reach and infect the tumor. Atasheva

et al. i.e. generated a mutant oncolytic HAdV-5 vector harboring a deletion and point mutation within HVR1 and HVR7 of hexon, respectively reducing the negative surface charge of the vector particle and ablated binding of IgM antibodies, components of the complement and FX to the vector capsid[376]. Additional substitution of the penton base-located RGD motif by a 48-amino acid sequence of the human laminin-α1 chain further avoided macrophage β3 integrin interactions while maintaining vector infectivity[376]. This mutant oncolytic vector showed significantly reduced toxicity after i.v. injection and thus allowed for repeated systemic administration, leading to remarkable anti-tumor efficacies in pre-clinical studies[376]. Repeated vector dosing, however, harbors the risk for emerging vector-directed immune responses, which may compromise the therapeutic efficacy of readministered vectors in an immunocompetent setting. Thus, efficient evasion of particle sequestration may be an additional step to further improve tumor targeting by HAdV-5 based oncolytic vectors. Site-specific attachment of small polyethylene glycol (PEG) shielding moieties to hexon i.e., as already applied by Krutzke *et al.*[227], may provide a suitable strategy to fulfill this requirement, as it significantly improves vector pharmacokinetics[227] and thus might expand the time window for i.v. injected vector particles to reach, distribute in, and transduce the tumor tissue. Altogether, effective delivery of vector particles to the tumor requires specific tumor targeting, diminished vector toxicity and reduced particle sequestration, with the latter probably being the most important.

6.12 The tumor stroma as a promising target for oncolytic virotherapy

Solid tumors comprise a highly heterogenous tissue architecture, composed out of cellular and non-cellular components, building up the so-called tumor stroma[377]. Beside the malignant cancer cell itself, stromal tissue accounts for most of the total tumor mass[284] with fibroblasts and extracellular matrix components being the major structural components[285]. The tumor cell by itself is firmly embedded into this stromal tissue and therewith efficiently shielded against systemic anti-tumor therapies[378,379]. As evident by the data gathered in the present study, the tumor stroma likewise reflects a substantial barrier for HAdV-5-based oncolytic virotherapy, limiting its therapeutic efficacy. Physically, it hinders i.v. injected vector particles to efficiently transduce targeted cancer cells due to intratumoral vessels tightly surrounded by stromal components. Alongside its structural

giving properties, the tumor stroma further generates an immune-suppressive and tumor growth-promoting tumor microenvironment (TME)[380]. Thus, different to so far existing anti-cancer therapies that primarily address the malignant tumor cell by itself, disruption of the tumor stroma and its related TME may provide an efficient anti-cancer therapy[381], since it may (re-)sensitizes the tumor against other anti-cancer interventions, which previously showed no effect[382]. Here, especially CAFs provide an attractive target as they represent the major cellular component of the tumor stroma and a main source for the *de novo* synthesis of various growth factors, promoting cancer cell proliferation and formation of metastasis[383]. CAFs have been already come into focus of various anti-tumor therapies including monoclonal antibodies (mAb)[304], CAR-T cell therapy[340,341], oncolytic adenoviral vectors[336,338], or AAV-based platforms[384]. As investigated in the present study, all these approaches have in common that they aimed to target CAFs via their cell-surface antigen FAP. The data provided by the present study further indicate that HAdV-5-based vectors can be successfully retargeted towards FAP as well, suggesting CAFs a suitable target cell type for oncolytic virotherapy. One of the major benefits targeting CAFs is their high abundancy and accessibility within the tumor. Different to the cancer cell itself, CAFs might be easier to access via the adjacent cardiovascular system. Disruption of the tumor stroma by virus replication may additionally attract the immune system due to the release of tumor stroma associated antigens, creating a bystander effect that additionally supports tumor depletion. Tumor stroma-directed oncolytic virotherapy thus represents a promising anti-cancer therapy and may be combined with standard of care interventions such as immuno-, chemo- or radiotherapy.

6.13 Cytotoxic transgenes as a tool to enhance the therapeutic efficacy of oncolytic adenoviruses

Sufficient infection of tumor cells or cells of the tumor stroma with subsequent virus replication is mandatory for efficient oncolytic virotherapy. To further augment the therapeutic efficacy, it might be beneficial to arm oncolytic adenoviruses with tumor-destructive transgenes, which support tumor disruption in addition to the process of virus-induced tumor cell lysis. Cytotoxic transgenes generate a bystander effect to address neighboring cells that have not been initially infected by the virus itself. A major

advantage using virus-encoded transgenes is their local amplification and expression at sites of the tumor, which reduces the risk for systemic side-effects. Different cytotoxic transgenes have been already genetically introduced into oncolytic adenoviruses such as pro-apoptotic proteins, (immuno)toxins or pro-drug converting enzymes[385]. One of the best characterized and investigated is the tumor suppressive p53[386]. *In vitro*, it was shown that virus-mediated p53 expression significantly enhances the cytotoxicity of a CRAd by improving the release of viral progeny and accelerating virus-induced cell death, leading to an overall >100-fold improved oncolytic potential[387]. Follow-up *in vivo* studies further showed that a p53-armed CRAd significantly delayed tumor growth of late-stage subcutaneous neuroblastoma xenografts[388]. Another potent cytotoxic agent is the bee venom derived melittin, which induced strong inhibitory effects in hepatocellular carcinoma cell lines and significantly improved the anti-tumor efficacy of a melittin-armed adenovirus *in vivo*[389]. More directed cytotoxic agents are so-called immunotoxins, which are toxins fused to mAbs or single chain variable fragments that specifically bind to defined cell types expressing tumor specific antigens[390]. An EGFR-directed immunotoxin expressed by an oncolytic adenovirus induced a potent and EGFR-directed bystander effect and significantly augmented the anti-tumor efficacy of the virus *in vivo*[391]. However, even though cytotoxic transgenes may enhance the potency of the encoding oncolytic virus, they likewise affect the infected host cell by itself, which may negatively interfere with efficient virus replication in tumors but also during the production of such viruses. To avoid such undesired side-effects, the usage of so-called “suicide genes” is a suitable strategy. Suicide genes are based on pro-drug converting enzymes, which by themselves are non-toxic, however, metabolize their respective substrates into cytotoxic agents. Exemplary enzymes are thymidine kinase (TK), which metabolizes ganciclovir (GCV) into ganciclovir-5-monophosphate[392] or cytosine deaminase (CD), which converts 5-fluorocytosine into 5-fluorouracil[393,394]. TK-armed oncolytic adenoviruses were shown to exhibit increased cytotoxicity and anti-tumoral response in preclinical pancreatic cancer[395] and retinoblastoma[396] models. An TK-encoding adenoviral vector showed even improved outcome in a phase-II clinical trial for high-grade recurrent glioma when co-administered with GCV[397]. Warmann *et al.* investigated a CD-encoding HAdV-5 vector in hepatoblastoma cell lines *in vitro* and showed increased CD-mediated cytotoxicity upon addition of 5-fluorocytosine[398].

Though, independent of the chosen arming-strategy, transgene expression must be restricted to sites of the tumor in order to avoid unwanted systemic adverse events. The use of tumor-specific promoters such as the survivin[399], telomere reverse transcriptase (TERT)[400] or carcinoembryonic antigen (CEA)[401] promoter may provide an effective strategy to meet this requirement. Transgene expression driven by the adenoviral major late promotor (MLP) provide another feasible strategy to directly link transgene expression to vector replication[402] and in the background of a conditionally replicating vector with selective replication in cancer cells, MLP driven transgene expression would be efficiently restricted to the tumor. Choosing transgenes specifically toxic to cancer cells such as the SAC domain[403] of prostate apoptosis response-4 (Par-4)[404–406] as already introduced into AAV[407] and adenoviral vectors[408], may additionally help to minimize the risk for potential side-effects and thus further improve the safety of armed oncolytic viruses. Additionally, the introduced transgene must not exceed a critical size[409] as an expansion of the adenoviral genome to more than 105% of the original size results in genomic vector instability and rearrangements[348].

6.14 Immune stimulatory oncolytic vectors

A major aspect favoring the use of adenoviruses for oncolytic virotherapy is their high immunogenicity that induces strong immune responses, augmenting their anti-tumor efficacy[315,410]. This feature becomes particularly important for the treatment of immunologically inert, so-called “cold tumors”, which do not respond to immune-based anti-cancer therapies due to different immune evasion mechanisms[411]. As virus induced cancer cell lysis results in the release of tumor-associated antigens, which attracts immune cells to invade the tumor, oncolytic adenoviruses by themselves already exhibit the potential to convert cold tumors to immunologically “visible”, thus turning them “hot”. To further enhance the virus replication-induced tumor-directed immune activation, oncolytic adenoviruses can be equipped with immunostimulatory transgenes to enhance their immunogenicity[143,412,413]. Especially cytokines represent interesting candidates as they are potent activators of various immune responses. Pro-inflammatory cytokines like Interleukine-12 (IL-12), tumor necrosis factor-α (TNF-α)[414,415] or granulocyte-macrophage colony stimulating factor (GM-CSF)[416] have been already identified as promising anti-cancer therapeutics[414–420], however, their clinical use is still limited due to toxicity upon

systemic administration[419,421]. Thus, tumor-restricted local cytokine expression by an oncolytic virus may circumvent such systemic toxicity[28]. In pre-clinical studies, oncolytic adenoviruses armed with IL-12, TNF-α or GM-CSF have been reported to induce strong immunological bystander effects, leading to improved anti-tumor efficacies while avoiding cytokine-related toxicities[422–426]. Most remarkably, in an immunocompetent Syrian hamster tumor model, a TNF-α and IL-2 encoding oncolytic adenovirus induced complete tumor destruction in all of the animals when combined with tumor-infiltrating lymphocyte therapy (TIL) and efficiently prevented tumor relapse when animals were re-challenged by injection of the same tumor cells, indicating for a robust anti-tumor memory immune response[425]. Cytokine-armed oncolytic adenoviruses such as Ad-RTS-hIL-12 (IL-12)[427], TILT-123 (TNF-α + IL-2)[428], CG0070 (GM-CSF)[429–431] and ONCOS-102 (GM-CSF)[426,432] have been already enrolled in phase I and phase II clinical trials and were reported to be well tolerated while showing encouraging results regarding their anti-tumor efficacy[426–432]. As an alternative to pro-inflammatory cytokines, the already introduced bispecific T-cell engagers (BiTEs) can also provide specific immune stimulators, as they induce T-cell-mediated immune responses against specific (tumor)cell-surface antigens[337]. BiTEs targeted against EGFR[433], human mucin 1 (MUC-1)[434] or the epithelial cell adhesion molecule (EpCAM)[435] have been genetically introduced into oncolytic adenoviruses, all of which inducing strong T-cell mediated bystander effects *in vitro* and *in vivo*, and significantly improved the anti-tumor efficacy of the respective virus[433–435]. Tumor stroma-targeted oncolytic adenoviruses encoding for FAP-targeted BiTEs have been discussed in a previous section, and showed potent anti-cancer efficacy *in vitro* and *in vivo* as well as in *ex vivo* tumor biopsies due to BiTE-mediated T-cell attraction[336,338]. To the best of our knowledge, BiTE-armed oncolytic adenoviruses have not reached the clinic yet, though results provided by various pre-clinical studies let suggest BiTE-armed oncolytic adenoviruses as promising candidates for continuing clinical studies. Altogether, oncolytic adenoviruses armed with immune stimulatory transgenes are promising “next generation” candidates for virus-based anti-tumor immunotherapies.

6.15 Combining oncolytic viruses with other anti-cancer therapies

In pre-clinical studies, oncolytic adenoviruses already showed significant anti-tumor efficacies. However, applied as a monotherapy, bench to bedside transition remains an

obstacle and therapeutic achievements are still limited. However, immune-based therapies such as checkpoint inhibitors or CAR-T cell therapy may significantly benefit from the immunostimulatory properties of oncolytic adenoviruses[410,436–438] as they are often compromised by an immune suppressive TME[439,440]. Disruption and break-down of the tumor stroma and its related TME using oncolytic viruses thus may render tumors more susceptible to such therapies and may overcome emerging resistances and bad tumor responses[437]. CAR-T cell therapies show poor efficiencies in solid tumors due to hampered T-cell infiltration caused by the tumor stroma and its related TME[437,441–443]. A set of pre-clinical studies demonstrated that tumor infiltration by CAR-T cells can be significantly enhanced when combined with oncolytic virotherapy[444]. Limited therapeutic efficacy of checkpoint inhibitors and other monoclonal antibody-based therapies may also be caused by the immune-suppressive TME and/or the physical barrier of the tumor stroma.[378,445,446] Oncolytic viruses are discussed as a promising synergistic tool to overcome this limitation[447] and combination therapies are already under clinical investigation for the treatment of various types of cancer including glioblastoma[448], melanoma[449], breast- and non-small lung carcinoma[450], bladder cancer[451] or epithelial tumors[452]. Virus-mediated tumor disruption could likewise render tumors more susceptible to standard of care treatments like chemo- or radiotherapy[453] as already proven in chemotherapy-resistant metastatic breast carcinoma[454]. Thus, the high number of ongoing pre-clinical and clinical studies utilizing oncolytic adenoviruses in combinatory therapies highlights their significance for the development of novel combinatory anti-cancer therapies. Thus, in addition to mono-therapeutic approaches, oncolytic adenoviruses may play a significant role as synergistic agents for conventional and novel anti-cancer therapies in the near future.

6.16 Evaluation and future prospects for adenoviral-based oncolytic virotherapy

During the last years, oncolytic adenoviral vectors underwent a remarkable and rapid development, rendering them one of the most promising novel anti-cancer therapies today[455]. An increased understanding of the adenovirus biology resulted in safer and more potent oncolytic vectors, many of which reaching clinical trials[24,29] and some having

achieved approval for the use in humans[17–19]. Genetic modifications enabled the development of oncolytic vectors with selective replication in cancer cells, altered viral tropism and increased tumor cell destruction efficacies by introducing cytotoxic and immune-stimulatory transgenes[315,412,456,457]. Simultaneously, a more detailed elucidation of the biological barriers[318] facilitated the improvement of adenoviral-based anti-cancer therapies regarding safety and efficacy. Over the years, a major focus has been the development of oncolytic adenoviruses based on HAdV-5, which established it as a kind of “working horse” in the field of oncolytic virotherapy. There are many HAdV-5-based oncolytic vectors showing promising results *in vitro* and in pre-clinical studies. However, pre-clinical studies are often performed in immunodeficient mice in order to allow for the engraftment of human tumor xenografts, which in turn allow for the replication of the species-restricted human adenoviruses. Lack of immunity, however, creates a rather artificial experimental environment, which only insufficiently mirrors the actual clinical situation in humans. Especially immune responses, independent on whether limiting or favoring the anti-tumor efficacy of the oncolytic virus cannot be evaluated. On the other hand, conclusions drawn from tumor models developed in immunocompetent mice[458–460], are generally limited by the severely suppressed replication of HAdV-5-based vectors in murine cells[351,352]. A thorough assessment of the efficacy and safety of HAdV-5-based oncolytic vectors thus cannot be sufficiently evaluated in mice. Poor tumor transduction efficiencies, insufficient intratumoral virus replication and spread, as well as a broad pre-existing immunity against HAdV-5 within the human population[180] additionally impede the anti-tumor efficacy of HAdV-5-based oncolytic virotherapy within the clinical use. Potentially emerging liver toxicities[183] due to the inherent liver tropism of HAdV-5-based vectors additionally rise concern about the safety of HAdV-5-based oncolytic virotherapy. To date, these barriers have not yet sufficiently overcome and still need to be addressed. In this point, new human adenovirus types are potential hopes. To date, there have been more than 80 different adenovirus types identified[33], however, only few have been characterized in more detail. Possibly, some of them might show improved oncolytic potential and an improved safety profile, so in-depth characterization is worthwhile. Especially types showing low seroprevalence[461–463], accelerated replication and spread[464] or less susceptibility to natural sequestration mechanisms in humans may provide promising platforms for the development of novel and potent oncolytic adenoviral vectors.

Furthermore, an expanded repertoire of oncolytic viruses based on different adenovirus types may provide the possibility to overcome poor tumor responses in patients with pre-existing and acquired immunity due to previous exposure and/or repeated vector dosing. Novel vectors may be further improved using already existing and well-established methods, developed using HAdV-5, such as cytotoxic or immune stimulatory transgenes. The repertoire of different adenovirus types available thus exhibits the potential for the development of novel oncolytic viruses with increased activity and may represent a future research direction in the area of novel anti-cancer virotherapies. Basic research on HAdV-5, however, will continue to provide the fundamental knowledge about the adenovirus biology and thus will further support and guide the development of novel oncolytic adenoviral vectors in the future.

7 Summary

The therapeutic efficacy of HAdV-5-based oncolytic vectors is limited by different biological barriers. Rapid particle sequestration and off-target tropism of particles upon vector administration severely limits efficient delivery of vector particles to the tumor and additionally poses the risk for vector-induced toxicity. Hence, enhancing tumor transduction efficiencies and reducing dose-limiting vector toxicity is mandatory to improve the therapeutic efficacy of HAdV-5-based oncolytic virotherapy.

In the present study two different tumor targeting strategies of HAdV-5-based vectors were evaluated. Firstly, two HAdV-5-based vectors, with the epidermal growth factor receptor (EGFR) affinity ligand Affilin covalently coupled to either the fiber or hexon protein of the vector capsid, were shown to exhibit remarkably enhanced transduction efficiency in EGFR-positive cancer cells *in vitro*. *In vivo*, these vectors further showed significantly reduced liver tropism upon intravenous injection, however, poor tumor transduction in EGFR-positive tumors, even after intratumoral injection. As the main reasons a broadly distributed on-target/off-tumor binding to EGFR within the cardiovascular system and poor accessibility of intratumoral EGFR were assumed. Thus, the EGFR was identified as a difficult-to-address receptor for HAdV-5-based oncolytic vectors.

As a second targeting strategy using a bispecific adapter molecule HAdV-5-based vectors were successfully retargeted to the fibroblast activation protein (FAP), a molecule that is almost exclusively expressed by cancer associated fibroblasts (CAFs) located in the tumor stroma. This data suggested FAP as an interesting target for HAdV-5-based oncolytic virotherapy with high tumor specificity, worthwhile to be further investigated.

Moreover, and as a major finding, the surface charge-modified mutant vector HAdV-5-HexPos3 was identified to not only exhibit improved tumor targeting but also distinctly reduced off-target organ tropism *in vivo*. The vector showed almost ablated hepatocyte transduction, absence of toxicity and intratumoral vector delivery detectable for up to 56 days after a single i.v. injection into tumor-bearing mice. Based on these findings, the net negative surface charge of HAdV-5 was identified as a major determinant

of particle fate and tropism, significantly reducing the anti-tumor efficacy of HAdV-5-based oncolytic vectors. Thus, due to its substantially reduced toxicity and maintained oncolytic potential, the HAdV-5-HexPos3 mutant holds promise as an oncolytic vector potentially with improved overall anti-tumor efficacy, which might be further enhanced if combined with additional retargeting and/or vector-arming strategies.

8 References

1. Gonçalves, G.A.R., and Paiva, R. de M.A. (2017). Gene therapy: advances, challenges and perspectives. Einstein (Sao Paulo) *15*, 369–375. 10.1590/S1679-45082017RB4024.

2. Das, S.K., Menezes, M.E., Bhatia, S., Wang, X.-Y., Emdad, L., Sarkar, D., and Fisher, P.B. (2015). Gene Therapies for Cancer: Strategies, Challenges and Successes. J Cell Physiol *230*, 259–271. 10.1002/jcp.24791.

3. Mali, S. (2013). Delivery systems for gene therapy. Indian J Hum Genet *19*, 3–8. 10.4103/0971-6866.112870.

4. Mollé, L.M., Smyth, C.H., Yuen, D., and Johnston, A.P.R. (2022). Nanoparticles for vaccine and gene therapy: Overcoming the barriers to nucleic acid delivery. Wiley Interdiscip Rev Nanomed Nanobiotechnol *14*, e1809. 10.1002/wnan.1809.

5. Lundstrom, K. (2018). Viral Vectors in Gene Therapy. Diseases *6*, 42. 10.3390/diseases6020042.

6. Bulcha, J.T., Wang, Y., Ma, H., Tai, P.W.L., and Gao, G. (2021). Viral vector platforms within the gene therapy landscape. Signal Transduct Target Ther *6*, 53. 10.1038/s41392-021-00487-6.

7. Raper, S.E., Chirmule, N., Lee, F.S., Wivel, N.A., Bagg, A., Gao, G., Wilson, J.M., and Batshaw, M.L. (2003). Fatal systemic inflammatory response syndrome in a ornithine transcarbamylase deficient patient following adenoviral gene transfer. Mol Genet Metab *80*, 148–158. 10.1016/j.ymgme.2003.08.016.

8. Zhao, Z., Anselmo, A.C., and Mitragotri, S. (2022). Viral vector-based gene therapies in the clinic. Bioeng Transl Med *7*, e10258. 10.1002/btm2.10258.

9. GTCT (FMS19) https://a873679.fmphost.com/fmi/webd/GTCT.

10. Ylä-Herttuala, S. (2012). Endgame: glybera finally recommended for approval as the first gene therapy drug in the European union. Mol Ther *20*, 1831–1832. 10.1038/mt.2012.194.

11. Burnett, J.R., and Hooper, A.J. (2009). Alipogene tiparvovec, an adeno-associated virus encoding the Ser(447)X variant of the human lipoprotein lipase gene for the treatment of patients with lipoprotein lipase deficiency. Curr Opin Mol Ther *11*, 681–691.

12. Russell, S., Bennett, J., Wellman, J.A., Chung, D.C., Yu, Z.-F., Tillman, A., Wittes, J., Pappas, J., Elci, O., McCague, S., et al. (2017). Efficacy and safety of voretigene neparvovec (AAV2-hRPE65v2) in patients with RPE65-mediated inherited retinal dystrophy: a randomised, controlled, open-label, phase 3 trial. Lancet *390*, 849–860. 10.1016/S0140-6736(17)31868-8.

References

13. Mendell, J.R., Al-Zaidy, S., Shell, R., Arnold, W.D., Rodino-Klapac, L.R., Prior, T.W., Lowes, L., Alfano, L., Berry, K., Church, K., et al. (2017). Single-Dose Gene-Replacement Therapy for Spinal Muscular Atrophy. N Engl J Med *377*, 1713–1722. 10.1056/NEJMoa1706198.

14. Ahmad, A. (2020). CAR-T Cell Therapy. Int J Mol Sci *21*, 4303. 10.3390/ijms21124303.

15. Maude, S.L., Frey, N., Shaw, P.A., Aplenc, R., Barrett, D.M., Bunin, N.J., Chew, A., Gonzalez, V.E., Zheng, Z., Lacey, S.F., et al. (2014). Chimeric antigen receptor T cells for sustained remissions in leukemia. N Engl J Med *371*, 1507–1517. 10.1056/NEJMoa1407222.

16. Fukuhara, H., Ino, Y., and Todo, T. (2016). Oncolytic virus therapy: A new era of cancer treatment at dawn. Cancer Sci *107*, 1373–1379. 10.1111/cas.13027.

17. Zhang, W.-W., Li, L., Li, D., Liu, J., Li, X., Li, W., Xu, X., Zhang, M.J., Chandler, L.A., Lin, H., et al. (2018). The First Approved Gene Therapy Product for Cancer Ad-p53 (Gendicine): 12 Years in the Clinic. Hum Gene Ther *29*, 160–179. 10.1089/hum.2017.218.

18. Wilson, J.M. (2005). Gendicine: The First Commercial Gene Therapy Product; Chinese Translation of Editorial. Human Gene Therapy *16*, 1014–1015. 10.1089/hum.2005.16.1014.

19. Liang, M. (2018). Oncorine, the World First Oncolytic Virus Medicine and its Update in China. Curr Cancer Drug Targets *18*, 171–176. 10.2174/1568009618666171129221503.

20. Johnson, D.B., Puzanov, I., and Kelley, M.C. (2015). Talimogene laherparepvec (T-VEC) for the treatment of advanced melanoma. Immunotherapy *7*, 611–619. 10.2217/imt.15.35.

21. Ferrucci, P.F., Pala, L., Conforti, F., and Cocorocchio, E. (2021). Talimogene Laherparepvec (T-VEC): An Intralesional Cancer Immunotherapy for Advanced Melanoma. Cancers (Basel) *13*, 1383. 10.3390/cancers13061383.

22. Todo, T., Ito, H., Ino, Y., Ohtsu, H., Ota, Y., Shibahara, J., and Tanaka, M. (2022). Intratumoral oncolytic herpes virus G47Δ for residual or recurrent glioblastoma: a phase 2 trial. Nat Med *28*, 1630–1639. 10.1038/s41591-022-01897-x.

23. Todo, T., Ino, Y., Ohtsu, H., Shibahara, J., and Tanaka, M. (2022). A phase I/II study of triple-mutated oncolytic herpes virus G47Δ in patients with progressive glioblastoma. Nat Commun *13*, 4119. 10.1038/s41467-022-31262-y.

24. Li, K., Zhao, Y., Hu, X., Jiao, J., Wang, W., and Yao, H. (2022). Advances in the clinical development of oncolytic viruses. Am J Transl Res *14*, 4192–4206.

25. Toth, K., Dhar, D., and Wold, W.S. (2010). Oncolytic (replication-competent) adenoviruses as anticancer agents. Expert Opinion on Biological Therapy *10*, 353–368. 10.1517/14712590903559822.

26. Mantwill, K., Klein, F.G., Wang, D., Hindupur, S.V., Ehrenfeld, M., Holm, P.S., and Nawroth, R. (2021). Concepts in Oncolytic Adenovirus Therapy. Int J Mol Sci *22*, 10522. 10.3390/ijms221910522.

27. Tian, Y., Xie, D., and Yang, L. (2022). Engineering strategies to enhance oncolytic viruses in cancer immunotherapy. Signal Transduct Target Ther *7*, 117. 10.1038/s41392-022-00951-x.

28. de Graaf, J.F., de Vor, L., Fouchier, R. a. M., and van den Hoogen, B.G. (2018). Armed oncolytic viruses: A kick-start for anti-tumor immunity. Cytokine Growth Factor Rev *41*, 28–39. 10.1016/j.cytogfr.2018.03.006.

29. Pol, J., Buqué, A., Aranda, F., Bloy, N., Cremer, I., Eggermont, A., Erbs, P., Fucikova, J., Galon, J., Limacher, J.-M., et al. (2016). Trial Watch-Oncolytic viruses and cancer therapy. Oncoimmunology *5*, e1117740. 10.1080/2162402X.2015.1117740.

30. Harui, A., Suzuki, S., Kochanek, S., and Mitani, K. (1999). Frequency and stability of chromosomal integration of adenovirus vectors. J Virol *73*, 6141–6146. 10.1128/JVI.73.7.6141-6146.1999.

31. Taxonomy browser (Adenoviridae) https://www.ncbi.nlm.nih.gov/Taxonomy/Browser/wwwtax.cgi?id=10508.

32. Rowe, W.P., Huebner, R.J., Gilmore, L.K., Parrott, R.H., and Ward, T.G. (1953). Isolation of a cytopathogenic agent from human adenoids undergoing spontaneous degeneration in tissue culture. Proc Soc Exp Biol Med *84*, 570–573. 10.3181/00379727-84-20714.

33. Dhingra, A., Hage, E., Ganzenmueller, T., Böttcher, S., Hofmann, J., Hamprecht, K., Obermeier, P., Rath, B., Hausmann, F., Dobner, T., et al. (2019). Molecular Evolution of Human Adenovirus (HAdV) Species C. Sci Rep *9*, 1039. 10.1038/s41598-018-37249-4.

34. Robinson, C.M., Singh, G., Lee, J.Y., Dehghan, S., Rajaiya, J., Liu, E.B., Yousuf, M.A., Betensky, R.A., Jones, M.S., Dyer, D.W., et al. (2013). Molecular evolution of human adenoviruses. Sci Rep *3*, 1812. 10.1038/srep01812.

35. Liu, H., Jin, L., Koh, S.B.S., Atanasov, I., Schein, S., Wu, L., and Zhou, Z.H. (2010). Atomic structure of human adenovirus by cryo-EM reveals interactions among protein networks. Science *329*, 1038–1043. 10.1126/science.1187433.

36. Knipe, D.M., and Howley, P.M. eds. (2013). Fields virology 6th ed. (Wolters Kluwer/Lippincott Williams & Wilkins Health).

37. Russell, W.C. (2009). Adenoviruses: update on structure and function. J Gen Virol *90*, 1–20. 10.1099/vir.0.003087-0.

38. Zubieta, C., Schoehn, G., Chroboczek, J., and Cusack, S. (2005). The structure of the human adenovirus 2 penton. Mol Cell *17*, 121–135. 10.1016/j.molcel.2004.11.041.

39. Chroboczek, J., Ruigrok, R.W., and Cusack, S. (1995). Adenovirus fiber. Curr Top Microbiol Immunol *199 (Pt 1)*, 163–200. 10.1007/978-3-642-79496-4_10.

40. Liu, H., Wu, L., and Zhou, Z.H. (2011). Model of the trimeric fiber and its interactions with the pentameric penton base of human adenovirus by cryo-electron microscopy. J Mol Biol *406*, 764–774. 10.1016/j.jmb.2010.11.043.

41. Bewley, M.C., Springer, K., Zhang, Y.B., Freimuth, P., and Flanagan, J.M. (1999). Structural analysis of the mechanism of adenovirus binding to its human cellular receptor, CAR. Science *286*, 1579–1583. 10.1126/science.286.5444.1579.

42. Henry, L.J., Xia, D., Wilke, M.E., Deisenhofer, J., and Gerard, R.D. (1994). Characterization of the knob domain of the adenovirus type 5 fiber protein expressed in Escherichia coli. J Virol *68*, 5239–5246. 10.1128/JVI.68.8.5239-5246.1994.

43. Bai, M., Harfe, B., and Freimuth, P. (1993). Mutations that alter an Arg-Gly-Asp (RGD) sequence in the adenovirus type 2 penton base protein abolish its cell-rounding activity and delay virus reproduction in flat cells. J Virol *67*, 5198–5205. 10.1128/JVI.67.9.5198-5205.1993.

44. Mathias, P., Wickham, T., Moore, M., and Nemerow, G. (1994). Multiple adenovirus serotypes use alpha v integrins for infection. J Virol *68*, 6811–6814. 10.1128/JVI.68.10.6811-6814.1994.

45. Wickham, T.J., Mathias, P., Cheresh, D.A., and Nemerow, G.R. (1993). Integrins alpha v beta 3 and alpha v beta 5 promote adenovirus internalization but not virus attachment. Cell *73*, 309–319.

46. Roberts, M.M., White, J.L., Grütter, M.G., and Burnett, R.M. (1986). Three-dimensional structure of the adenovirus major coat protein hexon. Science *232*, 1148–1151. 10.1126/science.3704642.

47. Crawford-Miksza, L., and Schnurr, D.P. (1996). Analysis of 15 adenovirus hexon proteins reveals the location and structure of seven hypervariable regions containing serotype-specific residues. J Virol *70*, 1836–1844. 10.1128/JVI.70.3.1836-1844.1996.

48. Alba, R., Bradshaw, A.C., Parker, A.L., Bhella, D., Waddington, S.N., Nicklin, S.A., van Rooijen, N., Custers, J., Goudsmit, J., Barouch, D.H., et al. (2009). Identification of coagulation factor (F)X binding sites on the adenovirus serotype 5 hexon: effect of mutagenesis on FX interactions and gene transfer. Blood *114*, 965–971. 10.1182/blood-2009-03-208835.

49. Waddington, S.N., McVey, J.H., Bhella, D., Parker, A.L., Barker, K., Atoda, H., Pink, R., Buckley, S.M.K., Greig, J.A., Denby, L., et al. (2008). Adenovirus serotype 5 hexon mediates liver gene transfer. Cell *132*, 397–409. 10.1016/j.cell.2008.01.016.

50. Alemany, R., Suzuki, K., and Curiel, D.T. (2000). Blood clearance rates of adenovirus type 5 in mice. J Gen Virol *81*, 2605–2609. 10.1099/0022-1317-81-11-2605.

51. Vellinga, J., Van der Heijdt, S., and Hoeben, R.C. (2005). The adenovirus capsid: major progress in minor proteins. J Gen Virol *86*, 1581–1588. 10.1099/vir.0.80877-0.

52. Kulanayake, S., and Tikoo, S.K. (2021). Adenovirus Core Proteins: Structure and Function. Viruses *13*, 388. 10.3390/v13030388.

53. Chroboczek, J., Bieber, F., and Jacrot, B. (1992). The sequence of the genome of adenovirus type 5 and its comparison with the genome of adenovirus type 2. Virology *186*, 280–285. 10.1016/0042-6822(92)90082-z.

54. Wu, M., Roberts, R.J., and Davidson, N. (1977). Structure of the inverted terminal repetition of adenovirus type 2 DNA. J Virol *21*, 766–777. 10.1128/JVI.21.2.766-777.1977.

55. Hay, R.T. (1985). The origin of adenovirus DNA replication: minimal DNA sequence requirement in vivo. EMBO J *4*, 421–426. 10.1002/j.1460-2075.1985.tb03645.x.

56. Rekosh, D.M., Russell, W.C., Bellet, A.J., and Robinson, A.J. (1977). Identification of a protein linked to the ends of adenovirus DNA. Cell *11*, 283–295. 10.1016/0092-8674(77)90045-9.

57. Pronk, R., and van der Vliet, P.C. (1993). The adenovirus terminal protein influences binding of replication proteins and changes the origin structure. Nucleic Acids Res *21*, 2293–2300. 10.1093/nar/21.10.2293.

58. Gräble, M., and Hearing, P. (1990). Adenovirus type 5 packaging domain is composed of a repeated element that is functionally redundant. J Virol *64*, 2047–2056. 10.1128/JVI.64.5.2047-2056.1990.

59. Schmid, S.I., and Hearing, P. (1995). Selective encapsidation of adenovirus DNA. Curr Top Microbiol Immunol *199 (Pt 1)*, 67–80. 10.1007/978-3-642-79496-4_5.

60. Hearing, P., Samulski, R.J., Wishart, W.L., and Shenk, T. (1987). Identification of a repeated sequence element required for efficient encapsidation of the adenovirus type 5 chromosome. J Virol *61*, 2555–2558. 10.1128/JVI.61.8.2555-2558.1987.

61. Pérez-Berná, A.J., Marion, S., Chichón, F.J., Fernández, J.J., Winkler, D.C., Carrascosa, J.L., Steven, A.C., Šiber, A., and San Martín, C. (2015). Distribution of DNA-condensing protein complexes in the adenovirus core. Nucleic Acids Res *43*, 4274–4283. 10.1093/nar/gkv187.

62. Westergren Jakobsson, A., Segerman, B., Wallerman, O., Lind, S.B., Zhao, H., Rubin, C.-J., Pettersson, U., and Akusjärvi, G. (2020). The Human Adenovirus Type 2 Transcriptome: An Amazing Complexity of Alternatively Spliced mRNAs. J Virol *95*, e01869-20, JVI.01869-20. 10.1128/JVI.01869-20.

63. Doerfler, W. (1996). Adenoviruses. In Medical Microbiology, S. Baron, ed. (University of Texas Medical Branch at Galveston).

64. Bergelson, J.M., Cunningham, J.A., Droguett, G., Kurt-Jones, E.A., Krithivas, A., Hong, J.S., Horwitz, M.S., Crowell, R.L., and Finberg, R.W. (1997). Isolation of a common receptor for Coxsackie B viruses and adenoviruses 2 and 5. Science *275*, 1320–1323.

65. Tomko, R.P., Xu, R., and Philipson, L. (1997). HCAR and MCAR: the human and mouse cellular receptors for subgroup C adenoviruses and group B coxsackieviruses. Proc. Natl. Acad. Sci. U.S.A. *94*, 3352–3356.

66. Zhang, Y., and Bergelson, J.M. (2005). Adenovirus receptors. J Virol *79*, 12125–12131. 10.1128/JVI.79.19.12125-12131.2005.

67. Meier, O., and Greber, U.F. (2004). Adenovirus endocytosis. J Gene Med *6 Suppl 1*, S152-163. 10.1002/jgm.553.

68. Nakano, M.Y., Boucke, K., Suomalainen, M., Stidwill, R.P., and Greber, U.F. (2000). The first step of adenovirus type 2 disassembly occurs at the cell surface, independently of endocytosis and escape to the cytosol. J. Virol. *74*, 7085–7095.

69. Greber, U.F., Willetts, M., Webster, P., and Helenius, A. (1993). Stepwise dismantling of adenovirus 2 during entry into cells. Cell *75*, 477–486. 10.1016/0092-8674(93)90382-z.

70. Greber, U.F., Webster, P., Weber, J., and Helenius, A. (1996). The role of the adenovirus protease on virus entry into cells. EMBO J *15*, 1766–1777.

71. Maier, O., Galan, D.L., Wodrich, H., and Wiethoff, C.M. (2010). An N-terminal domain of adenovirus protein VI fragments membranes by inducing positive membrane curvature. Virology *402*, 11–19. 10.1016/j.virol.2010.03.043.

72. Moyer, C.L., Wiethoff, C.M., Maier, O., Smith, J.G., and Nemerow, G.R. (2011). Functional genetic and biophysical analyses of membrane disruption by human adenovirus. J Virol *85*, 2631–2641. 10.1128/JVI.02321-10.

73. Wiethoff, C.M., Wodrich, H., Gerace, L., and Nemerow, G.R. (2005). Adenovirus protein VI mediates membrane disruption following capsid disassembly. J Virol *79*, 1992–2000. 10.1128/JVI.79.4.1992-2000.2005.

74. Bremner, K.H., Scherer, J., Yi, J., Vershinin, M., Gross, S.P., and Vallee, R.B. (2009). Adenovirus transport via direct interaction of cytoplasmic dynein with the viral capsid hexon subunit. Cell Host Microbe *6*, 523–535. 10.1016/j.chom.2009.11.006.

75. Leopold, P.L., Kreitzer, G., Miyazawa, N., Rempel, S., Pfister, K.K., Rodriguez-Boulan, E., and Crystal, R.G. (2000). Dynein- and microtubule-mediated translocation of adenovirus serotype 5 occurs after endosomal lysis. Hum Gene Ther *11*, 151–165. 10.1089/10430340050016238.

76. Mabit, H., Nakano, M.Y., Prank, U., Saam, B., Döhner, K., Sodeik, B., and Greber, U.F. (2002). Intact microtubules support adenovirus and herpes simplex virus infections. J Virol *76*, 9962–9971. 10.1128/jvi.76.19.9962-9971.2002.

77. Smith, J.G., Cassany, A., Gerace, L., Ralston, R., and Nemerow, G.R. (2008). Neutralizing antibody blocks adenovirus infection by arresting microtubule-dependent cytoplasmic transport. J Virol *82*, 6492–6500. 10.1128/JVI.00557-08.

78. Wodrich, H., Henaff, D., Jammart, B., Segura-Morales, C., Seelmeir, S., Coux, O., Ruzsics, Z., Wiethoff, C.M., and Kremer, E.J. (2010). A capsid-encoded PPxY-motif facilitates adenovirus entry. PLoS Pathog *6*, e1000808. 10.1371/journal.ppat.1000808.

79. Cassany, A., Ragues, J., Guan, T., Bégu, D., Wodrich, H., Kann, M., Nemerow, G.R., and Gerace, L. (2015). Nuclear import of adenovirus DNA involves direct interaction of hexon with an N-terminal domain of the nucleoporin Nup214. J Virol *89*, 1719–1730. 10.1128/JVI.02639-14.

80. Trotman, L.C., Mosberger, N., Fornerod, M., Stidwill, R.P., and Greber, U.F. (2001). Import of adenovirus DNA involves the nuclear pore complex receptor CAN/Nup214 and histone H1. Nat Cell Biol *3*, 1092–1100. 10.1038/ncb1201-1092.

81. Walkiewicz, M.P., Morral, N., and Engel, D.A. (2009). Accurate single-day titration of adenovirus vectors based on equivalence of protein VII nuclear dots and infectious particles. J Virol Methods *159*, 251–258. 10.1016/j.jviromet.2009.04.010.

82. Xue, Y., Johnson, J.S., Ornelles, D.A., Lieberman, J., and Engel, D.A. (2005). Adenovirus protein VII functions throughout early phase and interacts with cellular proteins SET and pp32. J Virol *79*, 2474–2483. 10.1128/JVI.79.4.2474-2483.2005.

83. Hindley, C.E., Lawrence, F.J., and Matthews, D.A. (2007). A role for transportin in the nuclear import of adenovirus core proteins and DNA. Traffic *8*, 1313–1322. 10.1111/j.1600-0854.2007.00618.x.

84. Wodrich, H., Cassany, A., D'Angelo, M.A., Guan, T., Nemerow, G., and Gerace, L. (2006). Adenovirus core protein pVII is translocated into the nucleus by multiple import receptor pathways. J Virol *80*, 9608–9618. 10.1128/JVI.00850-06.

85. Flint, J., and Shenk, T. (1997). Viral transactivating proteins. Annu Rev Genet *31*, 177–212. 10.1146/annurev.genet.31.1.177.

86. Berk, A.J. (1986). Functions of adenovirus E1A. Cancer Surv *5*, 367–387.

87. Nakajima, T., Masuda-Murata, M., Hara, E., and Oda, K. (1987). Induction of cell cycle progression by adenovirus E1A gene 13S- and 12S-mRNA products in quiescent rat cells. Mol Cell Biol *7*, 3846–3852. 10.1128/mcb.7.10.3846-3852.1987.

88. Whyte, P., Buchkovich, K.J., Horowitz, J.M., Friend, S.H., Raybuck, M., Weinberg, R.A., and Harlow, E. (1988). Association between an oncogene and an anti-oncogene: the adenovirus E1A proteins bind to the retinoblastoma gene product. Nature *334*, 124–129. 10.1038/334124a0.

89. Ikeda, M.A., and Nevins, J.R. (1993). Identification of distinct roles for separate E1A domains in disruption of E2F complexes. Mol Cell Biol *13*, 7029–7035. 10.1128/mcb.13.11.7029-7035.1993.

90. Fattaey, A.R., Harlow, E., and Helin, K. (1993). Independent regions of adenovirus E1A are required for binding to and dissociation of E2F-protein complexes. Mol Cell Biol *13*, 7267–7277. 10.1128/mcb.13.12.7267-7277.1993.

91. Liu, X., and Marmorstein, R. (2007). Structure of the retinoblastoma protein bound to adenovirus E1A reveals the molecular basis for viral oncoprotein inactivation of a tumor suppressor. Genes Dev *21*, 2711–2716. 10.1101/gad.1590607.

92. Bagchi, S., Raychaudhuri, P., and Nevins, J.R. (1990). Adenovirus E1A proteins can dissociate heteromeric complexes involving the E2F transcription factor: a novel mechanism for E1A trans-activation. Cell *62*, 659–669. 10.1016/0092-8674(90)90112-r.

93. Marton, M.J., Baim, S.B., Ornelles, D.A., and Shenk, T. (1990). The adenovirus E4 17-kilodalton protein complexes with the cellular transcription factor E2F, altering its DNA-binding properties and stimulating E1A-independent accumulation of E2 mRNA. J Virol *64*, 2345–2359. 10.1128/JVI.64.5.2345-2359.1990.

94. Kovesdi, I., Reichel, R., and Nevins, J.R. (1986). Identification of a cellular transcription factor involved in E1A trans-activation. Cell *45*, 219–228. 10.1016/0092-8674(86)90386-7.

95. Shan, B., and Lee, W.H. (1994). Deregulated expression of E2F-1 induces S-phase entry and leads to apoptosis. Mol Cell Biol *14*, 8166–8173. 10.1128/mcb.14.12.8166-8173.1994.

96. Lowe, S.W., and Ruley, H.E. (1993). Stabilization of the p53 tumor suppressor is induced by adenovirus 5 E1A and accompanies apoptosis. Genes Dev *7*, 535–545. 10.1101/gad.7.4.535.

97. Debbas, M., and White, E. (1993). Wild-type p53 mediates apoptosis by E1A, which is inhibited by E1B. Genes Dev *7*, 546–554. 10.1101/gad.7.4.546.

98. Perricaudet, M., Le Moullec, J.M., and Pettersson, U. (1980). Predicted structure of two adenovirus tumor antigens. Proc Natl Acad Sci U S A *77*, 3778–3782. 10.1073/pnas.77.7.3778.

99. Tarodi, B., Subramanian, T., and Chinnadurai, G. (1993). Functional similarity between adenovirus e1b 19k gene and bcl2 oncogene - mutant complementation and suppression of cell-death induced by DNA-damaging agents. Int J Oncol *3*, 467–472. 10.3892/ijo.3.3.467.

100. Chiou, S.K., Tseng, C.C., Rao, L., and White, E. (1994). Functional complementation of the adenovirus E1B 19-kilodalton protein with Bcl-2 in the inhibition of apoptosis in infected cells. J Virol *68*, 6553–6566. 10.1128/JVI.68.10.6553-6566.1994.

101. Cuconati, A., Mukherjee, C., Perez, D., and White, E. (2003). DNA damage response and MCL-1 destruction initiate apoptosis in adenovirus-infected cells. Genes Dev *17*, 2922–2932. 10.1101/gad.1156903.

102. Farrow, S.N., White, J.H., Martinou, I., Raven, T., Pun, K.T., Grinham, C.J., Martinou, J.C., and Brown, R. (1995). Cloning of a bcl-2 homologue by interaction with adenovirus E1B 19K. Nature *374*, 731–733. 10.1038/374731a0.

103. Han, J., Sabbatini, P., Perez, D., Rao, L., Modha, D., and White, E. (1996). The E1B 19K protein blocks apoptosis by interacting with and inhibiting the p53-inducible and death-promoting Bax protein. Genes Dev *10*, 461–477. 10.1101/gad.10.4.461.

104. Han, J., Modha, D., and White, E. (1998). Interaction of E1B 19K with Bax is required to block Bax-induced loss of mitochondrial membrane potential and apoptosis. Oncogene *17*, 2993–3005. 10.1038/sj.onc.1202215.

105. Sundararajan, R., and White, E. (2001). E1B 19K blocks Bax oligomerization and tumor necrosis factor alpha-mediated apoptosis. J Virol *75*, 7506–7516. 10.1128/JVI.75.16.7506-7516.2001.

106. White, E. (2001). Regulation of the cell cycle and apoptosis by the oncogenes of adenovirus. Oncogene *20*, 7836–7846. 10.1038/sj.onc.1204861.

107. Wei, M.C., Zong, W.X., Cheng, E.H., Lindsten, T., Panoutsakopoulou, V., Ross, A.J., Roth, K.A., MacGregor, G.R., Thompson, C.B., and Korsmeyer, S.J. (2001). Proapoptotic BAX and BAK: a requisite gateway to mitochondrial dysfunction and death. Science *292*, 727–730. 10.1126/science.1059108.

108. Spangler, R., Bruner, M., Dalie, B., and Harter, M.L. (1987). Activation of adenovirus promoters by the adenovirus E1A protein in cell-free extracts. Science *237*, 1044–1046. 10.1126/science.2956686.

109. Gaynor, R.B., and Berk, A.J. (1983). Cis-acting induction of adenovirus transcription. Cell *33*, 683–693. 10.1016/0092-8674(83)90011-9.

110. Liu, H., Naismith, J.H., and Hay, R.T. (2003). Adenovirus DNA replication. Curr Top Microbiol Immunol *272*, 131–164. 10.1007/978-3-662-05597-7_5.

111. Lichtenstein, D.L., Toth, K., Doronin, K., Tollefson, A.E., and Wold, W.S.M. (2004). Functions and mechanisms of action of the adenovirus E3 proteins. Int Rev Immunol *23*, 75–111. 10.1080/08830180490265556.

112. Weitzman, M.D. (2005). Functions of the adenovirus E4 proteins and their impact on viral vectors. Front Biosci *10*, 1106–1117. 10.2741/1604.

113. Thomas, G.P., and Mathews, M.B. (1980). DNA replication and the early to late transition in adenovirus infection. Cell *22*, 523–533. 10.1016/0092-8674(80)90362-1.

114. Leong, K., Lee, W., and Berk, A.J. (1990). High-level transcription from the adenovirus major late promoter requires downstream binding sites for late-phase-specific factors. J Virol *64*, 51–60. 10.1128/JVI.64.1.51-60.1990.

115. Farley, D.C., Brown, J.L., and Leppard, K.N. (2004). Activation of the early-late switch in adenovirus type 5 major late transcription unit expression by L4 gene products. J Virol *78*, 1782–1791. 10.1128/jvi.78.4.1782-1791.2004.

116. Wodrich, H., Guan, T., Cingolani, G., Von Seggern, D., Nemerow, G., and Gerace, L. (2003). Switch from capsid protein import to adenovirus assembly by cleavage of nuclear transport signals. EMBO J *22*, 6245–6255. 10.1093/emboj/cdg614.

117. Ostapchuk, P., and Hearing, P. (2005). Control of adenovirus packaging. J Cell Biochem *96*, 25–35. 10.1002/jcb.20523.

118. Mangel, W.F., and San Martín, C. (2014). Structure, function and dynamics in adenovirus maturation. Viruses *6*, 4536–4570. 10.3390/v6114536.

119. Braithwaite, A.W., and Russell, I.A. (2001). Induction of cell death by adenoviruses. Apoptosis *6*, 359–370. 10.1023/a:1011338119712.

120. Georgi, F., and Greber, U.F. (2020). The Adenovirus Death Protein - a small membrane protein controls cell lysis and disease. FEBS Lett *594*, 1861–1878. 10.1002/1873-3468.13848.

121. Wigand, R., and Kümel, G. (1977). The kinetics of adenovirus infection and spread in cell cultures infected with low multiplicity. Arch Virol *54*, 177–187. 10.1007/BF01314784.

122. Berkner, K.L. (1988). Development of adenovirus vectors for the expression of heterologous genes. Biotechniques *6*, 616–629.

123. Benihoud, K., Yeh, P., and Perricaudet, M. (1999). Adenovirus vectors for gene delivery. Curr Opin Biotechnol *10*, 440–447. 10.1016/s0958-1669(99)00007-5.

124. Haddada, H., Cordier, L., and Perricaudet, M. (1995). Gene therapy using adenovirus vectors. Curr Top Microbiol Immunol *199 (Pt 3)*, 297–306. 10.1007/978-3-642-79586-2_14.

125. Capasso, C., Garofalo, M., Hirvinen, M., and Cerullo, V. (2014). The evolution of adenoviral vectors through genetic and chemical surface modifications. Viruses *6*, 832–855. 10.3390/v6020832.

126. Graham, F.L., Smiley, J., Russell, W.C., and Nairn, R. (1977). Characteristics of a human cell line transformed by DNA from human adenovirus type 5. J Gen Virol *36*, 59–74. 10.1099/0022-1317-36-1-59.

127. Schiedner, G., Hertel, S., and Kochanek, S. (2000). Efficient transformation of primary human amniocytes by E1 functions of Ad5: generation of new cell lines for adenoviral vector production. Hum Gene Ther *11*, 2105–2116. 10.1089/104303400750001417.

128. Fallaux, F.J., Bout, A., van der Velde, I., van den Wollenberg, D.J., Hehir, K.M., Keegan, J., Auger, C., Cramer, S.J., van Ormondt, H., van der Eb, A.J., et al. (1998). New helper cells and matched early region 1-deleted adenovirus vectors prevent generation of replication-competent adenoviruses. Hum Gene Ther *9*, 1909–1917. 10.1089/hum.1998.9.13-1909.

129. Wold, W.S., Tollefson, A.E., and Hermiston, T.W. (1995). E3 transcription unit of adenovirus. Curr Top Microbiol Immunol *199 (Pt 1)*, 237–274. 10.1007/978-3-642-79496-4_13.

130. Tsien, R.Y. (1998). The green fluorescent protein. Annu Rev Biochem *67*, 509–544. 10.1146/annurev.biochem.67.1.509.

131. England, C.G., Ehlerding, E.B., and Cai, W. (2016). NanoLuc: A Small Luciferase Is Brightening Up the Field of Bioluminescence. Bioconjug Chem *27*, 1175–1187. 10.1021/acs.bioconjchem.6b00112.

132. Gould, S.J., and Subramani, S. (1988). Firefly luciferase as a tool in molecular and cell biology. Anal Biochem *175*, 5–13. 10.1016/0003-2697(88)90353-3.

133. Imperiale, M.J., Kao, H.T., Feldman, L.T., Nevins, J.R., and Strickland, S. (1984). Common control of the heat shock gene and early adenovirus genes: evidence for a cellular E1A-like activity. Mol Cell Biol *4*, 867–874. 10.1128/mcb.4.5.867-874.1984.

134. Tatsis, N., and Ertl, H.C.J. (2004). Adenoviruses as vaccine vectors. Mol Ther *10*, 616–629. 10.1016/j.ymthe.2004.07.013.

135. Gorziglia, M.I., Lapcevich, C., Roy, S., Kang, Q., Kadan, M., Wu, V., Pechan, P., and Kaleko, M. (1999). Generation of an adenovirus vector lacking E1, e2a, E3, and all of E4 except open reading frame 3. J Virol *73*, 6048–6055. 10.1128/JVI.73.7.6048-6055.1999.

136. Gorziglia, M.I., Kadan, M.J., Yei, S., Lim, J., Lee, G.M., Luthra, R., and Trapnell, B.C. (1996). Elimination of both E1 and E2 from adenovirus vectors further improves prospects for in vivo human gene therapy. J Virol *70*, 4173–4178. 10.1128/JVI.70.6.4173-4178.1996.

137. Schaack, J. (2005). Adenovirus vectors deleted for genes essential for viral DNA replication. Front Biosci *10*, 1146–1155. 10.2741/1607.

138. Gao, G.P., Yang, Y., and Wilson, J.M. (1996). Biology of adenovirus vectors with E1 and E4 deletions for liver-directed gene therapy. J Virol *70*, 8934–8943. 10.1128/JVI.70.12.8934-8943.1996.

139. Liu, J., and Seol, D.-W. (2020). Helper virus-free gutless adenovirus (HF-GLAd): a new platform for gene therapy. BMB Rep *53*, 565–575. 10.5483/BMBRep.2020.53.11.185.

140. Alba, R., Bosch, A., and Chillon, M. (2005). Gutless adenovirus: last-generation adenovirus for gene therapy. Gene Ther *12 Suppl 1*, S18-27. 10.1038/sj.gt.3302612.

141. Parks, R.J., Chen, L., Anton, M., Sankar, U., Rudnicki, M.A., and Graham, F.L. (1996). A helper-dependent adenovirus vector system: removal of helper virus by Cre-mediated excision of the viral packaging signal. Proc Natl Acad Sci U S A *93*, 13565–13570. 10.1073/pnas.93.24.13565.

142. Palmer, D., and Ng, P. (2003). Improved system for helper-dependent adenoviral vector production. Mol Ther *8*, 846–852. 10.1016/j.ymthe.2003.08.014.

143. Zhao, Y., Liu, Z., Li, L., Wu, J., Zhang, H., Zhang, H., Lei, T., and Xu, B. (2021). Oncolytic Adenovirus: Prospects for Cancer Immunotherapy. Front Microbiol *12*, 707290. 10.3389/fmicb.2021.707290.

144. Biegert, G.W.G., Rosewell Shaw, A., and Suzuki, M. (2021). Current development in adenoviral vectors for cancer immunotherapy. Mol Ther Oncolytics *23*, 571–581. 10.1016/j.omto.2021.11.014.

145. Kim, E., Kim, J.-H., Shin, H.-Y., Lee, H., Yang, J.M., Kim, J., Sohn, J.-H., Kim, H., and Yun, C.-O. (2003). Ad-mTERT-delta19, a conditional replication-competent adenovirus driven by the human telomerase promoter, selectively replicates in and elicits cytopathic effect in a cancer cell-specific manner. Hum Gene Ther *14*, 1415–1428. 10.1089/104303403769211637.

146. Lee, S.-J., Zhang, Y., Lee, S.D., Jung, C., Li, X., Kim, H.-S., Bae, K.-H., Jeng, M.-H., Kao, C., and Gardner, T. (2004). Targeting prostate cancer with conditionally replicative adenovirus using PSMA enhancer. Mol Ther *10*, 1051–1058. 10.1016/j.ymthe.2004.08.028.

147. Bühler, P., Wolf, P., and Elsässer-Beile, U. (2009). Targeting the prostate-specific membrane antigen for prostate cancer therapy. Immunotherapy *1*, 471–481. 10.2217/imt.09.17.

148. Doronin, K., Kuppuswamy, M., Toth, K., Tollefson, A.E., Krajcsi, P., Krougliak, V., and Wold, W.S. (2001). Tissue-specific, tumor-selective, replication-competent adenovirus vector for cancer gene therapy. J Virol *75*, 3314–3324. 10.1128/JVI.75.7.3314-3324.2001.

149. Whyte, P., Williamson, N.M., and Harlow, E. (1989). Cellular targets for transformation by the adenovirus E1A proteins. Cell *56*, 67–75. 10.1016/0092-8674(89)90984-7.

150. Hanahan, D., and Weinberg, R.A. (2000). The hallmarks of cancer. Cell *100*, 57–70. 10.1016/s0092-8674(00)81683-9.

151. Fueyo, J., Gomez-Manzano, C., Alemany, R., Lee, P.S., McDonnell, T.J., Mitlianga, P., Shi, Y.X., Levin, V.A., Yung, W.K., and Kyritsis, A.P. (2000). A mutant oncolytic adenovirus targeting the Rb pathway produces anti-glioma effect in vivo. Oncogene *19*, 2–12. 10.1038/sj.onc.1203251.

152. Hemann, M.T., and Lowe, S.W. (2006). The p53-Bcl-2 connection. Cell Death Differ *13*, 1256–1259. 10.1038/sj.cdd.4401962.

153. Sauthoff, H., Heitner, S., Rom, W.N., and Hay, J.G. (2000). Deletion of the adenoviral E1b-19kD gene enhances tumor cell killing of a replicating adenoviral vector. Hum Gene Ther *11*, 379–388. 10.1089/10430340050015851.

154. Harrison, D., Sauthoff, H., Heitner, S., Jagirdar, J., Rom, W.N., and Hay, J.G. (2001). Wild-type adenovirus decreases tumor xenograft growth, but despite viral persistence complete tumor responses are rarely achieved--deletion of the viral E1b-19-kD gene increases the viral oncolytic effect. Hum Gene Ther *12*, 1323–1332. 10.1089/104303401750270977.

155. Kim, J., Cho, J.Y., Kim, J.-H., Jung, K.C., and Yun, C.-O. (2002). Evaluation of E1B gene-attenuated replicating adenoviruses for cancer gene therapy. Cancer Gene Ther *9*, 725–736. 10.1038/sj.cgt.7700494.

156. Liu, T.-C., Hallden, G., Wang, Y., Brooks, G., Francis, J., Lemoine, N., and Kirn, D. (2004). An E1B-19 kDa gene deletion mutant adenovirus demonstrates tumor necrosis factor-enhanced cancer selectivity and enhanced oncolytic potency. Mol. Ther. *9*, 786–803. 10.1016/j.ymthe.2004.03.017.

157. Wold, W.S., and Gooding, L.R. (1989). Adenovirus region E3 proteins that prevent cytolysis by cytotoxic T cells and tumor necrosis factor. Mol Biol Med *6*, 433–452.

158. Cox, J.H., Bennink, J.R., and Yewdell, J.W. (1991). Retention of adenovirus E19 glycoprotein in the endoplasmic reticulum is essential to its ability to block antigen presentation. J Exp Med *174*, 1629–1637. 10.1084/jem.174.6.1629.

159. Hermiston, T.W., Tripp, R.A., Sparer, T., Gooding, L.R., and Wold, W.S. (1993). Deletion mutation analysis of the adenovirus type 2 E3-gp19K protein: identification of sequences within the endoplasmic reticulum lumenal domain that are required for class I antigen binding and protection from adenovirus-specific cytotoxic T lymphocytes. J Virol *67*, 5289–5298. 10.1128/JVI.67.9.5289-5298.1993.

160. Natarajan, K., Li, H., Mariuzza, R.A., and Margulies, D.H. (1999). MHC class I molecules, structure and function. Rev Immunogenet *1*, 32–46.

161. Rawle, F.C., Tollefson, A.E., Wold, W.S., and Gooding, L.R. (1989). Mouse anti-adenovirus cytotoxic T lymphocytes. Inhibition of lysis by E3 gp19K but not E3 14.7K. J Immunol *143*, 2031–2037.

162. Cornel, A.M., Mimpen, I.L., and Nierkens, S. (2020). MHC Class I Downregulation in Cancer: Underlying Mechanisms and Potential Targets for Cancer Immunotherapy. Cancers (Basel) *12*, 1760. 10.3390/cancers12071760.

163. Sauthoff, H., Hu, J., Maca, C., Goldman, M., Heitner, S., Yee, H., Pipiya, T., Rom, W.N., and Hay, J.G. (2003). Intratumoral spread of wild-type adenovirus is limited after local injection of human xenograft tumors: virus persists and spreads systemically at late time points. Hum Gene Ther *14*, 425–433. 10.1089/104303403321467199.

164. Wang, W.-C., Sayedahmed, E.E., and Mittal, S.K. (2022). Significance of Preexisting Vector Immunity and Activation of Innate Responses for Adenoviral Vector-Based Therapy. Viruses *14*, 2727. 10.3390/v14122727.

165. Di Paolo, N.C., Miao, E.A., Iwakura, Y., Murali-Krishna, K., Aderem, A., Flavell, R.A., Papayannopoulou, T., and Shayakhmetov, D.M. (2009). Virus binding to a plasma membrane receptor triggers interleukin-1 alpha-mediated proinflammatory macrophage response in vivo. Immunity *31*, 110–121. 10.1016/j.immuni.2009.04.015.

166. Bilzer, M., Roggel, F., and Gerbes, A.L. (2006). Role of Kupffer cells in host defense and liver disease. Liver Int *26*, 1175–1186. 10.1111/j.1478-3231.2006.01342.x.

167. Alemany, R., and Curiel, D.T. (2001). CAR-binding ablation does not change biodistribution and toxicity of adenoviral vectors. Gene Ther *8*, 1347–1353. 10.1038/sj.gt.3301515.

168. Smith, J.S., Xu, Z., Tian, J., Stevenson, S.C., and Byrnes, A.P. (2008). Interaction of systemically delivered adenovirus vectors with Kupffer cells in mouse liver. Hum Gene Ther *19*, 547–554. 10.1089/hum.2008.004.

169. Smith, T., Idamakanti, N., Kylefjord, H., Rollence, M., King, L., Kaloss, M., Kaleko, M., and Stevenson, S.C. (2002). In vivo hepatic adenoviral gene delivery occurs independently of the coxsackievirus-adenovirus receptor. Mol Ther *5*, 770–779. 10.1006/mthe.2002.0613.

170. Haisma, H.J., Boesjes, M., Beerens, A.M., van der Strate, B.W.A., Curiel, D.T., Plüddemann, A., Gordon, S., and Bellu, A.R. (2009). Scavenger receptor A: a new route for adenovirus 5. Mol Pharm *6*, 366–374. 10.1021/mp8000974.

171. Mukhopadhyay, S., and Gordon, S. (2004). The role of scavenger receptors in pathogen recognition and innate immunity. Immunobiology *209*, 39–49. 10.1016/j.imbio.2004.02.004.

172. Xu, Z., Tian, J., Smith, J.S., and Byrnes, A.P. (2008). Clearance of adenovirus by Kupffer cells is mediated by scavenger receptors, natural antibodies, and complement. J Virol *82*, 11705–11713. 10.1128/JVI.01320-08.

173. Shayakhmetov, D.M., Gaggar, A., Ni, S., Li, Z.-Y., and Lieber, A. (2005). Adenovirus binding to blood factors results in liver cell infection and hepatotoxicity. J Virol *79*, 7478–7491. 10.1128/JVI.79.12.7478-7491.2005.

174. Manickan, E., Smith, J.S., Tian, J., Eggerman, T.L., Lozier, J.N., Muller, J., and Byrnes, A.P. (2006). Rapid Kupffer cell death after intravenous injection of adenovirus vectors. Mol Ther *13*, 108–117. 10.1016/j.ymthe.2005.08.007.

175. Lieber, A., He, C.Y., Meuse, L., Schowalter, D., Kirillova, I., Winther, B., and Kay, M.A. (1997). The role of Kupffer cell activation and viral gene expression in early liver toxicity after infusion of recombinant adenovirus vectors. J Virol *71*, 8798–8807. 10.1128/JVI.71.11.8798-8807.1997.

176. Zhang, Y., Chirmule, N., Gao, G.P., Qian, R., Croyle, M., Joshi, B., Tazelaar, J., and Wilson, J.M. (2001). Acute cytokine response to systemic adenoviral vectors in mice is mediated by dendritic cells and macrophages. Mol Ther *3*, 697–707. 10.1006/mthe.2001.0329.

177. Xu, Z., Qiu, Q., Tian, J., Smith, J.S., Conenello, G.M., Morita, T., and Byrnes, A.P. (2013). Coagulation factor X shields adenovirus type 5 from attack by natural antibodies and complement. Nat Med *19*, 452–457. 10.1038/nm.3107.

178. Qiu, Q., Xu, Z., Tian, J., Moitra, R., Gunti, S., Notkins, A.L., and Byrnes, A.P. (2015). Impact of natural IgM concentration on gene therapy with adenovirus type 5 vectors. J Virol *89*, 3412–3416. 10.1128/JVI.03217-14.

179. Carlisle, R.C., Di, Y., Cerny, A.M., Sonnen, A.F.-P., Sim, R.B., Green, N.K., Subr, V., Ulbrich, K., Gilbert, R.J.C., Fisher, K.D., et al. (2009). Human erythrocytes bind and inactivate type 5 adenovirus by presenting Coxsackie virus-adenovirus receptor and complement receptor 1. Blood *113*, 1909–1918. 10.1182/blood-2008-09-178459.

180. Mast, T.C., Kierstead, L., Gupta, S.B., Nikas, A.A., Kallas, E.G., Novitsky, V., Mbewe, B., Pitisuttithum, P., Schechter, M., Vardas, E., et al. (2010). International epidemiology of human pre-existing adenovirus (Ad) type-5, type-6, type-26 and type-36 neutralizing antibodies: correlates of high Ad5 titers and implications for potential HIV vaccine trials. Vaccine *28*, 950–957. 10.1016/j.vaccine.2009.10.145.

181. Fausther-Bovendo, H., and Kobinger, G.P. (2014). Pre-existing immunity against Ad vectors: humoral, cellular, and innate response, what's important? Hum Vaccin Immunother *10*, 2875–2884. 10.4161/hv.29594.

182. Lyons, M., Onion, D., Green, N.K., Aslan, K., Rajaratnam, R., Bazan-Peregrino, M., Phipps, S., Hale, S., Mautner, V., Seymour, L.W., et al. (2006). Adenovirus type 5 interactions with human blood cells may compromise systemic delivery. Mol Ther *14*, 118–128. 10.1016/j.ymthe.2006.01.003.

183. Wang, Z., and Zhang, X. (2021). Adenovirus vector-attributed hepatotoxicity blocks clinical application in gene therapy. Cytotherapy *23*, 1045–1052. 10.1016/j.jcyt.2021.07.013.

184. Martin, K., Brie, A., Saulnier, P., Perricaudet, M., Yeh, P., and Vigne, E. (2003). Simultaneous CAR- and alpha V integrin-binding ablation fails to reduce Ad5 liver tropism. Mol Ther *8*, 485–494. 10.1016/s1525-0016(03)00182-5.

185. Nicol, C.G., Graham, D., Miller, W.H., White, S.J., Smith, T.A.G., Nicklin, S.A., Stevenson, S.C., and Baker, A.H. (2004). Effect of adenovirus serotype 5 fiber and penton modifications on in vivo tropism in rats. Mol Ther *10*, 344–354. 10.1016/j.ymthe.2004.05.020.

186. Bayo-Puxan, N., Cascallo, M., Gros, A., Huch, M., Fillat, C., and Alemany, R. (2006). Role of the putative heparan sulfate glycosaminoglycan-binding site of the adenovirus type 5 fiber shaft on liver detargeting and knob-mediated retargeting. J Gen Virol *87*, 2487–2495. 10.1099/vir.0.81889-0.

187. Smith, T.A.G., Idamakanti, N., Marshall-Neff, J., Rollence, M.L., Wright, P., Kaloss, M., King, L., Mech, C., Dinges, L., Iverson, W.O., et al. (2003). Receptor interactions involved in adenoviral-mediated gene delivery after systemic administration in non-human primates. Hum Gene Ther *14*, 1595–1604. 10.1089/104303403322542248.

188. Bradshaw, A.C., Parker, A.L., Duffy, M.R., Coughlan, L., van Rooijen, N., Kähäri, V.-M., Nicklin, S.A., and Baker, A.H. (2010). Requirements for receptor engagement during infection by adenovirus complexed with blood coagulation factor X. PLoS Pathog *6*, e1001142. 10.1371/journal.ppat.1001142.

189. Duffy, M.R., Bradshaw, A.C., Parker, A.L., McVey, J.H., and Baker, A.H. (2011). A cluster of basic amino acids in the factor X serine protease mediates surface attachment of adenovirus/FX complexes. J Virol *85*, 10914–10919. 10.1128/JVI.05382-11.

190. Descamps, D., and Benihoud, K. (2009). Two key challenges for effective adenovirus-mediated liver gene therapy: innate immune responses and hepatocyte-specific transduction. Curr Gene Ther *9*, 115–127. 10.2174/156652309787909544.

191. Heinz, S., and Braspenning, J. (2015). Measurement of Blood Coagulation Factor Synthesis in Cultures of Human Hepatocytes. Methods Mol Biol *1250*, 309–316. 10.1007/978-1-4939-2074-7_23.

192. Mammen, E.F. (1992). Coagulation abnormalities in liver disease. Hematol Oncol Clin North Am *6*, 1247–1257.

193. Liu, Q., and Muruve, D.A. (2003). Molecular basis of the inflammatory response to adenovirus vectors. Gene Ther *10*, 935–940. 10.1038/sj.gt.3302036.

194. Christ, M., Louis, B., Stoeckel, F., Dieterle, A., Grave, L., Dreyer, D., Kintz, J., Ali Hadji, D., Lusky, M., and Mehtali, M. (2000). Modulation of the inflammatory properties and hepatotoxicity of recombinant adenovirus vectors by the viral E4 gene products. Hum Gene Ther *11*, 415–427. 10.1089/10430340050015888.

195. Engler, H., Machemer, T., Philopena, J., Wen, S.-F., Quijano, E., Ramachandra, M., Tsai, V., and Ralston, R. (2004). Acute hepatotoxicity of oncolytic adenoviruses in mouse models is associated with expression of wild-type E1a and induction of TNF-alpha. Virology *328*, 52–61. 10.1016/j.virol.2004.06.043.

196. Alba, R., Bradshaw, A.C., Coughlan, L., Denby, L., McDonald, R.A., Waddington, S.N., Buckley, S.M.K., Greig, J.A., Parker, A.L., Miller, A.M., et al. (2010). Biodistribution and retargeting of FX-binding ablated adenovirus serotype 5 vectors. Blood *116*, 2656–2664. 10.1182/blood-2009-12-260026.

197. Jain, R.K., and Stylianopoulos, T. (2010). Delivering nanomedicine to solid tumors. Nat Rev Clin Oncol *7*, 653–664. 10.1038/nrclinonc.2010.139.

198. Zheng, M., Huang, J., Tong, A., and Yang, H. (2019). Oncolytic Viruses for Cancer Therapy: Barriers and Recent Advances. Mol Ther Oncolytics *15*, 234–247. 10.1016/j.omto.2019.10.007.

199. Wojton, J., and Kaur, B. (2010). Impact of tumor microenvironment on oncolytic viral therapy. Cytokine Growth Factor Rev *21*, 127–134. 10.1016/j.cytogfr.2010.02.014.

200. Jee, Y.S., Lee, S.G., Lee, J.C., Kim, M.J., Lee, J.J., Kim, D.Y., Park, S.W., Sung, M.-W., and Heo, D.S. (2002). Reduced expression of coxsackievirus and adenovirus receptor (CAR) in tumor tissue compared to normal epithelium in head and neck squamous cell carcinoma patients. Anticancer Res. *22*, 2629–2634.

201. Wunder, T., Schumacher, U., and Friedrich, R.E. (2012). Coxsackie adenovirus receptor expression in carcinomas of the head and neck. Anticancer Res *32*, 1057–1062.

202. Sachs, M.D., Rauen, K.A., Ramamurthy, M., Dodson, J.L., De Marzo, A.M., Putzi, M.J., Schoenberg, M.P., and Rodriguez, R. (2002). Integrin alpha(v) and coxsackie adenovirus receptor expression in clinical bladder cancer. Urology *60*, 531–536. 10.1016/s0090-4295(02)01748-x.

203. Ma, Y.-Y., Wang, X.-J., Han, Y., Li, G., Wang, H.-J., Wang, S.-B., Chen, X.-Y., Liu, F.-L., He, X.-L., Tong, X.-M., et al. (2016). Loss of coxsackie and adenovirus receptor expression in human colorectal cancer: A potential impact on the efficacy of adenovirus-mediated gene therapy in Chinese Han population. Mol Med Rep *14*, 2541–2547. 10.3892/mmr.2016.5536.

204. Boucher, Y., Baxter, L.T., and Jain, R.K. (1990). Interstitial pressure gradients in tissue-isolated and subcutaneous tumors: implications for therapy. Cancer Res *50*, 4478–4484.

205. Jain, R.K. (1987). Transport of molecules in the tumor interstitium: a review. Cancer Res *47*, 3039–3051.

206. Roelvink, P.W., Mi Lee, G., Einfeld, D.A., Kovesdi, I., and Wickham, T.J. (1999). Identification of a conserved receptor-binding site on the fiber proteins of CAR-recognizing adenoviridae. Science *286*, 1568–1571. 10.1126/science.286.5444.1568.

207. Schiedner, G., Hertel, S., Johnston, M., Dries, V., van Rooijen, N., and Kochanek, S. (2003). Selective depletion or blockade of Kupffer cells leads to enhanced and prolonged hepatic transgene expression using high-capacity adenoviral vectors. Mol Ther *7*, 35–43. 10.1016/s1525-0016(02)00017-5.

208. Wolff, G., Worgall, S., van Rooijen, N., Song, W.R., Harvey, B.G., and Crystal, R.G. (1997). Enhancement of in vivo adenovirus-mediated gene transfer and expression by prior depletion of tissue macrophages in the target organ. J Virol *71*, 624–629. 10.1128/JVI.71.1.624-629.1997.

209. Kuzmin, A.I., Finegold, M.J., and Eisensmith, R.C. (1997). Macrophage depletion increases the safety, efficacy and persistence of adenovirus-mediated gene transfer in vivo. Gene Ther *4*, 309–316. 10.1038/sj.gt.3300377.

210. Stein, C.S., Pemberton, J.L., van Rooijen, N., and Davidson, B.L. (1998). Effects of macrophage depletion and anti-CD40 ligand on transgene expression and redosing with recombinant adenovirus. Gene Ther *5*, 431–439. 10.1038/sj.gt.3300616.

211. Haisma, H.J., Kamps, J.A.A.M., Kamps, G.K., Plantinga, J.A., Rots, M.G., and Bellu, A.R. (2008). Polyinosinic acid enhances delivery of adenovirus vectors in vivo by preventing sequestration in liver macrophages. J Gen Virol *89*, 1097–1105. 10.1099/vir.0.83495-0.

212. Tao, N., Gao, G.P., Parr, M., Johnston, J., Baradet, T., Wilson, J.M., Barsoum, J., and Fawell, S.E. (2001). Sequestration of adenoviral vector by Kupffer cells leads to a nonlinear dose response of transduction in liver. Mol Ther *3*, 28–35. 10.1006/mthe.2000.0227.

213. Weaver, E.A., Hillestad, M.L., Khare, R., Palmer, D., Ng, P., and Barry, M.A. (2011). Characterization of species C human adenovirus serotype 6 (Ad6). Virology *412*, 19–27. 10.1016/j.virol.2010.10.041.

214. Khare, R., May, S.M., Vetrini, F., Weaver, E.A., Palmer, D., Rosewell, A., Grove, N., Ng, P., and Barry, M.A. (2011). Generation of a Kupffer cell-evading adenovirus for systemic and liver-directed gene transfer. Mol Ther *19*, 1254–1262. 10.1038/mt.2011.71.

215. O'Riordan, C.R., Lachapelle, A., Delgado, C., Parkes, V., Wadsworth, S.C., Smith, A.E., and Francis, G.E. (1999). PEGylation of adenovirus with retention of infectivity and protection from neutralizing antibody in vitro and in vivo. Hum Gene Ther *10*, 1349–1358. 10.1089/10430349950018021.

216. Vetter, A., Virdi, K.S., Espenlaub, S., Rödl, W., Wagner, E., Holm, P.S., Scheu, C., Kreppel, F., Spitzweg, C., and Ogris, M. (2013). Adenoviral vectors coated with PAMAM dendrimer conjugates allow CAR independent virus uptake and targeting to the EGF receptor. Mol Pharm *10*, 606–618. 10.1021/mp300366f.

217. Wortmann, A., Vöhringer, S., Engler, T., Corjon, S., Schirmbeck, R., Reimann, J., Kochanek, S., and Kreppel, F. (2008). Fully detargeted polyethylene glycol-coated adenovirus vectors are potent genetic vaccines and escape from pre-existing anti-adenovirus antibodies. Mol Ther *16*, 154–162. 10.1038/sj.mt.6300306.

218. Subr, V., Kostka, L., Selby-Milic, T., Fisher, K., Ulbrich, K., Seymour, L.W., and Carlisle, R.C. (2009). Coating of adenovirus type 5 with polymers containing quaternary amines prevents binding to blood components. J Control Release *135*, 152–158. 10.1016/j.jconrel.2008.12.009.

219. Danielsson, A., Elgue, G., Nilsson, B.M., Nilsson, B., Lambris, J.D., Tötterman, T.H., Kochanek, S., Kreppel, F., and Essand, M. (2010). An ex vivo loop system models the toxicity and efficacy of PEGylated and unmodified adenovirus serotype 5 in whole human blood. Gene Ther *17*, 752–762. 10.1038/gt.2010.18.

220. Tian, J., Xu, Z., Smith, J.S., Hofherr, S.E., Barry, M.A., and Byrnes, A.P. (2009). Adenovirus activates complement by distinctly different mechanisms in vitro and in vivo: indirect complement activation by virions in vivo. J Virol *83*, 5648–5658. 10.1128/JVI.00082-09.

221. Green, N.K., Herbert, C.W., Hale, S.J., Hale, A.B., Mautner, V., Harkins, R., Hermiston, T., Ulbrich, K., Fisher, K.D., and Seymour, L.W. (2004). Extended plasma circulation time and decreased toxicity of polymer-coated adenovirus. Gene Ther *11*, 1256–1263. 10.1038/sj.gt.3302295.

222. Croyle, M.A., Le, H.T., Linse, K.D., Cerullo, V., Toietta, G., Beaudet, A., and Pastore, L. (2005). PEGylated helper-dependent adenoviral vectors: highly efficient vectors with an enhanced safety profile. Gene Ther *12*, 579–587. 10.1038/sj.gt.3302441.

223. Mok, H., Palmer, D.J., Ng, P., and Barry, M.A. (2005). Evaluation of polyethylene glycol modification of first-generation and helper-dependent adenoviral vectors to reduce innate immune responses. Mol Ther *11*, 66–79. 10.1016/j.ymthe.2004.09.015.

224. Kreppel, F., Gackowski, J., Schmidt, E., and Kochanek, S. (2005). Combined genetic and chemical capsid modifications enable flexible and efficient de- and retargeting of adenovirus vectors. Mol. Ther. *12*, 107–117. 10.1016/j.ymthe.2005.03.006.

225. Prill, J.-M., Espenlaub, S., Samen, U., Engler, T., Schmidt, E., Vetrini, F., Rosewell, A., Grove, N., Palmer, D., Ng, P., et al. (2011). Modifications of adenovirus hexon allow for either hepatocyte detargeting or targeting with potential evasion from Kupffer cells. Mol Ther *19*, 83–92. 10.1038/mt.2010.229.

226. Corjon, S., Wortmann, A., Engler, T., van Rooijen, N., Kochanek, S., and Kreppel, F. (2008). Targeting of adenovirus vectors to the LRP receptor family with the high-affinity ligand RAP via combined genetic and chemical modification of the pIX capsomere. Mol Ther *16*, 1813–1824. 10.1038/mt.2008.174.

227. Krutzke, L., Prill, J.M., Engler, T., Schmidt, C.Q., Xu, Z., Byrnes, A.P., Simmet, T., and Kreppel, F. (2016). Substitution of blood coagulation factor X-binding to Ad5 by position-specific PEGylation: Preventing vector clearance and preserving infectivity. J Control Release *235*, 379–392. 10.1016/j.jconrel.2016.06.022.

228. Wienen, F., Nilson, R., Allmendinger, E., Graumann, D., Fiedler, E., Bosse-Doenecke, E., Kochanek, S., and Krutzke, L. (2022). Affilin-based retargeting of adenoviral vectors to the epidermal growth factor receptor. Biomater Adv *144*, 213208. 10.1016/j.bioadv.2022.213208.

229. Niemann, J., and Kühnel, F. (2020). Tumor Targeting of Oncolytic Adenoviruses Using Bispecific Adapter Proteins. Methods Mol Biol *2058*, 31–49. 10.1007/978-1-4939-9794-7_3.

230. Reetz, J., Herchenröder, O., and Pützer, B.M. (2014). Peptide-based technologies to alter adenoviral vector tropism: ways and means for systemic treatment of cancer. Viruses *6*, 1540–1563. 10.3390/v6041540.

231. Sharma, A., Li, X., Bangari, D.S., and Mittal, S.K. (2009). Adenovirus receptors and their implications in gene delivery. Virus Res *143*, 184–194. 10.1016/j.virusres.2009.02.010.

232. Murakami, M., Ugai, H., Belousova, N., Pereboev, A., Dent, P., Fisher, P.B., Everts, M., and Curiel, D.T. (2010). Chimeric adenoviral vectors incorporating a fiber of human adenovirus 3 efficiently mediate gene transfer into prostate cancer cells. Prostate *70*, 362–376. 10.1002/pros.21070.

233. Zheng, S., Ulasov, I.V., Han, Y., Tyler, M.A., Zhu, Z.B., and Lesniak, M.S. (2007). Fiber-knob modifications enhance adenoviral tropism and gene transfer in malignant glioma. J Gene Med *9*, 151–160. 10.1002/jgm.1008.

234. Reddy, P.S., Ganesh, S., and Yu, D.-C. (2006). Enhanced Gene Transfer and Oncolysis of Head and Neck Cancer and Melanoma Cells by Fiber Chimeric Oncolytic Adenoviruses. Clin Cancer Res *12*, 2869–2878. 10.1158/1078-0432.CCR-05-2397.

235. Kawakami, Y., Li, H., Lam, J.T., Krasnykh, V., Curiel, D.T., and Blackwell, J.L. (2003). Substitution of the adenovirus serotype 5 knob with a serotype 3 knob enhances multiple steps in virus replication. Cancer Res *63*, 1262–1269.

236. Gall, J., Kass-Eisler, A., Leinwand, L., and Falck-Pedersen, E. (1996). Adenovirus type 5 and 7 capsid chimera: fiber replacement alters receptor tropism without affecting primary immune neutralization epitopes. J Virol *70*, 2116–2123. 10.1128/JVI.70.4.2116-2123.1996.

237. Yu, L., Takenobu, H., Shimozato, O., Kawamura, K., Nimura, Y., Seki, N., Uzawa, K., Tanzawa, H., Shimada, H., Ochiai, T., et al. (2005). Increased infectivity of adenovirus type 5 bearing type 11 or type 35 fibers to human esophageal and oral carcinoma cells. Oncol. Rep. *14*, 831–835.

238. Wu, H., Han, T., Belousova, N., Krasnykh, V., Kashentseva, E., Dmitriev, I., Kataram, M., Mahasreshti, P.J., and Curiel, D.T. (2005). Identification of sites in adenovirus hexon for foreign peptide incorporation. J Virol *79*, 3382–3390. 10.1128/JVI.79.6.3382-3390.2005.

239. Stepanenko, A.A., and Chekhonin, V.P. (2018). Tropism and transduction of oncolytic adenovirus 5 vectors in cancer therapy: Focus on fiber chimerism and mosaicism, hexon and pIX. Virus Res. *257*, 40–51. 10.1016/j.virusres.2018.08.012.

240. Campos, S.K., and Barry, M.A. (2006). Comparison of adenovirus fiber, protein IX, and hexon capsomeres as scaffolds for vector purification and cell targeting. Virology *349*, 453–462. 10.1016/j.virol.2006.01.032.

241. Vigne, E., Mahfouz, I., Dedieu, J.F., Brie, A., Perricaudet, M., and Yeh, P. (1999). RGD inclusion in the hexon monomer provides adenovirus type 5-based vectors with a fiber knob-independent pathway for infection. J Virol *73*, 5156–5161. 10.1128/JVI.73.6.5156-5161.1999.

242. Wu, H., Seki, T., Dmitriev, I., Uil, T., Kashentseva, E., Han, T., and Curiel, D.T. (2002). Double modification of adenovirus fiber with RGD and polylysine motifs improves coxsackievirus-adenovirus receptor-independent gene transfer efficiency. Hum Gene Ther *13*, 1647–1653. 10.1089/10430340260201734.

243. Majhen, D., Richardson, J., Vukelić, B., Dodig, I., Cindrić, M., Benihoud, K., and Ambriović-Ristov, A. (2012). The disulfide bond of an RGD4C motif inserted within the Hi loop of the adenovirus type 5 fiber protein is critical for retargeting to αv -integrins. J Gene Med *14*, 788–797. 10.1002/jgm.2686.

244. Davydova, J., Le, L.P., Gavrikova, T., Wang, M., Krasnykh, V., and Yamamoto, M. (2004). Infectivity-enhanced cyclooxygenase-2-based conditionally replicative adenoviruses for esophageal adenocarcinoma treatment. Cancer Res. *64*, 4319–4327. 10.1158/0008-5472.CAN-04-0064.

245. Wickham, T.J., Tzeng, E., Shears, L.L., Roelvink, P.W., Li, Y., Lee, G.M., Brough, D.E., Lizonova, A., and Kovesdi, I. (1997). Increased in vitro and in vivo gene transfer by adenovirus vectors containing chimeric fiber proteins. J Virol *71*, 8221–8229. 10.1128/JVI.71.11.8221-8229.1997.

246. Uusi-Kerttula, H., Legut, M., Davies, J., Jones, R., Hudson, E., Hanna, L., Stanton, R.J., Chester, J.D., and Parker, A.L. (2015). Incorporation of Peptides Targeting EGFR and FGFR1 into the Adenoviral Fiber Knob Domain and Their Evaluation as Targeted Cancer Therapies. Hum. Gene Ther. *26*, 320–329. 10.1089/hum.2015.015.

247. MacLeod, S.H., Elgadi, M.M., Bossi, G., Sankar, U., Pisio, A., Agopsowicz, K., Sharon, D., Graham, F.L., and Hitt, M.M. (2012). HER3 targeting of adenovirus by fiber modification increases infection of breast cancer cells in vitro, but not following intratumoral injection in mice. Cancer Gene Ther *19*, 888–898. 10.1038/cgt.2012.79.

248. Xia, H., Anderson, B., Mao, Q., and Davidson, B.L. (2000). Recombinant human adenovirus: targeting to the human transferrin receptor improves gene transfer to brain microcapillary endothelium. J Virol *74*, 11359–11366. 10.1128/jvi.74.23.11359-11366.2000.

249. Dmitriev, I.P., Kashentseva, E.A., and Curiel, D.T. (2002). Engineering of adenovirus vectors containing heterologous peptide sequences in the C terminus of capsid protein IX. J Virol *76*, 6893–6899. 10.1128/jvi.76.14.6893-6899.2002.

250. Magnusson, M.K., Hong, S.S., Henning, P., Boulanger, P., and Lindholm, L. (2002). Genetic retargeting of adenovirus vectors: functionality of targeting ligands and their influence on virus viability. J Gene Med *4*, 356–370. 10.1002/jgm.285.

251. Nettelbeck, D.M. (2011). Bispecific Antibodies and Gene Therapy. Bispecific Antibodies, 327–347. 10.1007/978-3-642-20910-9_18.

252. Douglas, J.T., Rogers, B.E., Rosenfeld, M.E., Michael, S.I., Feng, M., and Curiel, D.T. (1996). Targeted gene delivery by tropism-modified adenoviral vectors. Nat Biotechnol *14*, 1574–1578. 10.1038/nbt1196-1574.

253. Watkins, S.J., Mesyanzhinov, V.V., Kurochkina, L.P., and Hawkins, R.E. (1997). The “adenobody” approach to viral targeting: specific and enhanced adenoviral gene delivery. Gene Ther. *4*, 1004–1012. 10.1038/sj.gt.3300511.

254. Haisma, H.J., Grill, J., Curiel, D.T., Hoogeland, S., van Beusechem, V.W., Pinedo, H.M., and Gerritsen, W.R. (2000). Targeting of adenoviral vectors through a bispecific single-chain antibody. Cancer Gene Ther. *7*, 901–904. 10.1038/sj.cgt.7700198.

255. Carette, J.E., Graat, H.C.A., Schagen, F.H.E., Mastenbroek, D.C.J., Rots, M.G., Haisma, H.J., Groothuis, G.M.M., Schaap, G.R., Bras, J., Kaspers, G.J.L., et al. (2007). A conditionally replicating adenovirus with strict selectivity in killing cells expressing epidermal growth factor receptor. Virology *361*, 56–67. 10.1016/j.virol.2006.11.011.

256. van Beusechem, V.W., Mastenbroek, D.C.J., van den Doel, P.B., Lamfers, M.L.M., Grill, J., Würdinger, T., Haisma, H.J., Pinedo, H.M., and Gerritsen, W.R. (2003). Conditionally replicative adenovirus expressing a targeting adapter molecule exhibits enhanced oncolytic potency on CAR-deficient tumors. Gene Ther. *10*, 1982–1991. 10.1038/sj.gt.3302103.

257. van Beusechem, V.W., Grill, J., Mastenbroek, D.C.J., Wickham, T.J., Roelvink, P.W., Haisma, H.J., Lamfers, M.L.M., Dirven, C.M.F., Pinedo, H.M., and Gerritsen, W.R. (2002). Efficient and selective gene transfer into primary human brain tumors by using single-chain antibody-targeted adenoviral vectors with native tropism abolished. J. Virol. *76*, 2753–2762. 10.1128/jvi.76.6.2753-2762.2002.

258. Nettelbeck, D.M., Miller, D.W., Jérôme, V., Zuzarte, M., Watkins, S.J., Hawkins, R.E., Müller, R., and Kontermann, R.E. (2001). Targeting of adenovirus to endothelial cells by a bispecific single-chain diabody directed against the adenovirus fiber knob domain and human endoglin (CD105). Mol. Ther. *3*, 882–891. 10.1006/mthe.2001.0342.

259. Wickham, T.J., Segal, D.M., Roelvink, P.W., Carrion, M.E., Lizonova, A., Lee, G.M., and Kovesdi, I. (1996). Targeted adenovirus gene transfer to endothelial and smooth muscle cells by using bispecific antibodies. J Virol *70*, 6831–6838. 10.1128/JVI.70.10.6831-6838.1996.

260. Tillman, B.W., de Gruijl, T.D., Luykx-de Bakker, S.A., Scheper, R.J., Pinedo, H.M., Curiel, T.J., Gerritsen, W.R., and Curiel, D.T. (1999). Maturation of dendritic cells accompanies high-efficiency gene transfer by a CD40-targeted adenoviral vector. J Immunol *162*, 6378–6383.

261. Goldman, C.K., Rogers, B.E., Douglas, J.T., Sosnowski, B.A., Ying, W., Siegal, G.P., Baird, A., Campain, J.A., and Curiel, D.T. (1997). Targeted gene delivery to Kaposi's sarcoma cells via the fibroblast growth factor receptor. Cancer Res *57*, 1447–1451.

262. Haisma, H.J., Pinedo, H.M., Rijswijk, A., der Meulen-Muileman, I., Sosnowski, B.A., Ying, W., Beusechem, V.W., Tillman, B.W., Gerritsen, W.R., and Curiel, D.T. (1999). Tumor-specific gene transfer via an adenoviral vector targeted to the pan-carcinoma antigen EpCAM. Gene Ther *6*, 1469–1474. 10.1038/sj.gt.3300969.

263. Johnson, D.E., Burtness, B., Leemans, C.R., Lui, V.W.Y., Bauman, J.E., and Grandis, J.R. (2020). Head and neck squamous cell carcinoma. Nat Rev Dis Primers *6*, 92. 10.1038/s41572-020-00224-3.

264. Gormley, M., Creaney, G., Schache, A., Ingarfield, K., and Conway, D.I. (2022). Reviewing the epidemiology of head and neck cancer: definitions, trends and risk factors. Br Dent J *233*, 780–786. 10.1038/s41415-022-5166-x.

265. Jethwa, A.R., and Khariwala, S.S. (2017). Tobacco-related carcinogenesis in head and neck cancer. Cancer Metastasis Rev *36*, 411–423. 10.1007/s10555-017-9689-6.

266. Kawakita, D., and Matsuo, K. (2017). Alcohol and head and neck cancer. Cancer Metastasis Rev *36*, 425–434. 10.1007/s10555-017-9690-0.

267. Hennessey, P.T., Westra, W.H., and Califano, J.A. (2009). Human papillomavirus and head and neck squamous cell carcinoma: recent evidence and clinical implications. J Dent Res *88*, 300–306. 10.1177/0022034509333371.

268. Alsahafi, E., Begg, K., Amelio, I., Raulf, N., Lucarelli, P., Sauter, T., and Tavassoli, M. (2019). Clinical update on head and neck cancer: molecular biology and ongoing challenges. Cell Death Dis *10*, 540. 10.1038/s41419-019-1769-9.

269. Kalyankrishna, S., and Grandis, J.R. (2006). Epidermal growth factor receptor biology in head and neck cancer. J. Clin. Oncol. *24*, 2666–2672. 10.1200/JCO.2005.04.8306.

270. Wee, P., and Wang, Z. (2017). Epidermal Growth Factor Receptor Cell Proliferation Signaling Pathways. Cancers (Basel) *9*, 52. 10.3390/cancers9050052.

271. Singh, B., Carpenter, G., and Coffey, R.J. (2016). EGF receptor ligands: recent advances. F1000Res *5*, F1000 Faculty Rev-2270. 10.12688/f1000research.9025.1.

272. Ferguson, K.M., Berger, M.B., Mendrola, J.M., Cho, H.S., Leahy, D.J., and Lemmon, M.A. (2003). EGF activates its receptor by removing interactions that autoinhibit ectodomain dimerization. Mol Cell *11*, 507–517. 10.1016/s1097-2765(03)00047-9.

273. Yarden, Y., and Schlessinger, J. (1987). Epidermal growth factor induces rapid, reversible aggregation of the purified epidermal growth factor receptor. Biochemistry *26*, 1443–1451. 10.1021/bi00379a035.

274. Dawson, J.P., Berger, M.B., Lin, C.-C., Schlessinger, J., Lemmon, M.A., and Ferguson, K.M. (2005). Epidermal growth factor receptor dimerization and activation require ligand-induced conformational changes in the dimer interface. Mol. Cell. Biol. *25*, 7734–7742. 10.1128/MCB.25.17.7734-7742.2005.

275. Zhang, X., Gureasko, J., Shen, K., Cole, P.A., and Kuriyan, J. (2006). An allosteric mechanism for activation of the kinase domain of epidermal growth factor receptor. Cell *125*, 1137–1149. 10.1016/j.cell.2006.05.013.

276. Downward, J., Parker, P., and Waterfield, M.D. (1984). Autophosphorylation sites on the epidermal growth factor receptor. Nature *311*, 483–485. 10.1038/311483a0.

277. Guo, G., Gong, K., Wohlfeld, B., Hatanpaa, K.J., Zhao, D., and Habib, A.A. (2015). Ligand-Independent EGFR Signaling. Cancer Res *75*, 3436–3441. 10.1158/0008-5472.CAN-15-0989.

278. Pines, G., Köstler, W.J., and Yarden, Y. (2010). Oncogenic mutant forms of EGFR: lessons in signal transduction and targets for cancer therapy. FEBS Lett *584*, 2699–2706. 10.1016/j.febslet.2010.04.019.

279. Nicholson, R.I., Gee, J.M., and Harper, M.E. (2001). EGFR and cancer prognosis. Eur J Cancer *37 Suppl 4*, S9-15. 10.1016/s0959-8049(01)00231-3.

280. Rowinsky, E.K. (2004). The erbB family: targets for therapeutic development against cancer and therapeutic strategies using monoclonal antibodies and tyrosine kinase inhibitors. Annu Rev Med *55*, 433–457. 10.1146/annurev.med.55.091902.104433.

281. Cai, W.-Q., Zeng, L.-S., Wang, L.-F., Wang, Y.-Y., Cheng, J.-T., Zhang, Y., Han, Z.-W., Zhou, Y., Huang, S.-L., Wang, X.-W., et al. (2020). The Latest Battles Between EGFR Monoclonal Antibodies and Resistant Tumor Cells. Front Oncol *10*, 1249. 10.3389/fonc.2020.01249.

282. Santos, E. da S., Nogueira, K.A.B., Fernandes, L.C.C., Martins, J.R.P., Reis, A.V.F., Neto, J. de B.V., Júnior, I.J. da S., Pessoa, C., Petrilli, R., and Eloy, J.O. (2021). EGFR targeting for cancer therapy: Pharmacology and immunoconjugates with drugs and nanoparticles. Int J Pharm *592*, 120082. 10.1016/j.ijpharm.2020.120082.

283. Dhillon, S. (2015). Gefitinib: a review of its use in adults with advanced non-small cell lung cancer. Target Oncol *10*, 153–170. 10.1007/s11523-015-0358-9.

284. Lindner, T., Loktev, A., Giesel, F., Kratochwil, C., Altmann, A., and Haberkorn, U. (2019). Targeting of activated fibroblasts for imaging and therapy. EJNMMI Radiopharm Chem *4*, 16. 10.1186/s41181-019-0069-0.

285. Liao, Z., Tan, Z.W., Zhu, P., and Tan, N.S. (2019). Cancer-associated fibroblasts in tumor microenvironment - Accomplices in tumor malignancy. Cell Immunol *343*, 103729. 10.1016/j.cellimm.2017.12.003.

286. Kalluri, R., and Zeisberg, M. (2006). Fibroblasts in cancer. Nat. Rev. Cancer *6*, 392–401. 10.1038/nrc1877.

287. Shiga, K., Hara, M., Nagasaki, T., Sato, T., Takahashi, H., and Takeyama, H. (2015). Cancer-Associated Fibroblasts: Their Characteristics and Their Roles in Tumor Growth. Cancers (Basel) *7*, 2443–2458. 10.3390/cancers7040902.

288. Xin, L., Gao, J., Zheng, Z., Chen, Y., Lv, S., Zhao, Z., Yu, C., Yang, X., and Zhang, R. (2021). Fibroblast Activation Protein-α as a Target in the Bench-to-Bedside Diagnosis and Treatment of Tumors: A Narrative Review. Front Oncol *11*, 648187. 10.3389/fonc.2021.648187.

289. Fitzgerald, A.A., and Weiner, L.M. (2020). The role of fibroblast activation protein in health and malignancy. Cancer Metastasis Rev *39*, 783–803. 10.1007/s10555-020-09909-3.

290. Park, J.E., Lenter, M.C., Zimmermann, R.N., Garin-Chesa, P., Old, L.J., and Rettig, W.J. (1999). Fibroblast activation protein, a dual specificity serine protease expressed in reactive human tumor stromal fibroblasts. J. Biol. Chem. *274*, 36505–36512. 10.1074/jbc.274.51.36505.

291. Waumans, Y., Baerts, L., Kehoe, K., Lambeir, A.-M., and De Meester, I. (2015). The Dipeptidyl Peptidase Family, Prolyl Oligopeptidase, and Prolyl Carboxypeptidase in the Immune System and Inflammatory Disease, Including Atherosclerosis. Front Immunol *6*, 387. 10.3389/fimmu.2015.00387.

292. Piñeiro-Sánchez, M.L., Goldstein, L.A., Dodt, J., Howard, L., Yeh, Y., Tran, H., Argraves, W.S., and Chen, W.T. (1997). Identification of the 170-kDa melanoma membrane-bound gelatinase (seprase) as a serine integral membrane protease. J Biol Chem *272*, 7595–7601. 10.1074/jbc.272.12.7595.

293. Scanlan, M.J., Raj, B.K., Calvo, B., Garin-Chesa, P., Sanz-Moncasi, M.P., Healey, J.H., Old, L.J., and Rettig, W.J. (1994). Molecular cloning of fibroblast activation protein alpha, a member of the serine protease family selectively expressed in stromal fibroblasts of epithelial cancers. Proc. Natl. Acad. Sci. U.S.A. *91*, 5657–5661. 10.1073/pnas.91.12.5657.

294. Rettig, W.J., Garin-Chesa, P., Healey, J.H., Su, S.L., Ozer, H.L., Schwab, M., Albino, A.P., and Old, L.J. (1993). Regulation and heteromeric structure of the fibroblast activation protein in normal and transformed cells of mesenchymal and neuroectodermal origin. Cancer Res. *53*, 3327–3335.

295. Sun, S., Albright, C.F., Fish, B.H., George, H.J., Selling, B.H., Hollis, G.F., and Wynn, R. (2002). Expression, purification, and kinetic characterization of full-length human fibroblast activation protein. Protein Expr Purif *24*, 274–281. 10.1006/prep.2001.1572.

296. Jacob, M., Chang, L., and Puré, E. (2012). Fibroblast activation protein in remodeling tissues. Curr Mol Med *12*, 1220–1243. 10.2174/156652412803833607.

297. Niedermeyer, J., Garin-Chesa, P., Kriz, M., Hilberg, F., Mueller, E., Bamberger, U., Rettig, W.J., and Schnapp, A. (2001). Expression of the fibroblast activation protein during mouse embryo development. Int J Dev Biol *45*, 445–447.

298. Bosma, G.C., Custer, R.P., and Bosma, M.J. (1983). A severe combined immunodeficiency mutation in the mouse. Nature *301*, 527–530. 10.1038/301527a0.

299. Fulop, G.M., and Phillips, R.A. (1990). The scid mutation in mice causes a general defect in DNA repair. Nature *347*, 479–482. 10.1038/347479a0.

300. Blunt, T., Finnie, N.J., Taccioli, G.E., Smith, G.C., Demengeot, J., Gottlieb, T.M., Mizuta, R., Varghese, A.J., Alt, F.W., Jeggo, P.A., et al. (1995). Defective DNA-dependent protein kinase activity is linked to V(D)J recombination and DNA repair defects associated with the murine scid mutation. Cell *80*, 813–823. 10.1016/0092-8674(95)90360-7.

301. Cao, X., Shores, E.W., Hu-Li, J., Anver, M.R., Kelsall, B.L., Russell, S.M., Drago, J., Noguchi, M., Grinberg, A., and Bloom, E.T. (1995). Defective lymphoid development in mice lacking expression of the common cytokine receptor gamma chain. Immunity *2*, 223–238. 10.1016/1074-7613(95)90047-0.

302. Pilder, S., Logan, J., and Shenk, T. (1984). Deletion of the gene encoding the adenovirus 5 early region 1b 21,000-molecular-weight polypeptide leads to degradation of viral and host cell DNA. J. Virol. *52*, 664–671.

303. Kirby, I., Davison, E., Beavil, A.J., Soh, C.P., Wickham, T.J., Roelvink, P.W., Kovesdi, I., Sutton, B.J., and Santis, G. (2000). Identification of contact residues and definition of the CAR-binding site of adenovirus type 5 fiber protein. J. Virol. *74*, 2804–2813.

304. Ostermann, E., Garin-Chesa, P., Heider, K.H., Kalat, M., Lamche, H., Puri, C., Kerjaschki, D., Rettig, W.J., and Adolf, G.R. (2008). Effective immunoconjugate therapy in cancer models targeting a serine protease of tumor fibroblasts. Clin. Cancer Res. *14*, 4584–4592. 10.1158/1078-0432.CCR-07-5211.

305. Haryadi, R., Ho, S., Kok, Y.J., Pu, H.X., Zheng, L., Pereira, N.A., Li, B., Bi, X., Goh, L.-T., Yang, Y., et al. (2015). Optimization of heavy chain and light chain signal peptides for high level expression of therapeutic antibodies in CHO cells. PLoS One *10*, e0116878. 10.1371/journal.pone.0116878.

306. BOSSE-DOENECKE, E., SETTELE, F., Fiedler, E., and Haupts, U. (2017). Novel egfr binding proteins.

307. Barrick, C.J., Roberts, R.B., Rojas, M., Rajamannan, N.M., Suitt, C.B., O'Brien, K.D., Smyth, S.S., and Threadgill, D.W. (2009). Reduced EGFR causes abnormal valvular differentiation leading to calcific aortic stenosis and left ventricular hypertrophy in C57BL/6J but not 129S1/SvImJ mice. Am J Physiol Heart Circ Physiol *297*, H65-75. 10.1152/ajpheart.00866.2008.

308. Barrick, C.J., Yu, M., Chao, H.-H., and Threadgill, D.W. (2008). Chronic pharmacologic inhibition of EGFR leads to cardiac dysfunction in C57BL/6J mice. Toxicol Appl Pharmacol *228*, 315–325. 10.1016/j.taap.2007.12.012.

309. Iwamoto, R., Yamazaki, S., Asakura, M., Takashima, S., Hasuwa, H., Miyado, K., Adachi, S., Kitakaze, M., Hashimoto, K., Raab, G., et al. (2003). Heparin-binding EGF-like growth factor and ErbB signaling is essential for heart function. Proc Natl Acad Sci U S A *100*, 3221–3226. 10.1073/pnas.0537588100.

310. Chen, B., Bronson, R.T., Klaman, L.D., Hampton, T.G., Wang, J.F., Green, P.J., Magnuson, T., Douglas, P.S., Morgan, J.P., and Neel, B.G. (2000). Mice mutant for Egfr and Shp2 have defective cardiac semilunar valvulogenesis. Nat Genet *24*, 296–299. 10.1038/73528.

311. Nilson, R., Lübbers, O., Schmidt, C.Q., Rojewski, M., Zeplin, P.H., Funk, W., Schrezenmeier, H., Kritzinger, A., Kochanek, S., and Krutzke, L. (2022). Hexon modification of human adenovirus type 5 vectors enables efficient transduction of human multipotent mesenchymal stromal cells. Mol Ther Methods Clin Dev *25*, 96–110. 10.1016/j.omtm.2022.03.004.

312. Fueyo, J., Gomez-Manzano, C., Alemany, R., Lee, P.S., McDonnell, T.J., Mitlianga, P., Shi, Y.X., Levin, V.A., Yung, W.K., and Kyritsis, A.P. (2000). A mutant oncolytic adenovirus targeting the Rb pathway produces anti-glioma effect in vivo. Oncogene *19*, 2–12. 10.1038/sj.onc.1203251.

313. Chinnadurai, G. (1998). Control of Apoptosis by Human Adenovirus Genes. Seminars in Virology *8*, 399–408. 10.1006/smvy.1997.0139.

314. Toth, K., and Wold, W.S.M. (2010). Increasing the efficacy of oncolytic adenovirus vectors. Viruses *2*, 1844–1866. 10.3390/v2091844.

315. Niemann, J., and Kühnel, F. (2017). Oncolytic viruses: adenoviruses. Virus Genes *53*, 700–706. 10.1007/s11262-017-1488-1.

316. Wold, W.S.M., and Toth, K. (2013). Adenovirus vectors for gene therapy, vaccination and cancer gene therapy. Curr Gene Ther *13*, 421–433.

317. Uusi-Kerttula, H., Hulin-Curtis, S., Davies, J., and Parker, A.L. (2015). Oncolytic Adenovirus: Strategies and Insights for Vector Design and Immuno-Oncolytic Applications. Viruses *7*, 6009–6042. 10.3390/v7112923.

318. Allen, R.J., and Byrnes, A.P. (2019). Interaction of adenovirus with antibodies, complement, and coagulation factors. FEBS Lett *593*, 3449–3460. 10.1002/1873-3468.13649.

319. Shaikh, H., Karivedu, V., and Wise-Draper, T.M. (2021). Managing Recurrent Metastatic Head and Neck Cancer. Hematol Oncol Clin North Am *35*, 1009–1020. 10.1016/j.hoc.2021.05.009.

320. Scherer, J., and Vallee, R.B. (2015). Conformational changes in the adenovirus hexon subunit responsible for regulating cytoplasmic dynein recruitment. J. Virol. *89*, 1013–1023. 10.1128/JVI.02889-14.

321. Hensen, L.C.M., Hoeben, R.C., and Bots, S.T.F. (2020). Adenovirus Receptor Expression in Cancer and Its Multifaceted Role in Oncolytic Adenovirus Therapy. Int J Mol Sci *21*, 6828. 10.3390/ijms21186828.

322. Nexø, E., and Hansen, H.F. (1985). Binding of epidermal growth factor from man, rat and mouse to the human epidermal growth factor receptor. Biochim Biophys Acta *843*, 101–106. 10.1016/0304-4165(85)90055-8.

323. Schreier, B., Döhler, M., Rabe, S., Schneider, B., Schwerdt, G., Ruhs, S., Sibilia, M., Gotthardt, M., Gekle, M., and Grossmann, C. (2011). Consequences of epidermal growth factor receptor (ErbB1) loss for vascular smooth muscle cells from mice with targeted deletion of ErbB1. Arterioscler Thromb Vasc Biol *31*, 1643–1652. 10.1161/ATVBAHA.111.223537.

324. Schreier, B., Rabe, S., Schneider, B., Bretschneider, M., Rupp, S., Ruhs, S., Neumann, J., Rueckschloss, U., Sibilia, M., Gotthardt, M., et al. (2013). Loss of epidermal growth factor receptor in vascular smooth muscle cells and cardiomyocytes causes arterial hypotension and cardiac hypertrophy. Hypertension *61*, 333–340. 10.1161/HYPERTENSIONAHA.112.196543.

325. Bacakova, L., Travnickova, M., Filova, E., Matějka, R., Stepanovska, J., Musilkova, J., Zarubova, J., and Molitor, M. (2018). The Role of Vascular Smooth Muscle Cells in the Physiology and Pathophysiology of Blood Vessels (IntechOpen) 10.5772/intechopen.77115.

326. Lau, T.-S., Chan, L.K.-Y., Wong, E.C.-H., Hui, C.W.-C., Sneddon, K., Cheung, T.-H., Yim, S.-F., Lee, J.H.-S., Yeung, C.S.-Y., Chung, T.K.-H., et al. (2017). A loop of cancer-stroma-cancer interaction promotes peritoneal metastasis of ovarian cancer via TNFα-TGFα-EGFR. Oncogene *36*, 3576–3587. 10.1038/onc.2016.509.

327. Brown, P.M., Debanne, M.T., Grothe, S., Bergsma, D., Caron, M., Kay, C., and O'Connor-McCourt, M.D. (1994). The extracellular domain of the epidermal growth factor receptor. Studies on the affinity and stoichiometry of binding, receptor dimerization and a binding-domain mutant. Eur J Biochem *225*, 223–233. 10.1111/j.1432-1033.1994.00223.x.

328. Nilson, R., Lübbers, O., Weiß, L., Singh, K., Scharffetter-Kochanek, K., Rojewski, M., Schrezenmeier, H., Zeplin, P.H., Funk, W., Krutzke, L., et al. (2021). Transduction Enhancers Enable Efficient Human Adenovirus Type 5-Mediated Gene Transfer into Human Multipotent Mesenchymal Stromal Cells. Viruses *13*, 1136. 10.3390/v13061136.

329. Tang, D., Gao, J., Wang, S., Ye, N., Chong, Y., Huang, Y., Wang, J., Li, B., Yin, W., and Wang, D. (2016). Cancer-associated fibroblasts promote angiogenesis in gastric cancer through galectin-1 expression. Tumour Biol. *37*, 1889–1899. 10.1007/s13277-015-3942-9.

330. Gaggioli, C., Hooper, S., Hidalgo-Carcedo, C., Grosse, R., Marshall, J.F., Harrington, K., and Sahai, E. (2007). Fibroblast-led collective invasion of carcinoma cells with differing roles for RhoGTPases in leading and following cells. Nat Cell Biol *9*, 1392–1400. 10.1038/ncb1658.

331. Zhang, J., and Liu, J. (2013). Tumor stroma as targets for cancer therapy. Pharmacol Ther *137*, 200–215. 10.1016/j.pharmthera.2012.10.003.

332. Hidaka, C., Milano, E., Leopold, P.L., Bergelson, J.M., Hackett, N.R., Finberg, R.W., Wickham, T.J., Kovesdi, I., Roelvink, P., and Crystal, R.G. (1999). CAR-dependent and CAR-independent pathways of adenovirus vector-mediated gene transfer and expression in human fibroblasts. J. Clin. Invest. *103*, 579–587. 10.1172/JCI5309.

333. Garin-Chesa, P., Old, L.J., and Rettig, W.J. (1990). Cell surface glycoprotein of reactive stromal fibroblasts as a potential antibody target in human epithelial cancers. Proc Natl Acad Sci U S A *87*, 7235–7239. 10.1073/pnas.87.18.7235.

334. Rettig, W.J., Su, S.L., Fortunato, S.R., Scanlan, M.J., Mohan Raj, B.K., Garin-Chesa, P., Healey, J.H., and Old, L.J. (1994). Fibroblast activation protein: Purification, epitope mapping and induction by growth factors. International Journal of Cancer *58*, 385–392. 10.1002/ijc.2910580314.

335. Pang, T., Wang, X., Gao, J., Chen, W., Shen, X.J., Nie, M.M., Luo, T., Yin, K., Fang, G., Wang, K.X., et al. (2017). Fiber-modified hexon-chimeric oncolytic adenovirus targeting cancer associated fibroblasts inhibits tumor growth in gastric carcinoma. Oncotarget *8*, 76468–76478. 10.18632/oncotarget.20273.

336. de Sostoa, J., Fajardo, C.A., Moreno, R., Ramos, M.D., Farrera-Sal, M., and Alemany, R. (2019). Targeting the tumor stroma with an oncolytic adenovirus secreting a fibroblast activation protein-targeted bispecific T-cell engager. J Immunother Cancer *7*, 19. 10.1186/s40425-019-0505-4.

337. Baeuerle, P.A., and Reinhardt, C. (2009). Bispecific T-cell engaging antibodies for cancer therapy. Cancer Res *69*, 4941–4944. 10.1158/0008-5472.CAN-09-0547.

338. Freedman, J.D., Duffy, M.R., Lei-Rossmann, J., Muntzer, A., Scott, E.M., Hagel, J., Campo, L., Bryant, R.J., Verrill, C., Lambert, A., et al. (2018). An Oncolytic Virus Expressing a T-cell Engager Simultaneously Targets Cancer and Immunosuppressive Stromal Cells. Cancer Res. *78*, 6852–6865. 10.1158/0008-5472.CAN-18-1750.

339. Bae, S., Park, C.W., Son, H.K., Ju, H.K., Paik, D., Jeon, C.-J., Koh, G.Y., Kim, J., and Kim, H. (2008). Fibroblast activation protein alpha identifies mesenchymal stromal cells from human bone marrow. Br. J. Haematol. *142*, 827–830. 10.1111/j.1365-2141.2008.07241.x.

340. Tran, E., Chinnasamy, D., Yu, Z., Morgan, R.A., Lee, C.-C.R., Restifo, N.P., and Rosenberg, S.A. (2013). Immune targeting of fibroblast activation protein triggers recognition of multipotent bone marrow stromal cells and cachexia. J Exp Med *210*, 1125–1135. 10.1084/jem.20130110.

341. Kakarla, S., Chow, K.K.H., Mata, M., Shaffer, D.R., Song, X.-T., Wu, M.-F., Liu, H., Wang, L.L., Rowley, D.R., Pfizenmaier, K., et al. (2013). Antitumor effects of chimeric receptor engineered human T cells directed to tumor stroma. Mol Ther *21*, 1611–1620. 10.1038/mt.2013.110.

342. Tollefson, A.E., Scaria, A., Saha, S.K., and Wold, W.S. (1992). The 11,600-MW protein encoded by region E3 of adenovirus is expressed early but is greatly amplified at late stages of infection. J Virol *66*, 3633–3642. 10.1128/JVI.66.6.3633-3642.1992.

343. Tollefson, A.E., Scaria, A., Hermiston, T.W., Ryerse, J.S., Wold, L.J., and Wold, W.S. (1996). The adenovirus death protein (E3-11.6K) is required at very late stages of infection for efficient cell lysis and release of adenovirus from infected cells. J Virol *70*, 2296–2306. 10.1128/JVI.70.4.2296-2306.1996.

344. Doronin, K., Toth, K., Kuppuswamy, M., Ward, P., Tollefson, A.E., and Wold, W.S. (2000). Tumor-specific, replication-competent adenovirus vectors overexpressing the adenovirus death protein. J. Virol. *74*, 6147–6155.

345. Subramanian, T., Vijayalingam, S., and Chinnadurai, G. (2006). Genetic identification of adenovirus type 5 genes that influence viral spread. J Virol *80*, 2000–2012. 10.1128/JVI.80.4.2000-2012.2006.

346. Scaria, A., Tollefson, A.E., Saha, S.K., and Wold, W.S. (1992). The E3-11.6K protein of adenovirus is an Asn-glycosylated integral membrane protein that localizes to the nuclear membrane. Virology *191*, 743–753. 10.1016/0042-6822(92)90250-s.

347. White, E., Blose, S.H., and Stillman, B.W. (1984). Nuclear envelope localization of an adenovirus tumor antigen maintains the integrity of cellular DNA. Mol Cell Biol *4*, 2865–2875. 10.1128/mcb.4.12.2865-2875.1984.

348. Bett, A.J., Prevec, L., and Graham, F.L. (1993). Packaging capacity and stability of human adenovirus type 5 vectors. J. Virol. *67*, 5911–5921.

349. Kew, M.C. (2000). Serum aminotransferase concentration as evidence of hepatocellular damage. Lancet *355*, 591–592. 10.1016/S0140-6736(99)00219-6.

350. Magami, Y., Azuma, T., Inokuchi, H., Kokuno, S., Moriyasu, F., Kawai, K., and Hattori, T. (2002). Cell proliferation and renewal of normal hepatocytes and bile duct cells in adult mouse liver. Liver *22*, 419–425. 10.1034/j.1600-0676.2002.01702.x.

351. Young, A.-M., Archibald, K.M., Tookman, L.A., Pool, A., Dudek, K., Jones, C., Williams, S.L., Pirlo, K.J., Willis, A.E., Lockley, M., et al. (2012). Failure of Translation of Human Adenovirus mRNA in Murine Cancer Cells Can be Partially Overcome by L4-100K Expression In Vitro and In Vivo. Mol Ther *20*, 1676–1688. 10.1038/mt.2012.116.

352. Blair, G.E., Dixon, S.C., Griffiths, S.A., and Zajdel, M.E. (1989). Restricted replication of human adenovirus type 5 in mouse cell lines. Virus Res. *14*, 339–346.

353. Tiegs, G., and Horst, A.K. (2022). TNF in the liver: targeting a central player in inflammation. Semin Immunopathol *44*, 445–459. 10.1007/s00281-022-00910-2.

354. Shuh, M., Bohorquez, H., Loss, G.E., and Cohen, A.J. (2013). Tumor Necrosis Factor-α: Life and Death of Hepatocytes During Liver Ischemia/Reperfusion Injury. Ochsner J *13*, 119–130.

355. Kiseleva, Y.V., Antonyan, S.Z., Zharikova, T.S., Tupikin, K.A., Kalinin, D.V., and Zharikov, Y.O. (2021). Molecular pathways of liver regeneration: A comprehensive review. World J Hepatol *13*, 270–290. 10.4254/wjh.v13.i3.270.

356. Atasheva, S., and Shayakhmetov, D.M. (2016). Adenovirus sensing by the immune system. Curr Opin Virol *21*, 109–113. 10.1016/j.coviro.2016.08.017.

357. Nowsheen, S., and Yang, E.S. (2012). The intersection between DNA damage response and cell death pathways. Exp Oncol *34*, 243–254.

358. Bartek, J., Lukas, C., and Lukas, J. (2004). Checking on DNA damage in S phase. Nat Rev Mol Cell Biol *5*, 792–804. 10.1038/nrm1493.

359. Palta, S., Saroa, R., and Palta, A. (2014). Overview of the coagulation system. Indian J Anaesth *58*, 515–523. 10.4103/0019-5049.144643.

360. Cichon, G., Schmidt, H.H., Benhidjeb, T., Löser, P., Ziemer, S., Haas, R., Grewe, N., Schnieders, F., Heeren, J., Manns, M.P., et al. (1999). Intravenous administration of recombinant adenoviruses causes thrombocytopenia, anemia and erythroblastosis in rabbits. J Gene Med *1*, 360–371. 10.1002/(SICI)1521-2254(199909/10)1:5<360::AID-JGM54>3.0.CO;2-Q.

361. Othman, M., Labelle, A., Mazzetti, I., Elbatarny, H.S., and Lillicrap, D. (2007). Adenovirus-induced thrombocytopenia: the role of von Willebrand factor and P-selectin in mediating accelerated platelet clearance. Blood *109*, 2832–2839. 10.1182/blood-2006-06-032524.

362. Wolins, N., Lozier, J., Eggerman, T.L., Jones, E., Aguilar-Córdova, E., and Vostal, J.G. (2003). Intravenous administration of replication-incompetent adenovirus to rhesus monkeys induces thrombocytopenia by increasing in vivo platelet clearance. Br J Haematol *123*, 903–905. 10.1046/j.1365-2141.2003.04719.x.

363. Raper, S.E., Yudkoff, M., Chirmule, N., Gao, G.-P., Nunes, F., Haskal, Z.J., Furth, E.E., Propert, K.J., Robinson, M.B., Magosin, S., et al. (2002). A pilot study of in vivo liver-directed gene transfer with an adenoviral vector in partial ornithine transcarbamylase deficiency. Hum Gene Ther *13*, 163–175. 10.1089/10430340152712719.

364. Jinna, S., and Khandhar, P.B. (2022). Thrombocytopenia. In StatPearls (StatPearls Publishing).

365. Nilson, R., Krutzke, L., Wienen, F., Rojewski, M., Zeplin, P.H., Funk, W., Schrezenmeier, H., Kochanek, S., and Kritzinger, A. (2023). Evaluation of Human Mesenchymal Stromal Cells as Carriers for the Delivery of Oncolytic HAdV-5 to Head and Neck Squamous Cell Carcinomas. Viruses *15*, 218. 10.3390/v15010218.

366. Ugurlu, B., and Karaoz, E. (2020). Comparison of similar cells: Mesenchymal stromal cells and fibroblasts. Acta Histochem *122*, 151634. 10.1016/j.acthis.2020.151634.

367. Jönsson, F., and Kreppel, F. (2017). Barriers to systemic application of virus-based vectors in gene therapy: lessons from adenovirus type 5. Virus Genes *53*, 692–699. 10.1007/s11262-017-1498-z.

368. Kreppel, F., and Kochanek, S. (2008). Modification of adenovirus gene transfer vectors with synthetic polymers: a scientific review and technical guide. Mol Ther *16*, 16–29. 10.1038/sj.mt.6300321.

369. Kreppel, F., Gackowski, J., Schmidt, E., and Kochanek, S. (2005). Combined genetic and chemical capsid modifications enable flexible and efficient de- and retargeting of adenovirus vectors. Mol Ther *12*, 107–117. 10.1016/j.ymthe.2005.03.006.

370. Beatty, M.S., and Curiel, D.T. (2012). Chapter two--Adenovirus strategies for tissue-specific targeting. Adv. Cancer Res. *115*, 39–67. 10.1016/B978-0-12-398342-8.00002-1.

371. Weklak, D., Pembaur, D., Koukou, G., Jönsson, F., Hagedorn, C., and Kreppel, F. (2021). Genetic and Chemical Capsid Modifications of Adenovirus Vectors to Modulate Vector-Host Interactions. Viruses *13*, 1300. 10.3390/v13071300.

372. Lusky, M. (2005). Good manufacturing practice production of adenoviral vectors for clinical trials. Hum Gene Ther *16*, 281–291. 10.1089/hum.2005.16.281.

373. Arjmand, B., Alavi-Moghadam, S., Payab, M., Goodarzi, P., Sheikh Hosseini, M., Tayanloo-Beik, A., Rezaei-Tavirani, M., and Larijani, B. (2021). GMP-Compliant Adenoviral Vectors for Gene Therapy. Methods Mol Biol *2286*, 237–250. 10.1007/7651_2020_284.

374. Poulin, K.L., McFall, E.R., Chan, G., Provost, N.B., Christou, C., Smith, A.C., and Parks, R.J. (2020). Fusion of Large Polypeptides to Human Adenovirus Type 5 Capsid Protein IX Can Compromise Virion Stability and DNA Packaging Capacity. J Virol *94*, e01112-20. 10.1128/JVI.01112-20.

375. Henning, P., Lundgren, E., Carlsson, M., Frykholm, K., Johannisson, J., Magnusson, M.K., Tång, E., Franqueville, L., Hong, S.S., Lindholm, L., et al. (2006). Adenovirus type 5 fiber knob domain has a critical role in fiber protein synthesis and encapsidation. J Gen Virol *87*, 3151–3160. 10.1099/vir.0.81992-0.

376. Atasheva, S., Emerson, C.C., Yao, J., Young, C., Stewart, P.L., and Shayakhmetov, D.M. (2020). Systemic cancer therapy with engineered adenovirus that evades innate immunity. Sci Transl Med *12*, eabc6659. 10.1126/scitranslmed.abc6659.

377. Werb, Z., and Lu, P. (2015). The Role of Stroma in Tumor Development. Cancer J *21*, 250–253. 10.1097/PPO.0000000000000127.

378. Son, B., Lee, S., Youn, H., Kim, E., Kim, W., and Youn, B. (2017). The role of tumor microenvironment in therapeutic resistance. Oncotarget *8*, 3933–3945. 10.18632/oncotarget.13907.

379. Ni, Y., Zhou, X., Yang, J., Shi, H., Li, H., Zhao, X., and Ma, X. (2021). The Role of Tumor-Stroma Interactions in Drug Resistance Within Tumor Microenvironment. Front Cell Dev Biol *9*, 637675. 10.3389/fcell.2021.637675.

380. Anderson, N.M., and Simon, M.C. (2020). The tumor microenvironment. Curr Biol *30*, R921–R925. 10.1016/j.cub.2020.06.081.

381. Xu, M., Zhang, T., Xia, R., Wei, Y., and Wei, X. (2022). Targeting the tumor stroma for cancer therapy. Mol Cancer *21*, 208. 10.1186/s12943-022-01670-1.

382. Wang, X., Zhong, L., and Zhao, Y. (2021). Oncolytic adenovirus: A tool for reversing the tumor microenvironment and promoting cancer treatment (Review). Oncol Rep *45*, 49. 10.3892/or.2021.8000.

383. Czekay, R.-P., Cheon, D.-J., Samarakoon, R., Kutz, S.M., and Higgins, P.J. (2022). Cancer-Associated Fibroblasts: Mechanisms of Tumor Progression and Novel Therapeutic Targets. Cancers (Basel) *14*, 1231. 10.3390/cancers14051231.

384. Kuklik, J., Michelfelder, S., Schiele, F., Kreuz, S., Lamla, T., Müller, P., and Park, J.E. (2021). Development of a Bispecific Antibody-Based Platform for Retargeting of Capsid Modified AAV Vectors. Int J Mol Sci *22*, 8355. 10.3390/ijms22158355.

385. Farrera-Sal, M., Fillat, C., and Alemany, R. (2020). Effect of Transgene Location, Transcriptional Control Elements and Transgene Features in Armed Oncolytic Adenoviruses. Cancers (Basel) *12*, 1034. 10.3390/cancers12041034.

386. Bressy, C., Hastie, E., and Grdzelishvili, V.Z. (2017). Combining Oncolytic Virotherapy with p53 Tumor Suppressor Gene Therapy. Mol Ther Oncolytics *5*, 20–40. 10.1016/j.omto.2017.03.002.

387. van Beusechem, V.W., van den Doel, P.B., Grill, J., Pinedo, H.M., and Gerritsen, W.R. (2002). Conditionally replicative adenovirus expressing p53 exhibits enhanced oncolytic potency. Cancer Res *62*, 6165–6171.

388. Geoerger, B., van Beusechem, V.W., Opolon, P., Morizet, J., Laudani, L., Lecluse, Y., Barrois, M., Idema, S., Grill, J., Gerritsen, W.R., et al. (2005). Expression of p53, or targeting towards EGFR, enhances the oncolytic potency of conditionally replicative adenovirus against neuroblastoma. J Gene Med *7*, 584–594. 10.1002/jgm.703.

389. Qian, C.-Y., Wang, K.-L., Fang, F.-F., Gu, W., Huang, F., Wang, F.-Z., Li, B., and Wang, L.-N. (2015). Triple-controlled oncolytic adenovirus expressing melittin to exert inhibitory efficacy on hepatocellular carcinoma. Int J Clin Exp Pathol *8*, 10403–10411.

390. Press, O.W. (1991). Immunotoxins. Biotherapy *3*, 65–76. 10.1007/BF02175100.

391. Fernández-Ulibarri, I., Hammer, K., Arndt, M.A.E., Kaufmann, J.K., Dorer, D., Engelhardt, S., Kontermann, R.E., Hess, J., Allgayer, H., Krauss, J., et al. (2015). Genetic delivery of an immunoRNase by an oncolytic adenovirus enhances anticancer activity. Int J Cancer *136*, 2228–2240. 10.1002/ijc.29258.

392. Beck, C., Cayeux, S., Lupton, S.D., Dörken, B., and Blankenstein, T. (1995). The thymidine kinase/ganciclovir-mediated “suicide” effect is variable in different tumor cells. Hum Gene Ther *6*, 1525–1530. 10.1089/hum.1995.6.12-1525.

393. Szary, J., Missol, E., and Szala, S. (1998). Characteristics of Cytosine Deaminase-5-Fluorocytosine System. In Gene Therapy of Cancer Advances in Experimental Medicine and Biology., P. Walden, U. Trefzer, W. Sterry, F. Farzaneh, and P. Zambon, eds. (Springer US), pp. 121–123. 10.1007/978-1-4615-5357-1_19.

394. Austin, E.A., and Huber, B.E. (1993). A first step in the development of gene therapy for colorectal carcinoma: cloning, sequencing, and expression of Escherichia coli cytosine deaminase. Mol Pharmacol *43*, 380–387.

395. Abate-Daga, D., Andreu, N., Camacho-Sánchez, J., Alemany, R., Herance, R., Millán, O., and Fillat, C. (2011). Oncolytic adenoviruses armed with thymidine kinase can be traced by PET imaging and show potent antitumoural effects by ganciclovir dosing. PLoS One *6*, e26142. 10.1371/journal.pone.0026142.

396. Ji, X., Zhang, J., Cheng, L., Wei, F., Li, H., Liu, X., Chen, X., Li, C., Wang, Y., and Huang, Q. (2009). Oncolytic adenovirus delivering herpes simplex virus thymidine kinase suicide gene reduces the growth of human retinoblastoma in an in vivo mouse model. Exp Eye Res *89*, 193–199. 10.1016/j.exer.2009.03.007.

397. Ji, N., Weng, D., Liu, C., Gu, Z., Chen, S., Guo, Y., Fan, Z., Wang, X., Chen, J., Zhao, Y., et al. (2016). Adenovirus-mediated delivery of herpes simplex virus thymidine kinase administration improves outcome of recurrent high-grade glioma. Oncotarget *7*, 4369–4378. 10.18632/oncotarget.6737.

398. Warmann, S.W., Armeanu, S., Heigoldt, H., Ruck, P., Vonthein, R., Heitmann, H., Seitz, G., Lemken, M.-L., Bitzer, M., Fuchs, J., et al. (2009). Adenovirus-mediated cytosine deaminase/5-fluorocytosine suicide gene therapy of human hepatoblastoma in vitro. Pediatr Blood Cancer *53*, 145–151. 10.1002/pbc.21956.

399. Chen, J.-S., Liu, J.-C., Shen, L., Rau, K.-M., Kuo, H.-P., Li, Y.M., Shi, D., Lee, Y.-C., Chang, K.-J., and Hung, M.-C. (2004). Cancer-specific activation of the survivin promoter and its potential use in gene therapy. Cancer Gene Ther *11*, 740–747. 10.1038/sj.cgt.7700752.

400. Yao, X., Yoshioka, Y., Eto, Y., Morishige, T., Okada, Y., Mizuguchi, H., Mukai, Y., Okada, N., and Nakagawa, S. (2007). TERT promoter-driven adenovirus vector for cancer gene therapy via systemic injection. Biochem Biophys Res Commun *362*, 419–424. 10.1016/j.bbrc.2007.08.001.

401. Brand, K., Löser, P., Arnold, W., Bartels, T., and Strauss, M. (1998). Tumor cell-specific transgene expression prevents liver toxicity of the adeno-HSVtk/GCV approach. Gene Ther *5*, 1363–1371. 10.1038/sj.gt.3300728.

402. Nettelbeck, D.M. (2008). Cellular genetic tools to control oncolytic adenoviruses for virotherapy of cancer. J Mol Med (Berl) *86*, 363–377. 10.1007/s00109-007-0291-1.

403. El-Guendy, N., Zhao, Y., Gurumurthy, S., Burikhanov, R., and Rangnekar, V.M. (2003). Identification of a unique core domain of par-4 sufficient for selective apoptosis induction in cancer cells. Mol. Cell. Biol. *23*, 5516–5525. 10.1128/mcb.23.16.5516-5525.2003.

404. Hebbar, N., Wang, C., and Rangnekar, V.M. (2012). Mechanisms of apoptosis by the tumor suppressor Par-4. J. Cell. Physiol. *227*, 3715–3721. 10.1002/jcp.24098.

405. Zhao, Y., and Rangnekar, V.M. (2008). Apoptosis and tumor resistance conferred by Par-4. Cancer Biol. Ther. *7*, 1867–1874. 10.4161/cbt.7.12.6945.

406. Cheratta, A.R., Thayyullathil, F., Pallichankandy, S., Subburayan, K., Alakkal, A., and Galadari, S. (2021). Prostate apoptosis response-4 and tumor suppression: it's not just about apoptosis anymore. Cell Death Dis *12*, 47. 10.1038/s41419-020-03292-1.

407. Qin, T.-J., Ma, W., Liu, S.-X., Yang, G.-X., Wang, Q.-Y., and Zhao, X.-H. (2010). Secretory expression of Par-4 SAC-HA2TAT following adeno-associated virus-mediated gene transfer induces apoptosis in HepG2 cells. Mol Med Rep *3*, 749–757. 10.3892/mmr.2010.343.

408. Chakraborty, M., Qiu, S.G., Vasudevan, K.M., and Rangnekar, V.M. (2001). Par-4 drives trafficking and activation of Fas and Fasl to induce prostate cancer cell apoptosis and tumor regression. Cancer Res. *61*, 7255–7263.

409. Kennedy, M.A., and Parks, R.J. (2009). Adenovirus virion stability and the viral genome: size matters. Mol Ther *17*, 1664–1666. 10.1038/mt.2009.202.

410. Kaufman, H.L., Kohlhapp, F.J., and Zloza, A. (2015). Oncolytic viruses: a new class of immunotherapy drugs. Nat Rev Drug Discov *14*, 642–662. 10.1038/nrd4663.

411. Bonaventura, P., Shekarian, T., Alcazer, V., Valladeau-Guilemond, J., Valsesia-Wittmann, S., Amigorena, S., Caux, C., and Depil, S. (2019). Cold Tumors: A Therapeutic Challenge for Immunotherapy. Front Immunol *10*, 168. 10.3389/fimmu.2019.00168.

412. Peter, M., and Kühnel, F. (2020). Oncolytic Adenovirus in Cancer Immunotherapy. Cancers (Basel) *12*, 3354. 10.3390/cancers12113354.

413. Tripodi, L., Vitale, M., Cerullo, V., and Pastore, L. (2021). Oncolytic Adenoviruses for Cancer Therapy. Int J Mol Sci *22*, 2517. 10.3390/ijms22052517.

414. van Horssen, R., Ten Hagen, T.L.M., and Eggermont, A.M.M. (2006). TNF-alpha in cancer treatment: molecular insights, antitumor effects, and clinical utility. Oncologist *11*, 397–408. 10.1634/theoncologist.11-4-397.

415. Mehta, A.K., Gracias, D.T., and Croft, M. (2018). TNF Activity and T cells. Cytokine *101*, 14–18. 10.1016/j.cyto.2016.08.003.

416. Hamilton, J.A., and Anderson, G.P. (2004). GM-CSF Biology. Growth Factors *22*, 225–231. 10.1080/08977190412331279881.

417. Colombo, M.P., and Trinchieri, G. (2002). Interleukin-12 in anti-tumor immunity and immunotherapy. Cytokine Growth Factor Rev *13*, 155–168. 10.1016/s1359-6101(01)00032-6.

418. Nguyen, K.G., Vrabel, M.R., Mantooth, S.M., Hopkins, J.J., Wagner, E.S., Gabaldon, T.A., and Zaharoff, D.A. (2020). Localized Interleukin-12 for Cancer Immunotherapy. Front Immunol *11*, 575597. 10.3389/fimmu.2020.575597.

419. Leonard, J.P., Sherman, M.L., Fisher, G.L., Buchanan, L.J., Larsen, G., Atkins, M.B., Sosman, J.A., Dutcher, J.P., Vogelzang, N.J., and Ryan, J.L. (1997). Effects of single-dose interleukin-12 exposure on interleukin-12-associated toxicity and interferon-gamma production. Blood *90*, 2541–2548.

420. Yan, W.-L., Shen, K.-Y., Tien, C.-Y., Chen, Y.-A., and Liu, S.-J. (2017). Recent progress in GM-CSF-based cancer immunotherapy. Immunotherapy *9*, 347–360. 10.2217/imt-2016-0141.

421. Roberts, N.J., Zhou, S., Diaz, L.A., and Holdhoff, M. (2011). Systemic use of tumor necrosis factor alpha as an anticancer agent. Oncotarget *2*, 739–751. 10.18632/oncotarget.344.

422. Wang, P., Li, X., Wang, J., Gao, D., Li, Y., Li, H., Chu, Y., Zhang, Z., Liu, H., Jiang, G., et al. (2017). Re-designing Interleukin-12 to enhance its safety and potential as an anti-tumor immunotherapeutic agent. Nat Commun *8*, 1395. 10.1038/s41467-017-01385-8.

423. Barrett, J.A., Cai, H., Miao, J., Khare, P.D., Gonzalez, P., Dalsing-Hernandez, J., Sharma, G., Chan, T., Cooper, L.J.N., and Lebel, F. (2018). Regulated intratumoral expression of IL-12 using a RheoSwitch Therapeutic System® (RTS®) gene switch as gene therapy for the treatment of glioma. Cancer Gene Ther *25*, 106–116. 10.1038/s41417-018-0019-0.

424. Hirvinen, M., Rajecki, M., Kapanen, M., Parviainen, S., Rouvinen-Lagerström, N., Diaconu, I., Nokisalmi, P., Tenhunen, M., Hemminki, A., and Cerullo, V. (2015). Immunological effects of a tumor necrosis factor alpha-armed oncolytic adenovirus. Hum Gene Ther *26*, 134–144. 10.1089/hum.2014.069.

425. Havunen, R., Siurala, M., Sorsa, S., Grönberg-Vähä-Koskela, S., Behr, M., Tähtinen, S., Santos, J.M., Karell, P., Rusanen, J., Nettelbeck, D.M., et al. (2017). Oncolytic Adenoviruses Armed with Tumor Necrosis Factor Alpha and Interleukin-2 Enable Successful Adoptive Cell Therapy. Mol Ther Oncolytics *4*, 77–86. 10.1016/j.omto.2016.12.004.

426. Bramante, S., Kaufmann, J.K., Veckman, V., Liikanen, I., Nettelbeck, D.M., Hemminki, O., Vassilev, L., Cerullo, V., Oksanen, M., Heiskanen, R., et al. (2015). Treatment of melanoma with a serotype 5/3 chimeric oncolytic adenovirus coding for GM-CSF: Results in vitro, in rodents and in humans. Int J Cancer *137*, 1775–1783. 10.1002/ijc.29536.

427. Chiocca, E.A., Yu, J.S., Lukas, R.V., Solomon, I.H., Ligon, K.L., Nakashima, H., Triggs, D.A., Reardon, D.A., Wen, P., Stopa, B.M., et al. (2019). Regulatable interleukin-12 gene therapy in patients with recurrent high-grade glioma: Results of a phase 1 trial. Sci Transl Med *11*, eaaw5680. 10.1126/scitranslmed.aaw5680.

428. TILT Biotherapeutics Ltd. (2021). A Phase 1, Open-Label, Dose-Escalation Clinical Trial of Tumor Necrosis Factor Alpha and Interleukin 2 Coding Oncolytic Adenovirus TILT-123 in Melanoma Patients Receiving Adoptive Cell Therapy With Tumor Infiltrating Lymphocytes (clinicaltrials.gov).

429. Ramesh, N., Ge, Y., Ennist, D.L., Zhu, M., Mina, M., Ganesh, S., Reddy, P.S., and Yu, D.-C. (2006). CG0070, a conditionally replicating granulocyte macrophage colony-stimulating factor--armed oncolytic adenovirus for the treatment of bladder cancer. Clin Cancer Res *12*, 305–313. 10.1158/1078-0432.CCR-05-1059.

430. Burke, J.M., Lamm, D.L., Meng, M.V., Nemunaitis, J.J., Stephenson, J.J., Arseneau, J.C., Aimi, J., Lerner, S., Yeung, A.W., Kazarian, T., et al. (2012). A first in human phase 1 study of CG0070, a GM-CSF expressing oncolytic adenovirus, for the treatment of nonmuscle invasive bladder cancer. J Urol *188*, 2391–2397. 10.1016/j.juro.2012.07.097.

431. Packiam, V.T., Lamm, D.L., Barocas, D.A., Trainer, A., Fand, B., Davis, R.L., Clark, W., Kroeger, M., Dumbadze, I., Chamie, K., et al. (2018). An open label, single-arm, phase II multicenter study of the safety and efficacy of CG0070 oncolytic vector regimen in patients with BCG-unresponsive non-muscle-invasive bladder cancer: Interim results. Urol Oncol *36*, 440–447. 10.1016/j.urolonc.2017.07.005.

432. Ranki, T., Pesonen, S., Hemminki, A., Partanen, K., Kairemo, K., Alanko, T., Lundin, J., Linder, N., Turkki, R., Ristimäki, A., et al. (2016). Phase I study with ONCOS-102 for the treatment of solid tumors - an evaluation of clinical response and exploratory analyses of immune markers. J Immunother Cancer *4*, 17. 10.1186/s40425-016-0121-5.

433. Fajardo, C.A., Guedan, S., Rojas, L.A., Moreno, R., Arias-Badia, M., de Sostoa, J., June, C.H., and Alemany, R. (2017). Oncolytic Adenoviral Delivery of an EGFR-Targeting T-cell Engager Improves Antitumor Efficacy. Cancer Res *77*, 2052–2063. 10.1158/0008-5472.CAN-16-1708.

434. Basnet, S., Santos, J.M., Quixabeira, D.C.A., Clubb, J.H.A., Grönberg-Vähä-Koskela, S.A.M., Arias, V., Pakola, S., Kudling, T.V., Heiniö, C., Havunen, R., et al. (2023). Oncolytic adenovirus coding for bispecific T cell engager against human MUC-1 potentiates T cell response against solid tumors. Mol Ther Oncolytics *28*, 59–73. 10.1016/j.omto.2022.12.007.

435. Freedman, J.D., Hagel, J., Scott, E.M., Psallidas, I., Gupta, A., Spiers, L., Miller, P., Kanellakis, N., Ashfield, R., Fisher, K.D., et al. (2017). Oncolytic adenovirus expressing bispecific antibody targets T-cell cytotoxicity in cancer biopsies. EMBO Mol Med *9*, 1067–1087. 10.15252/emmm.201707567.

436. Hwang, J.K., Hong, J., and Yun, C.-O. (2020). Oncolytic Viruses and Immune Checkpoint Inhibitors: Preclinical Developments to Clinical Trials. Int J Mol Sci *21*, 8627. 10.3390/ijms21228627.

437. Rezaei, R., Esmaeili Gouvarchin Ghaleh, H., Farzanehpour, M., Dorostkar, R., Ranjbar, R., Bolandian, M., Mirzaei Nodooshan, M., and Ghorbani Alvanegh, A. (2022). Combination therapy with CAR T cells and oncolytic viruses: a new era in cancer immunotherapy. Cancer Gene Ther *29*, 647–660. 10.1038/s41417-021-00359-9.

438. Zou, H., Mou, X.-Z., and Zhu, B. (2023). Combining of Oncolytic Virotherapy and Other Immunotherapeutic Approaches in Cancer: A Powerful Functionalization Tactic. Glob Chall *7*, 2200094. 10.1002/gch2.202200094.

439. Murciano-Goroff, Y.R., Warner, A.B., and Wolchok, J.D. (2020). The future of cancer immunotherapy: microenvironment-targeting combinations. Cell Res *30*, 507–519. 10.1038/s41422-020-0337-2.

440. Sadeghi Rad, H., Monkman, J., Warkiani, M.E., Ladwa, R., O'Byrne, K., Rezaei, N., and Kulasinghe, A. (2021). Understanding the tumor microenvironment for effective immunotherapy. Med Res Rev *41*, 1474–1498. 10.1002/med.21765.

441. Pan, J., Yang, J.F., Deng, B.P., Zhao, X.J., Zhang, X., Lin, Y.H., Wu, Y.N., Deng, Z.L., Zhang, Y.L., Liu, S.H., et al. (2017). High efficacy and safety of low-dose CD19-directed CAR-T cell therapy in 51 refractory or relapsed B acute lymphoblastic leukemia patients. Leukemia *31*, 2587–2593. 10.1038/leu.2017.145.

442. Hartmann, J., Schüßler-Lenz, M., Bondanza, A., and Buchholz, C.J. (2017). Clinical development of CAR T cells-challenges and opportunities in translating innovative treatment concepts. EMBO Mol Med *9*, 1183–1197. 10.15252/emmm.201607485.

443. Moon, E.K., Wang, L.-C., Dolfi, D.V., Wilson, C.B., Ranganathan, R., Sun, J., Kapoor, V., Scholler, J., Puré, E., Milone, M.C., et al. (2014). Multifactorial T-cell hypofunction that is reversible can limit the efficacy of chimeric antigen receptor-transduced human T cells in solid tumors. Clin Cancer Res *20*, 4262–4273. 10.1158/1078-0432.CCR-13-2627.

444. McGrath, K., and Dotti, G. (2021). Combining Oncolytic Viruses with Chimeric Antigen Receptor T Cell Therapy. Hum Gene Ther *32*, 150–157. 10.1089/hum.2020.278.

445. Petitprez, F., Meylan, M., de Reyniès, A., Sautès-Fridman, C., and Fridman, W.H. (2020). The Tumor Microenvironment in the Response to Immune Checkpoint Blockade Therapies. Front Immunol *11*, 784. 10.3389/fimmu.2020.00784.

446. Cruz, E., and Kayser, V. (2019). Monoclonal antibody therapy of solid tumors: clinical limitations and novel strategies to enhance treatment efficacy. Biologics *13*, 33–51. 10.2147/BTT.S166310.

447. LaRocca, C.J., and Warner, S.G. (2018). Oncolytic viruses and checkpoint inhibitors: combination therapy in clinical trials. Clin Transl Med *7*, 35. 10.1186/s40169-018-0214-5.

448. DNAtrix, Inc. (2021). A Phase II, Multi-center, Open-label Study of a Conditionally Replicative Adenovirus (DNX-2401) With Pembrolizumab (KEYTRUDA®) for Recurrent Glioblastoma or Gliosarcoma (CAPTIVE/KEYNOTE-192) (clinicaltrials.gov).

449. Targovax Oy (2021). A Pilot Study of Sequential ONCOS-102, an Engineered Oncolytic Adenovirus Expressing GMCSF, and Pembrolizumab in Patients With Advanced or Unresectable Melanoma Progressing After PD1 Blockade (clinicaltrials.gov).

450. MD, J.C.C. (2022). Phase II Window of Opportunity Trial of Stereotactic Body Radiation Therapy and In Situ Oncolytic Virus Therapy in Metastatic Triple Negative Breast Cancer and Metastatic Non-Small Cell Lung Cancer Followed by Pembrolizumab (clinicaltrials.gov).

451. CG Oncology, Inc. (2022). A Phase 2, Single Arm Study of CG0070 Combined With Pembrolizumab in Patients With Non Muscle Invasive Bladder Cancer (NMIBC) Unresponsive to Bacillus Calmette-Guerin (BCG) (clinicaltrials.gov).

452. Akamis Bio (2021). A Phase I Multicenter, Open Label Study of Enadenotucirev Combined With PD-1 Inhibitor in Subjects With Metastatic or Advanced Epithelial Tumors (clinicaltrials.gov).

453. Kumar, S., Gao, L., Yeagy, B., and Reid, T. (2008). Virus combinations and chemotherapy for the treatment of human cancers. Curr Opin Mol Ther *10*, 371–379.

454. Sakhawat, A., Ma, L., Muhammad, T., Khan, A.A., Chen, X., and Huang, Y. (2019). A tumor targeting oncolytic adenovirus can improve therapeutic outcomes in chemotherapy resistant metastatic human breast carcinoma. Sci Rep *9*, 7504. 10.1038/s41598-019-43668-8.

455. Zhang, S., and Rabkin, S.D. (2021). The discovery and development of oncolytic viruses: are they the future of cancer immunotherapy? Expert Opin Drug Discov *16*, 391–410. 10.1080/17460441.2021.1850689.

456. Jounaidi, Y., Doloff, J.C., and Waxman, D.J. (2007). Conditionally replicating adenoviruses for cancer treatment. Curr Cancer Drug Targets *7*, 285–301.

457. Moaven, O., Mangieri, C.W., Stauffer, J.A., Anastasiadis, P.Z., and Borad, M.J. (2021). Strategies to Develop Potent Oncolytic Viruses and Enhance Their Therapeutic Efficacy. JCO Precis Oncol *5*, PO.21.00003. 10.1200/PO.21.00003.

458. Halldén, G., Hill, R., Wang, Y., Anand, A., Liu, T.-C., Lemoine, N.R., Francis, J., Hawkins, L., and Kirn, D. (2003). Novel immunocompetent murine tumor models for the assessment of replication-competent oncolytic adenovirus efficacy. Mol Ther *8*, 412–424. 10.1016/s1525-0016(03)00199-0.

459. Basel, M.T., Narayanan, S., Ganta, C., Shreshta, T.B., Marquez, A., Pyle, M., Hill, J., Bossmann, S.H., and Troyer, D.L. (2018). Developing a xenograft human tumor model in immunocompetent mice. Cancer Lett. *412*, 256–263. 10.1016/j.canlet.2017.10.009.

460. Zhang, L., Hedjran, F., Larson, C., Perez, G.L., and Reid, T. (2015). A novel immunocompetent murine model for replicating oncolytic adenoviral therapy. Cancer Gene Ther. *22*, 17–22. 10.1038/cgt.2014.64.

461. Klann, P.J., Wang, X., Elfert, A., Zhang, W., Köhler, C., Güttsches, A.-K., Jacobsen, F., Weyen, U., Roos, A., Ehrke-Schulz, E., et al. (2022). Seroprevalence of Binding and Neutralizing Antibodies against 39 Human Adenovirus Types in Patients with Neuromuscular Disorders. Viruses *15*, 79. 10.3390/v15010079.

462. Mennechet, F.J.D., Paris, O., Ouoba, A.R., Salazar Arenas, S., Sirima, S.B., Takoudjou Dzomo, G.R., Diarra, A., Traore, I.T., Kania, D., Eichholz, K., et al. (2019). A review of 65 years of human adenovirus seroprevalence. Expert Rev Vaccines *18*, 597–613. 10.1080/14760584.2019.1588113.

463. Wang, X., Kerkmann, L., Hetzel, M., Windmann, S., Trilling, M., Zhang, W., Ehrhardt, A., and Bayer, W. (2022). Analysis of the Prevalence of Binding and Neutralizing Antibodies against 39 Human Adenovirus Types in Student Cohorts Reveals Low-Prevalence Types and a Decline in Binding Antibody Levels during the SARS-CoV-2 Pandemic. J Virol *96*, e0113322. 10.1128/jvi.01133-22.

464. Shashkova, E.V., May, S.M., and Barry, M.A. (2009). Characterization of human adenovirus serotypes 5, 6, 11, and 35 as anticancer agents. Virology *394*, 311–320. 10.1016/j.virol.2009.08.038.

Acknowledgements

First, I would like to thank Prof. Dr. Jan Tuckermann, director of the Institute of Comparative Molecular Endocrinology at University Ulm for being my first supervisor and for giving me the opportunity to do my PhD in the field of gene therapy.

Furthermore, I would like to greatly thank Prof. Dr. Stefan Kochanek, head of the Department of Gene Therapy at University Ulm for offering me the possibility to realize my thesis in his laboratory. Thank you for all the inspiring scientific discussions, valuable advices and for your everlasting support over the whole duration of my PhD.

Special thanks go to my laboratory supervisor Dr. Lea Krutzke. From the very beginning of my PhD, you exceptionally supported me in every conceivable way and not rarely far beyond your duties. With your scientific experience and expertise, you significantly contributed to this work, taught me valuable lectures in aim-orientated working, how to analyze and solve problems and not at least how to deal with frustrating times. Thank you for all your patience, all your motivating words, all the great discussion we had and for always supporting me throughout all the phases of my PhD. The way I was looked after by you was truly exceptional, working with you was always so much fun and I feel very grateful to have had such a great supervisor who contributed so substantially to make my PhD an unforgettable and special time in my life!

I also would like to thank all my current and former colleagues of the Department of Gene Therapy. After already accomplishing my Bachelor thesis at your institute, it really felt like a “home-coming” when starting my PhD. I am thankful for all the great moments I had with you and feel privileged for being part of your group for so many years. Much thanks to all of you for being part of this “journey” and for the intense and great time I had, which I will keep in best remembrance and definitely will never forget!

Lastly, I would like to express my heartfelt thanks to my family and friends for supporting me by every possible means and being with me through all the ups and downs over the last few years. Thank you for all the encouraging words, for always believing in me and for all the heartful support I experienced, especially during hard times. Without your support, this work may have never been finished and I am infinitely thankful for all of you!

Statutory declaration

I hereby declare that I wrote the present dissertation with the topic:

“Development and characterization of oncolytic adenoviral vectors for the treatment of head and neck cancer”

independently and used no other aids than those cited. In each individual case, I have clearly identified the source of the passages that are taken word for word or paraphrased from other works.

I also hereby declare that I have carried out my scientific work according to the principles of good scientific practice in accordance with the current “Satzung der Universität Ulm zur Sicherung guter wissenschaftlicher Praxis” [Rules of the University of Ulm for Assuring Good Scientific Practice]

Ulm,……

……

Frederik Wienen